

Thermoplastic Graphene Composites for Mechanical, Thermal Stability and Conductive Applications

**A thesis presented in fulfilment for the Degree of Doctor of
Philosophy**

Michael Czajka

BAppSc (Chemistry) Honours 1

School of Science

College of Science, Engineering and Health

RMIT University

October 2016

Declaration

I certify that except where due acknowledgement has been made, the work is that of the author alone; the work has not been submitted previously, in whole or in part, to qualify for any other academic award; the content of the thesis is the result of work which has been carried out since the official commencement date of the approved research program; any editorial work, paid or unpaid, carried out by a third party is acknowledged; and, ethics procedures and guidelines have been followed.

Michael Czajka

Date: 2/10/2016

Acknowledgements

Professor Emeritus Robert Shanks (senior supervisor) who provided regular advice. He has been exceedingly patient, generously sharing his expertise and giving his time. This thesis would not have been possible without his assistance.

Associate Professor Helmut Hugel (associate supervisor) for ideas (especially reduction).

Trevor Rook (associate supervisor) for encouraging a green chemistry approach, finding problems before they became serious and being there when others could not.

Dr Michelle Spencer (associate supervisor) for performing the DFT calculations, generating the images, analysing data and providing advice. Hang Tran also for running calculations, analysing data and creating some of the images.

Dr Mathew Leonard and Dr Anthony Lingham for assistance with synthetic mechanisms.

Dr David Tonkin for assisting with the tube furnace and being exceedingly helpful.

Dr Jeff Huges for timely and well-considered advice.

Dr Pandiyan Murugaraj for assistance with conductivity testing.

Daniel Oldfield for TEM assistance.

Special thanks to the RMIT Polymer Research Group who made life a lot more enjoyable especially Nabeen Dulal, Firoozeh Pourjavaheri, Isaac Martinez who took the time to find standards, demonstrate equipment and make useful suggestions on data processing and Dr Ing Kong for assistance and encouragement.

The equipment and facilities provided by the RMIT University School of Science have played a major part in achieving the research goals. A special thanks to Frank Antolasic, Nadia Zakhartchouk, Peter Laming, Mike Allan (Engineering) and Phil Francis (microscopy) who provided technical expertise, assistance and advice.

The authors acknowledge the facilities and technical assistance of the Australian Microscopy and Microanalysis Research Facility at RMIT University Microscopy and Microanalysis Facility.

The DFT calculations were undertaken with the assistance of resources from the National Computational Infrastructure (NCI), which is supported by the Australian Government, the Pawsey Supercomputing Centre with funding from the Australian Government and the Government of Western Australia, the Multimodal Australian ScienceS Imaging and Visualisation Environment (MASSIVE), and the Victorian Partnership for Advanced Computing Limited (VPAC Ltd.) through the V3 Alliance, Australia.

The Australian Commonwealth government for an Australian Postgraduate Award (APA) and RMIT University School of Science which topped up the APA.

17 Group for encouragement and assistance in applying for a provisional patent.

My mother (Stanisława), father (Michał), brother Chris and sister Elizabeth, who were always supportive of a PhD.

My Aunty Tosia (Antonina) Czajka, Uncle Kazik Czajka and Aunt June Dampier whose assistance made this course of study much easier.

To the many others who offered time or advice freely, thank you.

God who blessed me with this PhD opportunity.

Publications

Journal Papers

CZAJKA M., Shanks R. A., Spencer M. and Oldfield D. (2017) **Hydrogen-Reduced Low-Defect Graphene with Poly(ethylene terephthalate) Composites.** *Polymer Research Journal*, Vol 10(4).

MUSTAPA I. R., Czajka M., Chandran S., Daud N., Kong I. and Shanks R.A. (2017). **Crystallization Behavior of Plasticized Poly(lactic acid)-Hemp Nanocomposites.** *Polymer Research Journal*, Vol 10(4).

SARATHCHANDRAN C., Czajka M., Chan C. H., Shanks R. A., and Thomas S. (2016) **Interfacial Interactions of Thermally Reduced Graphene in Poly(trimethylene terephthalate)-Epoxy Resin Based Composites.** *Polymer*, vol 106: 140-151.

CZAJKA M., Shanks R. A. and Kong I. (2015) **Preparation of Graphene and Inclusion in Composites with Poly(styrene-*b*-butadiene-*b*-styrene).** *Science and Engineering of Composite Materials*, vol 22(1): 7-16.

POURJAVAHERI F., Mohaddes F., Shanks R.A., Czajka M., and Gupta A. (2014) **Effects of Different Purification Methods on Chicken Feather Keratin.** *Advanced Materials Research*, Trans Tech Publ, vol 941-944: 1184-87.

MUKHERJEE T. and Czajka M. (2014) **Dispersion Study of Nanofibrillated Cellulose Based Poly(butylene adipate-co-terephthalate) Composites.** *Carbohydrate Polymers* 102(0): 537-542.

CZAJKA M. (2012) **Systemic Effects of Fluoridation.** *J Orthomolecular Medicine*, vol 27, number 3.

Provisional Patent

CZAJKA M., Shanks R. A. and Hugel H. (2015) **Graphene Production Method.** WIPO/PCT WO 2015/164916 A1

Refereed Conference Papers

CZAJKA M., Shanks R. A. and Oldfield D. (2015) **Carbon Monoxide Reduced Low-Defect Graphene Nanocomposites with Poly(styrene-*b*-butadiene-*b*-styrene) Composites.** *Antec*, Orlando, Florida, USA, 23-25 March.

CZAJKA M., Shanks R. A. and Oldfield D. (2015) **CO-Reduced Low-Defect Graphene in Poly(styrene-*b*-butadiene-*b*-styrene) Composites.** *Antec*, Orlando, Florida, USA, 23-25 March.

CZAJKA M., Shanks R. A. and Oldfield D. (2015) **Low Defect CO-Reduced Graphene in Poly(styrene-*b*-butadiene-*b*-styrene) Composites.** *Nanolytica*, Melbourne, Australia, 9 February.

POURJAVAHERI F., Shanks R., Czajka M. and Gupta A. (2014) **Purification and Characterisation of Feathers Prior to Keratin Extraction.** *International Chemical Engineering Congress and Exhibition*, Kish, Iran.

POURJAVAHERI F., Mohaddes F., Shanks R., Czajka M. and Gupta A. (2014). **Effects of Different Purification Methods on Chicken Feather Keratin.** *International Conference on Manufacturing Science and Engineering*, (19 - 20 April) Shanghai, China.

CZAJKA M., Shanks R. A. and Oldfield D. (2013) **Poly(ethylene terephthalate) Composites with Low-defect Hydrogen-Reduced Graphene.** *International Conference on Advanced Polymeric Materials*, Kerala, India, 11-13 October p.68

MUSTAPA I. R., Czajka M., Chandran S., Daud N., Kong I. and Shanks R. A. (2013) **Crystallization Behavior of Plasticized Poly(lactic acid) Nanocomposites.** *Proc. International Conference on Advanced Polymeric Materials*, Kerala, India.

CZAJKA M., Shanks R. A. and Oldfield D. (2013) **Low Defect Hydrogen Reduced Graphene in Poly(ethylene terephthalate) Composites.** *OzCarbon*, Melbourne, Australia.

POURJAVAHERI-JAD F., Shanks R. A., Czajka M. and Gupta A. (2013) **Purification Methods for Chicken Feather Keratin.** *International Conference on Advanced Polymeric Materials*, Kerala, India, 11-13 October p.141

CZAJKA M., Kong I. and Shanks R. A. (2012), **Preparation of Graphene and Inclusion in Composites with Poly(styrene-*b*-butadiene-*b*-styrene)**. *International Conference on Composites/Nano Engineering*, Beijing, China, 22-28 July.

CZAJKA M., Kong I. and Shanks R. A. (2012), **Graphene Preparation from Intercalated Graphite via Rapid Heating under Reductive Conditions**. *International Conference on Composites/Nano Engineering*, Beijing, China, 22-28 July.

CZAJKA M., Kong I. and Shanks R. A. (2012), **Graphene Composites in Poly(styrene-*b*-butadiene-*b*-styrene)**. *International Conference on Composites/Nano Engineering*. Beijing, China, 22-28 July.

CZAJKA M., Kong I. and Shanks R.A. (2011), **Graphene Preparation and Composites with Poly(styrene-*b*-butadiene-*b*-styrene)**, *Australian-Indian Joint Symposium on Smart Nano-Materials in Victoria*, RMIT University 2-4 November.

SHANKS R. A., Spoljaric S., Kong I., CZAJKA M., Daud N., Mustapa I. R. and Zhai Y. M. (2011), **Preparation of Functional Nano-Particles for Dispersion to Form Polymer Nano-Composites**. *Australia-India Joint Symposium on Smart Nanomaterials in Victoria* (p. 62): RMIT University 2-4 November.

CZAJKA M. and Shanks R. A. (2011), **Graphite Layer Nano-Composites with Polyurethane Matrix**. *TechConnect World 2011 Proceedings: Nanotech, Clean Technology, Microtech, Bio Nanotech*, Taylor and Francis, Boston, MA, USA, pp. 196-199 (NSTI-Nanotech)

Table of Contents

Declaration	ii
Acknowledgements	iv
Publications	vi
List of Figures	xvi
List of Tables	xxiv
Abbreviations and Nomenclature	xxvi
Summary	xxx
Chapter 1 Introduction	1
<i>1.1 Overview</i>	<i>1</i>
1.1.1 Structure	1
1.1.2 History	2
1.1.3 Future	2
1.1.4 Polymers	2
<i>1.2 Rationale</i>	<i>3</i>
<i>1.3 Aim</i>	<i>4</i>
<i>1.4 Objectives</i>	<i>4</i>
<i>1.5 Research Questions</i>	<i>4</i>
<i>1.6 Thesis Structure</i>	<i>5</i>
Chapter 2 Literature Review	7
<i>2.1 Introduction</i>	<i>7</i>
2.1.1 Opportunities	8
2.1.2 Challenges	9
2.1.3 Potential	9
<i>2.2 Properties</i>	<i>9</i>

Table of Contents

<i>2.3 Production</i>	<i>10</i>
2.3.1 Top Down	10
2.3.2 Bottom Up	12
<i>2.4 Reduction of Oxidised Graphene</i>	<i>13</i>
2.4.1 Chemical Reduction	13
2.4.2 Microwave Activated Chemical Reduction	13
2.4.3 Biomaterial Enhanced Reduction	14
2.4.4 Thermally Induced Reduction	14
2.4.5 Gamma Radiation Activation Under an Inert or Reducing Gas	14
<i>2.5 Solvation Assisted Dispersion</i>	<i>15</i>
2.5.1 Dispersion	16
<i>2.6 Characterisation</i>	<i>17</i>
2.6.1 Raman Spectroscopy	17
2.6.2 Edges	18
2.6.3 Transmission Electron Microscopy	18
2.6.4 Scrolling	19
2.6.5 Other	19
<i>2.7 Metal-Graphene Combinations</i>	<i>20</i>
<i>2.8 Polymer-Graphene Composites</i>	<i>20</i>
2.8.1 Thermoplastic Elastomers	21
<i>2.9 Biocompatibility</i>	<i>22</i>
<i>2.10 Applications</i>	<i>23</i>
2.10.1 Electronics	23
2.10.2 Lubricants	28
2.10.3 Adhesives	28
2.10.4 Filtration	28
2.10.5 Analysis	29
2.10.6 Construction Materials	30
2.10.7 Armoured Materials	30
Chapter 3 Experimental	31
<i>3.1 Introduction</i>	<i>31</i>

Table of Contents

<i>3.2 Materials</i>	31
3.2.1 Polymer Matrices	31
3.2.2 Filler Reinforcement	32
3.2.3 Solvents	33
3.2.4 Non-Solvents	33
3.2.5 Alkalis	33
3.2.6 Metals	33
<i>3.3 Filler Synthesis and Dispersion</i>	33
3.3.1 Graphene Preparation	33
3.3.2 Ultrasonication	35
<i>3.4 Preparation of Nanocomposites</i>	36
3.4.1 Magnetic-Grafted Graphene	36
3.4.2 Solvent Dispersion	36
3.4.3 Melt Dispersion	36
3.4.4 Film Preparation	37
3.4.5 Microtomy Preparation	38
<i>3.5 Characterisation</i>	39
3.5.1 Microstructure	39
3.5.2 Vibrational Spectroscopy	40
3.5.3 Electron Spectroscopy	41
3.5.4 Composition and Thermal Stability	41
3.5.5 Wide Angle X-Ray Scattering	42
3.5.6 Thermomechanical Analysis (TMA)	43
3.5.7 Electrical Conductivity	44
3.5.8 Surface Area	44
3.5.9 Particle Size	45
3.5.10 Surface Energy	46
3.5.11 Molecular Modelling	47
Chapter 4 Graphene Preparation from Intercalated Graphite via Rapid Heating under Reductive Conditions	49
<i>4.1 Introduction</i>	49
<i>4.2 Experimental</i>	50

Table of Contents

<i>4.3 Results and Discussion</i>	50
4.3.1 Microscopy	50
4.3.2 Vibrational Spectroscopy	52
4.3.3 Composition and Thermal Stability	55
4.3.4 Surface Energy	56
4.3.5 Electrical Conductivity	57
4.3.6 Particle Size	58
4.3.7 Surface Area	59
4.3.8 Dispersion	60
<i>4.4 Conclusion</i>	62
Chapter 5 Preparation of graphene and inclusion in composites with poly(styrene-<i>b</i>-butadiene-<i>b</i>-styrene)	63
<i>5.1 Introduction</i>	63
<i>5.2 Experimental</i>	63
<i>5.3 Results and Discussion</i>	64
5.3.1 Microscopy	64
5.3.2 Vibrational Spectroscopy	65
5.3.3 Dynamic Mechanical Analysis	66
5.3.4 Wide Angle X-ray Scattering	68
5.3.5 Thermal Stability	70
5.3.6 Electrical Properties	70
5.3.7 Surface Modification	71
<i>5.4 Conclusion</i>	72
Chapter 6 Carbon Monoxide Reduced Low-Defect Graphene Nanocomposites with Poly(styrene-<i>b</i>-butadiene-<i>b</i>-styrene)	75
<i>6.1 Introduction</i>	75
<i>6.2 Experimental</i>	76
<i>6.3 Results and Discussion</i>	76
6.3.1 Vibrational Spectroscopy	77
6.3.2 Thermal Stability	78

Table of Contents

6.3.3 Microscopy	78
6.3.4 Mechanical Properties	79
6.3.5 Dispersion	81
<i>6.4 Interpretation</i>	83
<i>6.5 Conclusions</i>	83
Chapter 7 Hydrogen Reduced Low-Defect Graphene with Poly(ethylene terephthalate) Composites	85
<i>7.1 Introduction</i>	85
<i>7.2 Experimental</i>	85
<i>7.3 Results and Discussion</i>	86
7.3.1 Vibrational Spectroscopy	86
7.3.2 WAXS	87
7.3.3 Microscopy	89
7.3.4 Mechanical Properties	91
7.3.5 Thermogravimetry	93
7.3.6 Permeation	94
7.3.7 Dispersion	95
7.3.8 Conductivity	96
<i>7.4 Conclusion</i>	97
Chapter 8 Carbon Monoxide Reduced Low-Defect Graphene with Poly(ethylene terephthalate) Composites	99
<i>8.1 Introduction</i>	99
<i>8.2 Experimental</i>	100
<i>8.3 Results and Discussion</i>	100
8.3.1 Visual Characterisation	100
8.3.2 Microscopy	101
8.3.3 Mechanical Properties	103
<i>8.4 Conclusion</i>	106
Chapter 9 Polycarbonate-Graphene Composites	107

Table of Contents

<i>9.1 Introduction</i>	<i>107</i>
<i>9.2 Experimental</i>	<i>108</i>
<i>9.3 Results and Discussion</i>	<i>108</i>
9.3.1 Visual Characterisation	109
9.3.2 Microscopy	109
9.3.3 Mechanical Properties	112
9.3.4 Dispersion	113
<i>9.4 Conclusion</i>	<i>116</i>
Chapter 10 Polyether Sulfone-Graphene Composites	117
<i>10.1 Introduction</i>	<i>117</i>
<i>10.2 Experimental</i>	<i>118</i>
<i>10.3 Results and Discussion</i>	<i>118</i>
10.3.1 Microscopy	118
10.3.2 Mechanical Properties	120
<i>10.4 Conclusion</i>	<i>124</i>
Chapter 11 Conclusion	125
<i>11.1 Conclusion</i>	<i>125</i>
<i>11.2 Applications of This Work</i>	<i>128</i>
<i>11.3 Future Ideas</i>	<i>128</i>
11.3.1 Improved Dispersions	128
11.3.2 Bonding With Other Polymers	128
11.3.3 Other Improved Properties	129
11.3.4 Improved Production Methods	130
11.3.5 Scalability	130
References	131
Appendix A: Publications	153

List of Figures

Figure 1-1 a) Graphene is a sheet of single carbons bonded together in a honeycomb structure b) AB (Bernal) stacking of graphite ⁸ c) Graphite (many layers of graphene)	1
Figure 1-2 Flow chart of thesis structure	6
Figure 2-1 Typical oxygen functional groups found at the edges and in the plane of graphene	7
Figure 2-2 Graphene to buckminsterfullerenes, nanotubes and graphite ^{3, 10}	8
Figure 2-3 a) Double-layer graphene sheet illustrated using coronene b) Model of graphene showing sheet distortion from planarity due to high surface energy	9
Figure 2-4 Preparation of graphene sheets ⁴¹	10
Figure 2-5 a) Expandable graphite ⁴⁹ showing intercalation (small molecules introduced between layers) b) SEM of graphite oxide before thermal expansion c) after thermal expansion ⁵⁰	12
Figure 2-6 Synthesis of graphene nanoribbon using PAH molecular precursors ⁵⁷	13
Figure 2-7 Solvents (from left to right) a) 1-methyl-2-pyrrolidone (NMP) b) dimethyl sulfoxide (DMSO) c) dimethyl formamide (DMF) d) γ -butyrolactone (GBL) e) water (H ₂ O) ⁶⁸	15
Figure 2-8 a) 3,3'-aminobis(N,N-dimethylpropylamine) (DMPA) b) N-[3-(dimethylamino)propyl]methacrylamide (DMAPMA) c) 2-(tert-butylamino)ethyl methacrylate (BAEMA) d) 2-(dimethylamino)ethyl methacrylate (MAEMA)	15
Figure 2-9 Hydrogen bonding demonstrating π -interactions a) OH- π b) NH ₂ - π (modified) ⁷⁴	17
Figure 2-10 a) Surface enhanced, with gold, Raman spectra of single layer graphene (upper) compared with no enhancement (lower) showing G and 2D peaks 785 nm b) Trilayer graphene-enhanced (upper) 2x magnified (lower) 633 nm (4 mW with 1 s exposure alpha300 S) ⁷⁸ .	17
Figure 2-11 a) Graphene, and carbon nanotubes b) Armchair (5,5) c) zig-zag (9,0)	18

List of Figures

Figure 2-12 Graphene scrolls (one-sided, diagonal and two-sided) ⁸⁵	19
Figure 2-13 SBS illustrated: a) Shows repeating polystyrene and polybutadiene groups in a simplified form ¹¹⁰ and b) the chemical composition showing repeating groups	21
Figure 2-14 Fullerene (C ₆₀) ¹²⁶	22
Figure 2-15 Upper: Periodic table ¹³⁷ Lower: Graphene monoxide ¹³⁸	24
Figure 2-16 a) GO film reduced by laser b) Copper tape applied c) Electrolytic coat applied d) 100 capacitors e) Flexible substrate ⁶⁷	25
Figure 2-17 TEM image of a sheet of Graphene with Fe ₃ O ₄ particles bonded to the surface ¹⁴¹	26
Figure 2-18 TEM images a) Multilayer graphene by CO reduction (~18 layers) ¹⁴⁸ b) ~10 layer graphene by chemical vapour deposition (CVD) ¹⁴⁹	27
Figure 2-19 Graphyne ¹⁵⁴	29
Figure 2-20 Comparison of concrete with different nanofillers ¹⁵⁹	30
Figure 3-1 a) SBS b) PET c) PC d) PES	32
Figure 3-2 Aromatic solvents plus hydrogen atoms a) <i>p</i> -xylene b) <i>o</i> -chlorophenol c) benzene	33
Figure 3-3 Tube furnace with one way vent	34
Figure 3-4 a) Ultrasonicator b) Rayleigh-Benard cell ¹⁶⁴ formed by H ₂ reduced graphene in <i>p</i> -xylene (after ultrasonication)	35
Figure 3-5 Haake Polylab 600 internal cavity mixer showing twin roller rotors	37
Figure 3-6 Heated press (IDM)	38
Figure 3-7 Leica Ultracut UCT (minus cryo-stage)	38
Figure 3-8 TEM JEOL 2100F	39

List of Figures

Figure 3-9 Perkin Elmer Raman Station 400 showing glass slide and camera (with protective hood raised)	40
Figure 3-10 Perkin Elmer TGA7	42
Figure 3-11 Bruker D8 used for x-ray diffraction (XRD)	42
Figure 3-12 a) Diamond DMA showing mounting of SBS-graphene composite b) $\text{Tan}(\delta) = \frac{\sin(\delta)}{\cos(\delta)} = \text{loss modulus/storage modulus}$	43
Figure 3-13 a) HP4192A impedance analyser b) circular electrode (showing composite being measured)	44
Figure 3-14 ASAP 2000 for BET surface analysis	45
Figure 3-15 Canty Particle sizing system	45
Figure 3-16 Dataphysics OCA 20 for contact angle measurement	46
Figure 4-1 Microscopy 2 μm , a) GT-Air with ultrasonication TEM, b) GT-N ₂ (inert gas to remove oxides) SEM, c) GT-H ₂ (reducing gas) SEM, d) CT #1 >700 m ² ·g ⁻¹ SEM e) GT-CO (reducing gas) with ultrasonication TEM (50 nm)	51
Figure 4-2 Raman spectra intensity of graphene (listed at the 2D peak from highest to lowest)	52
Figure 4-3 Graphene a) Types of edges b) D/G ratio versus production method	53
Figure 4-4 Raman graphene G band position versus production method	54
Figure 4-5 Suggested mechanism for GT-CO reduction and repair	55
Figure 4-6 TGA of graphene mass loss (oxygen content) versus production method	56
Figure 4-7 GT graphene a) water drop on compressed GT-CO b) contact angle c) surface energy	57
Figure 4-8 Resistivity of graphene versus production method	58
Figure 4-9 Size distribution of GT-CO graphene by count	59

List of Figures

Figure 4-10 BET surface analysis measuring surface area versus graphene production method	60
Figure 4-11 Optimised structure of <i>p</i> -xylene adsorbed on graphene a) top down view b) side view (C-blue, H-orange and graphene C-grey) c) electron localisation function (ELF) of <i>p</i> -xylene d) graphene	61
Figure 5-1 SBS and graphene illustrating van der Waal interactions AB stacking geometry between the respective planes a) in solution b) without solvent	64
Figure 5-2 Electron microscopy a) GT-N ₂ 500 μm 80x SEM and 20,000x (2 μm) b) GT-Air with ultrasonication TEM c) GT-N ₂ SEM d) CT #1 SEM	65
Figure 5-3 Raman spectra a) Listed from highest to lowest at the D peak b) Comparing D peak intensity of graphene produced using four different methods	66
Figure 5-4 DMA of SBS-graphene 1 % composites a) Storage modulus b) Loss modulus c) Tan(δ) (Legend ordered at -120 °C highest to lowest)	67
Figure 5-5 Diffractogram SBS-graphene composites a) Relative intensity versus scattering angle (listed in order of peak intensity) b) Graphene peak intensity c) Graphene interlayer distance	69
Figure 5-6 TGA mass versus temperature with the first derivative of SBS and graphene (1 %) composites created with GT and CT (listed in order of lowest to highest temperature of decomposition)	70
Figure 5-7 SBS-graphene composites a) Resistance b) Capacitance	71
Figure 5-8 Microscopy (TEM) showing GT-Fe ₃ O ₄ (Fe ₃ O ₄ particles on a graphene sheet)	72
Figure 6-1 Graphene production by intercalation, thermal exfoliation with reduction and ultrasonication (simplified)	76
Figure 6-2 Raman spectra of graphene a) Listed in order of 2D peak b) D/G ratio	77
Figure 6-3 TGA of graphene mass loss (oxygen content) versus production method	78
Figure 6-4 TEM JEOL 2100 graphene a) GT-CO b) SBS 1 % GT-CO	79

List of Figures

- Figure 6-5 TMA of SBS GT-CO (0-20 %·w/w) at room temperature (25 °C) a) engineering stress versus strain b) tangent modulus at 0.25 % strain c) change in recovery strain 80
- Figure 6-6 Optimised structures of SBS monomer adsorbed on graphene after a simulation time of a) 2.5 ps b) 5 ps 82
- Figure 6-7 Aromatic interaction geometries a) Edge to face (aka T-shaped or edge on) b) offset face-to-face (aka slipped or skewed) c) face-to-face (aka eclipsed)^{74, 203, 204} 83
- Figure 7-1 Poly(ethylene terephthalate) and graphene showing DFT preferred van der Waal AB- π stacking geometry a) in solution b) without solvent 86
- Figure 7-2 Raman spectra comparing a) CT research grade graphene, GT-H₂ reduced graphene and GT-Air expanded graphene (listed in order of the 2D peak) b) D/G ratio of graphenes (calculated from unsmoothed data) 86
- Figure 7-3 PET a) WAXS (ordered by peak intensity) b) Interlayer distances c) Crystallinity versus crystal size 89
- Figure 7-4 SEM images with 20 μ m scale a) PET-Neat MD b) PET 1 % MD c) PET 1 % SD (left to right) 90
- Figure 7-5 TEM images with 20 nm scale a) PET-Neat MD b) PET 1 % MD c) PET 1 % SD (left to right) 90
- Figure 7-6 PET with a ramped force of 18 N applied a) Stress (MPa) versus strain (%) curve b) Tangent modulus 92
- Figure 7-7 DMA of PET composites a) Storage modulus b) Loss modulus c) Tan(δ) 93
- Figure 7-8 TGA pyrolysis under nitrogen a) PET degradation curve b) PET degradation temperature 94
- Figure 7-9 PET-graphene composites oxygen permeability 94
- Figure 7-10 Methyl terminated PET monomer adsorbed on graphene a) Side view b) Top down view (C-Blue H-White O-Red Graphene C-Grey) c) Electron localisation function (ELF) of PET adsorbed on graphene, aligned so the slice cuts through the C atoms in the ring of the methyl terminated PET molecule 96

List of Figures

Figure 8-1 Photographs of melt dispersed PET and graphene (GT-CO 1 %) composites a) neat b) graphene c) ultrasonicated graphene	100
Figure 8-2 PET (without glass) melt dispersed composites with 200 μm scale bar a) neat b) GT-CO 1 % c) GT-CO 1 % ultrasonicated	101
Figure 8-3 TEM images of PET with melt dispersed GT-CO 1 % (without ultrasonication) a) 500 nm b) 100 nm c) 50 nm d) 20 nm	102
Figure 8-4 TEM images of melt dispersed PET with melt dispersed ultrasonicated GT-CO 1 % a) 500 nm b) 100 nm c) 50 nm d) 20 nm	103
Figure 8-5 SS-MA of PET GT-CO 1 % melt dispersed with and without ultrasonication a) Stress-strain curve b) End strain (%) c) Tangent modulus (0.05 % Strain)	104
Figure 8-6 DMA of melt dispersed PET GT-CO 1 % graphene with and without ultrasonication a) Storage Modulus b) Loss Modulus c) Tan Delta (with bar graphs comparing properties at 25 °C)	105
Figure 9-1 Molecular representation of the polycarbonate monomer and graphene sheet	107
Figure 9-2 Photograph of polycarbonate melt dispersed with 0.1% ultrasonicated graphene a) neat b) GT-H ₂ c) GT-CO (from left to right)	109
Figure 9-3 PC melt dispersed with 0.1 % ultrasonicated graphene with 200 μm scale bar a) Neat b) GT-H ₂ c) GT-CO	110
Figure 9-4 TEM images of PC GT-H ₂ 0.1 % US MD a) 2 μm b) 500 nm c) 100 nm d) 20 nm	110
Figure 9-5 TEM images of PC GT-CO 0.1 % US MD a) 2 μm b) 500 nm c) 200 nm d) 100 nm	111
Figure 9-6 Polycarbonate with ultrasonication and melt dispersion of Neat, GT-H ₂ and GT-CO 0.1 % composites a) Storage Modulus b) Loss Modulus c) TanDelta	112

List of Figures

Figure 9-7 Three R'-CH/graphene complexes demonstrating weak hydrogen bonds (R' = H, phenyl, xylene or variable R = carbon part of molecular network) where a) is the most stable (modified from reference) ²³⁵	114
Figure 9-8 Optimised structures of PC monomer adsorbed on graphene after a simulation time of a) 3.5 ps and b) 5.3 ps	115
Figure 10-1 Molecular representation of the PES monomer and graphene sheet	117
Figure 10-2 TEM images of PES GT-H ₂ 1 % US and SD a) 200 nm b) 100 nm c) 50 nm d) 20 nm	119
Figure 10-3 TEM images of PES GT-CO 1 % US and SD a) 500 nm b) 200 nm c) 100 nm d) 20 nm	120
Figure 10-4 Stress-strain mechanical analysis a) Hysteresis curves b) Tangent modulus c) Max strain d) End strain	121
Figure 10-5 PES CO 1 % SD a) Storage modulus b) Loss Modulus c) Tan Delta	123

List of Tables

Table 3-1 Graphene summarised by supplier and production method (temperature, gas and ultrasonication)

34

Abbreviations and Nomenclature

θ	Angle of diffraction	CT	Cheap tubes (HDplas) graphene
Å	Angstrom (1 Å = 0.1 nm)	c	Centi (10^{-2})
λ	Wavelength	C	Carbon
Δ	Change (large)	C ₆₀	Buckminster fullerene (aka Buckyball)
°	Degree	CO	Carbon monoxide (reduction)
μ	Micro (10^{-6})	CVD	Chemical vapour deposition
Ω	Ohm (unit of electrical resistance)	DC	Direct current
%	Percent	d	Change (small)
/	Per (divide)	D	Defect (peak)
π	Pi (3.141)	DFT	Density functional theory
	Covalent bonds where two orbitals overlap	DMA	Dynamic mechanical analysis
AC	Alternating Current	f	Femto (10^{-15})
AFM	Atomic-force microscopy	F	Farad (unit of electrical capacitance)
Air	Atmospheric: nitrogen (~78 %), oxygen (~21 %), argon (~1 %)	ELF	Electron localisation function
aka	Also known as	g	Gram
at.%	Atomic percentage	G	Giga (10^9)
BE	Binding energy	GIC	Graphite intercalation compound
BET	Brunauer Emmett Teller	GO	Graphene oxide
BU	Bottom up	GT	Graftech

Abbreviations and Nomenclature

GT-Air	Air expanded graphene	N	Newton (unit of force)
GT-CO	CO reduced graphene	NMR	Nuclear magnetic resonance
GT-H ₂	Hydrogen reduced graphene	Oxidation	Loss of electrons (oxidant)
GT-N ₂	Nitrogen-expanded graphene	p	Pico (10 ⁻¹²)
h	Hour	Pa	Pascal (unit of pressure)
Hz	Hertz (unit of frequency) 1 cycle/second	PAH	Polycyclic aromatic hydrocarbon
H ₂	Hydrogen (a reducing gas)	PAW	Projector augmented wave (method)
Hg	Mercury	PC	Polycarbonate
J	Joule (unit of energy)	PES	Poly(ether sulfone)
k	Kilo (10 ³)	PET	Poly(ethylene terephthalate)
K	Kelvin (unit of temperature)	PS	Polystyrene
N ₂	Nitrogen (inert gas)	PTFE	Polytetrafluoroethylene
m	Metre	Reduction	Gain of electrons (anti-oxidant)
	Milli (10 ⁻³) when used with other units e.g. mm, mL	RPM	Revolutions per minute
mf	Modulated force	s	Second
M	Mega (10 ⁶)	SBS	Poly(styrene- <i>b</i> -butadiene- <i>b</i> - styrene)
MD	Melt dispersion	SD	Solvent dispersion
MD	Molecular Dynamics	SEM	Scanning electron microscope
min	Minute	SS-MA	Stress-strain (tensile) mechanical analysis
MWCNT	Multi-walled carbon nanotubes	T	Tera (10 ¹²)
n	Nano (10 ⁻⁹)	T _b	Temperature boiling

Abbreviations and Nomenclature

T_g	Temperature glass transition: change from hard (glassy) to soft (rubberlike) ¹
T_m	Temperature melting
TM	Thermomechanometry
TD	Top down
TEM	Transmission electron microscope
TGA	Thermo gravimetric analysis (thermogravimetry)
TMA	Thermomechanical analysis
US	Ultrasonication/ultrasonicator
UV	Ultraviolet (10 – 380 nm)
V	Volts (unit of electromotive force)
W	Watt (unit of power) 1 J/s
WAXS	Wide-angle X-ray Scattering (aka XRD)
w/w	weight/weight
XPS	X-ray photoelectron spectroscopy
XRD	X-ray diffraction (aka WAXS)

Summary

The aim of this research was to prepare graphenes, to reactively modify their surface to enhance exfoliation and to facilitate bonding to chosen matrix polymers, to characterise the prepared materials and determine their physical and mechanical properties. This investigation was motivated by the exceptional performance characteristics of graphene to find new ways of creating and dispersing graphene in polymers, so polymer-graphene composites were fabricated. Composites enhanced by the properties of graphene were prepared inspired by the unique nanostructure of graphene that imparts high strength, stiffness and resistance to deformation.

Graphenes were prepared using thermal expansion in an oxidising atmosphere (air), an inert atmosphere (nitrogen N₂) and a reducing atmosphere (hydrogen H₂ or carbon monoxide CO). The reduction of graphene using thermal expansion with simultaneous CO reduction was granted a provisional patent (Appendix A).

The graphenes were characterised using thermogravimetry (TGA), Raman spectroscopy, electrical resistance and surface energy measurements. All graphenes showed a mass loss in TGA which was attributed to oxygen-containing functional groups present on the graphene surface. The mass loss was lowest for the inert and reducing atmospheres. Raman spectroscopy (using the D/G peak ratio) showed that graphene had the fewest defects in the order CO<H₂<N₂<air and produced the fewest layers (as measured using the highest 2D/G ratio) under a CO reducing atmosphere. The electrical resistance (as measured using a compressed pellet) was lowest for graphene prepared under a reducing or inert atmosphere and highest under air. The contact angle was measured and used to calculate the surface energy which was found to be lower when produced under a reducing or inert atmosphere and highest when produced under air (CO<N₂<H₂<air). This increased hydrophobicity was consistent with a reduction in surface oxides, healing of surface defects and scrolling of graphenes, which was supported by transmission electron microscopy (TEM). The graphene produced had a surface area greater than commercially produced graphene. All of this suggests that the CO reduced graphene is superior to other graphene production methods.

The graphenes were then used to produce four different polymer composites including a thermoplastic elastomer (poly(styrene-*b*-butadiene-*b*-styrene); SBS at two compositions), a semi-crystalline thermoplastic (polyethylene terephthalate; PET at two compositions) and

Summary

two high-performance amorphous polymers (polycarbonate (PC) and poly(ether sulfone) (PES)). The composites were prepared by dispersion of the graphene into polymer solutions using ultrasonication and high torque melt dispersion.

The SBS-graphene (1 %·w/w) composites were produced using graphenes prepared in air, N₂ and H₂ and using solvent dispersion (SD). The greatest changes occurred using the H₂ reduced graphene which showed increased stored energy (storage modulus), energy absorption (loss modulus) and damping (tan delta) in SBS. The damping effect (move to a more liquid state and greater free volume) was largest at low temperatures as a result of the large size of the graphene sheets used. Functionalising the graphene with Fe₃O₄ before combining it with SBS resulted in a composite that displayed magnetic properties.

The SBS-graphene (0-20 %·w/w) composites were produced using GT-CO reduced graphenes and using solvent dispersion. Stress-strain measurements showed a progressive decrease in deformation and increase in damping as the graphene content increased suggesting uniform dispersion in the SBS. The presence of aromatic interactions and hydrogen bonding between the SBS and graphene was supported by density functional theory calculations. Some scrolling of graphene was observed in this SBS composite.

The PET-graphene (1 %·w/w) composites produced using the GT-H₂ reduced graphene were prepared using solvent dispersion (with ultrasonication) and melt dispersion (without ultrasonication). Nucleation of PET did not occur using the low defect graphene although oxygen permeation of the composite increased which was attributed to an increased free volume. The results suggested that using a combination of ultrasonication and melt dispersion of graphene to produce the composite would increase the exfoliation and dispersion further.

The PET-graphene (1 %·w/w) composites using GT-CO reduced graphenes were prepared using melt dispersion (MD) alone or combined with ultrasonication. When using ultrasonication graphene agglomeration in PET was diminished, and reduction of the graphene could be seen by a darkening of the colour of the composite. PET deformation (ductility) increased with ultrasonication and melt dispersion of graphene.

The PC-graphene (0.1 %·w/w) composites using GT-H₂ or GT-CO reduced graphene with low filler content were prepared using melt dispersion with ultrasonication. The storage modulus of PC-graphene composites was greater than PC alone indicating stronger interfacial interactions existed with graphene. The time-dependent loss of energy (loss modulus) and

Summary

damping (greater liquid properties) increased when graphene was added to PC. The increase in damping suggested an increase in free volume. DFT calculations indicated that the interactions between graphene and PC were due to a combination of π - π and CH/ π bonding. Despite being relatively weak, the interaction of the aromatic rings and the H atoms on the methyl groups, in the monomer, both play a significant role in the attraction with graphene.

The PES-graphene (1 %·w/w) composites using GT-H₂ or GT-CO reduced graphenes were prepared using solvent dispersion with ultrasonication. GT-CO reduced graphene showed evidence of rolling or scrolling in PES which increases cross-sectional area. Interactions between PES GT-CO increased indicating a move to a more solid state and an increase in elasticity. The results demonstrated that PES binds well with graphene using only non-covalent bonding.

In each case, the polymer-graphene composites demonstrated good dispersion which establishes that π -interactions and hydrogen bonding are an effective way to disperse graphene. Where similar or comparable data was found for covalent bonding, it demonstrated that non-covalent bonding gave similar results. By using only non-covalent bonding, the pristine nature of the graphene was maintained creating low defect polymer-graphene composites. Low defect graphenes have advantages such as improved electrical and thermal conductivity, fewer contaminants, greater biocompatibility and the benefit of a less dangerous processing method. The optimal processing method combined ultrasonication and melt dispersion which are synergistic reducing (signalled by darker colour) and exfoliating graphene further. The scrolling of low defect GT-CO reduced graphene is of particular interest because the increased cross-sectional area gives it the potential to improve thermal and electrical conductivity.

Chapter 1 Introduction

1.1 Overview

Graphene was first proven to exist in 2004. It is the strongest material known with a Young's modulus of 1 TPa and ultimate strength of 130 GPa². It has a greater surface area (2630 m²/g) and is more electrically conductive (6000 S/cm)³ than any other material. Graphene is impermeable to gases⁴, resists high temperatures (estimated $T_m = 4900$ K)⁵ and is highly thermally conductive (5000 W/(m·K))³. It has been the most cited substance in science since the 2010 Nobel Prize in Physics was awarded to Andre Geim and Konstantin Novoselov for exfoliating one layer of graphene from a pencil (graphite) using adhesive tape (demonstrating weak interlayer forces) and obtaining an image of the graphene⁶.

1.1.1 Structure

Graphene is a form of carbon, with a structure of one-atom-thick planar sheets of sp^2 -bonded carbon atoms that are densely packed in a hexagonal crystal lattice (aka a single graphite layer). The aromatic rings which make up graphene sheets are the basic structural component of Buckminsterfullerenes (which also contain some five-membered rings), carbon nanotubes and graphite. Graphite is just many layers of graphene (0.333⁷ - 0.335 nm gap) stacked in an offset manner (Figure 1-1). The in-plane covalent bonds between carbon atoms are some of the strongest in nature (~5.9 eV, stronger than diamond) while the interlayer van der Waals forces (~50 meV) in graphite are some of the weakest⁸.

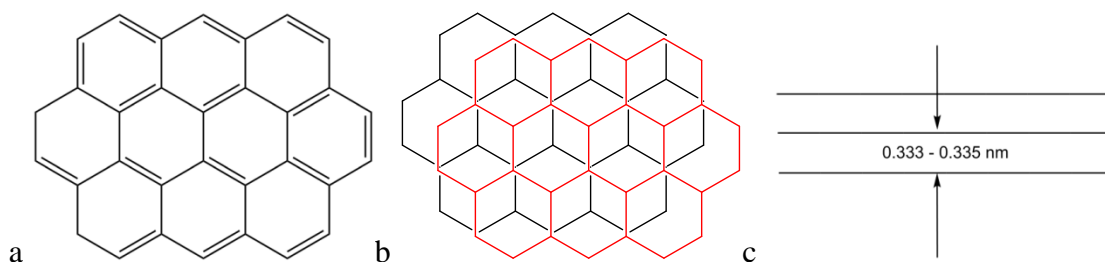


Figure 1-1 a) Graphene is a sheet of single carbons bonded together in a honeycomb structure b) AB (Bernal) stacking of graphite⁸ c) Graphite (many layers of graphene)

Graphene is defined as a single layer, but few layers (~2 or 3) or even multi-layers (up to 10 layers^{9, 10} or more^{11, 12}) are commonly called graphene because they still retain many exceptional properties of graphene. For example, each layer of multi-layer graphene absorbs

2.3 %^{3, 13} of light (single layer graphene 2.6 %¹⁴). Thus touch screens (for mobile phones) made of ten-layer graphene (replacing indium tin oxide) would still transmit ~77 % of light.

1.1.2 History

Carbon nanocomposites have traditionally been used in the rubber industry where many elastomers are compounded with carbon blacks (carbon particles of nano-dimension). It is now known that carbon nanotubes, composed of cylinders of fused hexagonal aromatic carbon rings, are responsible for the flexibility, strength and extreme sharpness of the near legendary Damascus steel swords^{15, 16}. Expandable graphites intercalated with oxides are used commercially in fire-retardant composites^{17, 18}.

1.1.3 Future

Graphenes are currently being produced in semi-commercial quantities, are already available in some commercial products and are expected to become a common component of advanced materials shortly. Graphenes are of great interest because they are simpler and cheaper to produce in large quantities while offering superior benefits to nanotubes for most uses. Graphenes have immediate applications in polymers, other composites and electronics. Graphenes can strengthen other materials, improve electron mobility, decrease gas permeation, improve flexibility, improve temperature resistance, improve durability and reduce mass. Graphenes are of theoretical interest since the individual sheets have a thickness of one carbon atom. Graphenes have an enormous surface energy since the surface to volume ratio is at a maximum at only one atom of carbon thick, but extending to relatively large lateral distances. Because graphenes have immediate commercial applications, they are likely to be commercialised more rapidly than any other recent discovery.

1.1.4 Polymers

Recently other nano-carbons have become available and are being evaluated for performance in polymers. Nano-carbons have been used in many polymers including epoxy resins¹⁹, polypropylene²⁰ and polycarbonate²¹. Nano-carbons are not particulates but are of nanoscale in at least one dimension. Graphenes are 2D single layers of fused hexagonal aromatic carbon rings in great sheets which can form percolated²² (conductive) networks in polymers at low concentration and are of nano-thickness.

This work describes the creation of polymer-graphene composites. The polymers were chosen so that they had aromatic groups in the structure making dispersion easier. The

polymers chosen avoided cross linking to ensure enhanced properties could only be attributed to the nano-carbon. The polymers were amorphous (no crystallinity or low crystallinity) so that interpretation could be simplified and so the graphene did not act as a source of nucleation.

Poly(styrene-*b*-butadiene-*b*-styrene), poly(ethylene terephthalate), polycarbonate and poly(ether sulfone) had the necessary characteristics to make good test polymers.

1.2 Rationale

Nanostructured materials are currently showing many potential applications. Nanostructured fillers provide high surface areas for functional processes to take place. Nanoparticles may be able to adsorb other molecules when placed at a surface or provide conductive pathways at relatively low concentration. An understanding of the underlying principles which determine production and dispersion of graphene is often lacking. Such knowledge can be used as a source of guidelines and ideas for the fabrication of new high-performance composites.

1. Nanocomposites are made from exfoliated layered structure fillers. In this project the layer material is graphene, and the oxidation of the layer surfaces has facilitated exfoliation. Exfoliation is assisted by interaction with the liquid in which it is being dispersed and by shear forces.
2. Nanocomposites are two-phase materials formed from a nanoparticle dispersed phase and a polymeric continuous phase. Nanocomposites provide a large surface area to volume ratio so that particle interactions with the matrix phase and with substances at the surface can be maximised.
3. The application for nanocomposites in this project is focused on their stiffening action. The presence of small active graphene particles embedded in a continuous polymeric matrix surface will be studied. The preparation of the nanoparticles in the polymeric phase will be the main part of the research, coupled with the characterisation of their structure and interaction with other substances from the liquid or gaseous state, or heat and light as physical interactions. The nanocomposites may be extruded as films or coated onto a surface.

1.3 Aim

The aim of this work was to prepare graphenes, reactively modify the surface to enhance exfoliation and facilitate bonding to chosen matrix polymers, characterise the prepared materials and determine physical and mechanical properties.

1.4 Objectives

The key objectives were to:

1. prepare low defect graphenes and enhance interfacial bonding to polymers;
2. prepare nanoparticle-graphene-polymer composites using π -interactions to bond with a chosen polymer;
3. prepare nanoplatelet graphene-polymer structures to develop thermally stable compositions, extruded profiles and mouldings;
4. measure composition by mass loss and thermal stability using thermogravimetry;
5. characterise the nanocomposites using materials characterisation instruments, such as Raman spectroscopy;
6. study the structure of the nanoparticle composites by wide angle X-ray diffraction to measure the inter-particle distance and the degree to which the layered structures have been separated and dispersed²³;
7. view the microstructure of the composites using scanning electron microscopy and transmission electron microscopy;
8. determine composite mechanical and viscoelastic performance with static, dynamic and modulated mechanical analysis with a variation of geometry, force, deformation, frequency and temperature;
9. model aromatic polymer-graphene interactions.

1.5 Research Questions

1. Can low defect graphene be created by thermal expansion or by repair?
2. Can graphene be dispersed in many polymers with aromatic rings using π -interactions?
3. Can aromatic solvents disperse graphenes in many aromatic polymers using π -interactions?
4. Can many weak π -interactions between graphene and a polymer provide effective dispersion and meaningful reinforcement?

5. What properties improve in polymers when low defect graphene is added?
6. Is there an optimal volume fraction of graphene for intermolecular interactions and surface adsorption of polymers? That is, do the properties of aromatic polymers change as the concentration of graphene increases?
7. Does the performance of aromatic polymers with low defect graphene exceed that with high defect graphene?

1.6 Thesis Structure

This thesis contains 11 chapters:

Chapter 1 is a general introduction describing the aims and objectives.

Chapter 2 is a review of relevant published literature.

Chapter 3 describes the experimental equipment and instruments used in this research.

Chapter 4 discusses the production of graphene.

Chapter 5 and 6 discuss the production of SBS-graphene composites. Firstly, different production methods are compared. Then, a low defect graphene was dispersed in SBS at 1-20 % w/w to establish how loading affects the properties.

Chapters 7 and 8 discuss PET-graphene composites. PET with glass fibre was compared using solvent and melt dispersion of graphene in chapter 7. PET without glass fibre was compared with and without ultrasonication of graphene in chapter 8.

Chapter 9 discusses polycarbonate-graphene composites using very low loadings of 0.1 % w/w. Melt dispersion and ultrasonication were used to optimise the dispersion of graphene in the polymer.

Chapter 10 discusses PES-graphene composites. Solvent dispersion and ultrasonication were used to disperse the graphene.

Chapter 11 presents the conclusion of the thesis and recommendations for future work.

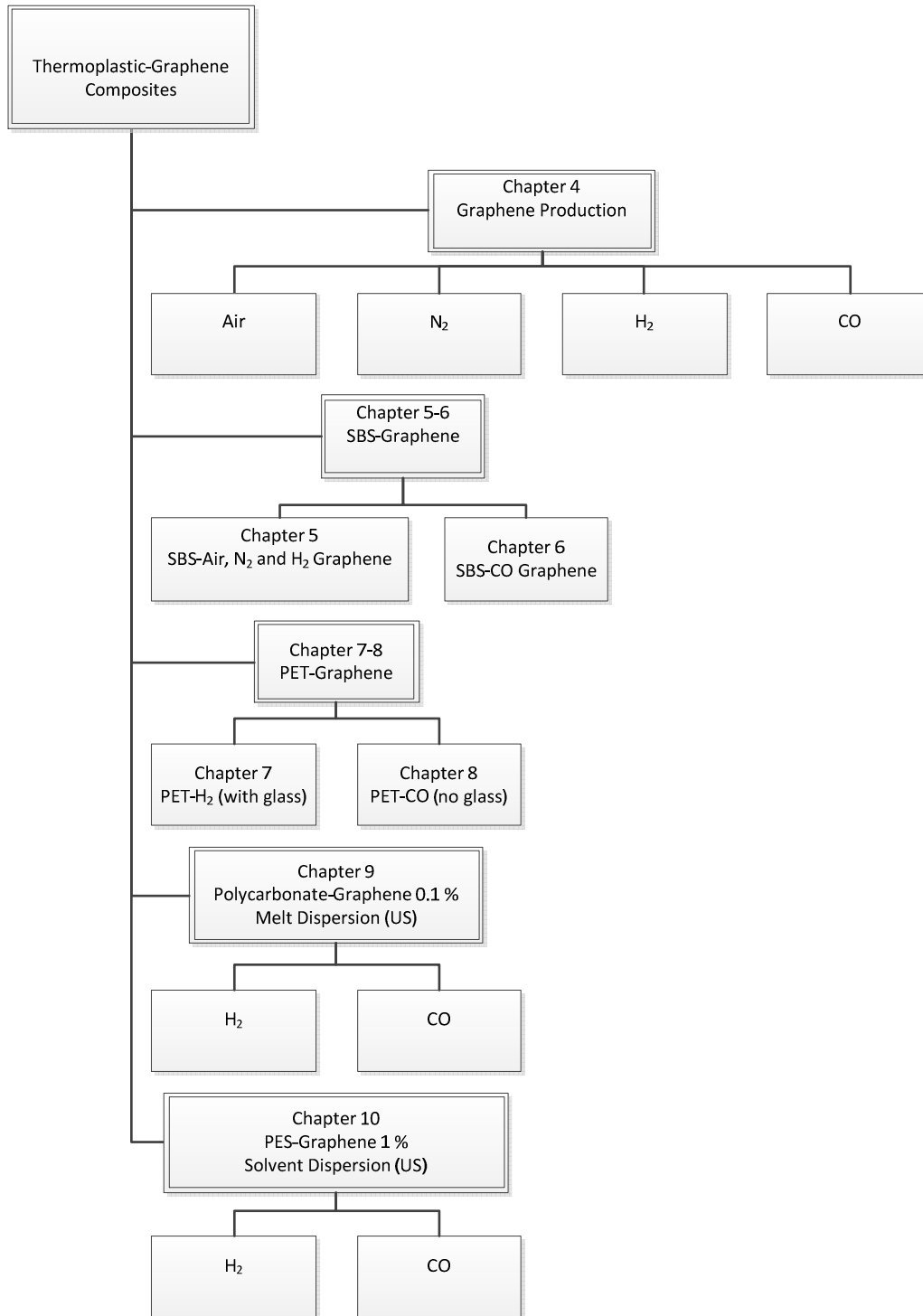


Figure 1-2 Flow chart of thesis structure

Chapter 2 Literature Review

2.1 Introduction

This literature review provides an overview of graphene, details of its properties, production, reduction, solvation, characterisation, metals, polymers, biocompatibility and applications.

Graphene was discovered in 2004, and Andre Geim and Konstantin Novoselov were recognised in 2010 with a Nobel Prize in Physics for separation of individual graphene sheets by a physical adhesion method^{24, 25}. Graphene is a one-atom-thick layer of aromatic carbon atoms arranged in a regular hexagonal pattern. It is the stiffest and strongest material yet discovered (tensile modulus 1 TPa and Ultimate Strength 130 GPa)^{2,26} is more electrically conductive (6000 S/cm) than any other material², exceptionally thermally conductive (5000 W/m·K)^{3, 4} and its properties (decomposition-resistant to $T_m \sim 4900 \text{ K}$ ⁵, large surface area $2630 \text{ m}^2/\text{g}^2$, impermeable to gases⁴ yet permeable to H_2O ²⁷) make it attractive for inclusion in composites provided suitable reactions, dispersants and dispersion techniques can be developed.

Graphenes can be exfoliated to a high degree to release individual graphene sheets to provide the optimum properties. Graphene sheets have extreme surface energy due to all carbon atoms being at a surface but are especially reactive at the edges²⁸. The large surface and high energy need to be stabilised to prevent flocculation (due to van der Waals forces) and to facilitate dispersion in a matrix phase. The unique properties of a graphene decrease as graphene sheets agglomerate but remain useful while under ten layers⁹.

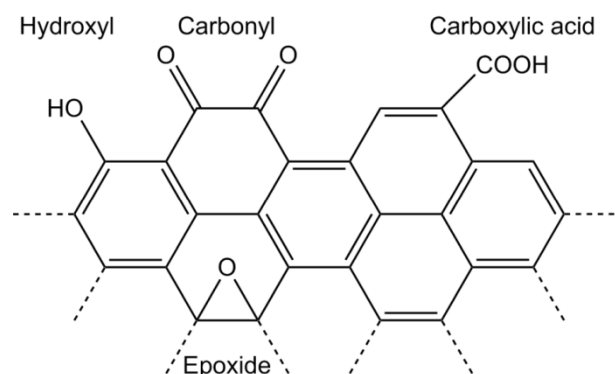


Figure 2-1 Typical oxygen functional groups found at the edges and in the plane of graphene

Oxygen functional groups (Figure 2-1) are commonly found at the edges of graphene, and these are primarily hydroxyl, carbonyl and carboxylic acid groups²⁹. In the plane epoxides

and hydroxyls are more common^{22, 30}. These defects can be reacted to graft other molecules onto graphene. Examples of reagents that can be reacted to graft onto graphene are isocyanates ($R-N=C=O$) with hydroxyl groups (to graft urethane)⁴, the hydroxyl group of poly(vinyl alcohol) (PVA) with carboxylic acid³¹, amide groups (NH_2) in chitosan which react with carbonyl³² and end-amine ($R^1-NR^2R^3$) groups in a commercial long chain surfactant which react with epoxide groups³³.

2.1.1 Opportunities

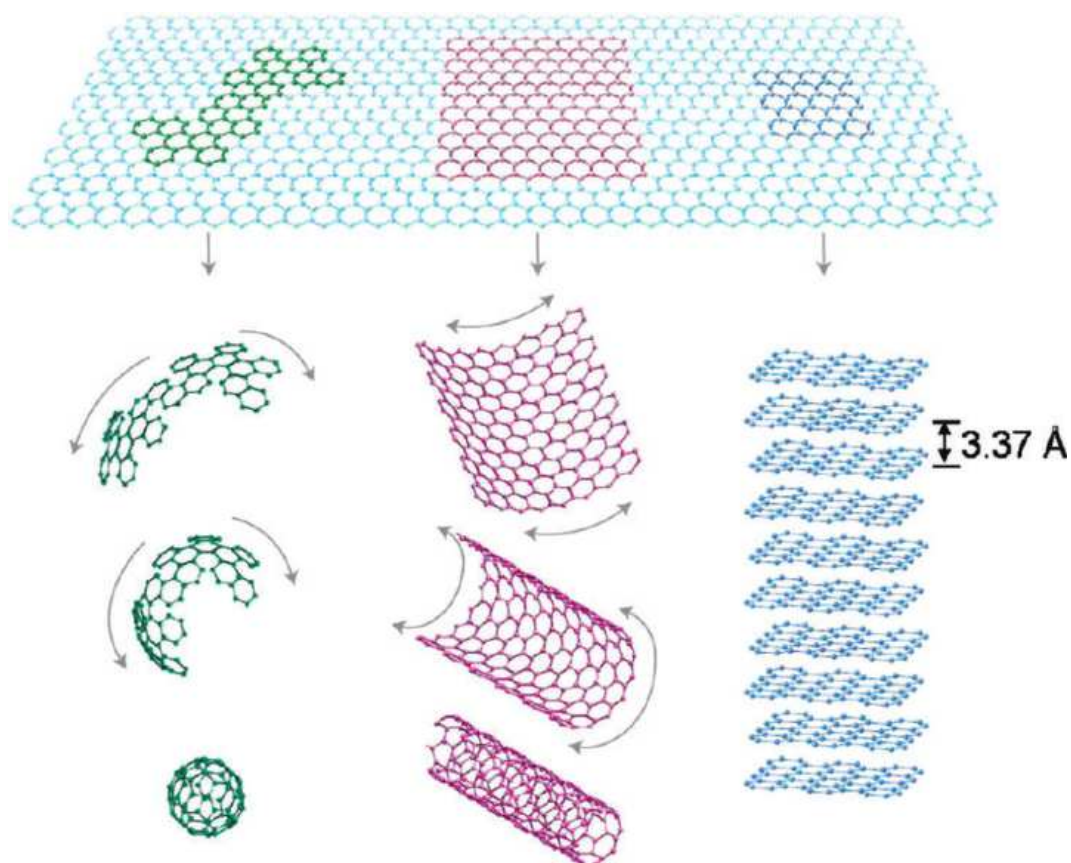


Figure 2-2 Graphene to buckminsterfullerenes, nanotubes and graphite^{3, 10}

Carbon allotropes (Figure 2-2) such as graphene, carbon nanotubes and Buckminsterfullerene are exceptionally high-performance nanomaterials. In particular, graphene has the highest tensile modulus, is stable at extreme temperatures and is highly conductive. Graphene needs to be supported in a matrix such as a polymer to give cohesion and allow its exceptional properties to be revealed. Graphene is more effective than traditional graphite for reinforcement of thermoplastics. Graphene has been found to conduct electricity when at low concentrations (0.02 % w/w) in polymer matrices³⁴. Applications for such conductive

polymer composites may include co-axial cables and electrostatic resistant films or mouldings.

2.1.2 Challenges

Formation of graphene nanostructures from graphite or carbon is the first challenge. The second challenge is to keep graphene dispersed so that it retains its unique properties. The exact solutions to these problems will vary depending on the intended purpose for the graphene.

2.1.3 Potential

Graphene is currently expensive and cannot be produced cheaply in quantity due to a lack of suitable method³⁵. Graphene is resistant to dispersion in polymers and typically contains up to 40 % structural defects^{30, 36}. These defects are holes and oxidised carbons at the edges or in the plane. The current research is aimed at producing larger amounts of graphene, finding new methods of dispersing it in polymers and producing low defect graphenes. This research will lead to stronger and lighter polymers with properties such as decreased gas permeation or increased conductivity. Areas such as aerospace currently have problems with fatigue and cracking of polymers (e.g. carbon fibre reinforced polymers) which such work can potentially eliminate.

2.2 Properties

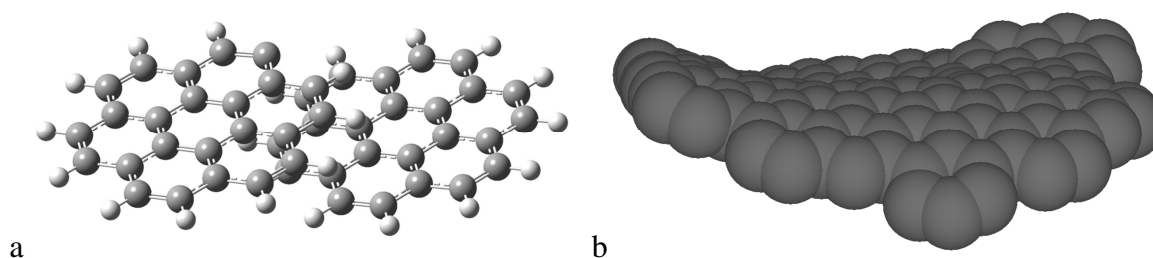


Figure 2-3 a) Double-layer graphene sheet illustrated using coronene b) Model of graphene showing sheet distortion from planarity due to high surface energy

Graphene sheets³⁷, C_mH_n where the ratio of carbon to hydrogen varies according to the size of the sheet (Figure 2-3), are extended conjugated systems that are 10 – 100 times larger than the size of common organic molecules. Defect free graphene is a pure aromatic carbon

system which is non-polar. Its properties include optical absorption including beyond the far infrared (2.3 % of incident white light is absorbed by one layer). This broad optical absorption has implications for non-degrading organic photonics components. Graphene is especially reactive along the edges.²⁸ Most properties typical of graphenes are lost when much more than ten graphene sheets agglomerate⁹.

The chemistry of carbon allotropes such as nanotubes³⁸ and buckminsterfullerenes is often identical to that of graphenes. Thus it is common to look to these allotropes when looking for supporting literature for graphene^{37, 39}.

2.3 Production

Graphene production can be characterised as:

1. Bottom up – building graphene one carbon atom at a time
2. Top down – separating or exfoliating graphite or graphite derivatives³

2.3.1 Top Down

The most common top-down methods are:

1. Chemical exfoliation (which requires a further reduction)⁴⁰
2. Mechanical exfoliation by removing one layer at a time from graphite with adhesive tape²⁵.

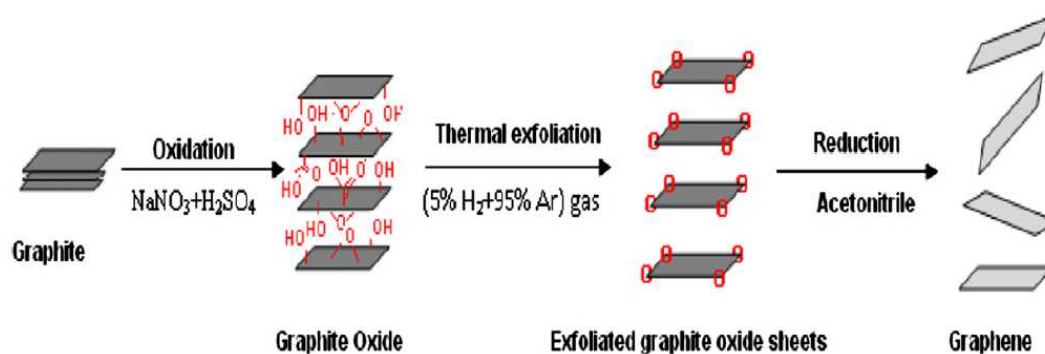


Figure 2-4 Preparation of graphene sheets⁴¹

A top down (Figure 2-4) approach holds the greatest promise for creating large amounts of graphene.

2.3.1.1 Chemical Exfoliation

Graphene can be created, by oxidising graphite with nitric acid and other oxidative acid mixtures such as sodium perchlorate or potassium permanganate⁴² in sulphuric acid (usually a modified Hummers method)^{40, 43}.

The resulting graphite oxide has interlayer oxidised carbons giving weakened interlayer adhesion (increasing interlayer spacing and weakening of van der Waals forces⁴⁴). If this oxidation is allowed to continue, it results in individual sheets of graphene. As a result, exfoliated-graphene sheets are often referred to as graphene oxide (GO)^{9, 45}.

Graphite intercalation compounds (GIC's Figure 2-5a) can involve any one of over 100 intercalators which can be either donor compounds (reducing alkali metals) or acceptor compounds (oxidising sulphuric or nitric acids)⁴⁶. The degree of intercalation is described by a stage number (1, 2, 3...) which refers to how many layers of carbon there are between each intercalated layer⁴⁴.

2.3.1.2 Thermal Exfoliation

If the oxidation of graphite is halted before exfoliation is complete, it becomes expandable.

A minimum graphite particle size of $75 \mu\text{m}^2$ is required for efficient intercalation and expansion⁴⁶. Heating rapidly to temperatures of 220 °C or higher (depending on the level of oxidation) causes the graphite layers to separate into individual oxidised graphene sheets or bundles of sheets by the expansion of gases (thermal shock)⁴⁷. The sheets are still partially attached in accordion-like structures (aka worms).

Graphite oxide (Figure 2-5b) is the raw material of choice because oxidation weakens graphene stacks and affords easy dispersion of functionalised graphenes in both aqueous and organic media. Thermal methods require the heating of graphite oxide: the higher the temperature, the purer the graphene sheets produced (>230 °C to ~3000 °C). Impure graphene sheets contain oxygen and other impurities such as sulphur that are volatilised at higher temperatures. Treatment of expanded graphite oxide (EGO) at 1000 °C over 8 h increased carbon content from 81 % to 97 % (initially expanded at 600 °C) and lowered resistivity from 1600 to 50 $\Omega\cdot\text{cm}$ ⁴⁸.

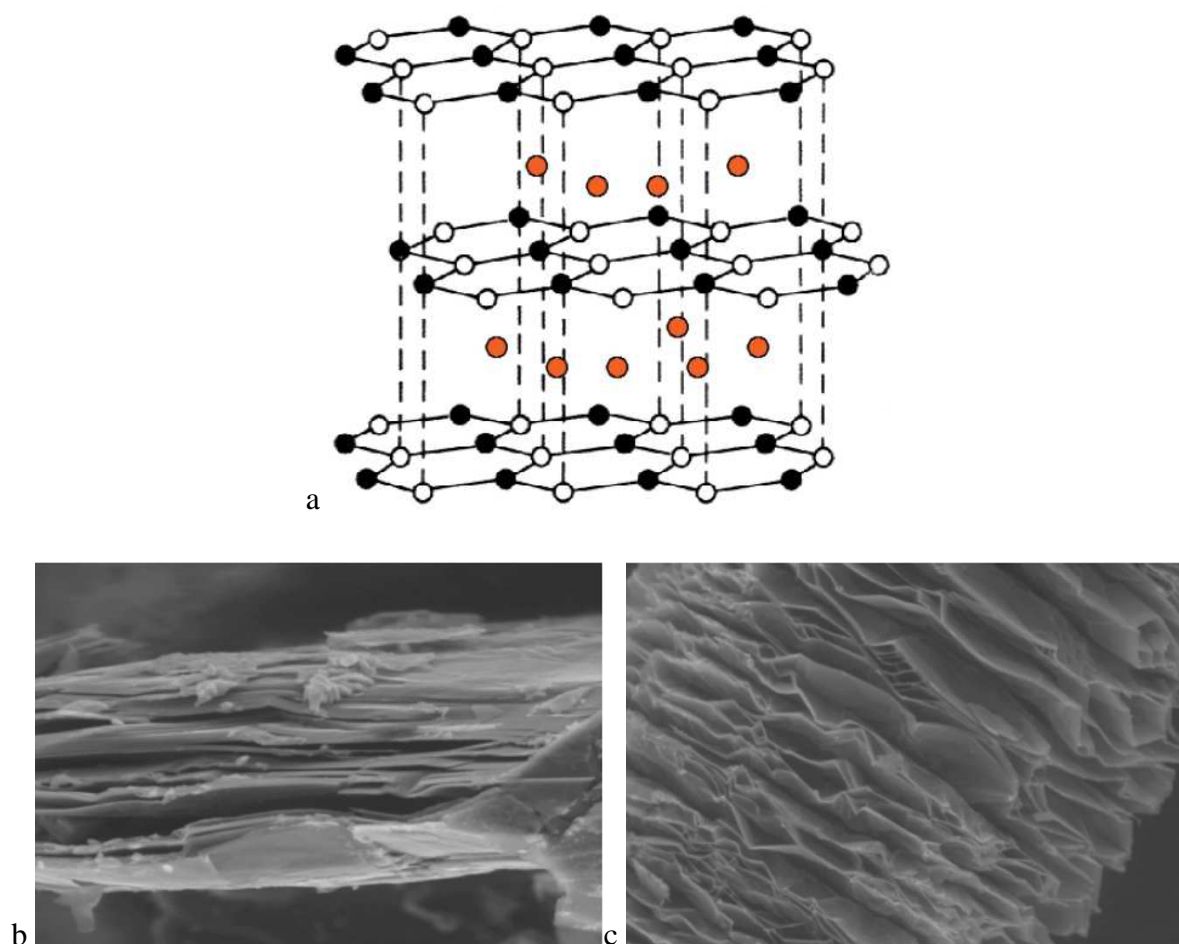


Figure 2-5 a) Expandable graphite⁴⁹ showing intercalation (small molecules introduced between layers) b) SEM of graphite oxide before thermal expansion c) after thermal expansion⁵⁰

2.3.1.3 Sonic Exfoliation

Sonication can be used for exfoliation of graphite, but graphene is fragmented, which is undesirable. However, sonication of graphite using N,N-dimethylformamide returned up to 50 % monolayer flakes^{28, 51}. An added advantage of sonic exfoliation of graphene oxide is increased reduction⁵² with hot spots of up to 5000 K, pressures of ~ 1000 bar and cooling rates of $>10^{10}$ K/s⁵³.

2.3.2 Bottom Up

Bottom-up (BU) graphene production offers exquisite control of graphene edges which is lacking in top-down (TD) approaches⁵⁴. The most popular method of bottom-up graphene production is chemical vapour deposition (CVD) and involves the deposition of gaseous

(100 μ L hydrazine hydrate, ethylenediamine or ammonium hydrate). The microwave is operated at full power (1000 W at 2.45 GHz) for 60 s (10 s on, 20 s stir: repeat 6 times). The yellow GO dispersion changes to black indicating a chemical reduction to graphene. The graphene is separated with a centrifuge at 5000 rpm (15 min) and dried overnight under vacuum. Supporting metal nanoparticles can prevent the formation of stacked graphitic structures (nanoparticles act as spacers) thus increasing surface area. Graphene sheets supporting nanoparticles of Pd, Cu, Pd, Cu, Au, Ag and much more have been created. Simultaneous reduction of the metal salt with GO results in well-dispersed nanoparticles on the graphene sheets: nanoparticles tend to assemble at the edges of the graphene sheets and between folded sheets⁶⁰.

2.4.3 Biomaterial Enhanced Reduction

Some green (low toxicity) methods of reduction have been used: L-tryptophan (an amino acid with an aromatic indole group) which was used to keep graphene in suspension (in water) using π - π interactions while the graphene was reduced with ascorbic acid⁶¹. Tea has been used to reduce graphene oxide⁶².

2.4.4 Thermally Induced Reduction

Thermal reduction⁶³ using expandable graphite⁶⁴ can be utilised for graphene production. Gases such as nitrogen⁶⁵ (inert), hydrogen⁶⁴ (reducing) or carbon monoxide⁶⁶ (reducing) can be used to remove oxides, reduce graphene further or heal the graphene.

Ultrasonication of graphene oxide reduces the number of GO bonds and increases the number of C-C bonds by at least 2 fold presumed to be by in-situ thermal reduction at the cavitating bubble-water interface⁵².

Visible light from a xenon flash, from a common digital camera, can instantly trigger a chemical-free reduction (with expansion) of graphite oxide by photothermal heating³⁵.

Lasers (visible monochromatic light) reduce graphene oxide cheaply, safely and effectively⁶⁷.

2.4.5 Gamma Radiation Activation Under an Inert or Reducing Gas

Gamma irradiation has been used to reduce graphene oxide under N₂ or H₂. The conductivity was improved 400 times, and the C/O ratio increased from 2.37 to 6.25 when using H₂. The reduction mechanism using H₂ was selective with mainly epoxy and hydroxyl groups being affected⁶⁴.

2.5 Solvation Assisted Dispersion

Solvents are often used to keep graphenes dispersed (without functionalisation) till they can be used or as part of the exfoliation process. A good solvent prevents graphenes from aggregating and forming graphite. Polar solvents are most effective at dispersing graphene.

Common solvents are listed in order of decreasing solvation (Figure 2-7):

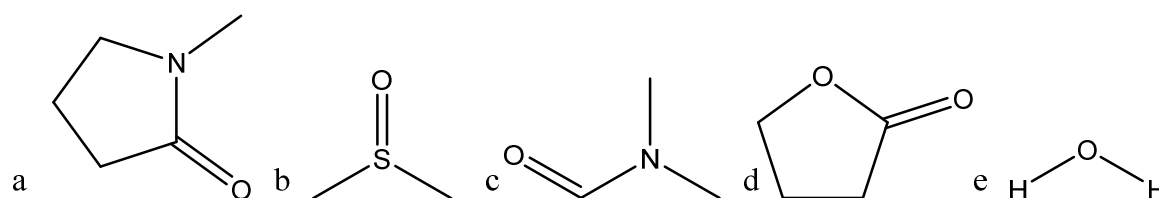


Figure 2-7 Solvents (from left to right) a) 1-methyl-2-pyrrolidone (NMP) b) dimethyl sulfoxide (DMSO) c) dimethyl formamide (DMF) d) γ -butyrolactone (GBL) e) water (H_2O)⁶⁸

All except water are dipolar (electrically neutral but having a partial positive and negative charge) aprotic (hydrogen is not bound to oxygen or nitrogen) organic solvents. Water is a protic solvent whose solubility is enhanced by the polar oxide groups common on graphene.

More recently organic amine-based solvents have outperformed NMP and surfactants for dispersing graphene listed in order of decreasing solvation (Figure 2-8)

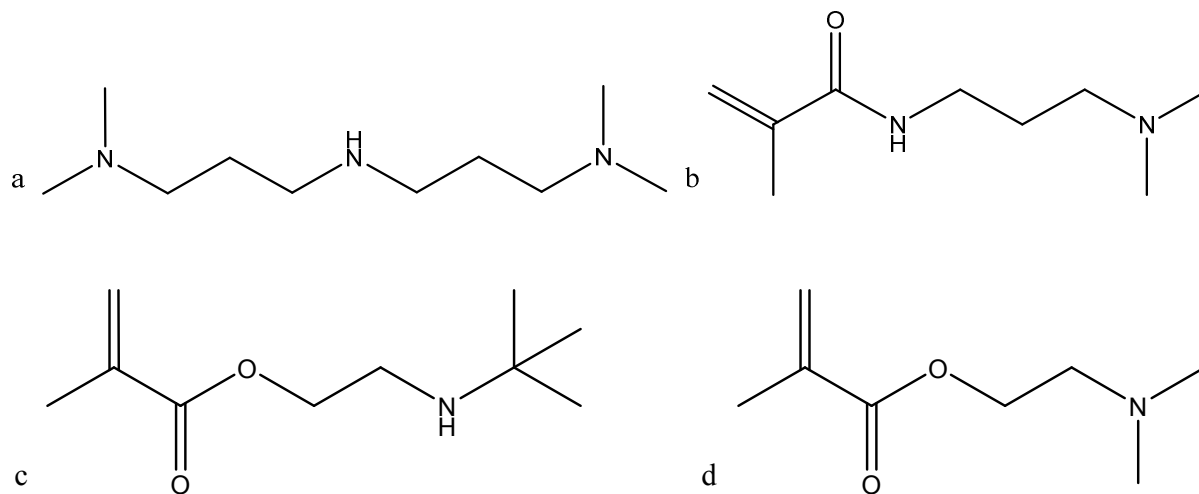


Figure 2-8 a) 3,3'-aminobis(N,N-dimethylpropylamine) (DMPA) b) N-[3-(dimethylamino)propyl]methacrylamide (DMAPMA) c) 2-(tert-butylamino)ethyl methacrylate (BAEMA) d) 2-(dimethylamino)ethyl methacrylate (MAEMA)

DMPA outperforms NMP by dispersing 50 % more graphene. Importantly DMAPMA, BAEMA and MAEMA are cheaper and less hazardous compared to NMP while dispersing more graphene⁶⁹.

2.5.1 Dispersion

2.5.1.1 Liquid Dispersion

Solvent dispersion can be used to prepare a polymer-graphene composite by mixing with a polymer solution, then precipitating. Graphene oxide sheets can be reduced to graphene while dispersed in a liquid. These graphene sheets tend to flocculate, but if they can be dispersed in a polymer solution, then graphene-polymer nanocomposites can be formed⁴⁵. Polymers such as poly(vinyl alcohol)(PVA) are sometimes used to coat the graphene and keep the layers that have separated from flocculating (agglomerating) together.

Separation of graphene sheets and dispersion in an organic liquid⁶² can be achieved with high shear. Graphene sheets functionalised at their edges with short branched alkanes (aka paraffin) afford stable dispersion in oils^{48, 70}. Alkyl functionalised graphene showed largely enhanced lipophilicity⁷¹.

Graphene is more likely to disperse in solvents which minimise interfacial tension. Graphene has a surface energy of 46.7 mN/m (GO 62.1 mN/m)⁷² which is similar to NMP 40 mN/m, DMF 37.1 mN/m, GBL 35.4 mN/m and o-dichlorobenzene 37 mN/m. Water has a surface energy of ~72 mN/m which is closer to that of GO^{42, 72}. Thus low interfacial tension is why GO is hydrophilic, but pristine graphene is hydrophobic.

2.5.1.2 Melt Dispersion

High shear in polymer solutions can be used for graphene dispersion and exfoliation. Melt compounding of isotactic poly(propylene), poly(styrene-co-acrylonitrile), polyamide-6 (nylon) and polycarbonate (PC). The degree of exfoliation with thermally reduced GO (TrGO) (based on theoretical surface area) has been estimated at around 50 %⁴⁸.

2.5.1.3 Chemical Dispersion

Functionalising graphene can help keep layers separated. Functionalisation can be either by π - π (non-covalent) stacking or C-C covalent coupling reactions²⁸. The π - π interactions increased in strength when the number of hydrogen atoms in benzene-like molecules increased⁷³. Hydrogen bonding (CH/ π) can also occur between a soft acid (CH) and a soft

base (π group) or hard acids (OH or NH) and soft bases (π -systems) increasing the amount of non-covalent bonding interactions (Figure 2-9)⁷⁴.

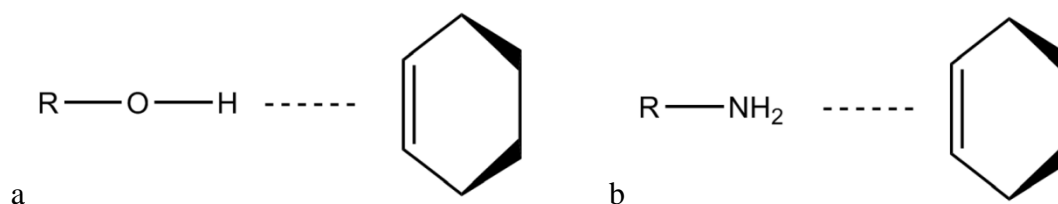


Figure 2-9 Hydrogen bonding demonstrating π -interactions a) OH- π b) NH₂- π (modified)⁷⁴

Graphene can be functionalised with many groups including fluorinated compounds⁷⁵. Non-ionic and ionic surfactants can be used to disperse graphene but add a potential contaminant while increasing complexity and thus cost⁴².

2.6 Characterisation

2.6.1 Raman Spectroscopy

Raman spectroscopy is considered the most useful characterisation technique for graphene because it quantifies many structural differences (vibrations of covalent bonds) that even an electron microscope cannot resolve. The Raman spectrum of graphene is characterised by three peaks: D (Defects: sp³ bonds, vacancies, implanted atoms^{76,77}), G (in-plane vibration of sp² bonds) and 2D (second order of the D peak). The D peak is found at ~ 1300 cm⁻¹, the G peak at ~ 1600 cm⁻¹ and the 2D peak at ~ 2600 cm⁻¹.

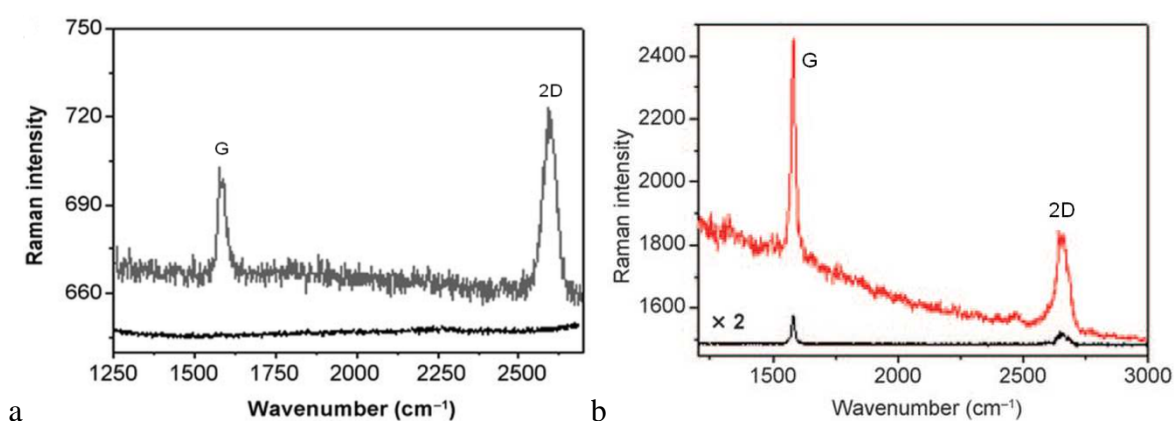


Figure 2-10 a) Surface enhanced, with gold, Raman spectra of single layer graphene (upper) compared with no enhancement (lower) showing G and 2D peaks 785 nm b) Trilayer graphene-enhanced (upper) 2x magnified (lower) 633 nm (4 mW with 1 s exposure alpha300 S)⁷⁸.

The D peak intensity⁷⁹ (lower is better) indicates the number of defects in graphene and defects are a measure of the quality of the graphene. The 2D peak height (higher is better) and shape (straight sides are better) can be used to determine the number of layers of graphene (Figure 2-10).

The differences between graphenes can be quantified using D/G ⁸⁰ (lower means fewer defects) or $2D/G$ ⁸¹ (higher means fewer layers) ratios. The 2D peak is higher than, or of similar height, to the G peak with monolayer graphene⁸². With two or three layer graphene the 2D peak is lower than the G peak⁷⁸.

The peak height and position vary according to the wavelength used. Commonly used wavelengths are ~532, 633 and 785 nm. Signal intensity varies with spot size, intensity and the instrument used. Signals can be boosted further by using a substrate of gold⁷⁸.

2.6.2 Edges

Graphene edges can be ordered either in a zig-zag or an armchair configuration. Armchair edges are a significant source of defects⁷⁷. Zig-zag edges do not generate a Raman D peak⁸³. Thus identifying the proportions of the two types is of particular interest.

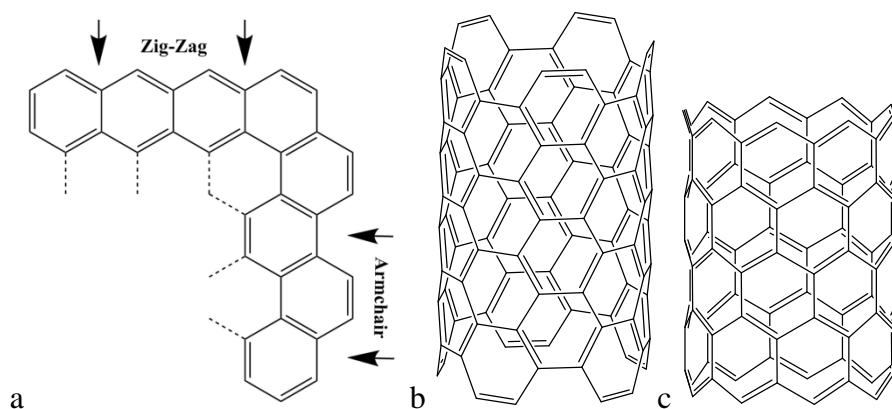


Figure 2-11 a) Graphene, and carbon nanotubes b) Armchair (5,5) c) zig-zag (9,0)

2.6.3 Transmission Electron Microscopy

Transmission electron microscopy (TEM) is a highly selective characterisation technique because it views such a small area it is not representative of the overall material or even the test specimen. However, it is capable of resolving individual graphene layers and allows the surface of the graphene to be viewed. Thus TEM allows Raman spectra to be reconciled with

images of the surface. Images are invaluable in resolving differences of opinion on graphene structure⁸⁴.

2.6.4 Scrolling

Graphene scrolls (Figure 2-12) have very little written about them. The lack of articles may reflect the difficulty in producing graphene scrolls in volume or with any consistency. Most work has been theoretical. One reason they are of interest is that the open ends and edges facilitate hydrogen storage. These open ends would be useful in supercapacitors and batteries. The π - π interactions between the inner and outer surfaces affect the electron transport and optical properties⁸⁵. Graphenes with fewer layers are more prone to scrolling to minimise surface energy. They have been observed in epoxy (with decreased fracturing) and polyurethane (with decreased gas permeability)^{4, 86}.

Ultrasonication was used to provide the necessary activation energy to graphene oxide to form nano-scrolls. Ultrasonication frequency, power density and duration were observed to control the dimensions of the scrolls. A thermal reduction (bubble vapour $T \sim 4000$ K and bubble interface ~ 800 K) during ultrasonication was suggested responsible for increasing C-C (sp^2) bonding at least two-fold (decreased C-O bonds). The results suggested that graphene with fewer defects had a lower scrolling activation energy. The work was identified as important for adsorptive (water purification) and capacitive processes⁵².

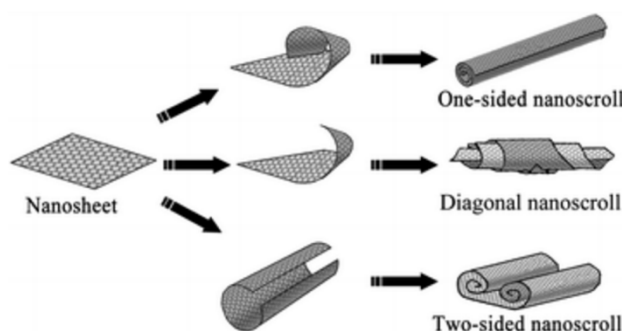


Figure 2-12 Graphene scrolls (one-sided, diagonal and two-sided)⁸⁵

2.6.5 Other

Other useful characterisation techniques are conductivity, atomic-force microscopy (AFM: number of layers and lateral sizes)^{47, 87} and scanning electron microscopy (SEM)⁸⁸. Less common are thermogravimetry (TGA)⁸⁷, contact angle, X-ray photoelectron spectroscopy (XPS: carbon ratios)⁸⁹, surface area (Brunauer Emmett Teller (BET))⁹⁰, nuclear magnetic

resonance (NMR)⁹¹, optical microscopy and particle sizing. Techniques such as Fourier transform infrared spectroscopy (FTIR)⁸⁷ and wide-angle x-ray scattering (WAXS)⁹¹ are usually only used once graphene is functionalised or dispersed in a polymer.

It is normal for two or more characterisation techniques to be combined when testing graphene as each test elicits different information.

2.7 Metal-Graphene Combinations

Single atomic layers of graphene have been used to strengthen metals such as copper (flow stress +250 %) and nickel (flow stress +230 %) by layering using CVD⁹². An alternative method used graphene encapsulated SiC particles added to an aluminium matrix which resulted in a 45 % increase in yield strength and 85 % increase in tensile ductility⁹³.

A graphene coating suppresses the oxidation of metals (the reduction of oxygen) making it the thinnest known corrosion protection⁹⁴. Graphene coating of nickel improved resistance to microbial induced corrosion by a factor of ~10 when compared to polyurethane (PU) and ~100 compared to parylene-C⁹⁵.

2.8 Polymer-Graphene Composites

Single sheets of graphene are not stable and tend to agglomerate. Dispersion in polymers helps stabilise graphene and can use π - π interactions⁴⁵ although covalent bonding is a more common approach²².

Dispersion in polymers provides one way to harness graphenes properties⁹⁶. For example, thermoplastic elastomer compounds based on block copolymers have low initial modulus and durability⁹⁷. Carbon nanocomposites can have enhanced thermal stability⁹⁸ and mechanical properties due to the large surface area to volume ratio of the carbon nanotubes or graphene sheets.

Graphenes have been incorporated into many different polymers including cellulose (enhanced conductivity)⁹⁹, chitosan (tensile strength +200 %)¹⁰⁰, rubber (increased tensile strength)¹⁰¹, epoxy (fracture toughness +900 % and improved tensile properties)^{11, 102}, polyurethane (improved EMI shielding)¹⁰³, polycarbonate (PC; improved thermal conductivity in foams)¹⁰⁴, polysulphone (PES; decreased filter fouling)¹⁰⁵, poly(ethylene terephthalate) (PET; decreased oxygen transmission)¹⁰⁶, nylon (improved ultimate tensile

strength, elongation at break, impact strength, toughness and permeation resistance)¹⁰⁷, polystyrene (conductivity at 0.1 %·v/v)⁹⁶, poly(styrene-*b*-butadiene-*b*-styrene) (SBS; 0.25 %·v/v electrical percolation threshold)³⁹ and many others.

2.8.1 Thermoplastic Elastomers

Thermoplastic elastomers are two-phase materials with the main elastomeric phase being the continuous phase, while a dispersed phase provides physical crosslinks for cohesion as the matrix is reversibly stretched. The properties of each can be enhanced with filler that provides a retardation of molecular segment motions and binds molecules together. Carbon nanocomposites are proposed to be particularly active fillers in these elastomers^{108, 109}.

More details about the SBS, PET, PC and PES that were used in this work are provided in the relevant chapters along with why they were chosen. In this work graphenes produced under different conditions are compared within the one polymer.

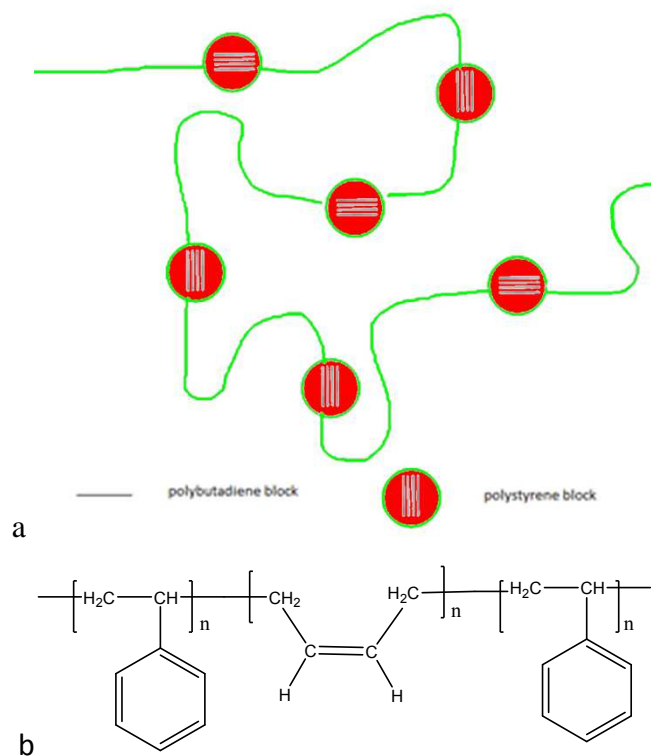


Figure 2-13 SBS illustrated: a) Shows repeating polystyrene and polybutadiene groups in a simplified form¹¹⁰ and b) the chemical composition showing repeating groups

2.9 Biocompatibility

Biocompatibility is of interest to most researchers if only to ensure that materials they work with do not pose a hazard to their health. Graphene is a newly recognised allotrope of carbon, so few studies on its toxicity are known. However, studies of the toxicity of the allotropes of carbon are more common.

Charcoal increased the lifespan of rats 43 %^{111, 112}. In farming the use of biochar (charcoal) shows beneficial effects such as adsorbing toxic compounds, increasing crop yields and promoting soil microbe populations¹¹³. Similarly, graphene oxide makes soil microbe populations richer and more diverse¹¹⁴. A review of charcoal across many industries found no evidence of harm even after long-term exposure. Many of these uses, such as treatment of poisoning, reduction of cholesterol^{115, 116} and treatment of kidney disease^{117, 118} require biocompatibility¹¹⁹.

Buckminsterfullerenes (C_{60} ¹²⁰⁻¹²²; Figure 2-14) are found in charcoal in small amounts and are present in many kinds of sooting flames¹²² including carbon black furnaces¹²³ and were initially discovered in soot¹²⁴. When fed to rats, buckyballs (C_{60}) almost doubled (+90 %) their lifespan¹²⁵.

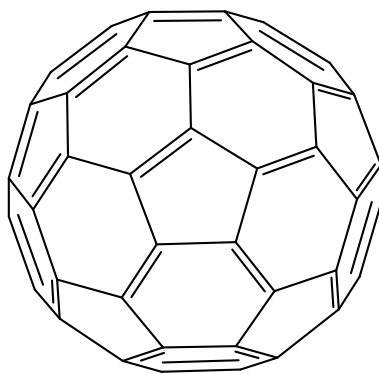


Figure 2-14 Fullerene (C_{60})¹²⁶

Graphene is found in charcoal in small amounts¹²⁷. Graphene has been found in both food and medicine without demonstrating any ill effects¹²⁸. Inhalation, the most likely route of ingestion, studies of graphene using rats showed a minimal toxic effect¹²⁹. Studies using graphene oxide and carboxyl graphene on cancer cells showed cytotoxicity¹³⁰ but did not demonstrate cytotoxicity in healthy cells. Reduced graphene oxide coated hydroxyapatite

composites stimulated human mesenchymal stem cells to differentiate into bone suggesting they would make good dental or orthopaedic bone fillers¹³¹.

A review of graphene biocompatibility suggested that the confounding effect in many graphene biocompatibility studies is probably the impurities⁶³. An example of a contaminant of concern is silica which is known to cause silicosis if inhaled. It is rare to see studies using pristine graphene (without impurities), but one such study concluded that graphene benefited wound healing and might also be an anti-diarrheal¹³². Graphene acts as an anti-oxidant with reduced graphene (low defect graphene) being more effectual than oxidised graphene (high defect). It worked both by preventative antioxidant activity (UV absorption) and $\bullet\text{OH}$ radical scavenging^{133, 134}.

As most of the carbon allotropes are found in charcoal and share much in common with graphene, their toxicity will be similar. The data suggests graphene without contaminants is highly biocompatible. Thus pristine graphene could be safely added to polymers for use in medical applications.

2.10 Applications

2.10.1 Electronics

Some of the most exciting potential applications for graphene exist in electronics.

2.10.1.1 Superconductivity

High doping of graphene (intentionally introducing impurities) may lead to room temperature superconductivity (also predicted for graphanes). High-frequency signals lose none of their energy when passing through graphene at room temperature and thus outperform superconductors¹³⁵. The low resistance is reflected in graphene's high electron mobility of $200,000 \text{ cm}^2/\text{V}\cdot\text{s}$ ²⁸

2.10.1.2 Semiconductors

P-doping can be induced in graphene by covalent bonding of electron-withdrawing oxygen functional groups. N-doping can be induced in graphene by electron-donating nitrogen functional groups²⁸. Thus the ability to modulate graphene's electrical properties makes it suitable for semiconductor use.

Metal adatoms can be adsorbed onto graphene to control electronic properties. Using density functional theory (DFT) it was found that the elements from groups I (Li, Na and K), II (Ca)

and III (Al, Ga, In) in the periodic table (Figure 2-15) gave results consistent with ionic bonding characterised by minimal change in graphene electronic state but large charge transfer. Transition (Ti, Fe), noble (Pd, Au) and group IV (Ti, Sn) metals gave results consistent with covalent bonding and were characterised by strong hybridisation with graphene¹³⁶.



Figure 2-15 Upper: Periodic table¹³⁷ Lower: Graphene monoxide¹³⁸

Placing five layer graphene on top of soda lime glass (normal window glass) using chemical vapour deposition (CVD) resulted in the sodium spontaneously correctly n-doping the graphene by surface transfer in a way that is cheap, effective, resilient, durable, tuneable and doesn't require high temperatures, vacuum or chemicals. Chemical doping of graphene yielded electron densities of $\leq 9.5 \times 10^{12} \text{ e/cm}^2$ while doping with sodium glass yielded $1.33 \times 10^{13} \text{ e/cm}^2$. Electron densities rise to $2.11 \times 10^{13} \text{ e/cm}^2$ when using a p-type copper

indium gallium diselenide (CIGS) on sodium glass. Sodium glass provides a scalable and low-cost doping method¹³⁹.

Thermal reduction of multilayered graphene oxide in a vacuum produced nanocrystalline (ordered) semiconducting (solid state) graphene monoxide (a double epoxide, Figure 2-15 lower) with a 1:1 O:C (stoichiometric) ratio and a calculated band gap of ~ 0.9 eV¹³⁸.

2.10.1.3 Capacitors

The energy density of the next generation of supercapacitors will improve using graphene⁶⁷. By placing graphene oxide on a PET sheet and reducing the graphene using the laser in a common computer LightScribe DVD drive (Figure 2-16) a supercapacitor with an energy density of 200 W/cm (among the highest for any supercapacitor) was created⁶⁷.

Hydration of graphene prevented restacking of chemically converted graphene sheets into graphite. Self-stacked solvated graphene exhibited unprecedented electrochemical performance in supercapacitors: Capacitance of 157 F/g at ultrafast charging rates of 1080 A/g, a maximum power density of 414 w/g and a discharge current of 108 A/g (1-3 orders of magnitude higher than competing techniques). It exhibited excellent cyclability retaining 97 % of capacitance over 10,000 cycles at a high charging current of 100 A/g¹⁴⁰

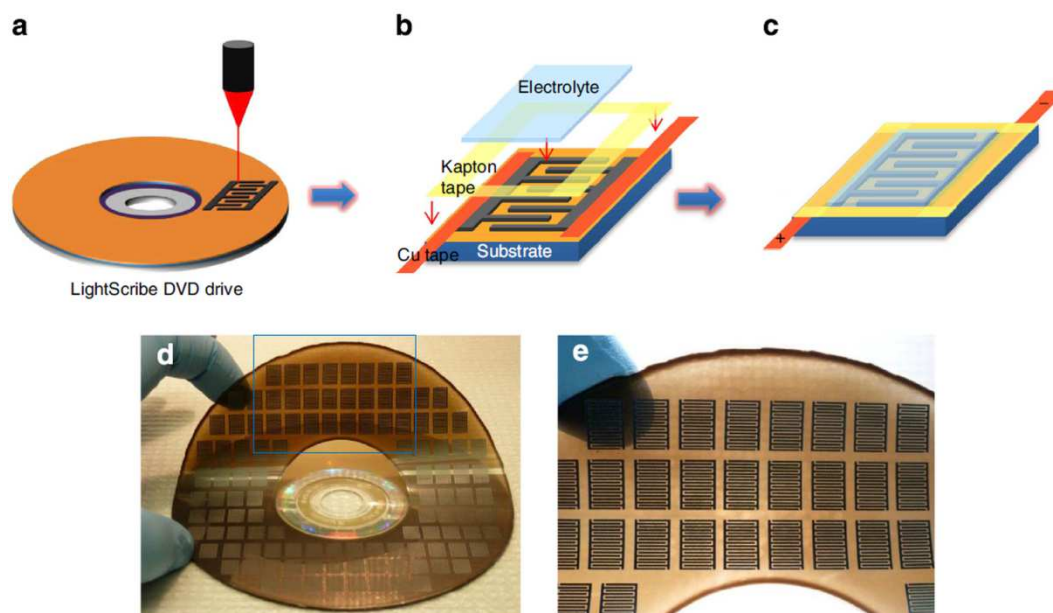


Figure 2-16 a) GO film reduced by laser b) Copper tape applied c) Electrolytic coat applied d) 100 capacitors e) Flexible substrate⁶⁷

2.10.1.4 Batteries

Graphene-Fe₃O₄ composites exhibit improved cycling stability and rate performance when used as an anode material in high-performance lithium-ion batteries¹⁴¹. Similarly, graphene encapsulated Fe₃O₄ nanoparticle aggregates made suitable as anode material for high-performance lithium-ion batteries due to good cycling stability and rapid cycling¹⁴². Graphene sheets can be used as anode material for lithium-ion batteries where reversible specific capacity was as high as 1264 mAh/g at a current density of 100 mA/g and after 40 cycles remained as high as 848 mA/g. Even at a high current density of 500 mA/g specific capacity remained at 718 mAh/g⁹⁰.

2.10.1.5 Magnetism

Fe₃O₄ was used to make a magnetic graphene nanocomposite (Figure 2-17) for the extraction of carbamate pesticides for measurement. The authors suggest that this method would work with any substance containing an aromatic ring (involving π -interactions)¹⁴³. Graphene-Fe₃O₄ composites were formed upon the reduction of graphite oxide and exhibited superparamagnetic (magnetic field much stronger than a normal magnet) behaviour. Fe₃O₄ particles as small as 7 nm were uniformly distributed across the graphene without aggregation¹⁴¹.

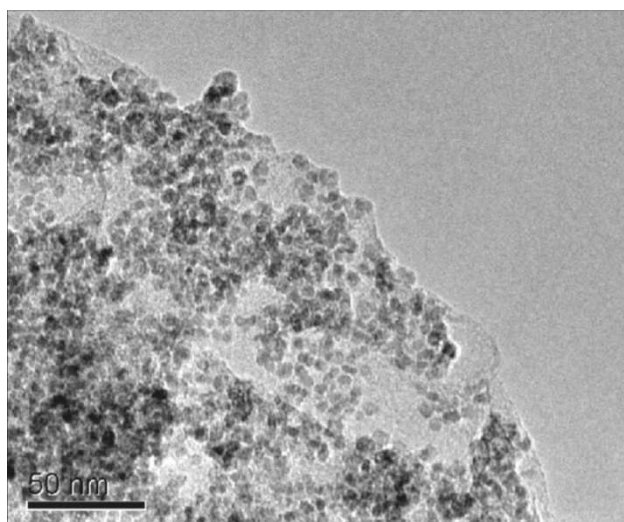


Figure 2-17 TEM image of a sheet of Graphene with Fe₃O₄ particles bonded to the surface¹⁴¹

Superparamagnetic graphene oxide-Fe₃O₄ (18.6 % w/w) was loaded with doxorubicin hydrochloride (1.08 mg/mg) and dispersed in an aqueous solution. It congregated under acidic conditions but redispersed under basic conditions and could be moved by a magnet.

The ability to load and move a drug makes graphene a good candidate for targeted drug delivery¹⁴⁴.

Ferromagnetism is theoretically possible by doping graphene with Ca, K or Pd due to the hybridisation of transition metals and carbon orbitals²⁸.

2.10.1.6 Flexible Electronics

Printable conductive graphene inks¹⁴⁵ are one of the first graphene applications to be commercialised. Flexible electronics are made possible with graphene⁴⁰. For example, graphene can replace indium tin oxide (ITO) in touch screens⁸⁷.

2.10.1.7 Conductive Polymers

Graphene has been shown to form percolated networks in polymers at concentrations as low as 1 %·w/w for carbon nanotubes and 0.02 %·w/w for graphenes¹⁴⁶. The percolated networks increment properties and exhibit electrical conductivity. Polymer-graphene foams lowered the percolation threshold (improve conductivity) and enhanced electromagnetic interference (EMI) shielding in polyurethane (PU) by absorption rather than reflection¹⁰³.

Many applications do not require exclusively single layer graphene. Multi-layer graphene^{104, 147} (Figure 2-18) is common in much graphene research although this is rarely explicitly acknowledged.

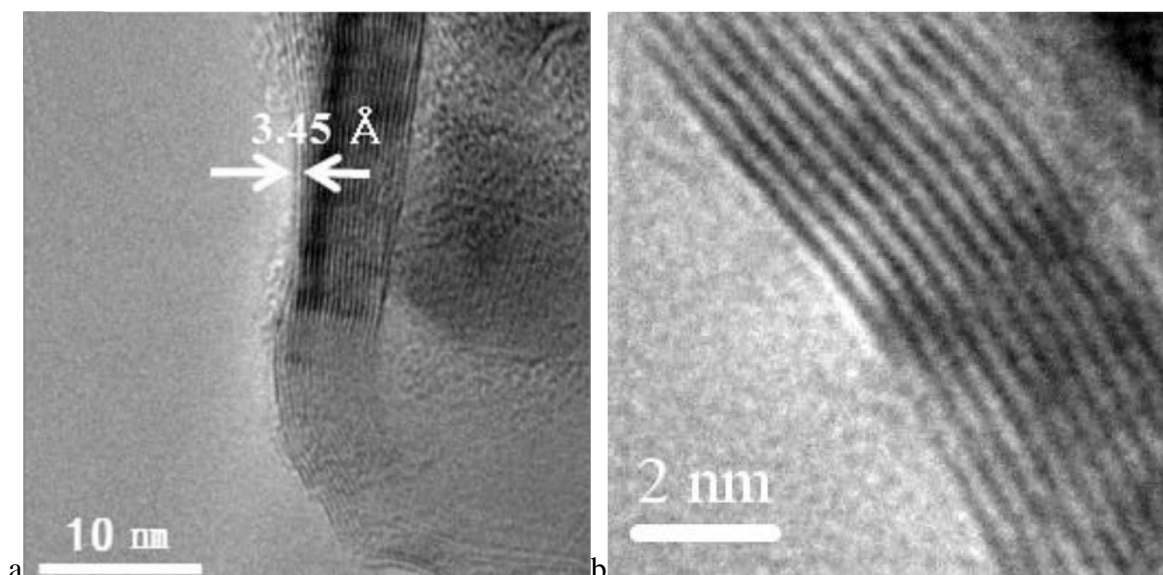


Figure 2-18 TEM images a) Multilayer graphene by CO reduction (~18 layers)¹⁴⁸ b) ~10 layer graphene by chemical vapour deposition (CVD)¹⁴⁹

2.10.1.8 Insulation

Graphene oxide (the most commonly produced graphene) has insulating properties²⁸ making it unsuitable for many electronic applications, at best it is a semiconductor⁶³.

Hydrogenation of graphene creates *graphane* (discovered 2008) a two-dimensional hydrocarbon and converts it into an insulator, as the electronic structures change from sp^2 to sp^3 ²⁸.

Thus graphene is a highly flexible material to work with because all three characteristics of electrical conductivity are present: conductivity, insulation and semi-conductivity.

2.10.2 Lubricants

Graphene nanoribbons sliding on gold, exhibit ultra-low friction (superlubricity) due to their high lateral stiffness and weak interaction with most materials¹⁵⁰. Graphene can be functionalised with fluorinated compounds²⁸, and total fluorination of C_{60} should represent the slickest molecular lubricant known to man³⁷. A boundary lubricant (Xcelplus) which permanently bonds with metal was hypothesised to involve Fe-Graphene-polytetrafluoroethylene (PTFE)¹⁵¹.

2.10.3 Adhesives

Mussel-inspired chemistry demonstrated the simultaneous reduction and surface functionalisation of graphite oxide using norepinephrine formed chemically adherent films on virtually all material surfaces including PTFE⁷⁵.

2.10.4 Filtration

Perfect graphene excludes even hydrogen while precisely sized nanopores can make it selectively permeable to many more molecules¹⁵². Graphene with nanopores (having oxide functional groups at their edges¹⁵³) is selectively permeable to water and transports water two orders of magnitude faster than predicted by classical continuum fluid dynamics¹⁵⁴. Capillary action between two graphene-oxide sheets completely excludes liquids, vapours and gases including helium while allowing the unimpeded permeation of water²⁷.

Modelling studies of graphene have shown that boron (1.3 eV) and nitrogen (3.2 eV) have low activation energies so that, by controlling annealing conditions, the selective passage of these and other atoms (with higher activation energies) would be allowed¹⁵⁵.

Modelling of graphene and hexagonal boron nitride (hBN) indicates that it is highly permeable to thermal protons at room temperature with an activation energy of only 0.3 eV making it a promising candidate for many hydrogen technologies¹⁵².

Graphyne (Figure 2-19)¹⁵⁶ a theoretical allotrope of carbon which is defined by three bonds between carbons (R-C≡C-R) may hold even greater promise for desalination because the gaps between carbons are large enough to permit water to pass through but small enough to exclude larger molecules and ions (including sodium and chloride). The advantage of graphyne is that the inter-carbon distances are exactly controlled whereas pore size in graphene is hard to control and requires functionalisation of the edges which can be inconsistent.

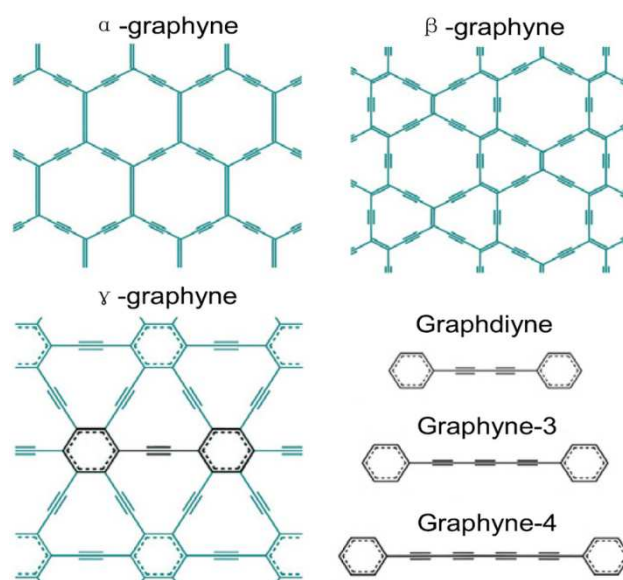


Figure 2-19 Graphyne¹⁵⁴

2.10.5 Analysis

Graphene, graphene oxide (GO) and their derivatives or composites have adsorption capacities much higher than that of current sorbents used in analytical chemistry. GO provides opportunities for hydrogen bonding or electrostatic interactions with oxygen or nitrogen functional groups. On graphene, compounds are mainly adsorbed by π - π interactions. However, covalent bonding to suitable support media like silica may improve service life and stability¹⁵⁷. Interestingly, the magnitude of π - π interactions increases significantly as the number of hydrogens in aromatic molecules increases and the energy of adsorption can be obtained by counting the number of carbons and hydrogens⁷³.

2.10.6 Construction Materials

Graphene oxide (Figure 2-20) at 0.05 %·w/w added to concrete increased compressive strength by 15-33 % and flexural strength by 41-59 %. Graphene oxide makes concrete ductile. Graphene oxide at 0.03 %·w/w improved compressive strength by 46.2 % while improving failure stress and strain. The strong interfacial interactions occur via covalent bonding. Functionalising graphene nanoplatelets tends to improve interfacial strength and mechanical properties¹⁵⁸. Graphene oxide outperforms carbon nanotubes in concrete at smaller concentrations. Agglomeration of graphenes in concrete indicates a need to develop a dispersion method¹⁵⁹.

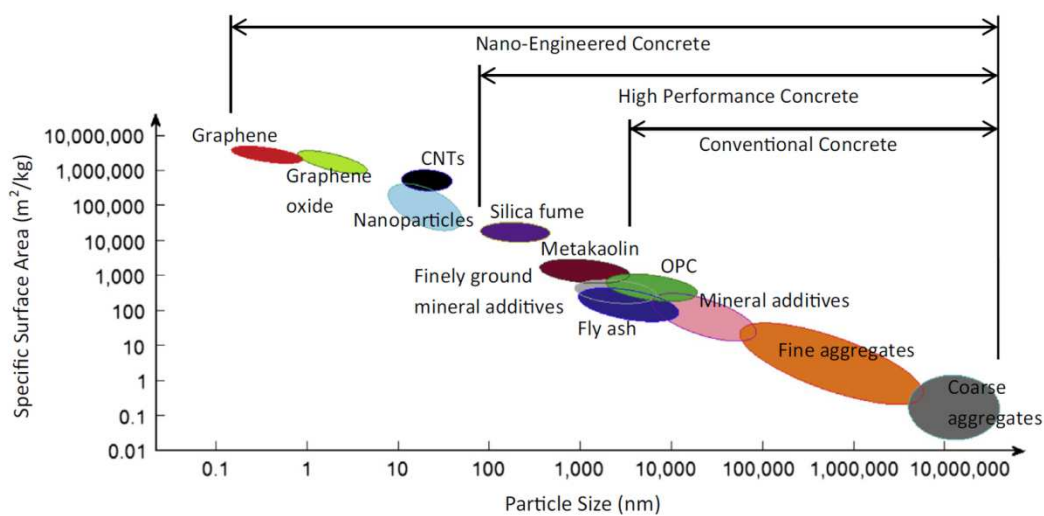


Figure 2-20 Comparison of concrete with different nanofillers¹⁵⁹

2.10.7 Armoured Materials

The specific penetration energy for multilayer graphene (10-100 nm) is ~10 times that of steel. Graphene was able to absorb 0.92 MJ/kg of ballistic energy compared to only 0.08 MJ/kg for steel¹⁴⁷. Thus graphene is ideal for body armour and other protective uses. The mass of body armour could be reduced while maintaining the same level of protection.

Chapter 3 Experimental

3.1 Introduction

This chapter provides details of materials and methods used in this research project. Several characterization techniques were employed throughout this research. The characterization aimed to obtain information on mechanical properties, thermal stability, crystalline structure, microstructure and surface morphology of polymer-graphene composites. Therefore, the techniques of thermo-mechanical analysis (TMA), thermogravimetry (TGA), wide-angle X-ray scattering (WAXS), surface area (BET), electrical resistance, surface energy, particle sizing, vibrational spectroscopy, optical microscopy, scanning electron microscopy (SEM), transmission electron microscopy (TEM) and computer modelling have been used.

3.2 Materials

3.2.1 Polymer Matrices

Poly(styrene-*b*-butadiene-*b*-styrene) (SBS) from Aldrich, NSW, Australia: CAS number [9003-55-8] Catalogue # 18,287-7 $[-\text{CH}_2\text{CH}(\text{C}_6\text{H}_5)-]_x-(-\text{CH}_2\text{CH}=\text{CHCH}_2-)_y-[\text{CH}_2\text{CH}(\text{C}_6\text{H}_5)-]_z$ or $(\text{C}_8\text{H}_8)_n-(\text{C}_4\text{H}_6)_n-(\text{C}_8\text{H}_8)_n$ 30 wt % styrene, density = 0.940 g/cm³ at 25 °C and average $M_w \sim 140,000$ g/mol (by GPC). Styrene monomer molecular mass 104.15 g/mol and elemental analysis C 92.26 % H 7.74 %. Butadiene monomer molecular mass 54.092 g/mol and elemental analysis 88.82 % C 11.18 % H (Ch. 5-6).

Poly(ethylene terephthalate) (PET) $(\text{C}_{10}\text{H}_8\text{O}_4)_n$ from Sigma-Aldrich, Australia: CAS number [25038-59-9] reinforced with 30 % glass fibre, $T_m \sim 225$ °C, $T_g \sim 70-80$ °C (Ch. 7).

Poly(ethylene terephthalate) (PET) WK-811 from Zhejiang Wankai New Material Co., Ltd via Martogg and Company, Dandenong, Australia: CAS number 25038-59-9 $T_m = 225$ °C, $T_g = 70-80$ °C. Monomer molecular mass 192.15 g/mol and elemental mass C 62.51 % H 4.2 % O 33.3 %. (Ch. 8)

Poly(bisphenol-A-carbonate) (PC) Lexan 124R supplied as transparent pellets from Sabic, Melbourne: CAS number [111211-39-3] $(\text{C}_{16}\text{H}_{14}\text{O}_3)_n$ and $T_g \sim 140-150$ °C. Monomer molecular mass 254.27 g/mol and elemental mass C 75.58 % H 5.55 % O 18.87 % (Ch. 9).

Poly(ether sulfone) (PES) supplied as transparent pellets from Aldrich: Average $M_w \sim 35,000$ g/mol (by light scattering): CAS number [25135-51-7] $(\text{C}_{27}\text{H}_{22}\text{O}_4\text{S})_n$ Average $M_n \sim 16,000$

g/mol (by MO). $T_g \sim 220-230^\circ\text{C}$ Monomer molecular mass 442.42 g/mol and elemental mass C 73.3 % H 5.01 % O 14.46 % S 7.23 % (Ch. 10).

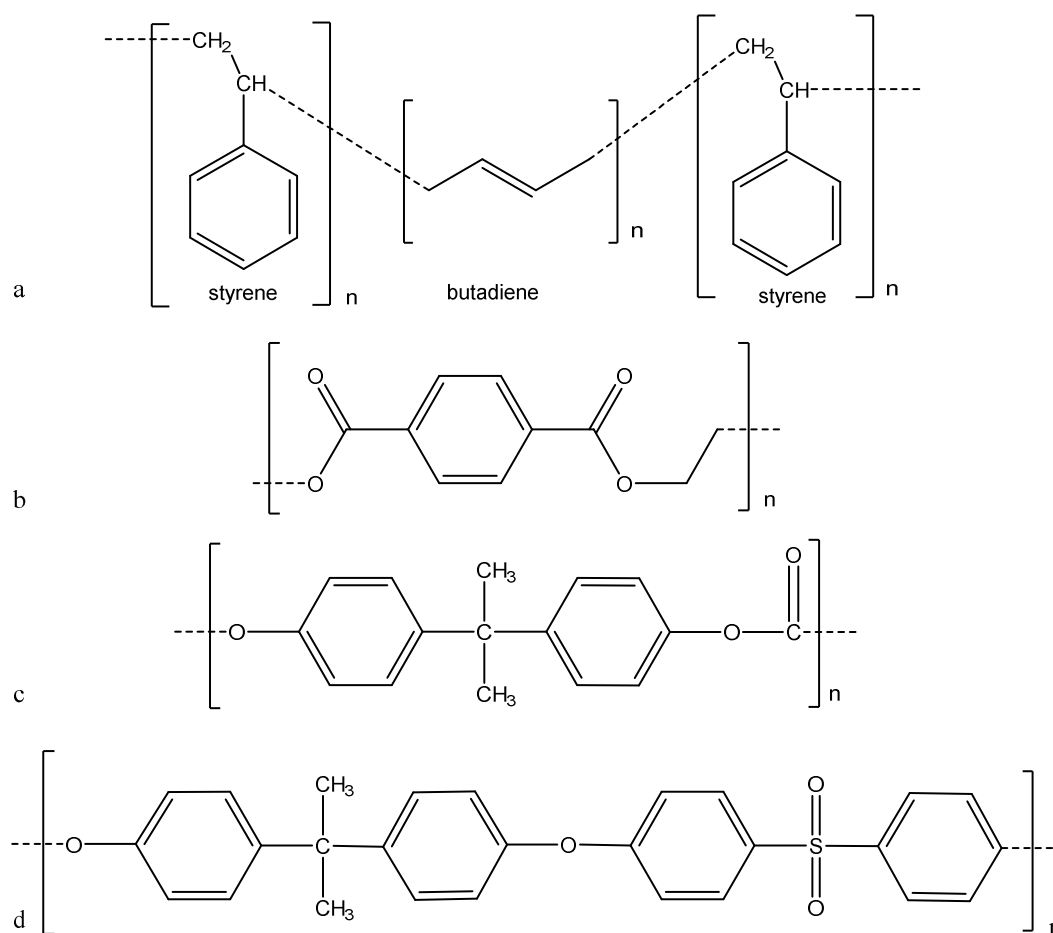


Figure 3-1 a) SBS b) PET c) PC d) PES

3.2.2 Filler Reinforcement

Graftech 220-50N (GT) expandable graphite from UCAR Carbon Company, Cleveland OH USA: 65 % on 50 mesh (nominal), an expansion onset of 220°C , typical mean particle size of $350\ \mu\text{m}$, expansion volume of $200\ \text{cm}^3/\text{g}$ at 600°C , neutral (N) or basic surface chemistry and specific volume of $1.25\ \text{cm}^3/\text{g}$ ($0.8\ \text{g}/\text{cm}^3$).

HDPlas (Cheap Tubes), USA Grade 4 (research quality) $>700\ \text{m}^2\cdot\text{g}^{-1}$ nanoplatelets, $1-2\ \mu\text{m}$ diameter, $< 3\ \text{nm}$ thickness, 1-3 graphene layers and 99 % w/w (two different materials denoted #1 and #2).

Expandable graphite was prepared using a modified Staudenmaier method where KClO_3 is halved. Graphite flakes were oxidised by concentrated nitric acid (HNO_3 69 %) and sulfuric acid (H_2SO_4 98 %). Graphite 10 g was used with powdered KClO_3 5 g ($2:1 \text{ g}\cdot\text{g}^{-1}$)¹⁶⁰⁻¹⁶³.

3.2.3 Solvents

p-Xylene (1,4-dimethylbenzene) from Merck, Germany CAS number 106-42-3 $T_b=138 \text{ }^\circ\text{C}$

o-Chlorophenol (2-chlorophenol) from ThermoFisher Scientific, Australia. CAS number 95-57-8 (Ch. 7)

1-Methyl-2-pyrrolidone (NMP) from Merck, Germany CAS number 872-50-4 $T_b = 202\text{-}204 \text{ }^\circ\text{C}$ (Ch. 4 and 6).

Benzene from Sigma-Aldrich, Australia CAS number 71-43-2 $T_b= 80.1 \text{ }^\circ\text{C}$ Ch. 6

Dichloromethane (DCM; CH_2Cl_2) from Merck, Germany CAS number 75-09-2 $T_b = 40 \text{ }^\circ\text{C}$ (Ch. 9 and 10).

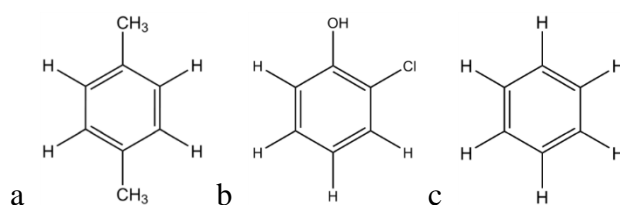


Figure 3-2 Aromatic solvents plus hydrogen atoms a) *p*-xylene b) *o*-chlorophenol c) benzene

3.2.4 Non-Solvents

Methanol (CH_3OH) AR grade from Merck, Germany CAS 67-56-1

3.2.5 Alkalis

Sodium hydroxide (NaOH) from Chem Supply Pty Ltd, Port Adelaide, South Australia (Ch. 5)

3.2.6 Metals

Iron(II) chloride tetrahydrate ($\text{FeCl}_2\cdot 4\text{H}_2\text{O}$) and iron(III) chloride hexahydrate ($\text{FeCl}_3\cdot 6\text{H}_2\text{O}$) from BDH Chemicals (VWR) Tingalpa, Queensland (Ch. 5).

3.3 Filler Synthesis and Dispersion

3.3.1 Graphene Preparation

GT (in 1 g amounts) was expanded in air for 30 s in a furnace preheated to $1000 \text{ }^\circ\text{C}$ to create expanded GT (hereafter called GT-Air). The GT was also heated in a ceramic tube furnace at

1000 °C for 8 h in an inert atmosphere of 100 % nitrogen (GT-N₂). A second GT was heated at 1000 °C for 8 h in a reducing atmosphere of hydrogen 5 % and argon 95 % (GT-H₂). A third GT was heated at 800 °C for 8 h in a reducing atmosphere of CO 100 % (GT-CO) (Table 3-1 and Figure 3-3) Flow rate of gases was 150 mL/min (Ch. 4, 6, 8, 9 and 10).

Table 3-1 Graphene summarised by supplier and production method (temperature, gas and ultrasonication)

Material	Step 1		Step 2		Gas	Step 3
	Temp (°C)	Time (s)	Temp (°C)	Time (h)		Ultrasonication (min)
Graftech 220-50N	1000	30	-	-	Air	10-20
Graftech 220-50N	1000	30	1000	8	N ₂ 100 %	10-20
Graftech 220-50N	1000	30	1000	8	H ₂ 5 % Ar 95 %	10-20
Graftech 220-50N	1000	30	800	8	CO 10 or 100 %	10-20
Graftech 220-50N	-	-	250	8	800 μm Hg	-
Cheap Tubes >700 m ² /g	-	-	-	-	-	10-20
10 g Graphite 5 g KClO ₃	Speed lite	ISO 800	-	-	-	-



Figure 3-3 Tube furnace with one way vent

GT was heated in a ceramic tube furnace at 1000 °C for 8 h in a reducing atmosphere of CO 10 % (GT-CO) (Ch. 6).

Disks of 2.85 cm diameter (~0.5 mm thick) were formed from expanded GT placed in a stainless steel 5 piece mould (top, bottom, two internal disks and a compression shaft) and applying a 9 t load for 5 min in a RIIK 30 ton lever-operated hydraulic press.

3.3.2 Ultrasonication

A Sonics Autotune series high-intensity Ultrasonic (20 kHz) Processor Model: GEX 500 (500 W) with a 13 mm tip was used (Figure 3-4). Ultrasonication, at an amplitude of 25 %, was continued until no more large (un-exfoliated) particles of graphene were visible.

Graphenes (10 mg) were ultrasonicated (as above) in *p*-xylene (2 mL) for 10 - 20 min (~1 min/mg). The energy required was ~128 J/mg for solvents and ~179 J/mg for polymer solutions (Ch. 4 and 5).

GT-CO at 1, 5, 10 and 20 %·w/w loadings in 2 mL benzene was ultrasonicated (as above) (Ch. 6).

Graphenes (H₂ reduced 1 % 100 mg) were ultrasonicated (as above) for 100 min (1 min/mg) in *o*-chlorophenol 14 mL for 100 min (Ch. 7).

Graphenes (CO reduced 1 % 500 mg), pressed into a disk, were ultrasonicated in 10 mL *p*-xylene for 5 h (300 min). It is more convenient to ultrasonicate the graphene in pressed form (less volume), but it is more effectual to ultrasonicate in expanded form (less dispersion required) (Ch. 8).



Figure 3-4 a) Ultrasonicator b) Rayleigh-Benard cell¹⁶⁴ formed by H₂ reduced graphene in *p*-xylene (after ultrasonication)

Graphenes 50 mg (1 %·w/w) H₂ and CO reduced were ultrasonicated for 50 min (1 min/mg) in 10 mL *p*-xylene (Ch. 9).

Graphenes 13 mg (1 %·w/w) H₂ and CO reduced were ultrasonicated for 13 min (1 min/mg) in 1 mL *p*-xylene (Ch. 10).

3.4 Preparation of Nanocomposites

3.4.1 Magnetic-Grafted Graphene

FeCl₂·4H₂O and FeCl₃·6H₂O (molar ratio 1:2) were dissolved in 100 mL of deoxygenated water (with constant stirring for 30 min). EGO was added to the Fe²⁺ - Fe³⁺ solution and dispersed with ultrasonication for 30 min under N₂. The solution was stirred at room temperature for a further 30 min. While stirring, NaOH was added dropwise to precipitate the magnetite particles onto the graphene. The black precipitate was magnetically isolated, and solution decanted. The magnetite (Fe₃O₄) coated graphene was repeatedly washed with water and dried in a vacuum oven at 35 °C for 24 h (Ch. 5).

3.4.2 Solvent Dispersion

SBS (1 g) was dissolved in xylene (10 mL) by standing overnight at 23 °C. Graphenes 1 %·w/w were ultrasonicated (as above). Ultrasonication was used to further increase the surface area of the graphenes by layer separation. SBS and graphene solutions were combined and ultrasonicated (to disperse graphene). Composites were precipitated with methanol and dried at 50 °C in a vacuum (25 in Hg) (Ch. 5).

SBS (1 g) was dissolved in benzene (10 mL) by standing overnight at 23 °C. SBS and graphene solutions were combined, precipitated and dried (as above). (Ch. 6)

PET 10 g was added to 100 mL *o*-chlorophenol heated to ~100 °C. PET and Graphene solutions were added together and ultrasonicated a further 30 min. The composite was precipitated (as above) and dried at 130 °C at 760 mm Hg overnight (Ch. 7).

PES 1.3 g was dissolved in 1 mL *p*-xylene and 10 mL dichloromethane (DCM) by standing overnight at 23 °C (Ch. 10).

3.4.3 Melt Dispersion

PET 50 g was vacuum heated to 165 °C for 4 h (to remove moisture).

A Haake Polylab 600 internal cavity mixer with twin roller rotors was used (Figure 3-5). The cavities were heated to 275 °C. PET granules were added and dispersed for 5 min. Graphenes GT-H₂ 1 % w/w were added and dispersed for 5 min (Ch. 7).

PET (as above): Graphenes (500 mg) GT-CO 1 % w/w (with and without ultrasonication) were added and dispersed for 5 min (Ch. 8).

PC 50 g was dried (as above): The cavities were heated to 275 °C. Graphenes ultrasonicated 50 mg 0.1 % w/w GT-H₂ and GT-CO were added (as above) (Ch. 9)



Figure 3-5 Haake Polylab 600 internal cavity mixer showing twin roller rotors

3.4.4 Film Preparation

Polytetrafluoroethylene (PTFE) sheets were placed on both sides of a round mould ~4.2 cm in diameter measuring 10 cm x 5 cm x 0.5 mm. The sheets were sandwiched between metal plates. The mould was ~30 % overfilled with composite to force out bubbles and voids. The composite was warmed for ≥ 5 min (till melted), pressed at 1 t for 5 min and 6 t pressure for 5 min. The plates were removed and cooled for ≥ 5 min before extracting the composite.

SBS composites were consolidated (as above) in an IDM (15 t Figure 3-6) heated press at 155 °C and 6 t pressure (Ch. 5 and 6).

PET composites were consolidated (as above) in a thermal press heated to 275 °C. The composite was pressed at 8000 N for 2 min (Ch. 7).

PC composites were consolidated at 260 °C (as above) (Ch. 9).

PES composites were consolidated at 285 °C (as above) (Ch. 10).



Figure 3-6 Heated press (IDM)

3.4.5 Microtomy Preparation

Cryo-ultramicrotomy was used to prepare SBS specimens. A Leica Ultracut UCT with a cryo-stage (liquid nitrogen) and Diatome diamond knife was used to create 60-120 nm sections of SBS at -130 °C (Ch. 6).

PET composites were cast in epoxy, shaped with a glass knife (forming a $\sim 0.25 \times \sim 0.25$ mm grid) using the microtome. Composites of ~ 70 nm thickness were cut with a Diatome diamond knife and floated off with water (Ch. 7).

PET, PC and PES composites were shaped and cut with a glass knife (Ch. 8, 9 and 10).



Figure 3-7 Leica Ultracut UCT (minus cryo-stage)

3.5 Characterisation

3.5.1 Microstructure

Optical microscopies were used to characterise dispersion. A Dino-Lite digital microscope (AM4013T-M40) from AnMon Electronics Co with Dino-Capture 2.0 operating software was used at a magnification of 250x (Ch. 8 and 9).

Electron microscopies were used to characterise surface morphology. A Philips XL30 Scanning Electron Microscope (SEM) was used with graphene mounted on conductive carbon tape in high vacuum mode used ($\sim 1.2 \times 10^{-5}$ mBar) (Ch. 4 and 5).

A Quanta 200 scanning electron microscope (SEM) was used in low vacuum mode. PET composites fractured in nitrogen were mounted on conductive carbon tape (without a conductive coating) (Ch. 7).

A JEOL 1010 Transmission Electron Microscope (TEM) at 100 kV was used to observe thermally expanded graphite (1000 °C for 30 s) 4 mg that was previously suspended in 3 mL N-methyl-2-pyrrolidone (NMP) and dispersed with 10 min of ultrasonication. A drop of suspended graphene was placed on GYCU200 Holey support film (200 mesh copper grid). The solvent was left to evaporate for 1 h before imaging (Ch. 4 and 5).



Figure 3-8 TEM JEOL 2100F

A JEOL 2100F TEM at 200 kV was used for thermally expanded GT-CO 4 mg that was previously suspended in 1 mL N-methylpyrrolidone (NMP) and dispersed for 10 min under ultrasonication. 10 μ L was taken and placed in 1 mL of NMP to dilute. A drop of the suspended graphene was deposited on a GYCU200 Holey support film (200 mesh copper grid). The solvent was left to evaporate (Ch. 6).

PET composites were placed on GYCU200 Holey support film (200 mesh copper grids) and dried overnight to remove water (Ch. 7).

PET, PC and PES composites were placed on Formvar GSCu200F-50 full strength solid carbon coated 200 mesh copper grids and dried overnight to remove water (Ch. 8, 9 and 10).

3.5.2 Vibrational Spectroscopy

Raman spectroscopy was used to measure inelastic scattering in the graphene. A Perkin Elmer Raman Station 400F with a laser wavelength of 785 nm (near infrared), 250 mW power and spot size of 100 μ m was used. 120 scans of 1 s were carried out, except for CT which required 30 scans of 5 s. The scan range was from 200 – 3200 cm^{-1} at a data interval of 2.00 cm^{-1} . The graphenes were compressed in a press (9 t for 5 min) to obtain a stronger response except for CT which was not compressed. Graphed data was smoothed using a 15 point moving average. Intensities were compared using unsmoothed data.

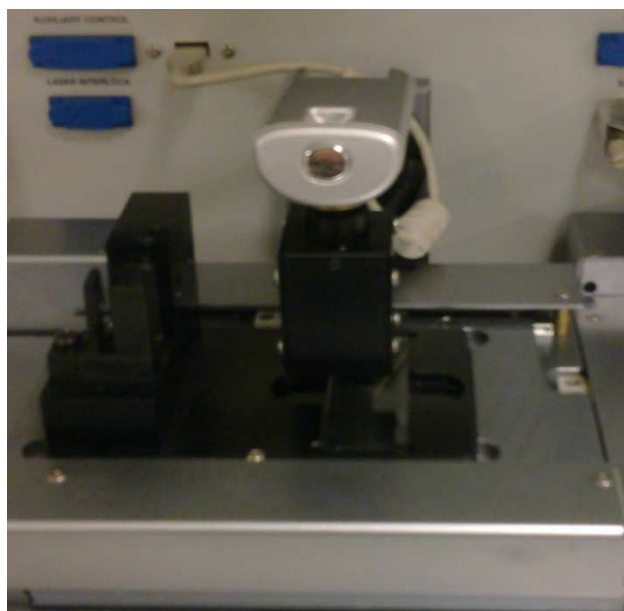


Figure 3-9 Perkin Elmer Raman Station 400 showing glass slide and camera (with protective hood raised)

3.5.3 Electron Spectroscopy

X-ray photoelectron Spectroscopy (XPS) was employed to measure the elements present. A XPS was performed using a Thermo K Alpha with an aluminium x-ray source, standard lens mode, constant analyser (pass) energy of 20.0 eV, spot size of 100 μm , energy step size of 0.100 eV and 100 scans. Four pressed disks of graphene (GT-Air, GT-N₂, GT-H₂ and GT-CO) were used for testing.

3.5.4 Composition and Thermal Stability

Thermogravimetry (TGA) was employed to determine thermal stability. TGA was performed using either a Perkin Elmer TGA7 or Pyris 1. Before each experiment, the pan was cleaned in nitric acid (>1 h at 75 °C). The nitric acid was neutralised with sodium bicarbonate and flushed with water. A thermal cleaning cycle was performed: heating in air at 40 K·min⁻¹ from 50–850 °C and held for 10 min.

Measurements on SBS composites were carried out with a PerkinElmer TGA7. Composites of ~2 mg mass were analysed in an open platinum pan. Composites were heated from 30-850 °C at 20 K/min in nitrogen at 20 mL/min. At 700 °C, the gas was switched back to air at 20 mL/min. Ch. 5

Measurements on graphene were carried out with a PerkinElmer Pyris 1 TGA. Graphenes of ~2 mg mass were analysed in an open platinum pan. Graphenes were left for 12–24 h in flowing nitrogen to remove adsorbed oxygen. Graphenes were heated from 30-1000 °C at 20 K/min in nitrogen at 20 mL/min. At 950 °C, the gas was switched back to air at 20 mL/min and held for 10 min. After 9 min the gas was switched back to nitrogen. Ch. 4 and 6.

Measurements on PET composites were carried out with a PerkinElmer Pyris TGA. Composites of ~2 mg mass were analysed in an open platinum pan. Composites were heated from 30-850 °C at 10 K/min in nitrogen at 20 mL/min. At 800 °C, the gas was switched back to air at 20 mL/min. It was held at 850 °C for 10 min. After 9 min the gas was switched back to nitrogen. Ch. 7



Figure 3-10 Perkin Elmer TGA7

3.5.5 Wide Angle X-Ray Scattering

Wide-angle X-ray scattering (WAXS) was employed to determine any change in the crystalline structure of the graphene. Measurements were carried out with a Bruker D8 Advance diffractometer XRD (Cu K α radiation with $\lambda = 0.154$ nm). The films were placed on a sample holder and analysed using a 1 μ m slit. The diffractograms were scanned in the 2θ range from 10 - 90° at a rate of $2^\circ/\text{min}$. Ch. 5 and 7

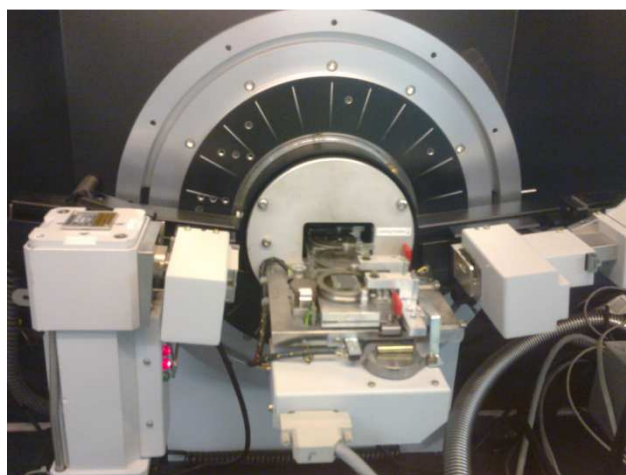


Figure 3-11 Bruker D8 used for x-ray diffraction (XRD)

3.5.6 Thermomechanical Analysis (TMA)

A Perkin-Elmer Diamond DMA (Dynamic Mechanical Analysis) used modulated force thermomechanometry (mf-TM) to measure viscoelastic properties with frequency and temperature. A standard target position of 10 mm, frequencies of 0.5, 1, 2, 5 and 10 Hz (only 1 Hz is reported) was used.

The SBS temperature range was -120-120 °C (Ch. 5).

The PET temperature range was 20-120 °C (Ch. 7) 20-200 °C (Ch. 8).

A TA Instruments DMA Q800 (in extension mode) used tensile mechanical analysis to measure stress (MPa) and strain (%). An isothermal temperature of 30 °C was maintained for 5 min, a ramped force of 1 N/min was applied until 11 N was obtained. A hysteresis curve was formed by returning the force to zero at the same rate. The SBS composite widths were 10.1 mm +/- 0.1 mm; the thickness was 0.515 +/- 0.025 mm and length ~10 – 20 mm (3.95 +/- 0.05 mm between the grips). Ch. 6

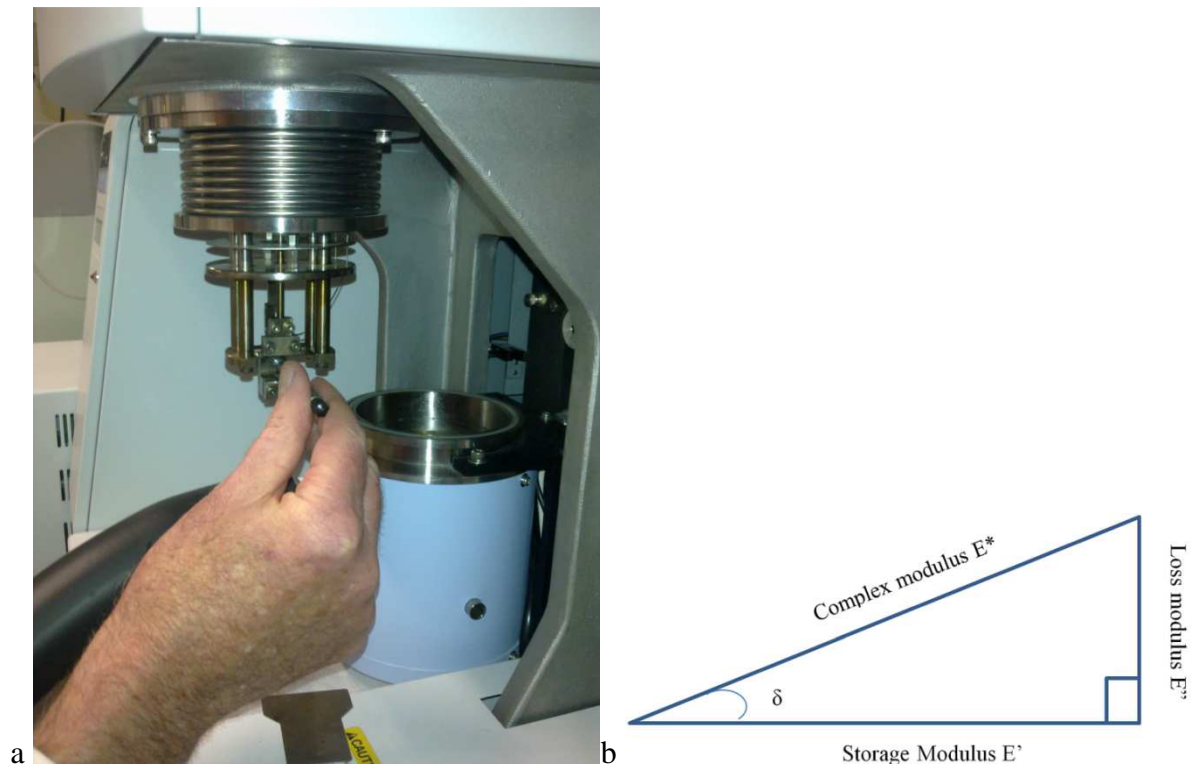


Figure 3-12 a) Diamond DMA showing mounting of SBS-graphene composite b) $\tan(\delta) = \sin(\delta)/\cos(\delta) = \text{loss modulus}/\text{storage modulus}$

PET composites were measured at room temperature. A ramped force was applied till 18 N was obtained (as above). Ch. 7 and 8

PC composites used mf-TM from 30-170 °C. The storage modulus, loss modulus and tan delta were measured at 1 Hz as the temperature was increased at 2 °C/min. Ch. 9

PES used mf-TM from 30-210 °C at 2 K/min. Data was smoothed at 3 °C. Ch. 10

3.5.7 Electrical Conductivity

Conductivity testing (DC measurement) was carried out with a HP 4192A 5 Hz -13 MHz LF impedance analyser and clamp with two 1.2 cm diameter circular electrodes. Measurements of resistance were carried out on pressed disks and composites (Ch. 4, 5 and 6)

SBS composites were measured for capacitance at 11 kHz AC (Ch. 5)

PET composites were measured for capacitance (Ch. 7)



Figure 3-13 a) HP4192A impedance analyser b) circular electrode (showing composite being measured)

3.5.8 Surface Area

Surface area was measured with a Micromeritics ASAP 2000 using Brunauer Emmett Teller (BET) surface area plots. GT was heated to 250 °C at 800 $\mu\text{m Hg}$ (equivalent to 489 °C at 760 mm Hg). Sample sizes were calculated to exceed a surface area of 5 $\text{m}^2 \cdot \text{g}^{-1}$ to achieve an accurate measurement.



Figure 3-14 ASAP 2000 for BET surface analysis

3.5.9 Particle Size

Particle sizing was performed using a vision-based Canty particle sizing system (PSS). The system consisted of a microscopic gigabit camera (30 fps), high-intensity light source (80 W) and a flow path between two windows.



Figure 3-15 Canty Particle sizing system

CO reduced expanded graphite (10 mg) was ultrasonicated for 20 min in 2.75 mL NMP. For tests 1 and 2 1 mL of the suspension was diluted with 250 mL isopropyl alcohol (IPA). For test 3 only 0.75 mL was used.

3.5.10 Surface Energy

Contact angle measurements were carried out using a Dataphysics (Filderstadt Germany) OCA20 from Particle and Surface Sciences. An electronically controlled syringe was used to drip (6.5 - 8.1 mg) deionised water onto pressed graphene disks (refer preparation) at room temperature. Water contact angle was evaluated using static measurements and the sessile drop method.

SCA20 software version 1.60 (build 81) was used with additional Frame grabber driver, image processing unit and profile analysis unit. Readings were averaged (5-8) to obtain an accurate measurement. The Neumann¹⁶⁵ equation of state theory was the method used for the free surface energy calculation.

$$\sigma_{sl} = \sigma_l + \sigma_s - 2\sqrt{\sigma_l \cdot \sigma_s} \cdot e^{-\beta(\sigma_l - \sigma_s)^2} \quad [1]$$

σ_{sl} Interfacial tension between the liquid (l) and the solid (s) (the unknown to be determined from the contact angle)

σ_l Surface tension of the liquid

σ_s Surface free energy of the solid

e Euler's constant 2.71828

β Constant with a value of 0.0001247



Figure 3-16 Dataphysics OCA 20 for contact angle measurement

3.5.11 Molecular Modelling

Graphene interactions with different polymers (SBS, PET and PC) and the solvent (*p*-xylene) were determined by employing density functional theory (DFT) calculations using the Vienna *Ab Initio* Simulation Package (VASP)¹⁶⁶⁻¹⁶⁸. The projector augmented wave method (PAW)¹⁶⁹ was employed with the exchange-correlation functional of PBE (Perdew-Burke-Ernzerhof)¹⁷⁰, together with the DFT-D2 method of Grimme¹⁷¹. A Gamma-centered kpoint mesh of 7x7x1 and a plane-wave cut-off energy of 400 eV was used.

The graphene unit cell had dimensions of $x = y = 1.968$ nm, $z = 2.0$ nm and angles $\alpha = \beta = 90^\circ$, $\gamma = 120^\circ$. Application of periodic boundary conditions in the x- and y- directions creates the extended surface of the graphene plane. The vacuum spacer in the z-direction prevents interaction between the graphene layers.

For the *p*-xylene solvent, the isolated molecule was optimised in the same size simulation cell and then adsorbed on the graphene sheet ~0.35-0.4 nm above the surface. All atoms were allowed to relax during the simulation until the total energy was converged to 10^{-4} eV and the Hellmann–Feynman force on each relaxed atom was less than 0.01 eV/Å. The results of these calculations are presented in Ch. 4

The polymers were modeled by terminating the monomeric unit with H atoms. Each monomer was then placed ~0.3 nm above the graphene plane. Each structure was initially optimised, followed by an *ab initio* molecular dynamics (MD) simulation (as implemented in VASP) at 300 K, using a plane-wave basis set expanded at the Gamma point only in the Brillouin zone. The MD was performed for up to ~5.3 ps using a timestep of 0.5 fs. At different stages, during the MD simulation, the structure was optimised and the total energy values compared to determine whether the structure had reached equilibrium. Some the optimised structures obtained towards the end of the MD simulations are presented in Chapter 6 for SBS, Chapter 7 for PET and Chapter 9 for PC.

Chapter 4 Graphene Preparation from Intercalated Graphite via Rapid Heating under Reductive Conditions

4.1 Introduction

This chapter introduces thermal exfoliation and carbon monoxide thermal reduction that is demonstrated to produce graphene with low defects, of quality that will enhance polymer composites, be scalable to yield significant mass or be converted to continuous production with a suitable furnace. Low defect graphene is a high-performance two-dimensional material with all atoms planar and at a surface in single layers and a huge aspect ratio giving reinforcement, fractal interconnection and percolation networks at low volume content. Thus graphene is of great interest to experimenters hampered only by the high price of most commercial graphenes and thus ready availability for experimentation^{3, 5, 35}.

Graphene top down (from graphite) production methods are ideal for mass production. However current chemical exfoliation⁴⁰ methods typically involve oxidation, intercalation and exfoliation conditions that introduce defects. Variations of the Hummers (H_2SO_4 , NaNO_3 and KMnO_4)⁴³, Studenmaier (H_2SO_4 , fuming HNO_3 and KClO_3)¹⁷² or Hofmann (H_2SO_4 , concentrated HNO_3 and KClO_3)^{173, 174} methods are used to oxidise graphite and separate layers of graphite with oxygen-containing functional groups. Unfortunately, functionalization is a defect and this approach to producing graphene results in up to 40 % defects, even after reduction³⁰, which may degrade the mechanical properties¹⁵⁹.

However, thermal exfoliation methods can be used to produce low defect graphene and maintain the exceptional properties that make graphene so useful. Minimising defects can be achieved when intercalating graphite with residual acids. Intercalation is the insertion of atoms or molecules of a different chemical species between sheets of graphite¹⁷⁵. Incomplete separation involves less covalent bonding^{176, 177} and thus produces fewer defects. The process uses similar methods (e.g. sulfuric (intercalant) and nitric acids (oxidising agent)¹⁷⁸) to chemical exfoliation, but the graphite sheets remain in close proximity. Oxygen-containing groups are placed between graphite layers (creating expandable graphite) then rapidly expanded. The high-temperature expansion removes any functional groups (sp^3 defects) that might have formed¹⁶⁰⁻¹⁶³. High temperatures separate the graphite sheets by increasing pressures of evolved gases and volatiles from the decomposition of oxygen-containing

groups^{3, 179}. The van der Waals attraction between the graphite layers that must be overcome is ~ 26 MPa. Water generates a maximum pressure in excess of 60 MPa and CO₂ greater than 100 MPa. However, as H₂O vaporisation is endothermic, it slows the heating process. Thus CO₂ evolution, which is exothermic, is the preferred mechanism for exfoliation¹⁸⁰. If the expansion takes place in air some oxide groups (defects) are formed as the graphene cools (edges are particularly reactive). Such oxides are often removed in solution using hazardous chemicals (hydrazine) but leave behind contaminants. Nitrogen (an inert gas), hydrogen or carbon monoxide (reducing gases) can be used to remove oxides without leaving behind any contaminants.

Sheets created by thermal expansion still contain some functional groups¹⁸⁰. They still need to be further separated and dispersed. To do this, new functional groups are often introduced or existing groups are used for covalent bonding creating further defects. One way of avoiding the creation of new defects is by using π -interactions and ultrasonication in an aromatic solvent¹⁸¹. Thermal expansion with ultrasonication can produce ~ 80 % (or more) single sheets of graphene^{179, 180} and ultrasonication reduces the graphene further⁵².

The aim was to use rapid thermal expansion and exfoliation of intercalated graphite oxide with high interlayer separation to produce graphene having a low defect concentration. An inert gas (N₂) or reductive conditions (H₂ or CO) were used to eliminate the need for a second solvent-based chemical reduction and repair of the graphene sp² structure.

4.2 Experimental

Material information, filler synthesis and preparation and characterisation methods are detailed in Chapter 3.

4.3 Results and Discussion

4.3.1 Microscopy

Four images were taken at a uniform resolution (Figure 1) allowing comparison. Image (a) shows GT-Air after disruption of connectivity by ultrasonication which increased exfoliation and decreased the width. Image (b) shows GT-N₂ long folds of carbon joined at the edges in an accordion-like fashion: expanded GT looks like this before ultrasonication or compression. Image (c) shows GT-H₂ after treatment with a reducing hydrogen atmosphere, resulting in thinner layers: the carbons are compressed, so the folds are not as marked. Image (d) shows

that a commercial graphene (Cheap Tubes) of 1 - 3 layers was comparable in thickness but had much smaller particle size. Image (e) shows single layer partially coiled graphene(s) (50 nm) produced in a reducing CO atmosphere (GT-CO) with ultrasonication to further separate, exfoliate and reduce⁵².

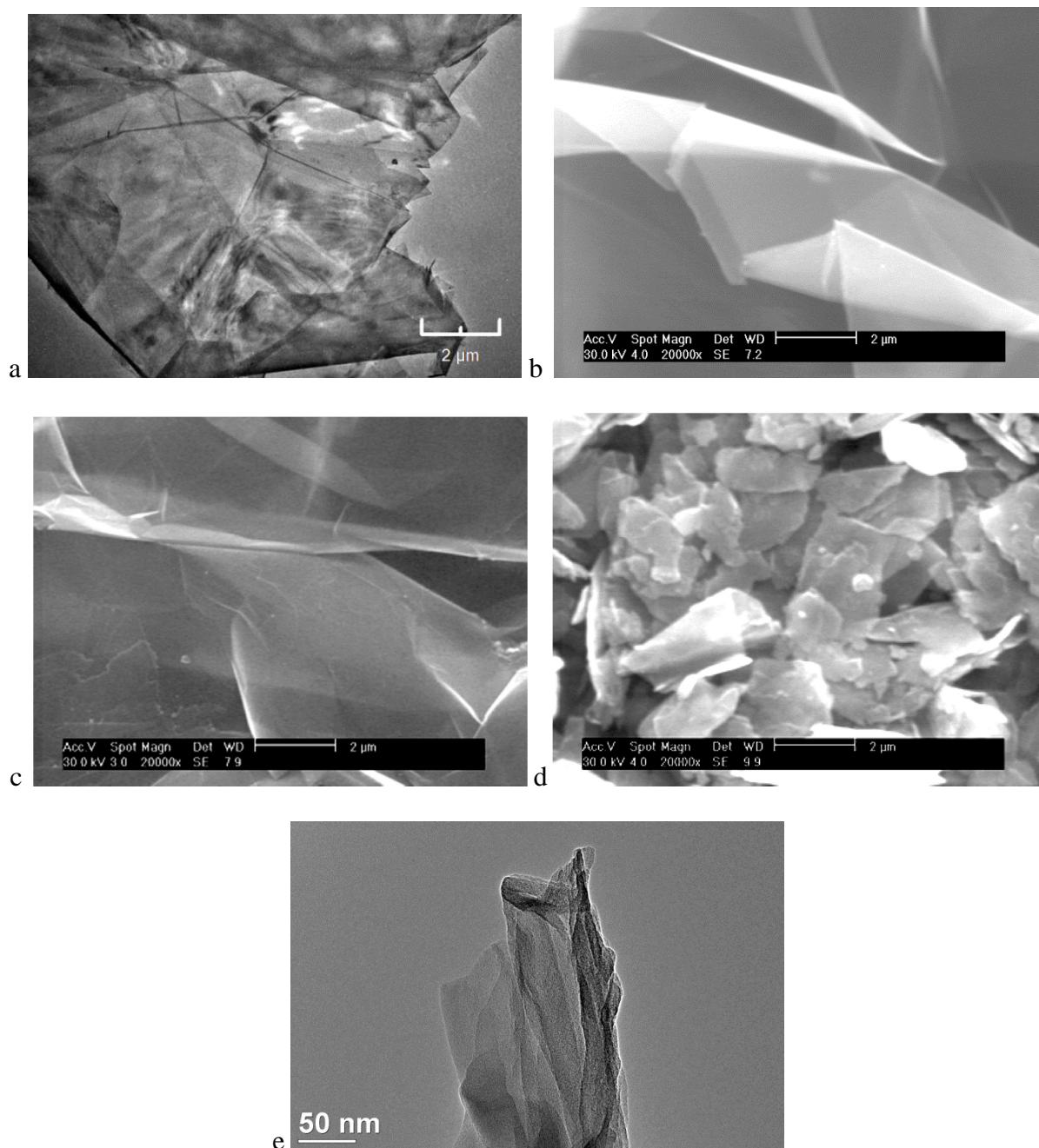


Figure 4-1 Microscopy 2 μm , a) GT-Air with ultrasonication TEM, b) GT-N₂ (inert gas to remove oxides) SEM, c) GT-H₂ (reducing gas) SEM, d) CT #1 $>700 \text{ m}^2 \cdot \text{g}^{-1}$ SEM e) GT-CO (reducing gas) with ultrasonication TEM (50 nm)

4.3.2 Vibrational Spectroscopy

Raman spectroscopy is the most common technique for characterising graphenes; it records vibrations of covalent bonds in molecules. It is sensitive to changes in polarisability (stretching and deformation) rather than infrared spectroscopy that is sensitive to changes in dipole moment. Raman spectroscopy is most sensitive to symmetrical bonds and slight changes in bond angle or bond strength. Thus it is particularly sensitive to changes in the sp^2 symmetry of graphenes⁷⁷.

The Raman spectra (Figure 4-2) show significant peaks at ~ 2650 , ~ 1580 and ~ 1314 cm^{-1} (2D, G and D bands).

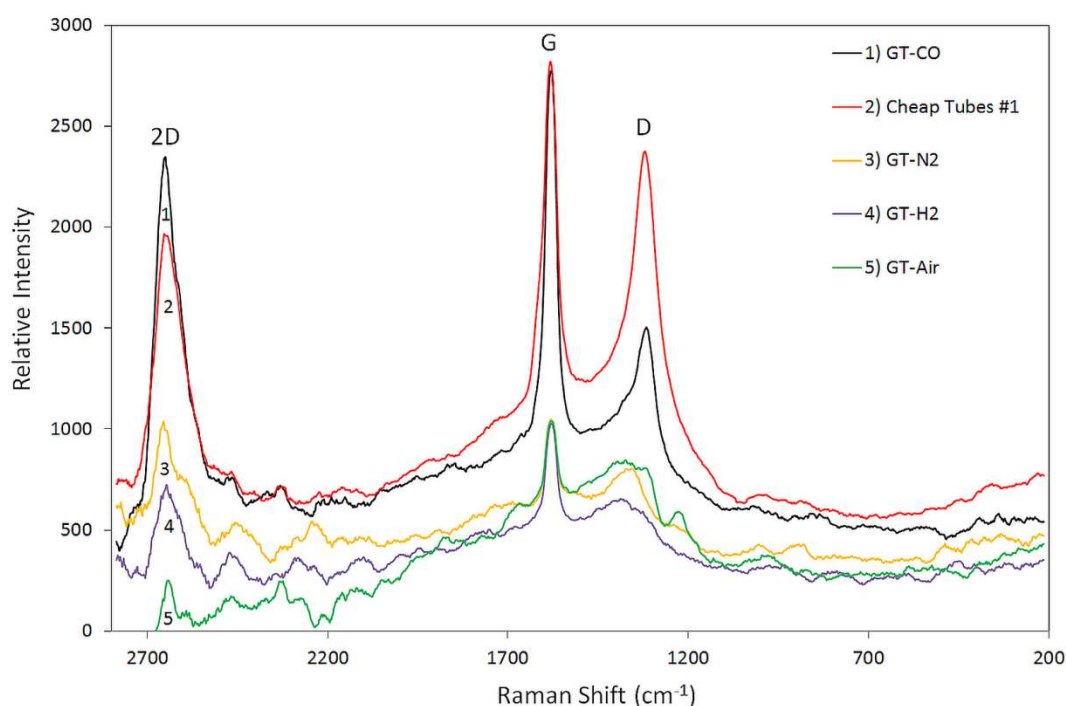


Figure 4-2 Raman spectra intensity of graphene (listed at the 2D peak from highest to lowest)

4.3.2.1 2D Peak

It is known that the 2D peak (second order of the D peak) is strongly influenced by strain, intercalants and charged impurities. Single layer graphene is indicated by a single 2D peak⁸³. Graftech (GT) CO (highest) and Cheap Tubes (CT) #1 (slightly lower) showed a symmetrical single Gaussian 2D peak at 2654 cm^{-1} (Figure 4-2) suggesting a single or few layer graphene. The other GT graphenes had significantly lower peaks that were not as well defined, indicating multi-layer graphene.

The 2D/G ratio is a quantitative measure of graphene layers⁸¹. A high 2D/G ratio indicates fewer layers and a lower 2D/G ratio indicates more layers. A rising 2D peak may also mean fewer defects⁸³. GT-CO had a higher 2D/G ratio (0.76) than CT (0.63). Thus the 2D/G ratio, the shape of the peak and the comparison with CT (known to be 2-3 layer) suggest GT-CO is 2-3 layer graphene.

4.3.2.2 D Peak

The D peak occurs when there are defects or disorder in the graphene matrix. Edges, grain boundaries, vacancies, implanted atoms^{76, 77} and changes from sp^2 to sp^3 carbon bonding can all cause defects¹⁸². A major source of defects comes from armchair edges (Figure 4-3a)⁷⁷. Defects that do not generate a D peak include perfect zig-zag edges (Figure 4-3a), charged impurities, intercalants and uni/biaxial strain⁸³. Defects adversely affect performance and limit the use of graphene. Defects are of particular relevance to applications which require pristine graphene. Any method of decreasing defects in graphene is noteworthy.

The Cheap Tubes graphene showed the largest D peak (2,394 intensity at 1314 cm^{-1}) compared with other graphenes (Figure 4-2). The GT based graphenes showed smaller D peaks. However, the D peak alone is not quantitative.

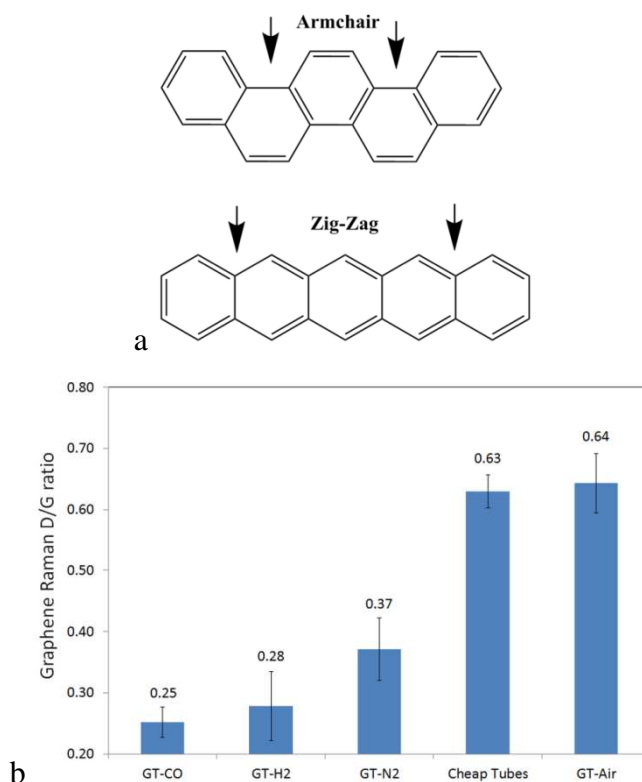


Figure 4-3 Graphene a) Types of edges b) D/G ratio versus production method

4.3.2.3 D/G Ratio

The D/G ratio is a quantitative measure of defects^{56, 183} which is more precise than D peak size alone: A high D/G ratio indicates more defects, a lower D/G ratio indicates fewer defects⁶¹. The GT-CO had the lowest D/G ratio (fewest defects) at 0.25 (Figure 4-3b). GT-H₂ was second lowest. GT-N₂ had a lower ratio than CT commercial graphene and GT produced in air had the highest ratio (most defects) at 0.64. These are all low ratios corresponding to considerable distances between defects (~17 nm), i.e. low-defect graphene^{77, 184}. The low ratios are typical of small defect peaks produced by zig-zag edges^{184, 185}.

4.3.2.4 G Peak

The G band is caused by in-plane vibration of the sp² bonds found in graphene. The position of the G band has been shown to correlate with the number of layers in graphene^{4, 186}. Single layers are indicated by a Raman shift to a higher wavenumber. Double or multiple layers are shown by a Raman shift to a lower wavenumber. The Cheap Tubes graphene G peak was at 1580 cm⁻¹. The GT based graphenes peaks were between 1580-1582 cm⁻¹ (Figure 4-4).

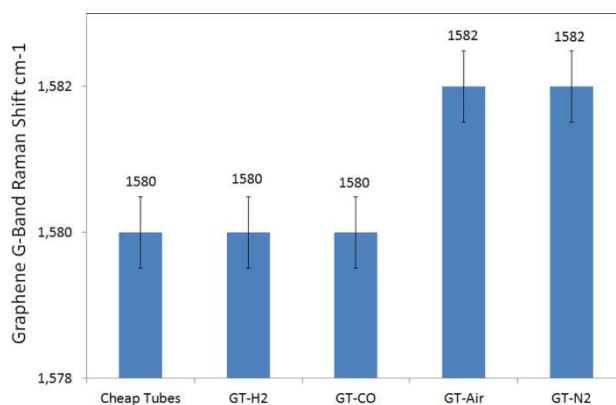


Figure 4-4 Raman graphene G band position versus production method

If the Cheap Tubes graphene is single or few-layer (as suggested by the 2D peak), then the position of the G peaks indicates the GT graphene also contains single or a few layers.

4.3.2.5 Mechanism

These results show that thermal exfoliation in nitrogen (an inert gas) prevents air from creating oxygen-containing functional groups hydroxyl (-OH), acid (-COOH), carbonyl (=O) and epoxides (-O-) primarily. Thermal exfoliation in hydrogen (a reducing gas) removed functional groups even more efficiently. CO is an even stronger reducing gas and resulted in a Raman spectrum indicating fewest defects in the graphene. It is energetically advantaged

for reduction i.e. CO has a low energy barrier of 0.06 eV for epoxides, 0.04 eV for hydroxyls and 0.09 eV for ketone pairs⁶⁶. The Boudouard reaction (Equation 1) of CO provides a source of carbon.

Boudouard reaction:



The low energy barrier, the ready source of carbon and the enhanced Raman spectra all suggest that the graphene matrix is being repaired. The proposed chemical transformation for the healing of graphene using carbon monoxide is shown in Figure 4-5.

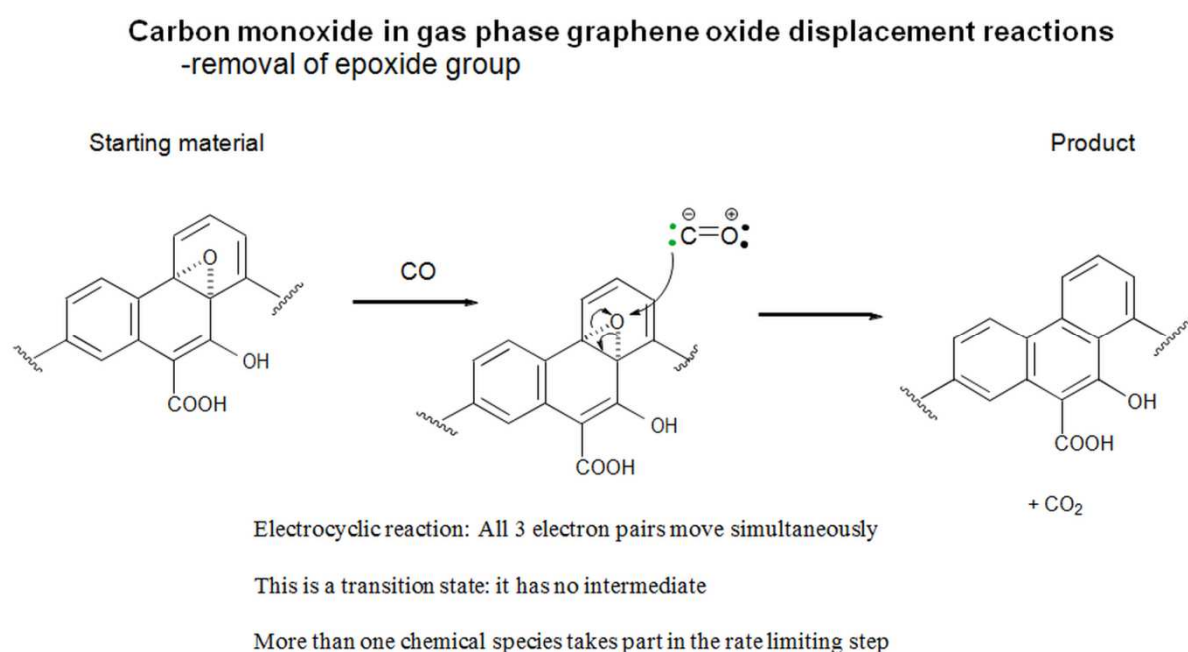


Figure 4-5 Suggested mechanism for GT-CO reduction and repair

4.3.3 Composition and Thermal Stability

4.3.3.1 Thermogravimetry

Thermogravimetry (TGA) has been used to compare graphenes^{187, 188}. Oxide groups (hydroxides, epoxides, carboxylic acids and ketones³⁰) on graphene are less thermally stable than a fully aromatic structure. Heating in an inert (N₂) or reducing (H₂ or CO) atmosphere removes these oxide groups. Thus, the mass loss can be used to provide a measure of oxide groups on the surface of graphene.

The results (Figure 4-6) show that the commercial CT graphene lost the greatest mass (2.4 %). GT expanded in air lost 0.7 % mass. The GT processed in inert N₂, reducing H₂ and reducing CO environment had the lowest mass loss (0.4 %).

These results demonstrate that the GT-N₂, GT-H₂ and GT-CO had the fewest oxide groups.

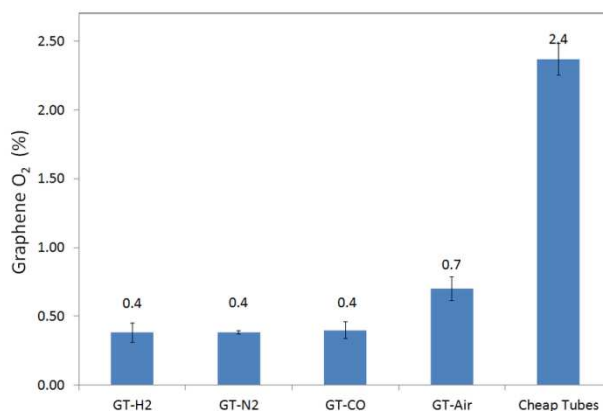


Figure 4-6 TGA of graphene mass loss (oxygen content) versus production method

4.3.3.2 Electron Spectroscopy

X-ray photoelectron spectroscopy (XPS) was carried out to investigate bonding of elements (except for hydrogen which is unable to be detected) with carbon in graphene. XPS was run on GT-Air, GT-N₂, GT-H₂ and GT-CO graphenes and the results were found to be inconclusive. The uncertainty is due to trying to find quantities of material <1 at.% through an adventitious carbon layer of variable thickness when XPS accuracy is in the 1-2 at.% range. Adventitious carbon is a thin layer (~1-2 nm) of non-graphitic carbon found on the surface of most air exposed samples¹⁸⁹.

4.3.4 Surface Energy

Contact angle (CA) measurements investigate surface tension, and they are used to calculate surface energy (SE). CA varies in graphene depending on the functional groups present. The most common groups on graphene are oxides which make graphene hydrophilic. Thus, fewer oxides make graphene more hydrophobic.

Contact angle measurement (Figure 4-7) showed an increase from 81° (GT-Air), 87° (GT-H₂), 89° (GT-N₂) to 107° (GT-CO). This is equivalent to surface energy (SE) of 34.7 (GT-Air), 30.9 (GT-H₂), 29.8 (GT-N₂) and 19.1 (GT-CO) mN·m⁻¹. No measurement of the CT graphene was possible because it did not provide a sufficiently large contact area for

measurement. These readings demonstrate that the strongest reducing agent (CO) resulted in the highest contact angle (greatest hydrophobicity). This indicates a change to the surface consistent with the removal of oxygen-containing functional groups.

An article in which graphene was modelled predicted a contact angle of 95-100°. The article suggested that contact angle predictions to 127° were excessive¹⁹⁰.

Comparison of the SE of PTFE (polytetrafluoroethylene) ($21.35 \text{ mN}\cdot\text{m}^{-1}$)¹⁹¹ a highly hydrophobic polymer, with GT-CO ($19.1 \text{ mN}\cdot\text{m}^{-1}$) demonstrates that the GT-CO had a lower SE than PTFE. A reduction in oxides and healing of the graphene is consistent with the observed increased contact angle and low SE of GT-CO. These observations fall at the extreme end of those observed for a hydrophobic material. This may explain the scrolling of the GT-CO in an effort to minimise surface energy.

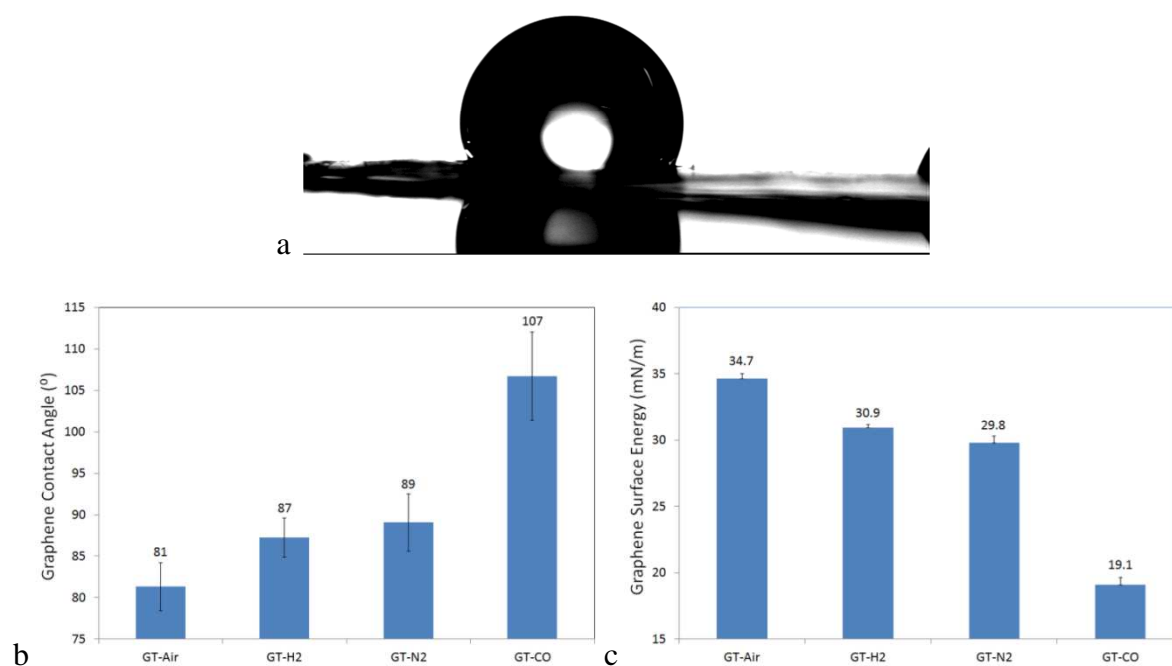


Figure 4-7 GT graphene a) water drop on compressed GT-CO b) contact angle c) surface energy

4.3.5 Electrical Conductivity

Graphene is normally conductive, making conductivity a potential method of characterisation. DC resistance measurements were carried out on the compressed graphene disks to provide some basis for comparison. Only GT graphenes could be compressed: the CT graphenes and unexpanded GT were too elastic and slipped from between the disks in the

press. Thus, four compressed graphenes were prepared. Such disks have different resistivity to uncompressed graphenes.

Equation 2 measured resistance as related to resistivity

$$R = \rho t/A \quad [2]$$

Equation 3 Resistivity is calculated (by re-organising equation 2)

$$\rho = RA/t \quad [3]$$

Where R is resistance, t is thickness, A is area and ρ is resistivity.

Graphene resistivity measurement was carried out for GT based graphenes before ultrasonication (Figure 4-8). The lowest resistivity was from GT treated in a reducing atmosphere of CO (238 $\Omega \cdot \text{cm}$). Resistivity was highest (1,203 $\Omega \cdot \text{cm}$) with GT-Air. There was some variation between different H₂ treated graphenes (239 versus 390 $\Omega \cdot \text{cm}$).

Oxidised graphene was less conductive, so any processing to remove oxide groups decreased resistance. By this measure, the CO reduction method was the most successful at removing oxide groups.

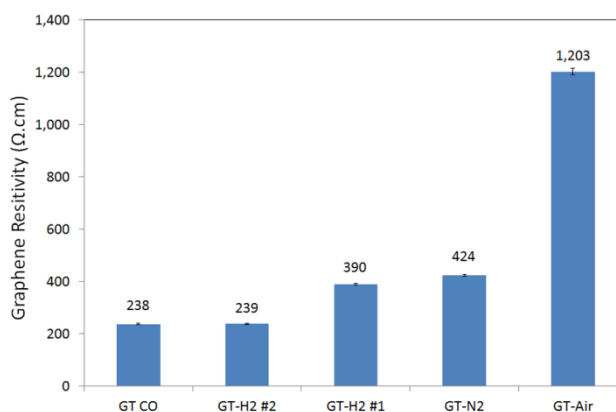


Figure 4-8 Resistivity of graphene versus production method

4.3.6 Particle Size

Particle size is an important consideration for many uses of graphene. For example, the properties of polymer composites are dependent upon the particle size of fillers and reinforcements.

Dynamic light scattering was attempted, however, due to the wide range of particle sizes, this was unsuccessful. A Cauty particle sizing system was used instead.

The particle size range for GT-CO was 2 – 56 μm with a mode of 7 – 8 μm , an average of 12 μm and up to 25 μm was within the 99th percentile (Figure 4-9). Compared with the CT graphenes (~1 – 3 μm) the ultrasonicated GT-CO is much larger (even after ultrasonication). Large particle size (referring to high aspect ratio and large surface area) is ideal for reinforcing polymers¹⁹².

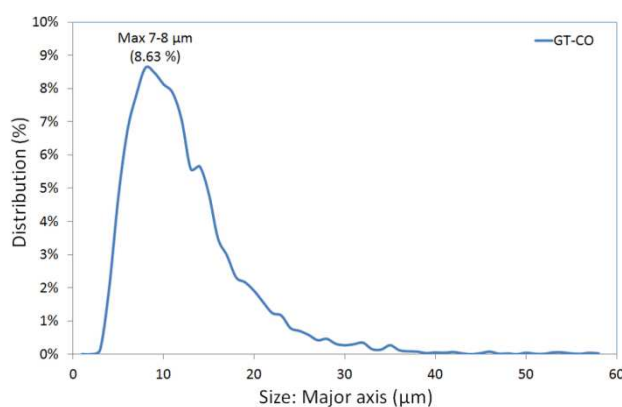


Figure 4-9 Size distribution of GT-CO graphene by count

4.3.7 Surface Area

Brunauer-Emmett-Teller (BET) surface area plots (Figure 4-10) showed an excellent fit to the data, but very low surface area measurements were obtained for all graphenes including CT which has a surface area known to be $>700 \text{ m}^2 \cdot \text{g}^{-1}$. It is believed that graphenes (which are stable to $>4,900 \text{ K}$) were not heated sufficiently ($250 \text{ }^\circ\text{C}$, $800 \text{ } \mu\text{m Hg}$ equivalent to $489 \text{ }^\circ\text{C}$ at 1 atm (760 mm Hg)) to drive off all surface adsorbed molecules. In other research, the adsorption of nitrogen was found to be significantly limited by the overlap of graphenes, in dry systems¹⁷⁹. Given that surface area measurements are reported in the literature, it appears that measurement varies according to surface functionalization of the graphene.

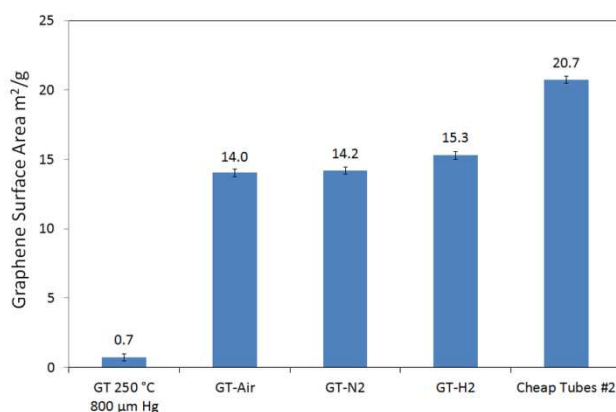


Figure 4-10 BET surface analysis measuring surface area versus graphene production method

4.3.8 Dispersion

Thermally expanded graphite is composed of graphene sheets in close proximity to each other. Ultrasonication in a solvent separates these sheets (especially after processing with N₂, H₂ or CO). Graphene disperses most effectively in polar solvents of which NMP is the most effective⁶⁸. However, agglomeration often occurs during processing unless the graphene is functionalised. To avoid covalent functionalization (defects) and prevent agglomeration non-polar aromatic solvents can be used utilising π -interactions for dispersion.

p-Xylene was used to create suspensions of graphenes. The interaction between *p*-xylene and graphene was modelled using DFT (Figure 4-11) and showed the ring of *p*-xylene preferred to be aligned above the graphene sheet so that the centre of the xylene ring lies directly above a carbon atom. This is the same stacking orientation as the AB (Bernal) stacking⁸ geometry.

The carbon-carbon bond lengths in graphene were calculated to be 0.142 nm, and the *p*-xylene was oriented $\sim 8^\circ$ from the axis of the graphene. The average distance of the *p*-xylene ring above the graphene sheet was ~ 0.333 nm: as measured between the average z-height of the 6C atoms in the ring and the height of the C atom in the graphene sheet located directly below the middle of the ring. This is similar to the experimental distance between layers in graphite of 0.3354 nm¹⁹³.

The electron localisation function (ELF) showed the covalent bonding in the graphene sheet and the *p*-xylene molecule. The ELF is plotted on a scale from 0 to 1 and gives an indication of the likelihood of formation of bonding and nonbonding electron pairs. Regions of red indicate a high probability and can be seen in the bonding region between the C atoms in the

C-ring structure. Previous experiments have demonstrated that the π -interaction stacking approach is effective with aromatic polymers¹⁸¹.

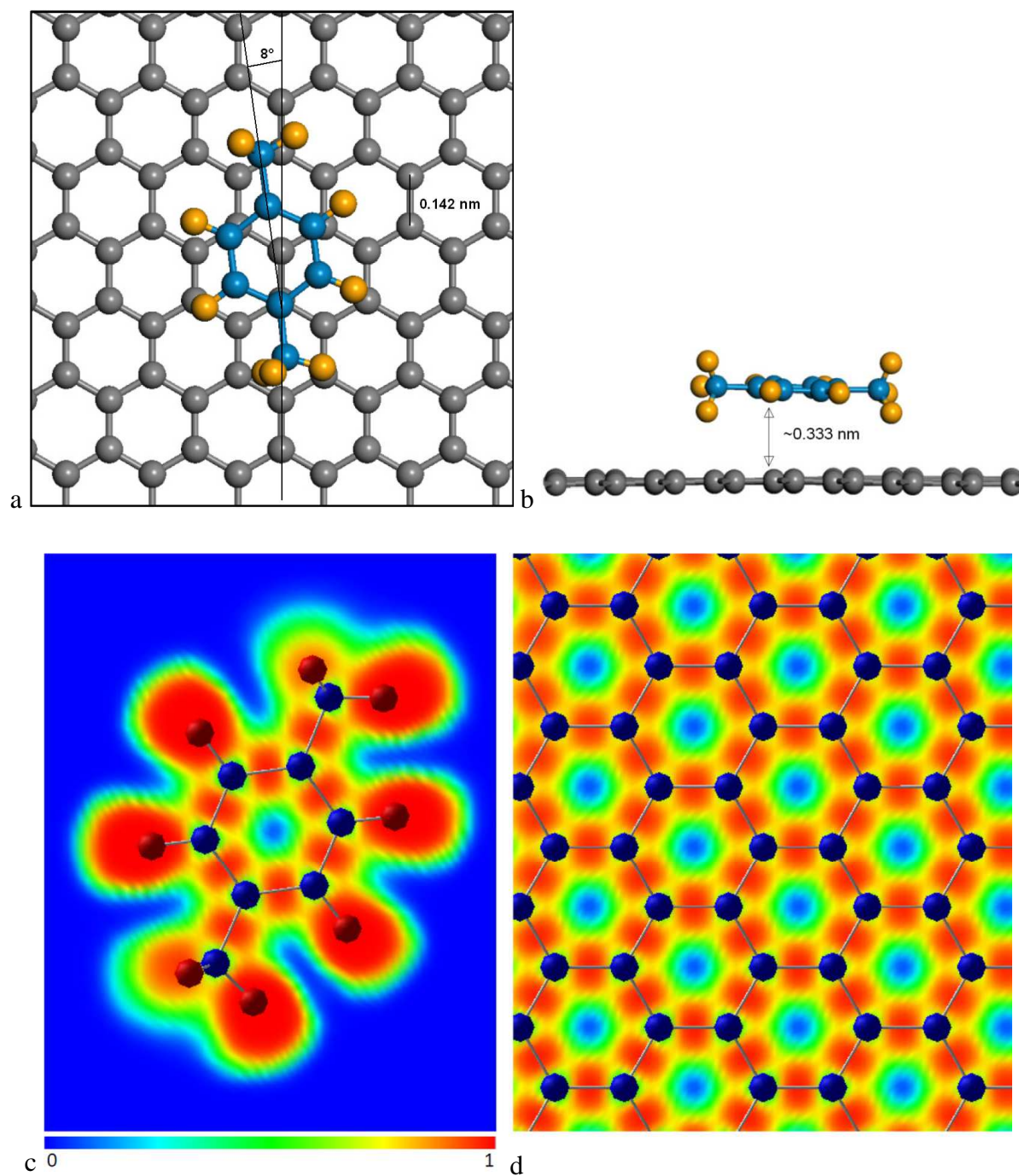


Figure 4-11 Optimised structure of *p*-xylene adsorbed on graphene a) top down view b) side view (C-blue, H-orange and graphene C-grey) c) electron localisation function (ELF) of *p*-xylene d) graphene

4.4 Conclusion

Graphene was prepared by exfoliation and thermal reduction of graphene oxide. Thermal exfoliation was performed under air, inert atmosphere (nitrogen) and reducing atmospheres of hydrogen (5 %) and carbon monoxide. The reducing atmospheres allowed removal of oxygen-containing functional groups (e.g. epoxides) from the graphene with the reduced introduction of defects into the graphene sheets. The resulting graphene sheets were further detached by dispersion in the aromatic liquid xylene using ultrasonication. DFT calculations showed that the p-xylene ring prefers to be aligned parallel to the preferred interaction between graphene. Graphene dispersions in xylene with ultrasonication further reduced the number of sheets in a stack and were suitable for solvent based preparations of graphene-polymer nanocomposites.

The graphenes prepared were characterised using Raman spectroscopy, contact angle surface energy, microscopy, thermogravimetry, resistivity and particle size distribution. From Raman spectroscopy, the GT-CO graphene appears to be single or few layer and has the least number of defects of all the samples that have been studied. Thermogravimetry showed a low mass loss due to decomposition of residual oxygenated groups. This was confirmed by electrical resistance measurements showing lowest resistance where defects or oxygenated groups were in the lower concentration. Contact angle surface energy was lowest for graphenes with lower oxygenated group concentrations with the graphene produced with carbon monoxide reduction exhibiting scrolling and a surface energy lower than polytetrafluoroethylene.

These results demonstrate that a high-quality graphene can be created using thermal expansion.

Chapter 5 Preparation of graphene and inclusion in composites with poly(styrene-*b*-butadiene-*b*-styrene)

5.1 Introduction

The preparation of SBS-graphene composites is described in this chapter. Non-covalent bonding (π -interactions) between SBS and graphene were used for dispersion. Graphene produced by thermal expansion in air, an inert gas (N₂) and a reducing gas (H₂) was used. SBS is a triblock copolymer thermoplastic elastomer that consists of two amorphous phases, a continuous polybutadiene phase and a dispersed polystyrene phase. Since SBS is amorphous, there is no crystallisation nucleation by dispersed graphene to add to the interpretation of the nanocomposite properties. Since SBS is a thermoplastic elastomer, there is no crosslinking reaction that could be inhibited or catalysed by graphene that could complicate the interpretation of nanocomposite structure and properties. The two-phase separation may be modified by graphene, or the graphene may selectively disperse in one of the phases. A hypothesis is that the styrene blocks in SBS selectively adsorb onto graphene improving dimensional stability even at low volume fractions. Surface modification of graphene may be used to modify the properties of SBS further.

The aim was to prepare and characterise nanocomposites containing graphene or surface modified graphene from intercalated graphite, characterise their structure, evaluate their electrical properties, response to modulated force and temperature.

5.2 Experimental

Material information, preparation of nanocomposites and characterisation methods are detailed in Chapter 3.

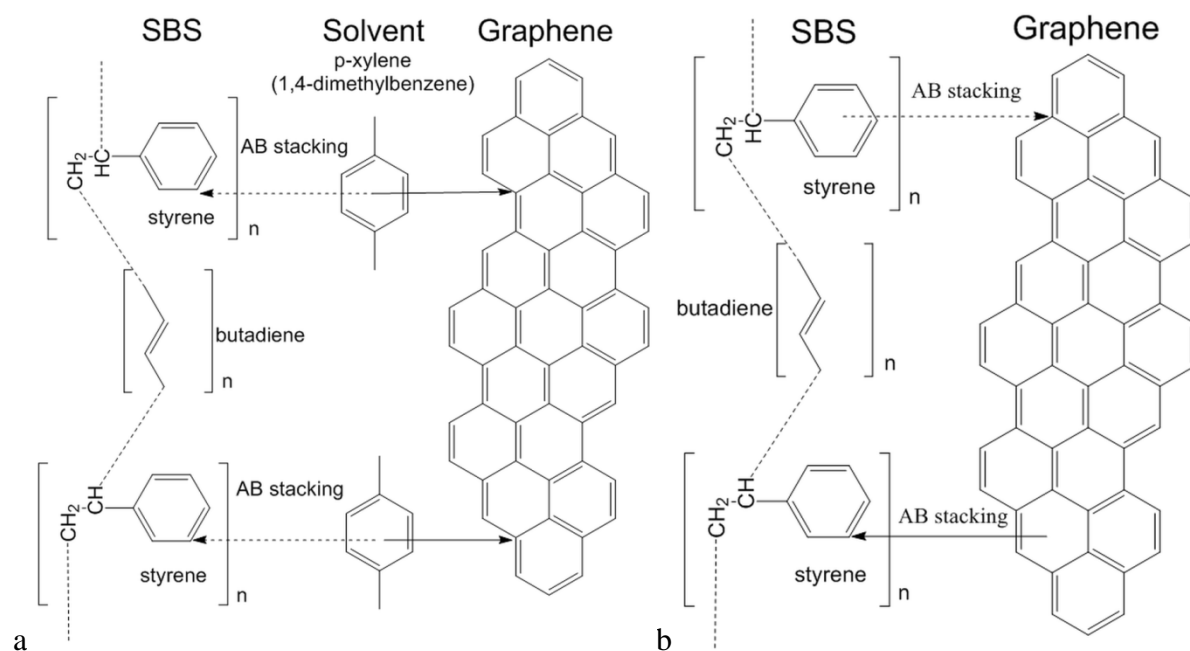


Figure 5-1 SBS and graphene illustrating van der Waal interactions AB stacking geometry between the respective planes a) in solution b) without solvent

5.3 Results and Discussion

5.3.1 Microscopy

Graphene was produced by rapid thermal expansion (TE) and compared to a high-quality commercial graphene (CT). The graphene was dispersed in poly(styrene-*b*-butadiene-*b*-styrene) (SBS) using π -interactions (Figure 5-1) to prevent agglomeration.

Figure 5-2 (a) was taken at low resolution (80x) to demonstrate the worm or accordion-like expansion which is typical of thermally expanded graphene. Three images were taken at 20,000x magnification allowing easy comparison: Figure 5-2 (b) demonstrates the effect of ultrasonication on the graphene: increases exfoliation and decreases the width. Figure 5-2 (c) shows long folds of carbon joined at the edges in an accordion-like or worm fashion; expanded graphite looks like this before ultrasonication or compression. Figure 5-2 (d) shows that a commercial graphene (CT) of 1-3 layers is comparable in thickness but has much smaller particle size.

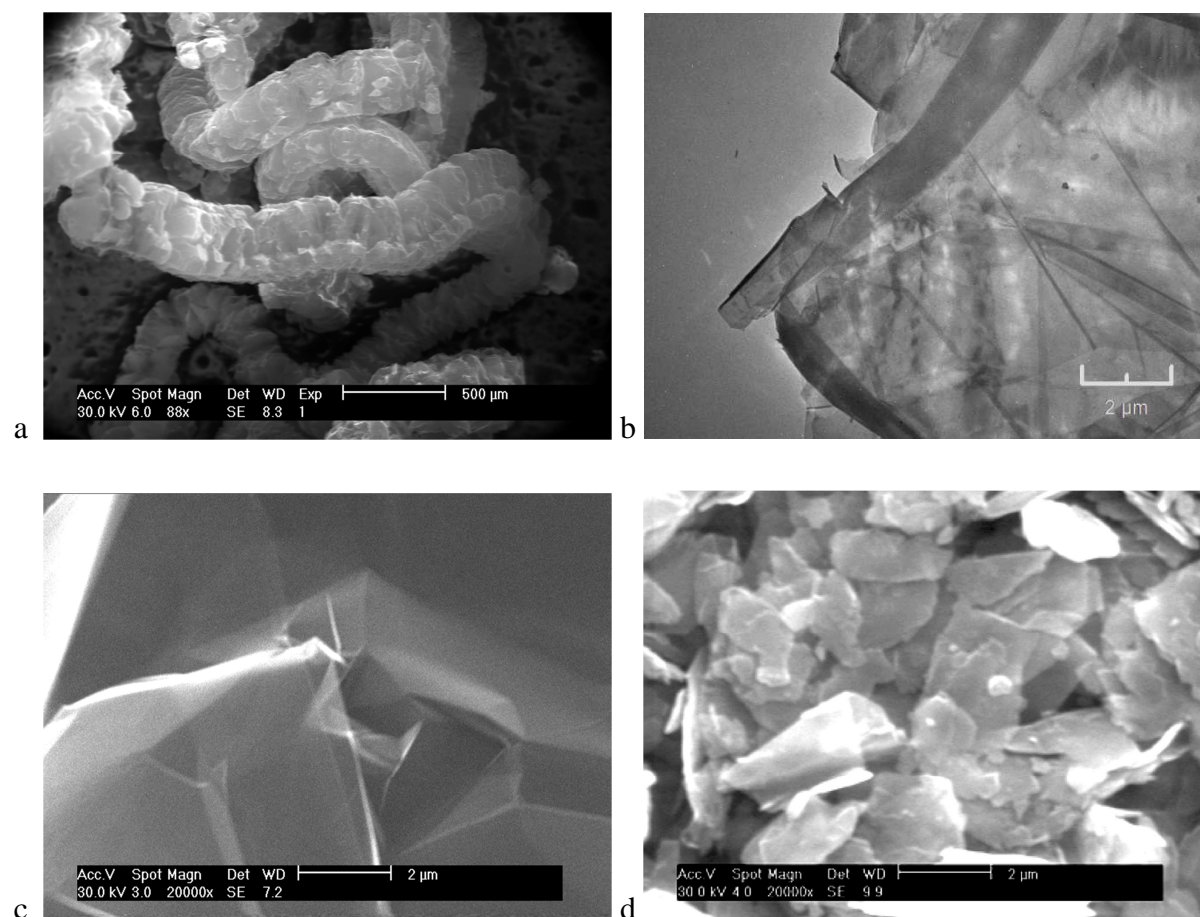


Figure 5-2 Electron microscopy a) GT-N₂ 500 μm 80x SEM and 20,000x (2 μm) b) GT-Air with ultrasonication TEM c) GT-N₂ SEM d) CT #1 SEM

5.3.2 Vibrational Spectroscopy

Raman spectroscopy (Figure 5-3a) was used to identify graphene defects via the defect (D) peak. The Raman spectra showed significant peaks at ~ 2654 (2D), ~ 1582 (G) and ~ 1316 cm^{-1} (D) bands.

The Cheap Tubes >700 m^2/g graphene showed a large peak in the D band at 1316 cm^{-1} whereas the 220-50N based graphenes showed smaller D peaks (Figure 5-3b). The order of these smaller D peaks corresponds to the amount of processing carried out on the 220-50N: 1) air (highest) 2) N₂ inert gas 3) H₂ reducing gas (lowest). Low defect graphene is usually the most desirable. The low D/G ratio, which is more objective, confirmed that GT-H₂ reduced graphene (0.28) has a low defect rate.

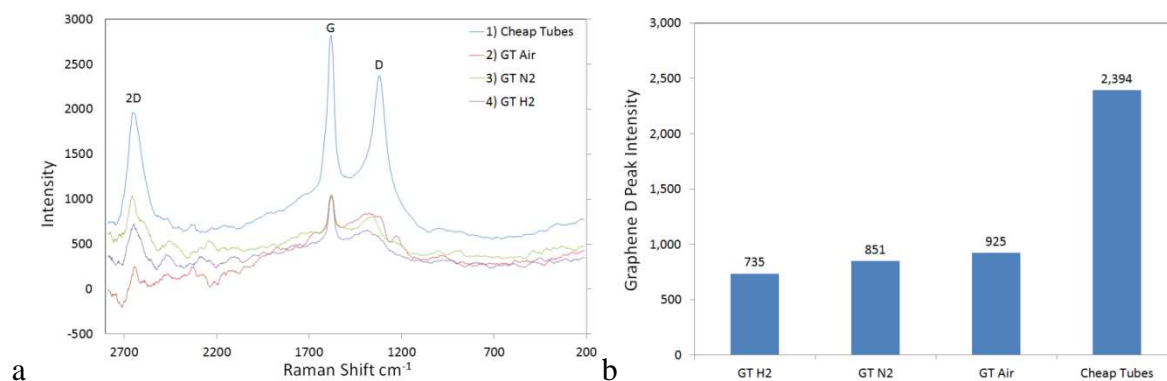


Figure 5-3 Raman spectra a) Listed from highest to lowest at the D peak b) Comparing D peak intensity of graphene produced using four different methods

5.3.3 Dynamic Mechanical Analysis

DMA (Figure 5-4) was used to compare SBS without graphene to SBS with graphene created by thermal reduction in various gases. At low temperatures (-120 °C) stored energy (tensile storage modulus) increased the most (+68 %) in SBS-graphene 1 %·w/w reduced in hydrogen compared to neat SBS which was the lowest. The increase in storage modulus indicated improved interfacial interactions with butadiene, suggesting the presence of weak hydrogen bonds $(\text{CH}/\pi)^{74}$.

At low temperatures (-120 °C) energy absorption (loss modulus) of SBS with GT-H₂ 1 % (+147 %) was highest compared to neat SBS (lowest). The increase in viscous properties (loss modulus) attributable to H₂ reduced graphene peaked at 2.43 GPa (-97.5 °C) compared with 1.69 GPa (-96.8 °C) for SBS. This peak represents T_g (glass transition temperature) for the butadiene phase and demonstrates that it was not affected by graphene. Unlike storage modulus which is elastic (responds instantly), loss modulus is time dependant and thus slower to respond. The viscous effect noted in the loss modulus occurs because adding graphene slows molecular response.

At low temperatures (-120 °C) damping ($\tan(\delta)$) of SBS elastomer with GT-H₂ 1 % (+47 %) was highest compared to neat SBS. The increase in $\tan \delta$ for GT-H₂ indicates a move to a more liquid state compared to neat SBS, which is in a more solid state.

At 25 °C, the storage modulus (+37 %) and loss modulus (+52 % energy lost as heat) of SBS-H₂ remained the highest compared to SBS-neat. However, damping ($\tan(\delta)$) increased the most with Cheap Tubes #2 graphene (+74 %). The increased damping of SBS with CT

graphenes, compared to GT graphenes suggests smaller sheet size (CT) might be a major performance feature at higher temperatures. However, if smaller sheet size is desired, longer ultrasonication, of GT graphenes, can be used to reduce sheet size⁴⁰.

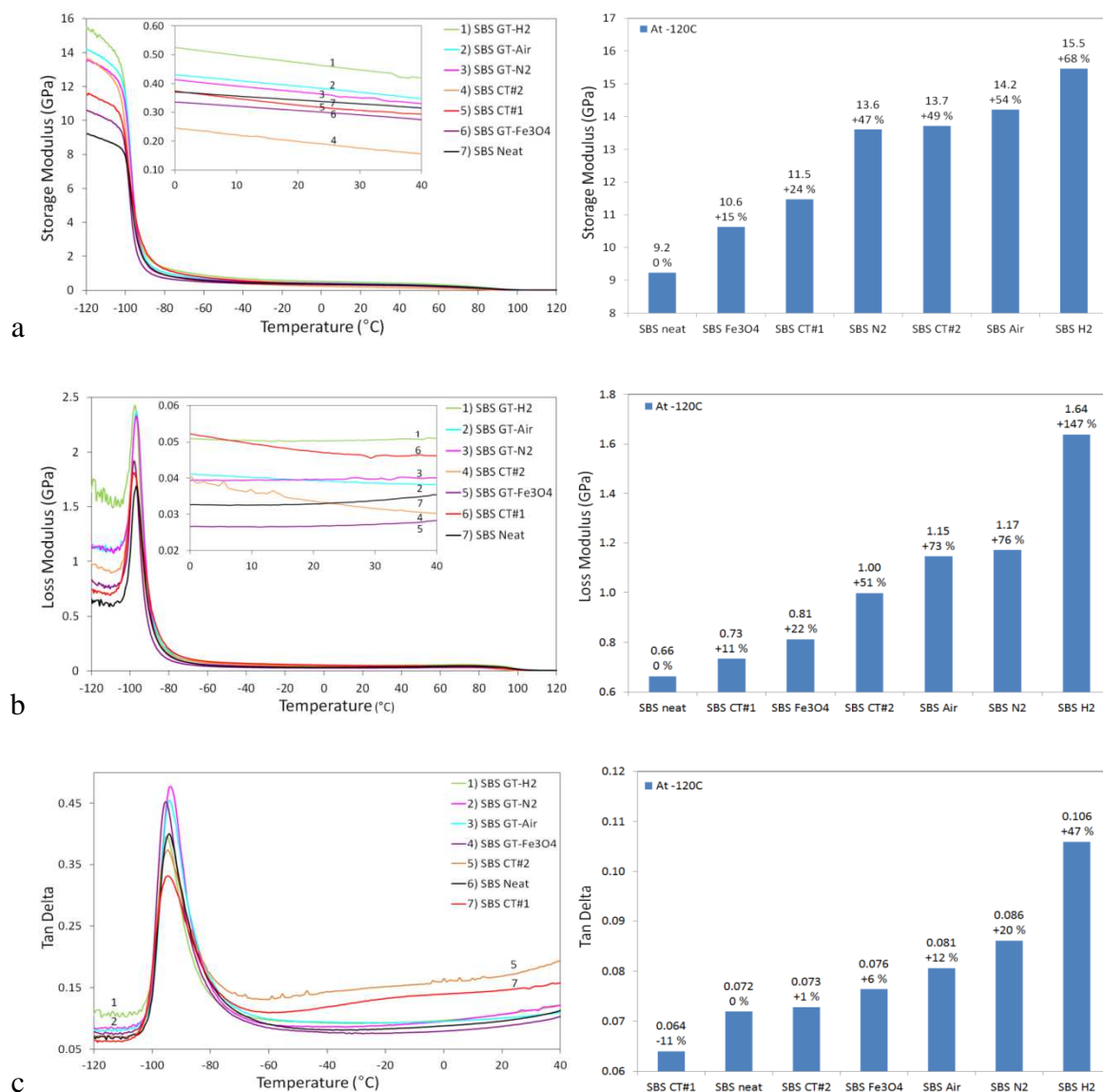


Figure 5-4 DMA of SBS-graphene 1 % composites a) Storage modulus b) Loss modulus c) Tan(δ) (Legend ordered at -120 °C highest to lowest)

In a similar study with styrene butadiene rubber (SBR) using covalent bonding of graphene, interfacial interactions with graphene increased while energy losses were decreased by reduced nanoscale friction between graphene sheets and rubber chains (due to relative slippage)¹⁹⁴. Thus the increased energy losses (loss modulus) with SBS GT-H₂ may be attributable to the differences in bonding (covalent versus non-covalent) and suggest

increased nanoscale friction between hydrogen reduced graphene sheets and the continuous phase of SBS (butadiene).

Graphene dispersion gave strong interactions (storage modulus) with the polymer to stabilise the dispersion against agglomeration. The modulus measured is due to the polybutadiene block which is the continuous phase while polystyrene block is dispersed as separated particles that bind the polybutadiene continuous phase. Styrene provides strength and rigidity to SBS, but any styrene π -interactions with graphene could not be considered since DMA scans cannot go into the polystyrene (PS) T_g region because SBS would become a liquid at the higher temperatures required.

5.3.4 Wide Angle X-ray Scattering

SBS-graphene composites display a series of well-resolved diffraction peaks superimposed on an amorphous background (Figure 5-5a). The peak of maximum intensity at $2\theta \sim 26.56^\circ$ is attributed to graphene⁹⁷. This peak corresponds to the 002 reflection (the plane in a crystal) of graphene¹⁴³ and is also the characteristic peak of pure graphite⁹⁷. Pure SBS has an amorphous halo at $\sim 19.60^\circ$ 2θ ¹⁹⁵. The diffraction patterns were similar for all SBS-graphene composites differing only in intensity. The tallest peak within the area of maximum intensity was the Cheap Tubes graphene whereas the pure SBS had no peak, as expected.

Each reflection is from a particular diffraction plane in the crystal. Therefore the composite with the greatest intensity for the 002 plane displays a preference for this crystal orientation (Figure 5-5b). The order of this preference is from (highest) 1) Cheap Tubes graphene 2) GT-Air (least processed) 3) GT-N₂ (an inert gas) 4) GT-H₂ (a reducing gas) 5) GT-Fe₃O₄ (to lowest). As single layer graphene has no layer stacking the reduction in intensity of the (002) peak implies a move towards single layer graphene.

Interlayer distance was measured using the Bragg law

$$\text{Equation } d = n\lambda/2\sin\theta \quad [1]$$

The interlayer distance of thermally exfoliated (GT) graphenes was higher than the comparable commercial (CT) graphene. After reduction with H₂ or surface modification with Fe₃O₄ (Magnetite), there was a slight decrease in interlayer distance. The highest interlayer distances were when using graphene prepared with air or N₂ atmospheres. The difference between the thermally produced (GT) and commercial (CT) graphenes may be a reflection of

the production method. Intercalation of the thermally exfoliated graphene (GT) is expected to increase the distance between graphene sheets. The results show that a reducing atmosphere of H₂ and surface modification with Fe₃O₄ decreased the interlayer distance of thermally exfoliated graphene compared to air or N₂. These small decreases probably reflect reductions in remaining intercalatants.

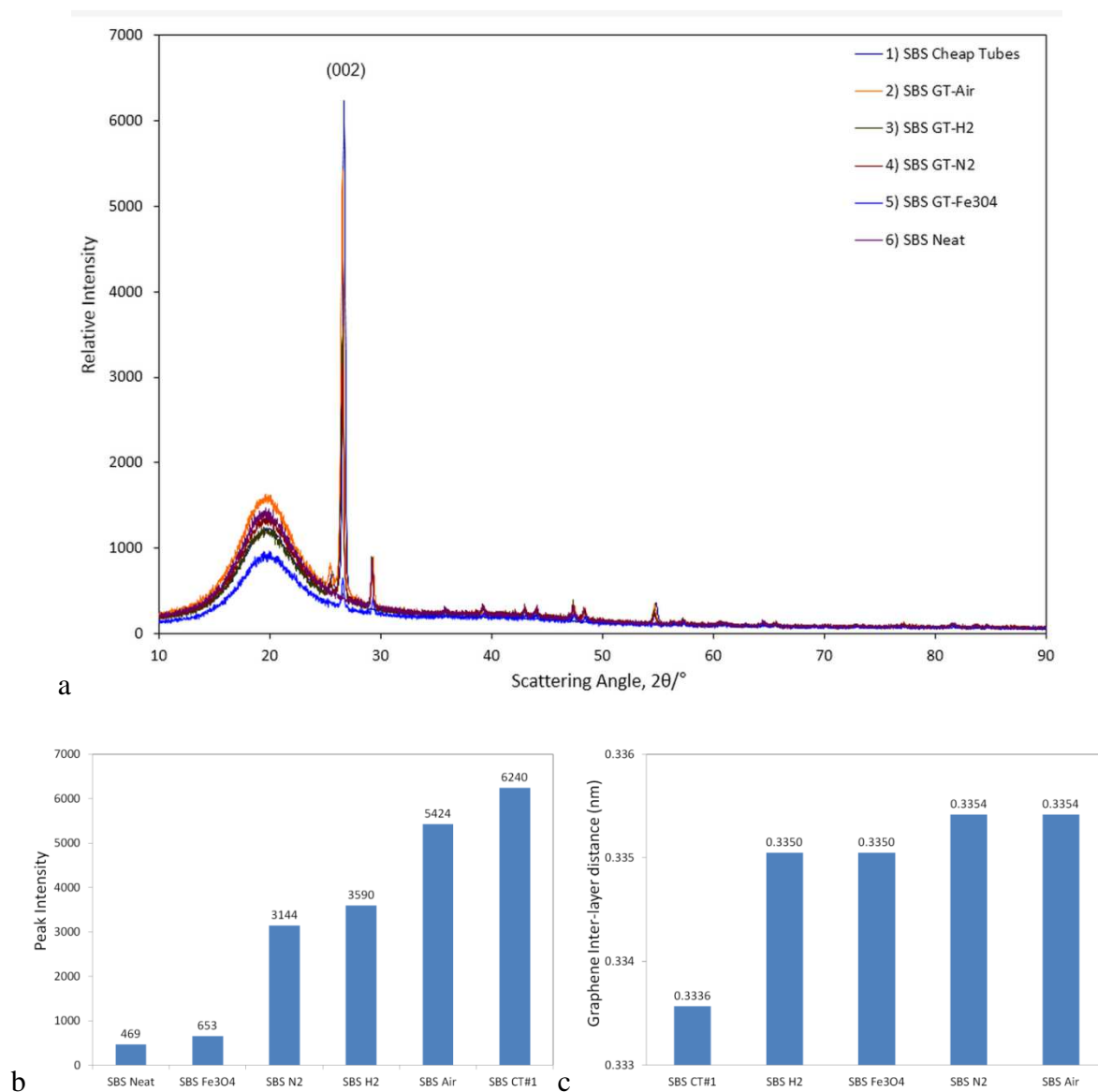


Figure 5-5 Diffractogram SBS-graphene composites a) Relative intensity versus scattering angle (listed in order of peak intensity) b) Graphene peak intensity c) Graphene interlayer distance

5.3.5 Thermal Stability

Thermal degradation of the SBS composites was measured using thermogravimetric analysis (TGA) (Figure 5-6). Thermogravimetry shows that degradation for all the SBS-graphene composites starts at ~ 350 °C, is greatest at ~ 474 °C (point of inflexion of the first derivative) and is completed by ~ 510 °C. SBS temperature of degradation is reduced by GT-Fe₃O₄ graphene and air expanded graphene (which has a poor Raman spectrum) while increasing when using graphenes with improved Raman spectra (GT-H₂, CT and GT-N₂). Often when multiple components are present (polystyrene, polybutadiene and graphene), the curve shows three deflections. Thus adding graphene to SBS does not significantly enhance the heat resistance of SBS. However, this is desirable as SBS already has a fairly high temperature of degradation i.e. low heat resistance makes moulding, disposal and reprocessing easier.

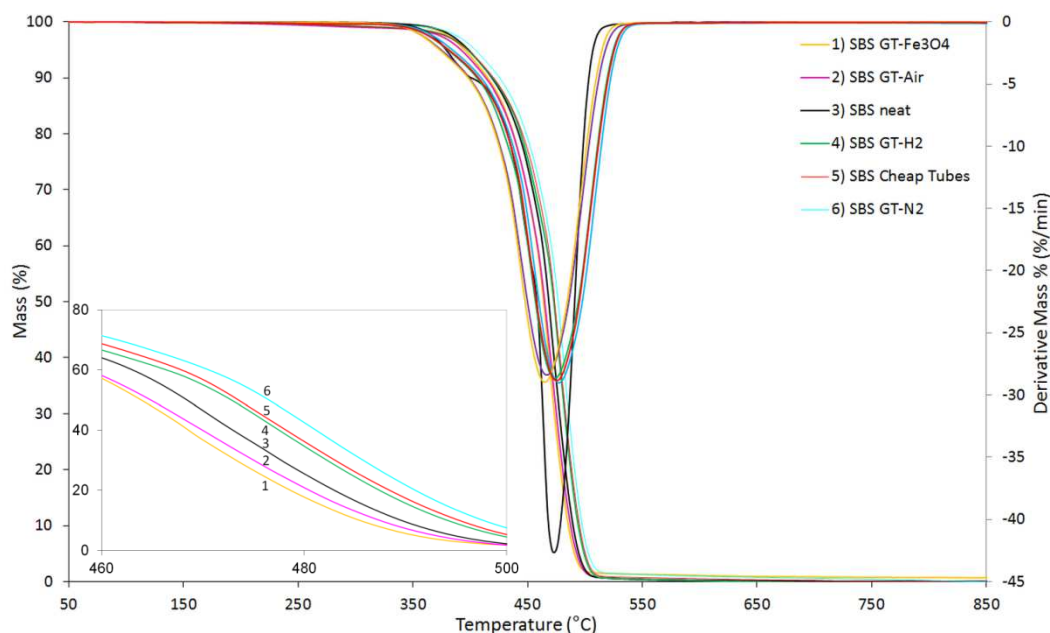


Figure 5-6 TGA mass versus temperature with the first derivative of SBS and graphene (1 %) composites created with GT and CT (listed in order of lowest to highest temperature of decomposition)

5.3.6 Electrical Properties

Electrical properties of SBS composites were measured to establish resistance and capacitance (Figure 5-7). Graphene and SBS were compatible due to π -interactions between their aromatic groups⁷⁴ resulting in uniform dispersion. The resistivity of neat SBS decreased with the addition of graphene at 1 %·w/w. The greatest decrease in resistance was achieved

with H₂ reduced graphene (-11 %). The capacitance of neat SBS was unchanged with GT-N₂ expanded and GT-Fe₃O₄ surface modified graphenes but increased with GT-H₂ reduced (+17 %), CT (+22 %) and GT-air expanded (+23 %) graphenes.

Conductivity (the inverse of resistance) at 1 %·w/w is low because the concentration has not reached the percolation threshold. Styrene in SBS is a dispersed phase in a continuous butadiene phase so graphene surrounded by styrene would not form a percolation network to enhance conductivity unless it was also distributed in the butadiene phase. The decrease in resistance shows that graphene dispersion is in the butadiene phase too.

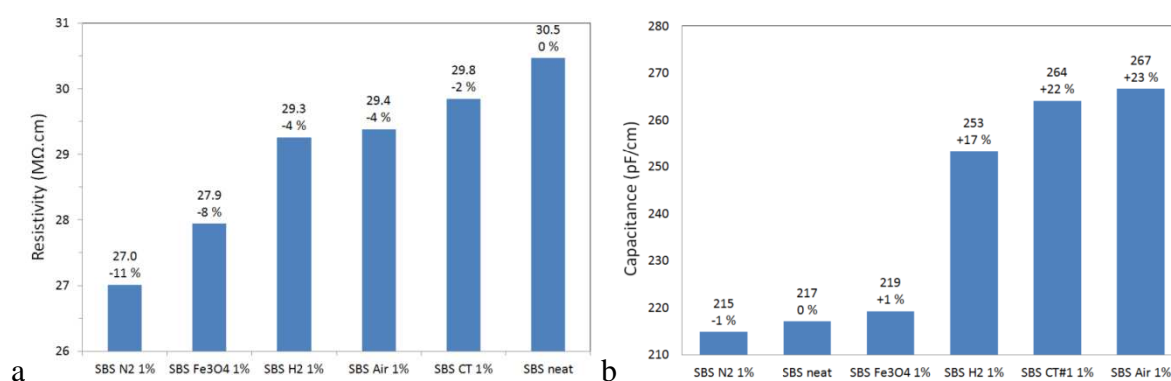


Figure 5-7 SBS-graphene composites a) Resistance b) Capacitance

5.3.7 Surface Modification

Graphene was functionalised with Fe₃O₄ (Figure 5-8) and its properties compared to neat SBS. DMA showed that at low temperatures (-120 °C) the stored energy (storage modulus) for SBS with GT-Fe₃O₄ 1 % was higher (+15 %) than neat SBS but lower than other types of graphenes in SBS. Absorbed energy (loss modulus) of SBS with GT-Fe₃O₄ was higher (+22 %) than SBS with CT#1 (+11 %) compared to neat SBS. Damping (tan delta) of SBS with GT-Fe₃O₄ was slightly higher (+6 %) than CT graphenes (CT#1 -11 % or CT#2 +1 %) when compared to neat SBS. At higher temperatures (25 °C) similar small increases were observed. WAXS results showed that SBS with GT-Fe₃O₄ had a peak intensity at 26.56° (653 relative intensity) which was the lowest of all graphenes, suggesting more single layer graphene. Interlayer spacing at 26.56° was not affected (0.3354 nm) and was the same as other GT graphenes. Thermogravimetry showed SBS with GT-Fe₃O₄ had the highest temperature of decomposition with a slight increase in temperature resistance.

Electrical measurements showed that resistance in SBS GT-Fe₃O₄ composites was slightly decreased (-8 % 27.9 MΩ.cm) compared to neat SBS (30.5 MΩ.cm), but capacitance of SBS GT-Fe₃O₄ barely increased (219 pF/cm) compared to neat SBS (217 pF/cm). TEM microscopy showed an even dispersion of Fe₃O₄ particles bonded to graphene which created a graphene responsive to magnetic fields. Except for magnetism measured SBS properties were less enhanced by GT-Fe₃O₄ graphene compared to other graphenes. However, as only 15 % of the mass fraction of GT-Fe₃O₄ was graphene (established by TGA), this explains why its performance was lower than expected.

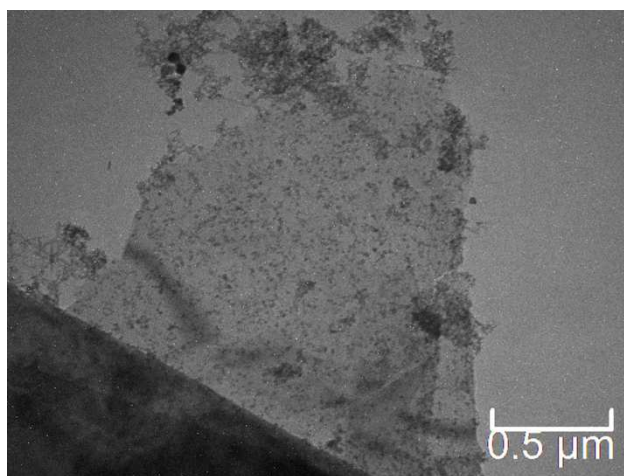


Figure 5-8 Microscopy (TEM) showing GT-Fe₃O₄ (Fe₃O₄ particles on a graphene sheet)

5.4 Conclusion

Graphene was formed by thermal expansion in air, inert N₂ and a reducing atmosphere. Sonication disrupted exfoliated structures dispersing in an aromatic liquid with dissolved SBS. The SBS solution-graphene dispersion was precipitated into a non-solvent to prevent flocculation that could occur with solvent evaporation.

SEM imaged graphene after expansion showing increased exfoliation and decreased width after sonication. Raman spectroscopy showed that in a H₂ reducing atmosphere the reduced graphene had the fewest defects. WAXS showed the diffraction due to thermally exfoliated graphene layers at ~26.56° ~0.335 nm demonstrating that not all graphene was single layer. DMA showed the polybutadiene continuous phase had an increased storage (elastic) modulus, loss modulus and damping with graphene added. It indicated that interfacial interactions and energy loss were greatest when using hydrogen reduced graphene. It showed damping was highest at low temperatures when graphenes were largest but at higher

temperatures smaller graphenes improved damping. SBS mass loss temperatures were unchanged with graphene. The percolation threshold was not reached to enhance conductivity. The surface of graphene was modified by formation of Fe_3O_4 by solution precipitation adding the property of magnetism.

These results demonstrate that π -interactions between SBS and graphene facilitate their dispersion.

Chapter 6 Carbon Monoxide Reduced Low-Defect Graphene Nanocomposites with Poly(styrene-*b*-butadiene-*b*-styrene)

6.1 Introduction

SBS is a block copolymer, thermoplastic elastomer used in adhesives, sealants and moulded or extruded products where flexibility and toughness are desirable. Fillers, such as carbon black, are added to SBS to increase toughness, reduce creep and permanent set. Graphene is a single layer of hexagonally bonded carbon atoms with high modulus, strength and conductivity^{2, 4, 24}. These are desirable properties to incorporate into a polymer. Graphene has high surface area per unit mass and extremely high aspect ratio, and these are expected to provide enhancement of SBS even when included in low volume fractions. The polystyrene block physical crosslinks in SBS are proposed to selectively adsorb onto graphene, increasing the dimensional stability of the SBS.

Most research into graphene polymer composites has concentrated on covalent bonding of graphenes with the chosen polymer matrix²². To achieve this, oxides (hydroxides, peroxides, carbonyls or carboxyls)¹⁹⁶ are added on to graphene to provide sites for bonding. However, these functional groups interrupt the perfect sp^2 matrix of graphene creating defects. Most methods of graphene production result in many voids, also a type of defect. It is common for graphenes to contain up to 40 % of such defects^{30, 145}. Even reduced graphene includes such defects³⁶. It is generally accepted that it is not possible to reinforce a polymer with graphene without these imperfections. However, a graphene production method such as thermal expansion removes most functional group defects¹⁹⁷. Additionally, π -interactions with a solvent can assist the dispersion of graphenes, eliminating the need to use covalent bonding¹⁹⁸. In previous research, it was demonstrated that such a reinforcing approach was possible with SBS¹⁸¹. However, research suggests that the mechanical percolation threshold for exfoliated graphite and graphenes in a polymer is 2-3 %·w/w¹⁹⁹⁻²⁰¹.

The aim of the research described in this chapter was to use CO reduced graphene to establish whether dispersion and reinforcement of SBS could be achieved at up to 20 %·w/w graphene with only π -interactions to bind SBS to graphene while maintaining the perfect sp^2 structure of a low defect graphene.

6.2 Experimental

Material information, preparation of nanocomposites and characterisation methods are detailed in Chapter 3.

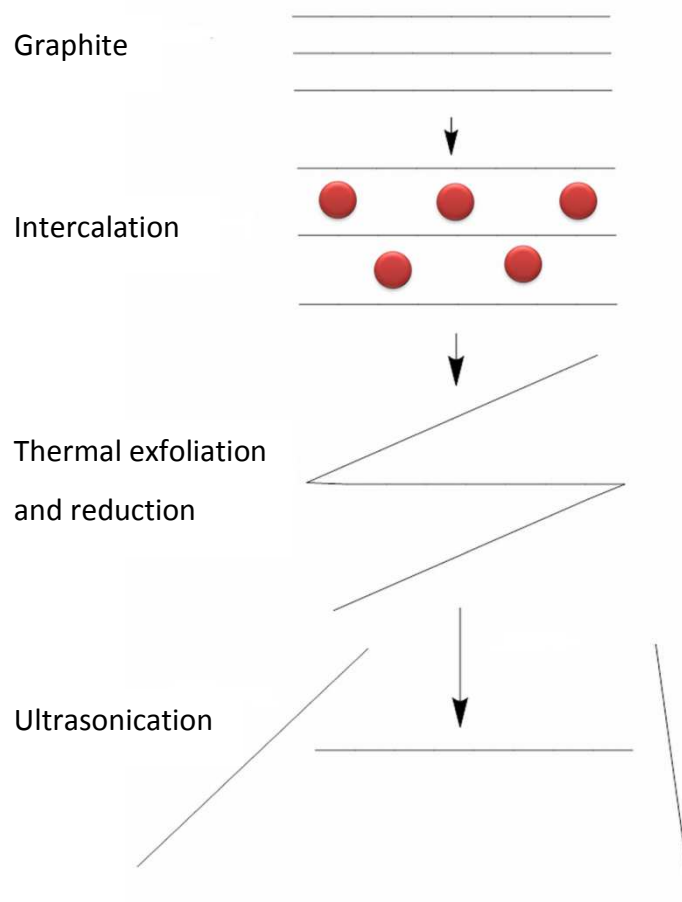


Figure 6-1 Graphene production by intercalation, thermal exfoliation with reduction and ultrasonication (simplified)

6.3 Results and Discussion

SBS was dissolved, and graphene dispersed using benzene, a solvent chosen for its potential π -electron interactions with polycyclic aromatic graphene structures⁷⁴ and because benzene-like carbons (those attached to a hydrogen) can increase the magnitude of π - π stacking interactions significantly⁷³. This solvent was found to assist suspension and dispersion of the graphenes, while ultrasonication was found to increase graphene interlayer exfoliation. Rapid precipitation of the composite into methanol prevented graphene agglomeration.

6.3.1 Vibrational Spectroscopy

Raman spectroscopy is the characterisation method of choice for graphenes. Raman spectroscopy involves the inelastic scattering of light: one frequency is input, but a different frequency is output and measured. Raman spectroscopy measures rotational, vibrational and similar low-frequency modes of the covalent bonds between molecules. Raman spectroscopy is particularly sensitive to any phenomenon that disrupts the symmetry of sp^2 carbons. The Raman spectra of graphene contain three characteristic peaks: D, G and 2D. The D peak occurs when there are defects in the graphene matrix. The G peak is caused by in-plane vibration of the sp^2 bonds in graphene. The 2D peak is the second order of the D peak. The 2D peak is influenced by strain, intercalates and charged impurities. A single symmetrical 2D peak indicates a single layer or few layer graphene.

Three types of graphenes were compared: a commercial graphene (CT), air expanded graphene (GT-Air) and CO reduced graphene (GT-CO). The commercial graphene (CT) provided a baseline for comparison as it had been characterised by HDPlas (the manufacturer) and had the largest defect peak. The defect peaks of both the thermally expanded graphenes (GT-Air and GT-CO) were lower. The G peak was similar between the CT and GT-CO graphenes suggesting the same sp^2 structure. The 2D peak of GT-CO was more intense and sharper than CT graphene indicating single or few layer graphene (Figure 6-2a).

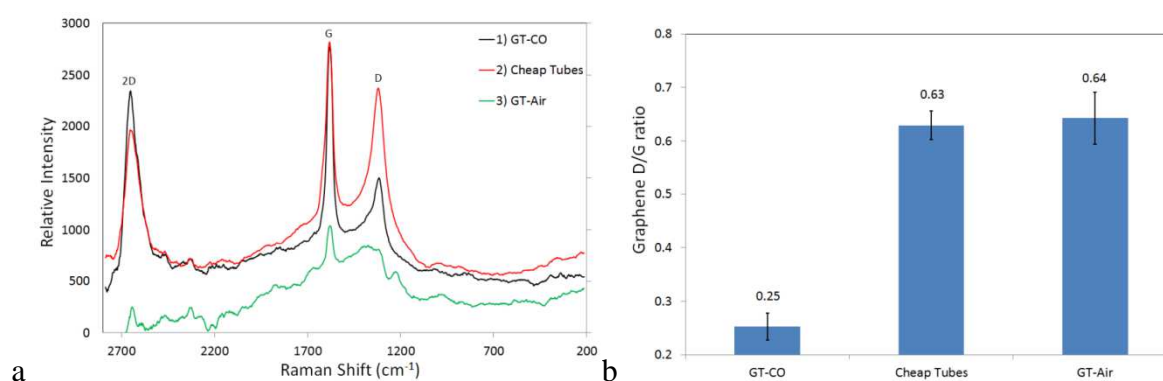


Figure 6-2 Raman spectra of graphene a) Listed in order of 2D peak b) D/G ratio

To quantify these differences more precisely a ratio of the D/G peaks was calculated. The GT-CO graphene had the lowest D/G ratio (0.25) while the CT (0.63) and GT-Air (0.64) had much higher ratios (Figure 6-2b). A low D/G ratio indicates the GT-CO is a low defect graphene.

The number of graphene layers was measured using the $2D/G^{81}$ ratio where an increasing number means fewer graphene layers. The $2D/G$ ratio of GT-CO (0.76) was higher than CT (0.63) signifying fewer layers which are highly desirable.

6.3.2 Thermal Stability

Thermogravimetry (TGA) (Figure 6-3) was used to measure thermal stability. Oxygen-containing groups (-OH, -O-, -COOH and =O) on graphene have low thermal stability. Heating in an inert nitrogen (N_2) environment removes these oxide groups. Thus the mass loss in a TGA can be used to measure the oxygen-containing groups on the surface of graphene.

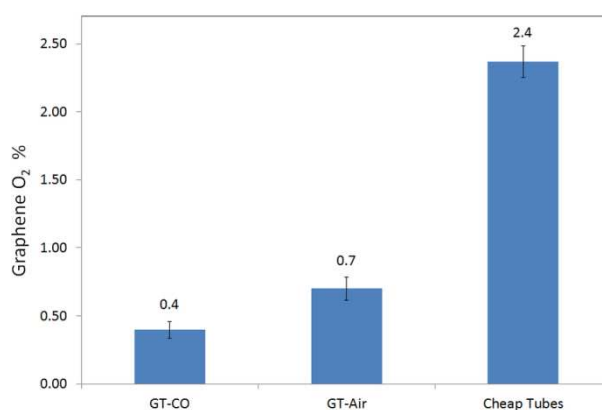


Figure 6-3 TGA of graphene mass loss (oxygen content) versus production method

TGA measured oxide levels by mass loss were 2.4 % for CT, 0.7 % for GT-Air and 0.4 % for GT-CO. The GT-CO had 84 % fewer oxide groups than the commercial graphene (CT). Low oxide content indicates a low defect graphene.

6.3.3 Microscopy

Electron microscopy (Figure 6-4) was used to characterise graphenes and poly(styrene-*b*-butadiene-*b*-styrene)-graphene composites. It was used to confirm the quality of the graphene and reveal detail about the structure of SBS-graphene composites.

Transmission electron microscopy (TEM) was required to resolve individual graphene layers. Individual graphene layers are often difficult to distinguish in a polymer. Graphenes usually cannot be identified if oriented edgewise in a specimen. Graphene without any supporting polymer is challenging to resolve as it tends to agglomerate. Agglomeration is minimised with sufficient dilution in an appropriate liquid with subsequent rapid evaporation.

Graphene images were collected at high resolution in SBS and after dispersing graphene in a solvent with ultrasonication. Both images showed that GT-CO graphene had a tendency to form scrolls although this was not a dominant feature. Both images show single layers of graphene with no visible defects.

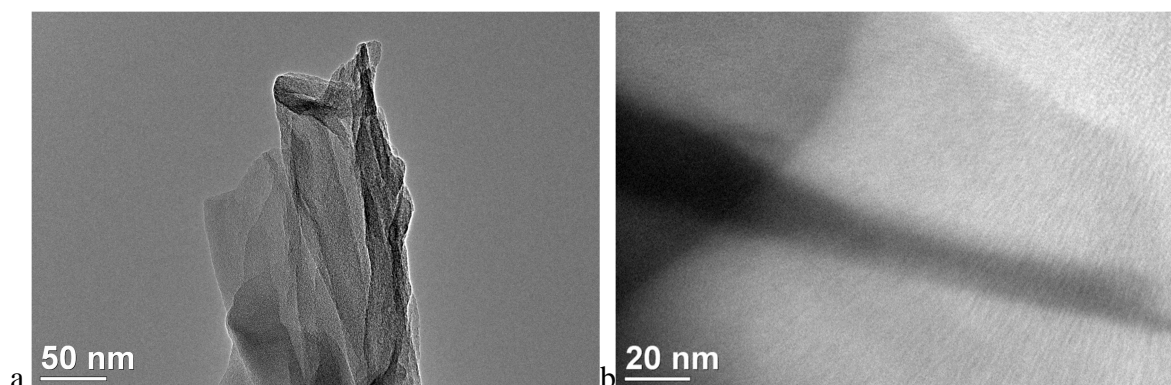


Figure 6-4 TEM JEOL 2100 graphene a) GT-CO b) SBS 1 % GT-CO

The TEM images show that single layer graphene existed before dispersion in SBS and that the single layers existed after dispersion in the SBS. This dispersion was aided by π -interactions.

6.3.4 Mechanical Properties

Stress-strain tensile mechanical analysis (TMA) was used for characterising and comparing the mechanical performance of SBS and the graphene nanocomposites. Enhancements in performance were detected, measured and graphically represented. TMA was used to measure stress-strain as a stress was increased and then decreased forming a hysteresis curve (Figure 6-5a). A hysteresis curve provides extra information about the reversible performance of the materials.

Tangent modulus (a measurement at a single point) was used because the line was curved (no linear region). It was measured from the initial area of the stress-strain curve (0.25 % strain) to avoid changes in cross-sectional area and length²⁰². The results show that at a strain of 0.25 % tangent modulus increased by up to 100 % (0.72 MPa) when graphene loading was 20 %·w/w (Figure 6-5b). Thus, the stiffness of SBS-graphene composites continued to increase as the GT-CO loading increased.

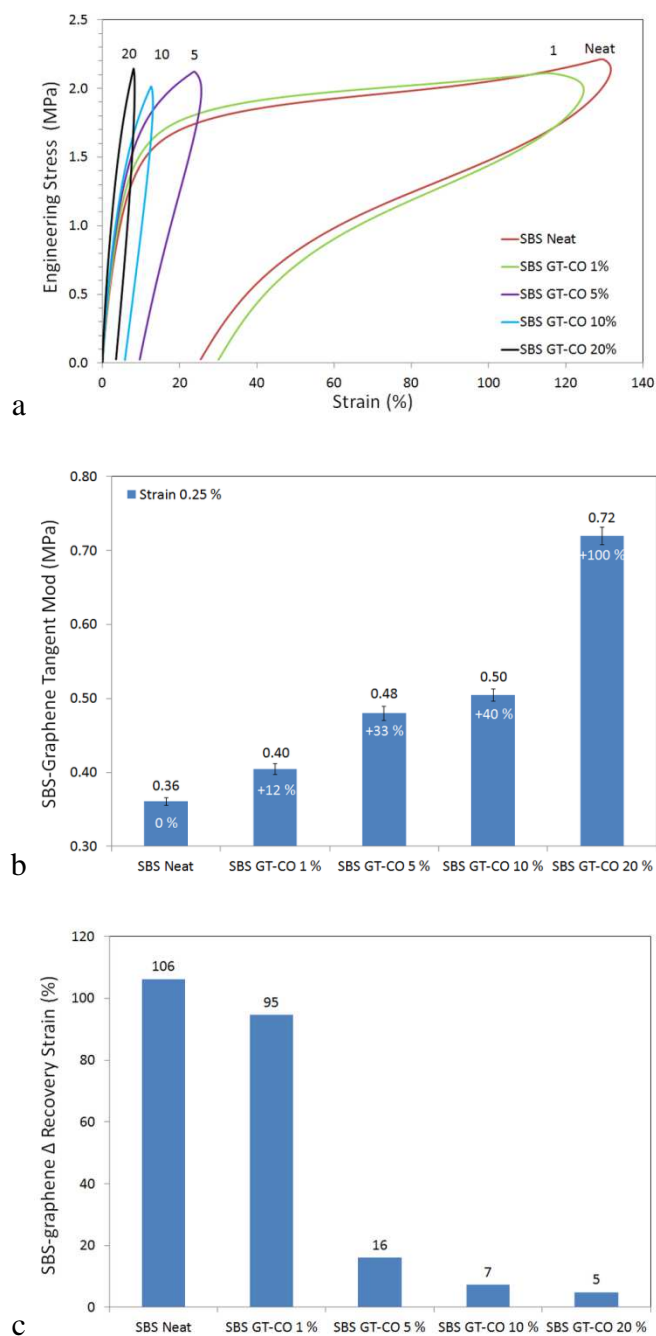


Figure 6-5 TMA of SBS GT-CO (0-20 % w/w) at room temperature (25 °C) a) engineering stress versus strain b) tangent modulus at 0.25 % strain c) change in recovery strain

Strain (%) measures the deformation of the polymer at a fixed force. As force was ramped to 11 N Engineering Stress (Force (N)/area (m²)) was calculated using the cross-sectional area (width x thickness) of the composite. The strain on recovery (Max strain – Final strain) was compared. It was found that recovery decreased from 106 % in neat SBS to only 5 % (-101 %) in SBS GT-CO 20 % (Figure 6-5c). Thus, deformation decreased as graphene

content increased. However, as ultrasonication times were static, it is likely that further improvements could be achieved if ultrasonication times were increased in a linear fashion.

6.3.5 Dispersion

DFT calculations were used to determine how SBS monomer interacts with the graphene sheet (Figure 6-6). The *ab initio* molecular dynamics simulations showed that the binding energy (BE) between the graphene and SBS was almost identical after 2.5 ps (-0.81 eV) and 5 ps (-0.78 eV) simulation time. The almost identical binding energy indicates the structure has reached equilibrium. The two adsorption geometries are not identical which shows that the polymer can take multiple forms on the graphene.

Overall the shortest distances between SBS and graphene as measured between the closest carbon atom on graphene (C_g) and a hydrogen atom on SBS (H_p) (0.249 nm) and a carbon atom on graphene and carbon atom on SBS (C_p) (0.329 nm), changed by only 0.002 nm during this time. These small changes indicate that the polymer remains at a similar distance above the graphene while allowing minor changes to its geometry. The magnitude of the adsorption distances and binding energy values indicate the SBS is weakly adsorbed on the graphene. The SBS ring structure is either aligned above the graphene in an AB or AA stacking geometry. However, it is worth noting that the plane of the ring does not lie parallel to the graphene as the butadiene group also interacts with the graphene.

The closest distance between an SBS hydrogen and graphene is 32 % closer than the closest SBS carbon. The side view shows that some SBS hydrogen atoms are oriented above the graphene sheet, suggesting there is an affinity between these atoms and graphene (Figure 6-7). The suggestion of a particular hydrogen affinity is consistent with previous calculations showing that hydrogen increases the binding strength of aromatic interactions (SBS has five hydrogen atoms on its aromatic rings)⁷³.

At 2.5 ps the aromatic ring in the SBS monomer is slightly rotated compared to the graphene ring below. At 5 ps the aromatic ring in the SBS is offset to the graphene in a similar fashion to the AB stacking of graphite⁸. Such skewed or offset stacking of the aromatic rings is common in aromatic π -interactions where π - σ attraction dominates⁷⁴.

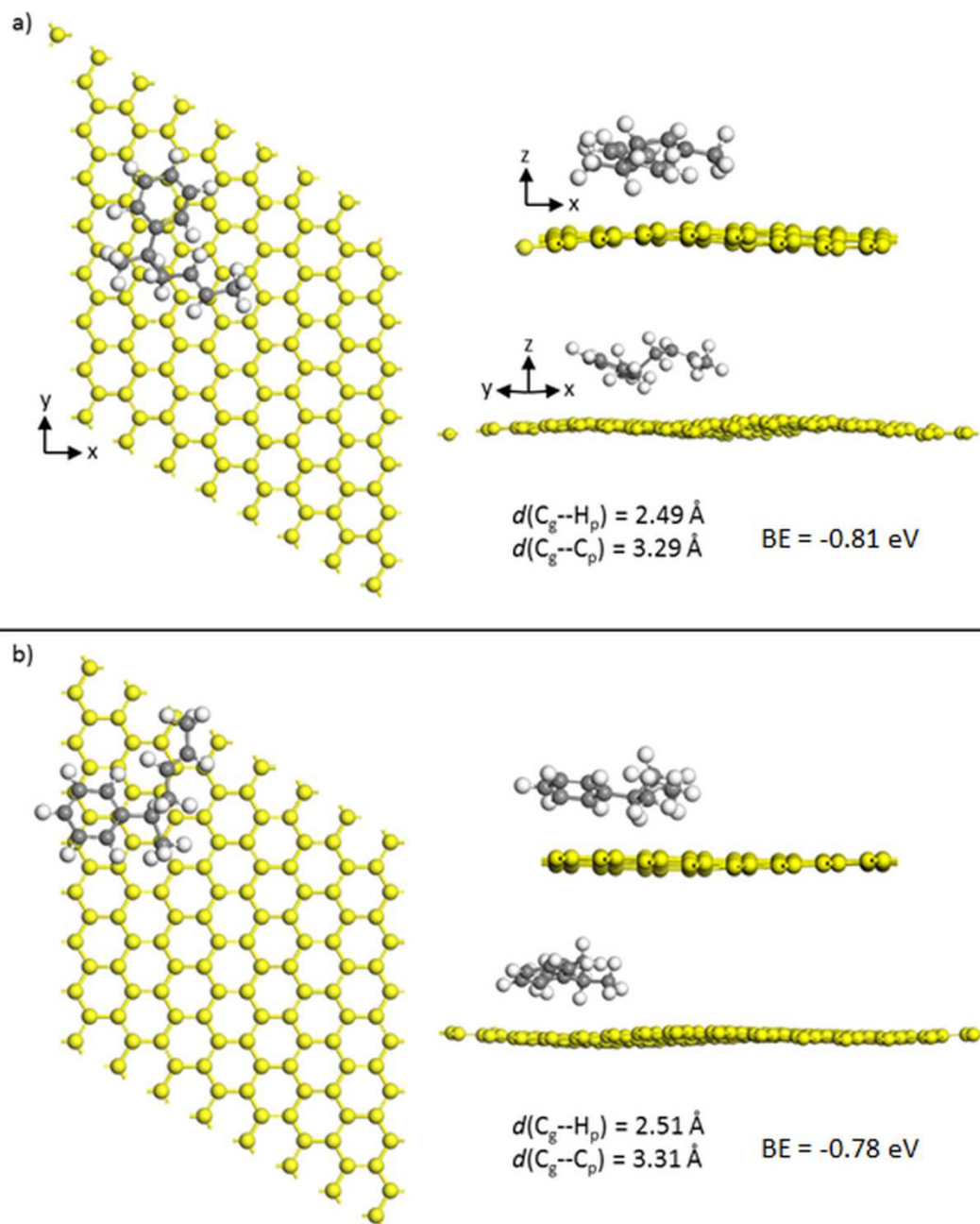


Figure 6-6 Optimised structures of SBS monomer adsorbed on graphene after a simulation time of a) 2.5 ps b) 5 ps

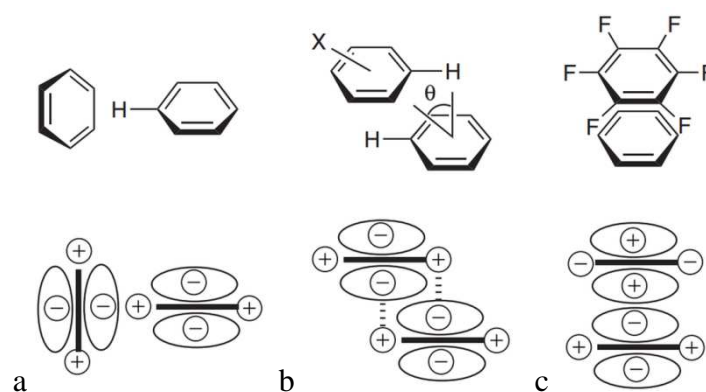


Figure 6-7 Aromatic interaction geometries a) Edge to face (aka T-shaped or edge on) b) offset face-to-face (aka slipped or skewed) c) face-to-face (aka eclipsed)^{74, 203, 204}

6.4 Interpretation

Low defect graphene (GT-CO) is of particular interest to explore and extend the unique properties of graphene because reduced graphene typically continues to contain functional groups (defects)³⁶. Reduced graphenes and low defect graphenes behave differently because of these differences. Hence the production of composites with low defect graphene will result in enhanced properties potentially broadening their uses in nanocomposites, electronics (e.g. capacitors⁶⁷, dielectrics²⁰⁵) and filtration²⁰⁶.

π -Interactions capable of dispersing graphenes up to a loading of 20 %·w/w provide an advantageous route to the dispersion of graphenes in aromatic liquids, polymers and related products. Given that hydration of graphene prevents it restacking into graphite¹⁴⁰ it is likely that aromatic polymers would likewise prevent the restacking of graphene, and much higher concentrations are possible.

6.5 Conclusions

Low defect graphene prepared by carbon monoxide reduction of a thermally expanded graphene was combined with SBS to create composites. The loading of the GT-CO was varied from 0 – 20 %·w/w with π -interactions to preserve the sp^2 matrix of the graphene. The use of low defect graphene, as verified by few oxides (TGA) and low D/G ratio (Raman), means that only π -interactions are necessary for graphene-polymer bonding. The effectiveness of the dispersion was demonstrated by the performance of the SBS that was positively affected by the GT-CO: deformation (recovery strain) decreased with 20 %·w/w GT-CO as stiffness increased. The existence of single layer graphene in SBS, with some

scrolling, was verified using TEM. The interaction between SBS and graphene was shown using DFT calculations which also suggested the existence of hydrogen bonding between the SBS and graphene and was consistent with hydrogen atoms increasing the strength of aromatic interactions.

Creation and dispersion of graphene with low defects is noteworthy. Thermal expansion in a reducing carbon monoxide atmosphere is an efficient and effective means to produce high-quality graphene, that is solution or melt dispersible in thermoplastics such as SBS. Longer ultrasonication at higher graphene loading would further improve performance.

Chapter 7 Hydrogen Reduced Low-Defect Graphene with Poly(ethylene terephthalate) Composites

7.1 Introduction

In this chapter, the preparation of poly(ethylene terephthalate) PET-graphene composites using solvent and melt dispersion is described (Figure 7-1). PET is a high-performance commodity; it is a semi-crystalline thermoplastic employed in bottles, films, fibres and moulded products. It is produced by the polymerisation of ethylene glycol and terephthalic acid. Its repeating group contains one aromatic ring and two ester (R-CO-O-R') groups. Polymer-graphene composites have the ability to enhance the properties of the polymer.

The dispersion of graphene in polymers is considered a major challenge. The most common method to enhance graphene dispersion is functionalisation (which requires the production of defects). However, the creation of defects can be avoided by using π -interactions²⁹ to disperse graphene²⁰⁷. There are many π -interactions compared to covalent bonds: π -interactions are considered to include ionic and hydrogen bonds⁷⁴. However weak forces are additive and can be quite strong jointly²⁰⁸. Thus using π -interactions, the final composite can retain low defect graphene and optimise properties. SBS-graphene composites have demonstrated that when the polymer and solvent both have aromatic rings graphenes (which have many aromatic rings) disperse well¹⁸¹. Platelet composites with PET were proposed to constrain gas permeation and to enhance modulus and creep resistance of thin container walls and films.

Thus the aim was to prepare composites of low defect graphene with PET using dispersion by sonication of solution (solvent dispersion (SD), using o-chlorophenol as solvent) and high torque melt shear (melt dispersion (MD)), characterising structure and morphology, measuring properties and comparing the composites according to dispersion technique.

7.2 Experimental

Material information, blend preparation procedures, and characterisation methods are detailed in Chapter 3.

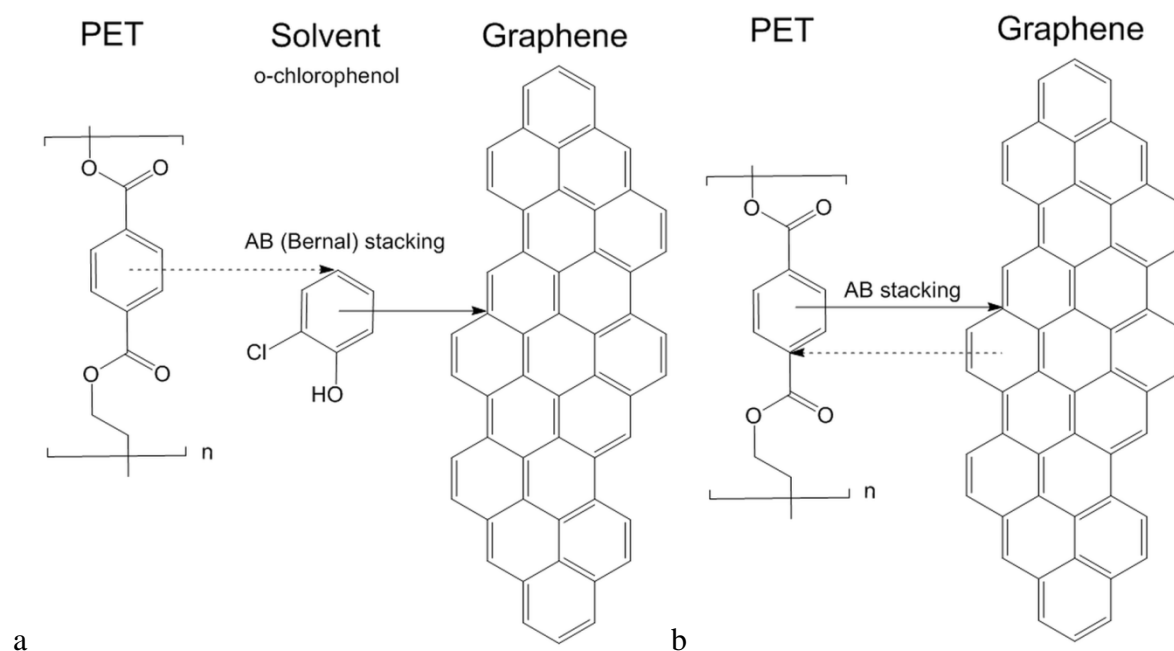


Figure 7-1 Poly(ethylene terephthalate) and graphene showing DFT preferred van der Waal AB- π stacking geometry a) in solution b) without solvent

7.3 Results and Discussion

7.3.1 Vibrational Spectroscopy

Raman spectroscopy was used to characterise the number of layers and the defects in graphene. Thermally expanded and H_2 reduced graphene was compared with Cheap Tubes graphene of the highest research grade available.

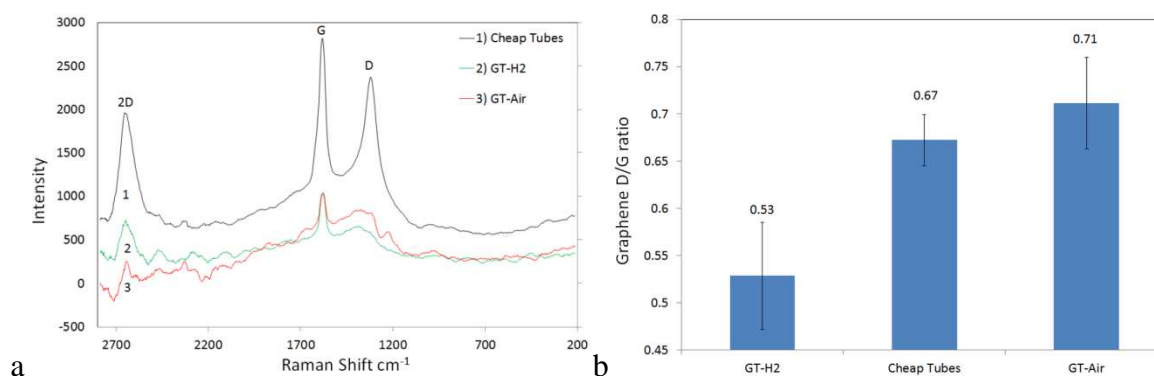


Figure 7-2 Raman spectra comparing a) CT research grade graphene, GT- H_2 reduced graphene and GT-Air expanded graphene (listed in order of the 2D peak) b) D/G ratio of graphenes (calculated from unsmoothed data)

The GT-H₂ graphene (Figure 7-2) shows a robust G peak, low D (defect) peak and a 2D peak: The 2D peak is the second order of the D peak. The 2D peak is strongly influenced by intercalants, charged impurities and strain. Single layer graphene is indicated by a single symmetrical 2D peak⁸³. CT graphene showed a clear single layer 2D peak at 2654 cm⁻¹ signifying a single layer graphene. The 2D peak shape of the GT-H₂ reduced graphene suggests that shoulders may be present indicating few layer graphene (smoothed with 15 point moving average).

Defects in graphene are most objectively compared using the D/G ratio¹⁸³. Comparing the materials shows that GT-H₂ graphene has a lower defect ratio (0.53) than that of the CT (highest quality research grade) graphene (0.67). GT-Air graphene had only a marginally higher D/G (0.71). Graphene with defects often has 40 % of its surface affected by the defects³⁰. Defects will significantly influence the performance of graphene. Thus low defect graphene would be expected to outperform high defect graphene.

7.3.2 WAXS

Wide-angle X-ray scattering (WAXS) is commonly used to establish the crystallinity, crystal size and interlayer distances of polymers and other crystalline structures. Graphite and few layer graphene both have identical crystalline structures (with a differing number of layers). Graphite has a characteristic reflection at 002 which is found at $2\theta \sim 26^\circ$ but the interlayer spacing, and thus 2θ , varies widely if intercalants are present ($0.333^{18} \sim 0.91 \text{ nm}^{41, 183}$). Graphene has also been described in this range^{97, 209, 210} and the crystalline peak of maximum intensity in the PET-graphene composites is found in this range (Figure 7-3a). Few-layer graphene will have a weak reflection and thus will be difficult to identify using WAXS. Single layer graphene is not crystalline and thus cannot be measured by WAXS. The four tallest peaks (16.4° , 17.9° , 23.0° and 26.3°) are characteristic of PET²¹¹.

Maximum peak intensity was lowest in PET-Neat MD (26.3°). PET with graphene (26.7°) increased the peak intensity significantly indicating increased crystallinity and that some un-exfoliated graphene exists. The peak intensity for graphenes differed by only 2 % (11,910 MD versus 11,657 SD) making it difficult to differentiate between them.

Interlayer spacing of PET-graphene composites was measured at the 002 peak using the Bragg equation

$$d = n\lambda/2\sin\theta \quad [1]$$

Where d is the interlayer distance, n is the order of reflection an integer (assume 1), λ (nm) is the wavelength of the x-ray source, and θ is the Bragg angle^{163, 212}.

Interlayer spacing was 0.339 nm for PET 0 % MD, 0.334 nm for PET 1 % MD and 0.333 nm for PET 1 % SD. The narrow gaps (0.334 versus 0.333 nm) mean there were no intercalating oxides present confirming effectual reduction.

Crystallinity (X_c) of the PET composites was calculated by measuring the intensity (I) of crystalline (c) and amorphous (a) regions

$$X_c = I_c / (I_c + I_a) \quad [2]$$

Crystallinity was highest for PET neat MD (33.0 %) with PET 1 % MD (28.7 %) and PET 1 % SD (29.6 %) both being lower. While this is only a small reduction in crystallinity, it shows that low defect graphene does not encourage PET nucleation.

The crystalline thickness of PET perpendicular to the reflection of the plane $L_{(hkl)}$ was calculated using the Scherrer equation.

$$L_{(hkl)} = K\lambda / (\beta_o \cos\theta) \quad [3]$$

Where K is the shape factor of crystalline thickness (normally 0.9), λ is the wavelength of the x-ray source (nm), β_o (radian) is full width at half maxima (FWHM), and θ is the Bragg angle^{163, 212}.

Compared to PET-Neat MD (14.8 nm) PET 1 %, MD (14.5 nm) crystalline structures had slightly smaller dimensions, and PET 1 % SD (15.8 nm) had slightly larger dimensions. The negligible increase in crystal size (+1 nm) of the SD composite demonstrated increased surface area, due to ultrasonication, did not affect nucleation.

Other research has found that graphene oxide provides a starting point for nucleation that can lead to an increase in crystal size and crystallinity similar to that found with multiwall carbon nanotubes (MWCNT)²¹³. Such research has found the nucleation effect was stronger for graphene oxide, the crystals were smaller, the π - π interactions were stronger, and the crystals were more perfect than for MWCNT²¹⁴. The nucleation effect was expected to increase as graphene loading increased²¹⁵.

These results demonstrate that low defect graphene behaves differently to high defect (high oxide) graphene in PET and may be particularly useful where a lack of nucleation is desired.

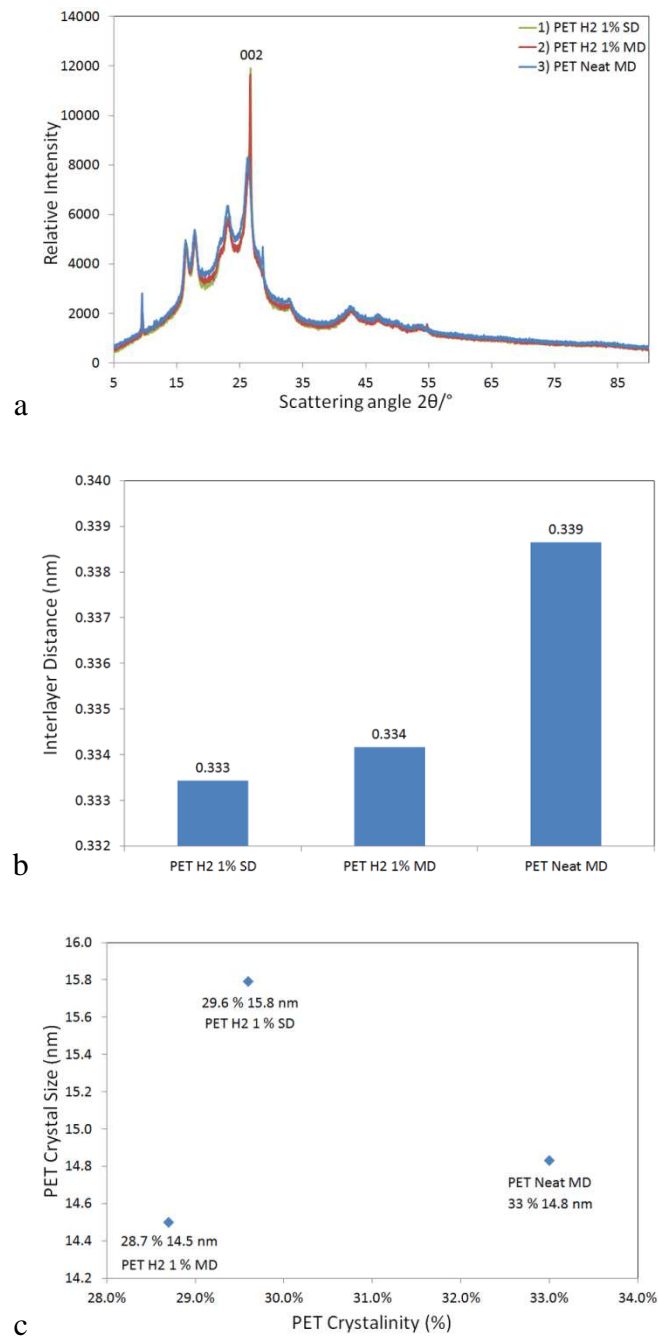


Figure 7-3 PET a) WAXS (ordered by peak intensity) b) Interlayer distances c) Crystallinity versus crystal size

7.3.3 Microscopy

PET composites fractured in N₂ (Figure 7-4) showed PET-Neat MD had a smooth surface with some raised fracture contours, PET 1 % MD had a smoother surface with fewer fracture contours (suggesting fewer graphene interactions) and PET 1 % SD had many raised fracture

contours signifying more graphene interactions (good interfacial bonding). Note the presence of reinforcing glass fibre in the first image.

The primary differentiating feature of the solvent dispersed (SD) composites is that the ultrasonication of the graphene gave better separated expanded graphene flakes. The ultrasonication increased the surface area available for interaction with PET and will result in more interfaces within the PET.

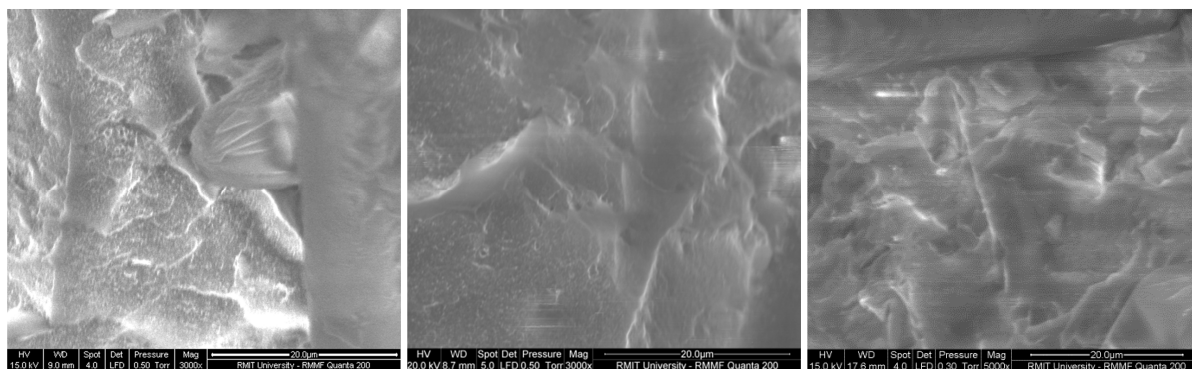


Figure 7-4 SEM images with 20 µm scale a) PET-Neat MD b) PET 1 % MD c) PET 1 % SD (left to right)

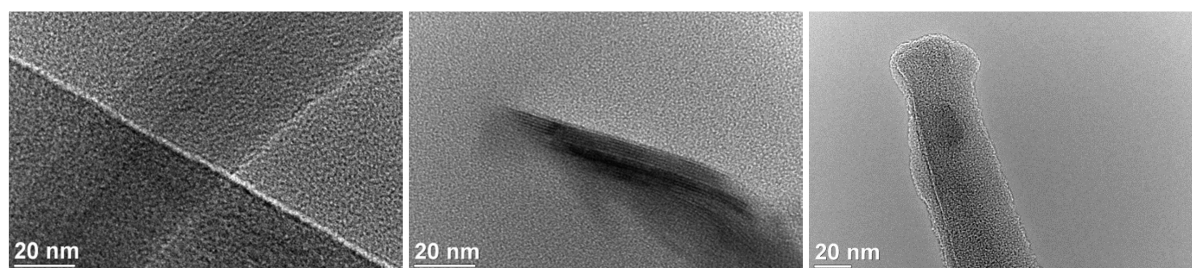


Figure 7-5 TEM images with 20 nm scale a) PET-Neat MD b) PET 1 % MD c) PET 1 % SD (left to right)

PET composites were compared to highlight graphene dispersal. Figure 7-5a shows a homogenous layer of PET lying on a second layer and with the copper grid visible underneath. In Figure 7-5b PET 1 % MD contained some visible multi-layer graphene. In Figure 7-5c PET 1 % SD no multi-layer graphene was visible and single layer graphene was hard to identify.

The MD graphene was included without ultrasonication to establish how effectively the melt mixing process separated the graphenes. It is clear that the ultrasonicated graphene significantly enhanced separation of graphene layers and facilitated dispersion in the PET.

Graphenes are only ~ 0.12 nm thick if oriented edge and the distance between individual molecular layers is ~ 0.36 nm. When a composite is melted and pressed, the nanocomposites tend to orient in-plane. The PET sheets were cut perpendicular to the surface. Thus any graphenes should be mostly edge on minimising the visible surfaces.

7.3.4 Mechanical Properties

7.3.4.1 Tensile Mechanical Analysis

Stress-strain tensile mechanical analysis (SS-MA) was used to compare the mechanical properties of the three composites using a ramped force of up to 18 N (Figure 7-6). Strain (L_t/L_0 % final versus original length) of the three composites was compared. PET-Neat MD (0.23 % strain) and the PET 1 % SD (0.24 % strain) performed similarly at the conclusion of the hysteresis loop. By comparison, the PET 1 % MD (0.03 % strain) created a much smaller hysteresis loop (indicating less stretching as the force was applied) and much less deformation (-86 % strain at the end) when force was removed from the composite. Thus extension was more reversible, and PET chains did not slide past each other as much.

The size of the hysteresis loop of the three composites was compared. PET-Neat MD had the largest hysteresis loop. PET 1 % MD had the smallest hysteresis loop due to a significant easing of strain reversibility. PET 1 % SD had the second largest hysteresis loop due to graphene limiting strain recovery.

The tangent modulus (slope of the curve) of neat PET at 0.05 % strain (41 MPa) was compared to the other composites. PET 1 % MD had the highest modulus (48 MPa +19 %), and PET 1 % SD (27 MPa -34 %) had the lowest modulus. The lowered modulus (a measure of stiffness) in the SD composite suggests that either some solvent remains or free volume had increased. As o-chlorophenol has a high boiling temperature (174.9 °C), it is likely that some solvent remained. These results demonstrate that the graphenes increase tangent modulus in PET when melt dispersed and decrease tangent modulus when solvent dispersed. The increase in tangent modulus is consistent with other research on graphene MD in PET which also showed an increase in Young's modulus but only as graphene loading rose to ≥ 5 %²¹⁶.

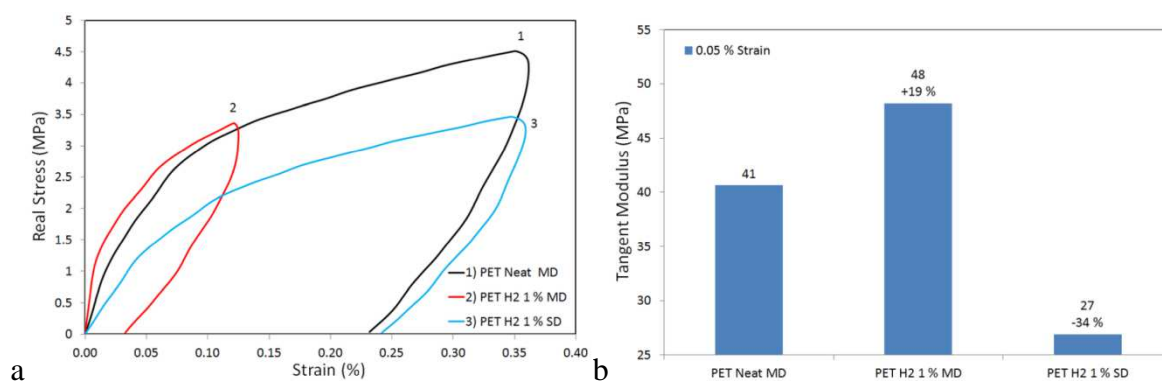


Figure 7-6 PET with a ramped force of 18 N applied a) Stress (MPa) versus strain (%) curve b) Tangent modulus

7.3.4.2 Dynamic Mechanical Analysis

DMA was used to compare PET without graphene to PET with graphene using both melt and solvent dispersion (Figure 7-7). The storage modulus (E') describes elasticity and was used to compare the three composites at 20 °C. PET 1 % MD showed an increase (+43 %) and PET 1 % SD showed a decrease (-52 %) compared with PET-Neat MD. Storage modulus also describes the interfacial interaction between PET and graphene which decreased with the SD graphene and increased with the MD graphene. The reduction in storage modulus for SD dispersed graphene may be due to some remaining solvent.

Loss modulus (E'') is a measure of energy absorption over time and was used to compare the three composites at 20 °C: The loss modulus increased (+26 %) in the PET 1 % SD and PET 1 % MD (+96 %), compared to PET-Neat MD. Thus the viscoelasticity increased most with MD graphene.

$\text{Tan}(\delta)$ represents damping which is the ability of material to dissipate energy over time (viscoelasticity) relative to releasing it immediately (elasticity). The three composites were compared at 20 °C. PET-Neat MD damping (0.039) increased in PET 1 % MD (0.053 +137 %) but increased most in PET 1 % SD (0.10 +259 %). Increased damping also indicates more liquid properties and that free volume is increasing. However, as the absolute numbers are small, any change is less significant.

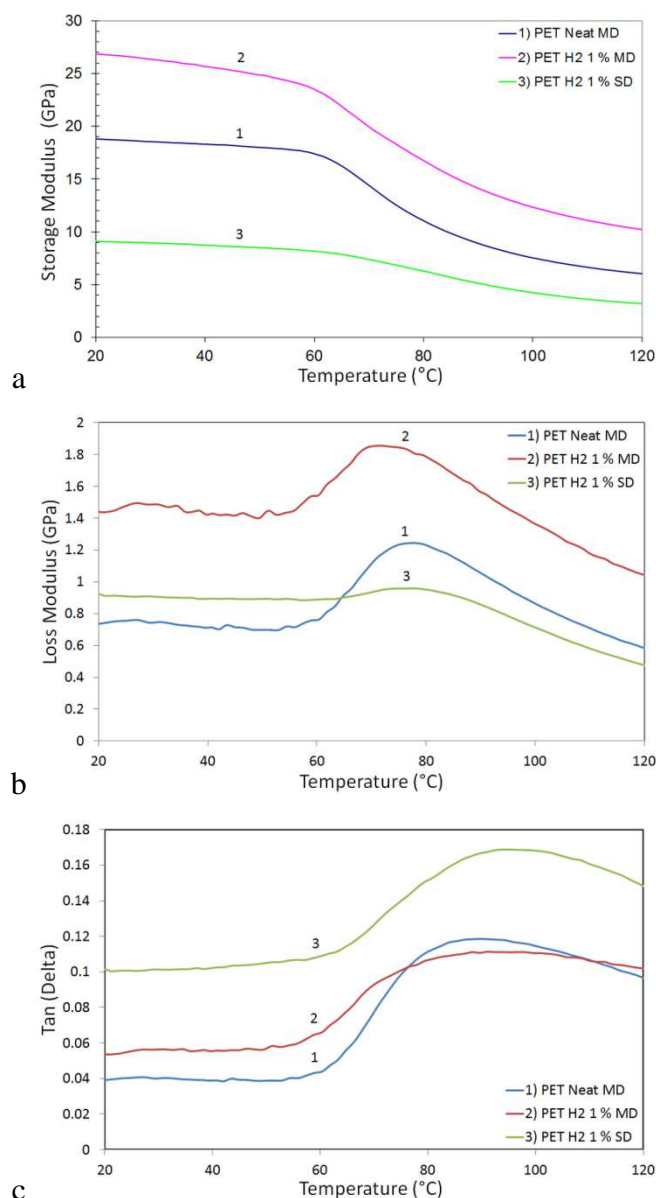


Figure 7-7 DMA of PET composites a) Storage modulus b) Loss modulus c) Tan(δ)

7.3.5 Thermogravimetry

Thermogravimetry (TGA) measured the effect of temperature on the PET composites in an inert nitrogen environment (Figure 7-8). The shape of the TGA curves was compared. All three curves exhibit a single mass loss event suggesting the graphenes are homogeneously distributed throughout the PET, and the materials degrade at similar rates.

The temperature of degradation of the three composites was compared. PET 1% MD with graphene showed no significant change in degradation temperature (434 °C) compared with PET-Neat MD and PET 1% SD (429 °C). Resistance to pyrolysis (+5 °C) of PET 1% MD is

suggested to be due to a failure to separate the graphene sheets entirely. These sheets when in close proximity act as insulators (similar to expandable graphite).

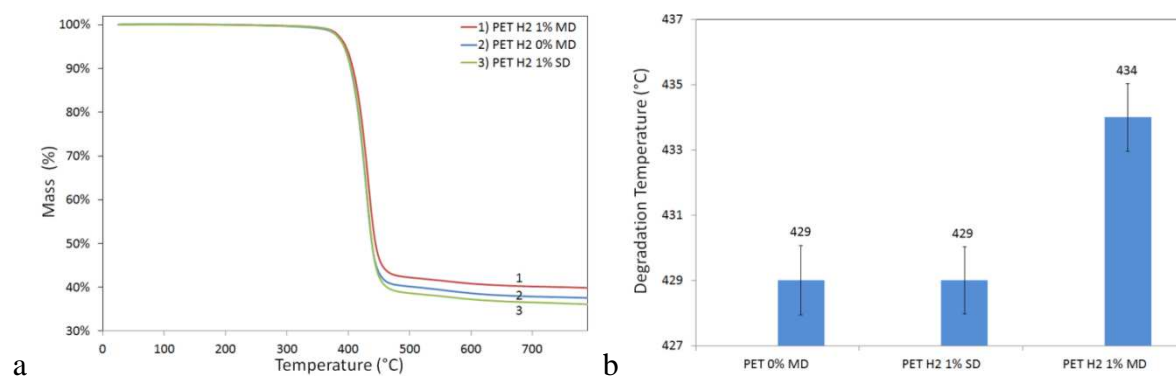


Figure 7-8 TGA pyrolysis under nitrogen a) PET degradation curve b) PET degradation temperature

7.3.6 Permeation

Permeation studies were undertaken to establish if reduced graphene dispersed in PET would decrease oxygen permeation (Figure 7-9). However oxygen permeation of neat PET (1.6 cc/(m²·day)) increased with PET 1 % MD (2.3 cc/(m²·day) +69 %) and with PET 1% SD (5.2 cc/(m²·day) +325 %). This conflicts with predictions that graphenes should decrease gas transmission because they present a tortuous path. However, this agrees with results reported by Yu that reduced graphene resulted in increased permeation and oxidised graphene resulted in reduced permeation. Yu suggested that the electronegative nature of the oxygen on the surface of oxidised graphene hindered the permeation of oxygen through the polymer¹⁰⁶ whereas increased oxygen permeation would be consistent with an increase in free volume²¹⁷ at the interface between the graphene and PET.

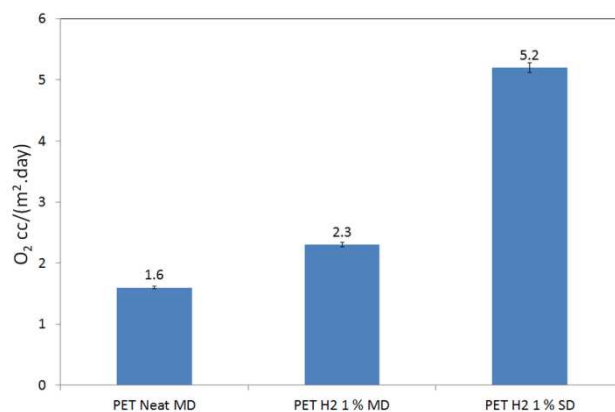


Figure 7-9 PET-graphene composites oxygen permeability

The increase in permeation in the ultrasonicated PET 1 % SD is consistent with an increase in surface area (better exfoliation and dispersion) creating more free volume.

7.3.7 Dispersion

Density functional theory (DFT) calculations of the molecular interactions of our system of interest were carried out to help validate the dispersion of graphene in PET (Figure 7-10): The PET ring was shown to orient itself above the graphene sheet so that the centre of the ring lies directly above a carbon atom. The same stacking orientation is present between layers in graphite which show an AB (Bernal) stacking geometry⁸. The average distance of the PET ring above the graphene sheet is ~0.328 nm: as measured between the average z-height of the 6C atoms in the ring and the height of the C atom in the graphene sheet located directly below the middle of the ring. This PET-graphene distance agrees well with the distance measured for benzene adsorbed on graphene of 0.36 nm²¹⁸ and the experimental distance between layers in graphite of 0.336 nm¹⁹³.

The electron localisation function (ELF) (Figure 7-10c) gives an indication of the likelihood of formation of nonbonding (0 = blue) and bonding (1 = red) electron pairs. Regions of red indicate a high probability and can be seen in the bonding region between the C atoms in the C-ring structure. This bonding is similar to that which occurs between multiple graphene sheets. Adsorption of methyl-terminated PET on the graphene sheet induces a minor redistribution of electrons such that there is a small donation of charge from the graphene layer to the molecule, of ~-0.03 eV.

This interaction between the PET and graphene thus confirms that π -interactions help disperse graphene in PET.

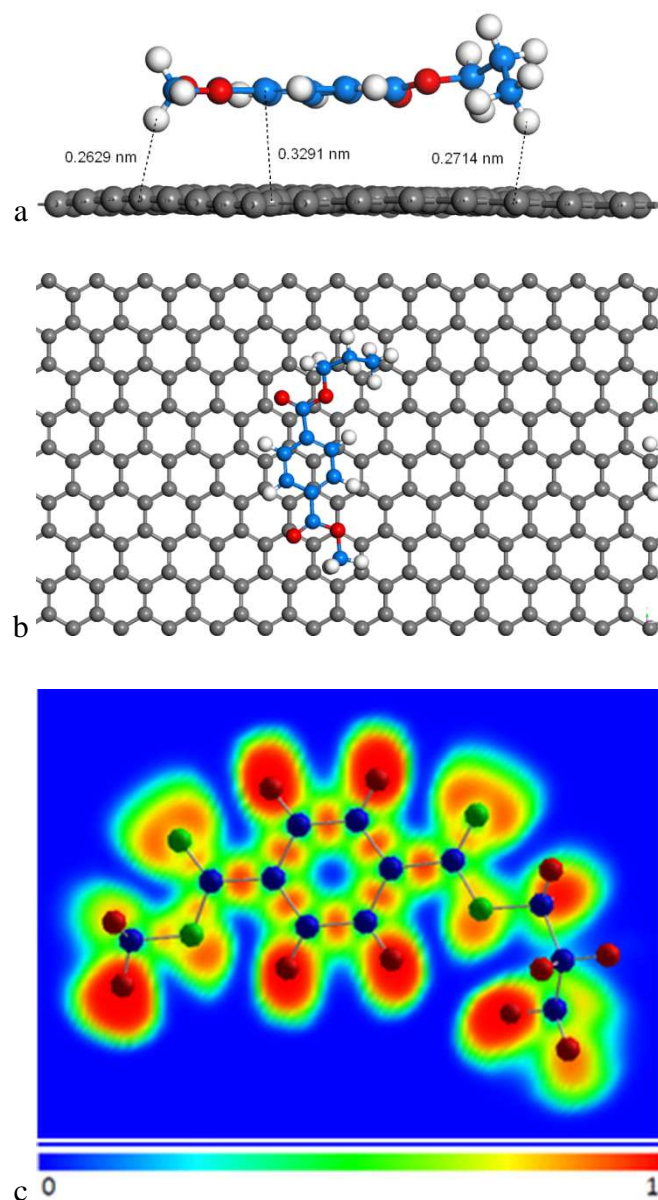


Figure 7-10 Methyl terminated PET monomer adsorbed on graphene a) Side view b) Top down view (C-Blue H-White O-Red Graphene C-Grey) c) Electron localisation function (ELF) of PET adsorbed on graphene, aligned so the slice cuts through the C atoms in the ring of the methyl terminated PET molecule

7.3.8 Conductivity

All three PET materials were non-conductive indicating the percolation threshold had not yet been reached.

7.4 Conclusion

PET GT-H₂ reduced low defect graphene (produced by a thermal expansion method) composites were characterised and compared using both melt dispersion (without ultrasonication) and solvent dispersion (with ultrasonication). Hydrogen reduced graphene had few defects and few layers as measured by Raman spectroscopy. PET crystallinity was not affected by graphene demonstrating that low defect graphene does not cause nucleation as measured by WAXS. SEM images suggested ultrasonication of graphene (PET 1 % SD) better separated and expanded graphene flakes. TEM showed that solvent dispersed ultrasonicated graphene (PET 1 % SD) had fewer layers than melt dispersed graphene (PET 1 % MD). SS-MA showed a reduction in deformation in PET 1 % MD. Tangent modulus (stiffness) increased slightly in PET 1 % MD. Interfacial interactions (storage modulus) increased for PET 1 % MD but decreased for PET 1 % SD which may be due to some remaining solvent. The viscoelastic time-dependent energy loss (loss modulus) increased in PET 1 % SD but was largest in PET 1 % MD. A move toward a liquid state and increased free volume (damping) increased in PET 1% MD, was highest in PET 1 % SD but the absolute changes were insignificant. TGA's smooth degradation curve demonstrated that the composites were uniformly dispersed. DFT calculations showed that PET prefers to be oriented with the ring lying parallel to the graphene plane in an AB stacking geometry. An increase in oxygen permeation with reduced graphene was attributed to an increase in free volume. Ultrasonication further increased permeation (free volume) by improving exfoliation plus dispersion of graphene (increasing accessible surface area). Despite good dispersion 1 %·w/w graphene did not result in measurable conductivity.

These results suggest that an ultrasonication treated thermally expanded and H₂ reduced graphene introduced into melt dispersed PET is likely to result in improved properties and should be investigated further since melt dispersion of PET by itself is insufficient to obtain the best results.

Chapter 8 Carbon Monoxide Reduced Low-Defect Graphene with Poly(ethylene terephthalate) Composites

8.1 Introduction

Poly(ethylene terephthalate) (PET) is a high-performance semi-crystalline thermoplastic polymer used in bottles²¹⁹, films, fibres and moulded products. In this chapter, melt dispersion is combined with ultrasonication of graphenes to exfoliate graphene to overcome insufficient shear during PET processing.

Melt dispersion is a high shear mixing method used by industry in the large scale production of polymers and has the added advantage of thermally reducing graphene in situ^{46, 205, 220-223}. Ultrasonication produces cavitation which helps wet, disperse, further exfoliate³⁰ and reduce⁵² graphene. Combining these techniques has the potential to improve the dispersion of graphene further and thus the properties of the polymer⁴⁶.

Ultrasonication in *p*-xylene provides potential π -electron interactions with the polycyclic aromatic graphene structures^{39, 181}. This non-polar aromatic solvent assists in suspension and dispersion of graphene. When added to PET at the high temperatures (275 °C) used in the MD process *p*-xylene ($T_b \sim 138$ °C)²²⁴ evaporates. PET makes a suitable choice of polymer because it has an aromatic structure which can continue to keep the graphene dispersed via π - π interactions²¹⁴. PET ($C_{10}H_8O_4$)_n also has eight hydrogen atoms per repeat unit (elemental analysis C 62.51 % H 4.2 %) and as the number of hydrogen atoms in an aromatic molecule increase (four hydrogen atoms per aromatic ring) the magnitude of the π - π interactions increases⁷³.

Low defect graphene³⁰ has not previously been available in sufficient quantities for polymer reinforcement²²⁵. Likewise, non-covalent bonding using π - π interactions (to avoid creating defects in graphene)³⁰ is an uncommon reinforcing technique. Thus it is of interest to establish whether low defect graphene can be used to reinforce a polymer using only π -interactions.

The aim of this experiment was to disperse graphene in an aromatic (semi-crystalline) polymer and determine if poly(ethylene terephthalate) (PET) mechanical performance could

be enhanced with ultrasonication (US) of low defect CO reduced graphene, at 1 %·w/w, using melt dispersion (MD). PET-graphene MD composites were compared with and without US.

8.2 Experimental

Material information, preparation of nanocomposites and characterisation methods are detailed in Chapter 3.

8.3 Results and Discussion

8.3.1 Visual Characterisation

Visual characterisation is often a simple yet accurate method of identifying differences. The unaided human eye can see a single layer of graphene²²⁶. However, it would be difficult to ascertain the number of graphene layers with certainty. It is even harder to view graphene in a polymer. The three PET test specimens could be clearly distinguished based on colour (Figure 8-1): Neat PET was an opaque cream colour. PET with melt dispersed graphene was a solid even blue-grey colour. PET with ultrasonicated and melt dispersed graphene was a solid even black colour. The black colour is typical of reduced graphene^{67, 222, 227}. The black colour also suggests improved dispersion and exfoliation. Thus combining ultrasonication and melt dispersion is desirable when creating polymer-graphene composites.

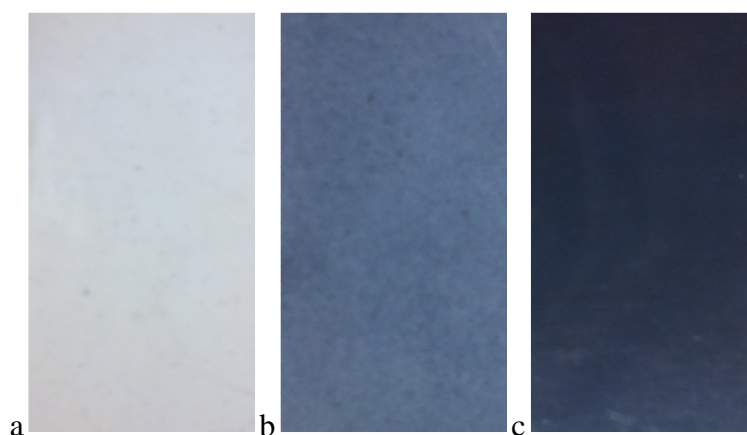


Figure 8-1 Photographs of melt dispersed PET and graphene (GT-CO 1 %) composites

a) neat b) graphene c) ultrasonicated graphene

8.3.2 Microscopy

8.3.2.1 Optical

Optical microscopy was used to characterise the macroscopic dispersion of graphene in PET composites. Individual graphene sheets cannot be definitively resolved using optical microscopy, but agglomerations, poor dispersion and poor exfoliation can be identified relatively easily.

PET images were collected using a light microscope (Figure 8-2). Three images of the edge of a pressed sheet of melt dispersed PET are shown a) Neat b) GT-CO c) GT-CO ultrasonicated (US). The images are at a uniform magnification (250x) with a 200 μm scale bar. The neat PET shows a clear edge without inclusions where an ultra-microtome glass knife had been cutting. The MD PET 1 % composite, shows poor dispersion resulting in visible inclusions of around 200 μm in size with a darker overall colour. The ultrasonicated PET composite with MD shows much-improved dispersion, small particle sizes of around 1 μm and a darker more even colour.



Figure 8-2 PET (without glass) melt dispersed composites with 200 μm scale bar a) neat b) GT-CO 1 % c) GT-CO 1 % ultrasonicated

The large particle sizes with agglomeration suggest that a high shear mixer (Haake) alone is not sufficient to disperse, exfoliate and wet the surface of thermally exfoliated graphenes in PET. The smaller particle sizes, reduced agglomeration and even colour of ultrasonicated graphenes with MD demonstrate that ultrasonication is necessary to optimise graphene dispersion in MD PET. High shear mixers alone are insufficient to create optimised composites. While it is likely that longer melt dispersion times would improve dispersions further, longer application of shear (via the Haake mixer) would never approach the dispersion achieved with ultrasonication.

8.3.2.2 Electron

Electron microscopy was used to characterise graphenes and PET-graphene composites. It was used to confirm the quality of the graphene and reveal detail about the structure of PET-graphene composites.

Transmission electron microscopy (TEM) was required to resolve individual graphene layers. Individual graphene layers are often difficult to distinguish in a polymer as they tend to be oriented edgewise.

PET GT-CO 1 % composites (without ultrasonication) show the good dispersion of graphene with no visible clumping or other indications of uneven dispersion at the microscopic level (Figure 8-3). It was possible to resolve individual layers of graphene at the nanoscopic level (20 nm) and demonstrate that melt dispersion (without ultrasonication) results in single layer graphene reinforcement.

Although no obvious multi-layer graphene is visible, it was possible to see multi-layer graphenes in other images.

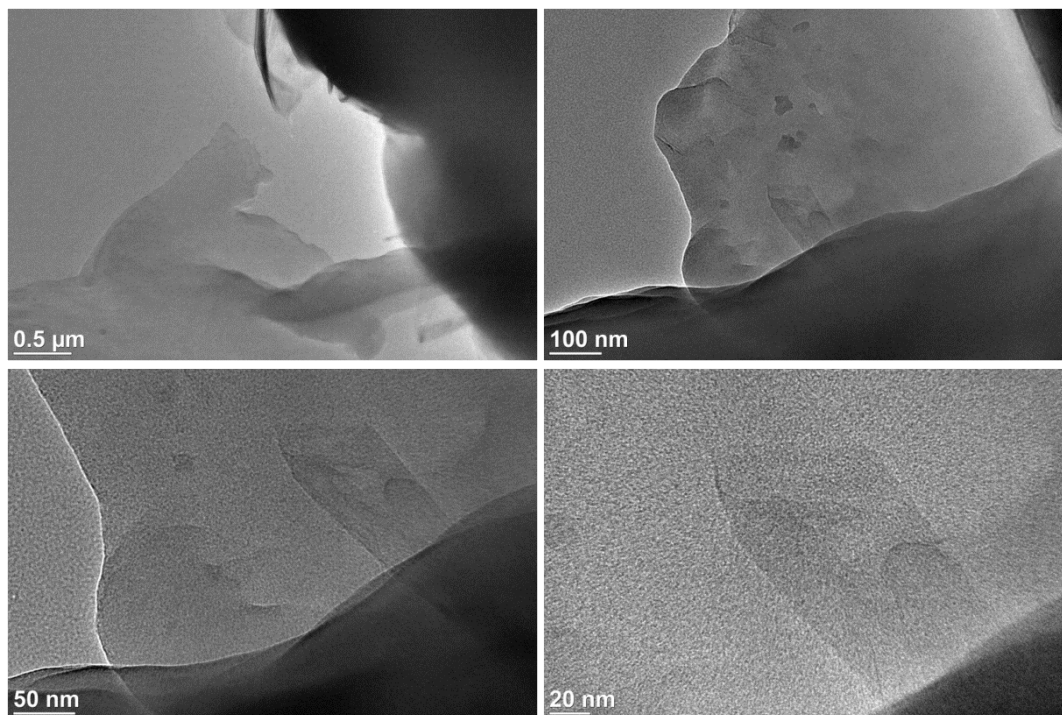


Figure 8-3 TEM images of PET with melt dispersed GT-CO 1 % (without ultrasonication) a) 500 nm b) 100 nm c) 50 nm d) 20 nm

PET GT-CO 1 % (with ultrasonication) shows the good dispersion of graphene with no visible clumping or other indications of uneven dispersion at the microscopic level (Figure 8-4). Three graphene sheets can be seen overlapping at the margins of the PET at the nanoscopic level (20 nm). Thus dark areas indicate a greater concentration of graphene and demonstrate that single layer graphene is present. The layering effect suggests more single layer graphene is present when ultrasonication is used.

No obvious multi-layer graphene was visible in these images. However, multi-layer graphene was visible in other images.

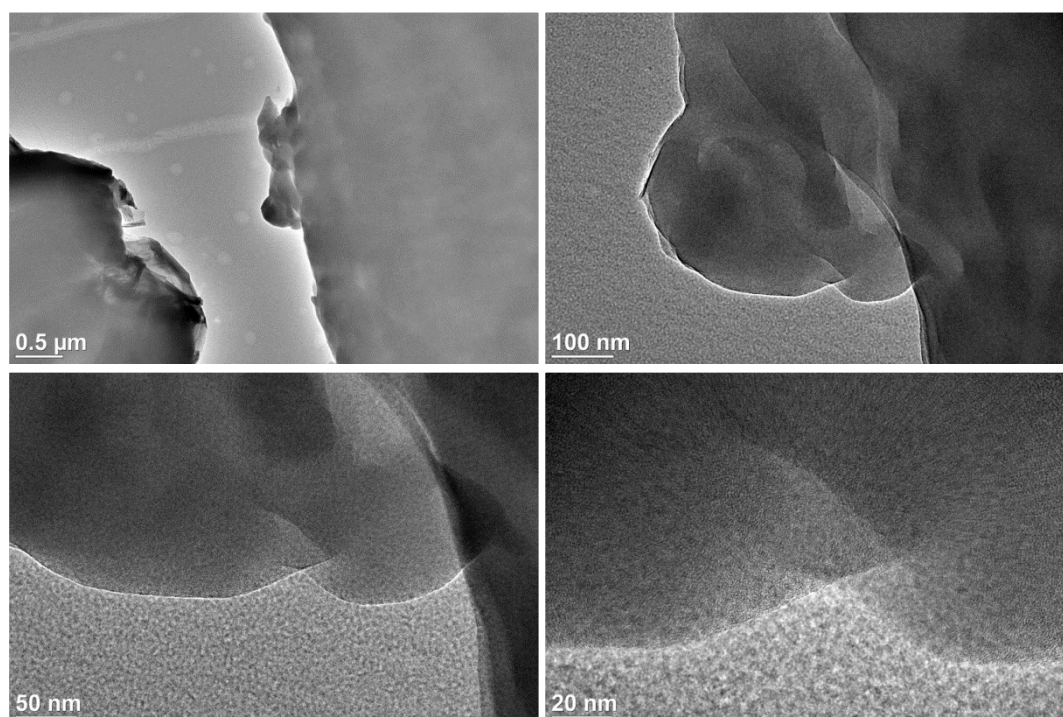


Figure 8-4 TEM images of melt dispersed PET with melt dispersed ultrasonicated GT-CO 1 % a) 500 nm b) 100 nm c) 50 nm d) 20 nm

8.3.3 Mechanical Properties

8.3.3.1 Tensile Mechanical Analysis

Stress-strain tensile mechanical analysis (SS-MA) was used for characterising and comparing the mechanical performance of PET and the graphene composites. Enhancements in performance were detected, measured and graphically represented. SS-MA was used to measure stress-strain as stress was increased and then decreased forming a hysteresis curve (Figure 8-5). A hysteresis curve provides further information about the reversible performance of the materials.

Comparing the three hysteresis curves for melt dispersed PET shows that the end strain, a measure of deformation, increased (+62 %) when ultrasonication was not used and increased further (+204 %) when GT-CO graphene was ultrasonicated. It is known that graphene increases elastoplasticity, viscoplasticity²²⁸, ductility¹⁵⁹ and fracture toughness of polymers¹¹, so increased deformation of stiff materials such as PET (reduced failure²¹⁵) is consistent with previous research. These reports are consistent with observations made during handling that adding graphene to PET made it more resistant to cracking, especially after ultrasonication.

Tangent modulus (stiffness) at 0.05 % strain increased (+6 %) with ultrasonication and melt dispersion (+14 %). Stiffness may have been increased slightly by adding ultrasonicated graphene and by withholding ultrasonication. However as this parameter scales logarithmically the difference is insignificant.

It appears that MD US graphene gives less reinforcement (weak interaction with PET) but retards recovery indicating a stronger interaction with PET. Thus ultrasonication should be carried out on graphene to increase ductility (end strain) of PET, but graphene did not affect stiffness significantly.

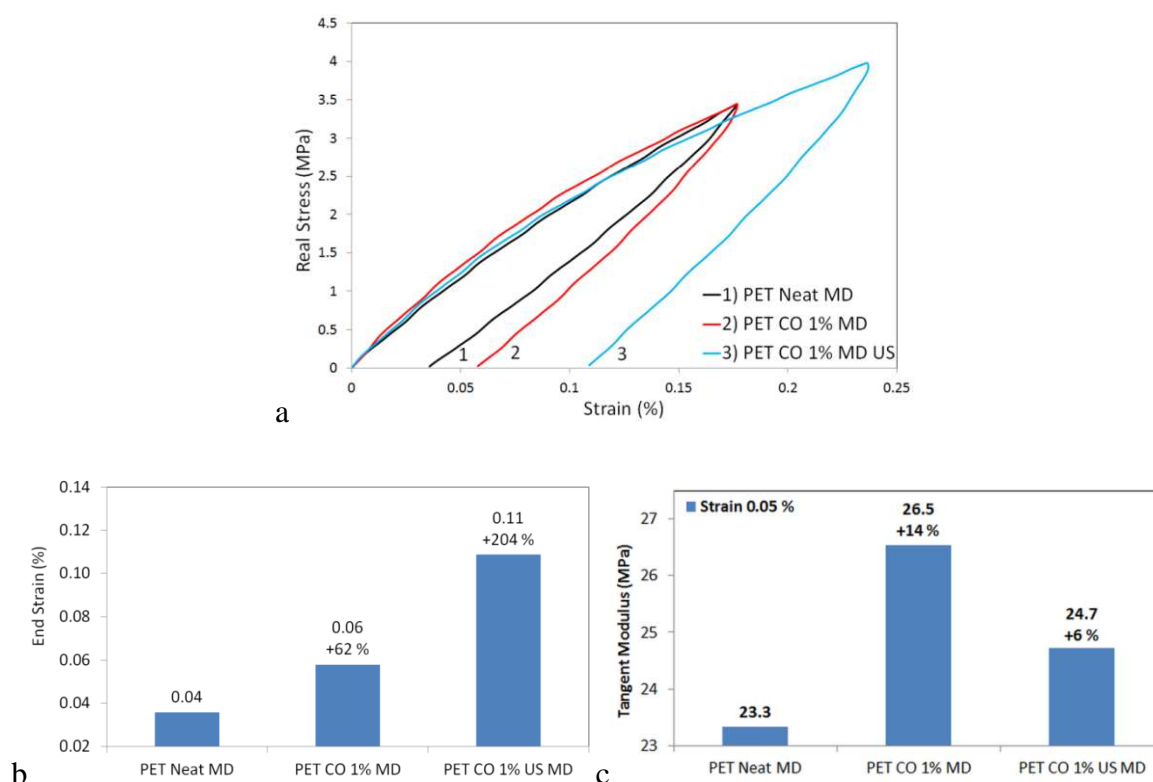


Figure 8-5 SS-MA of PET GT-CO 1 % melt dispersed with and without ultrasonication

a) Stress-strain curve b) End strain (%) c) Tangent modulus (0.05 % Strain)

8.3.3.2 Dynamic Mechanical Analysis

Dynamic mechanical analysis (DMA) is used to measure elasticity, viscoelasticity, damping of materials and their temperature and frequency dependence.

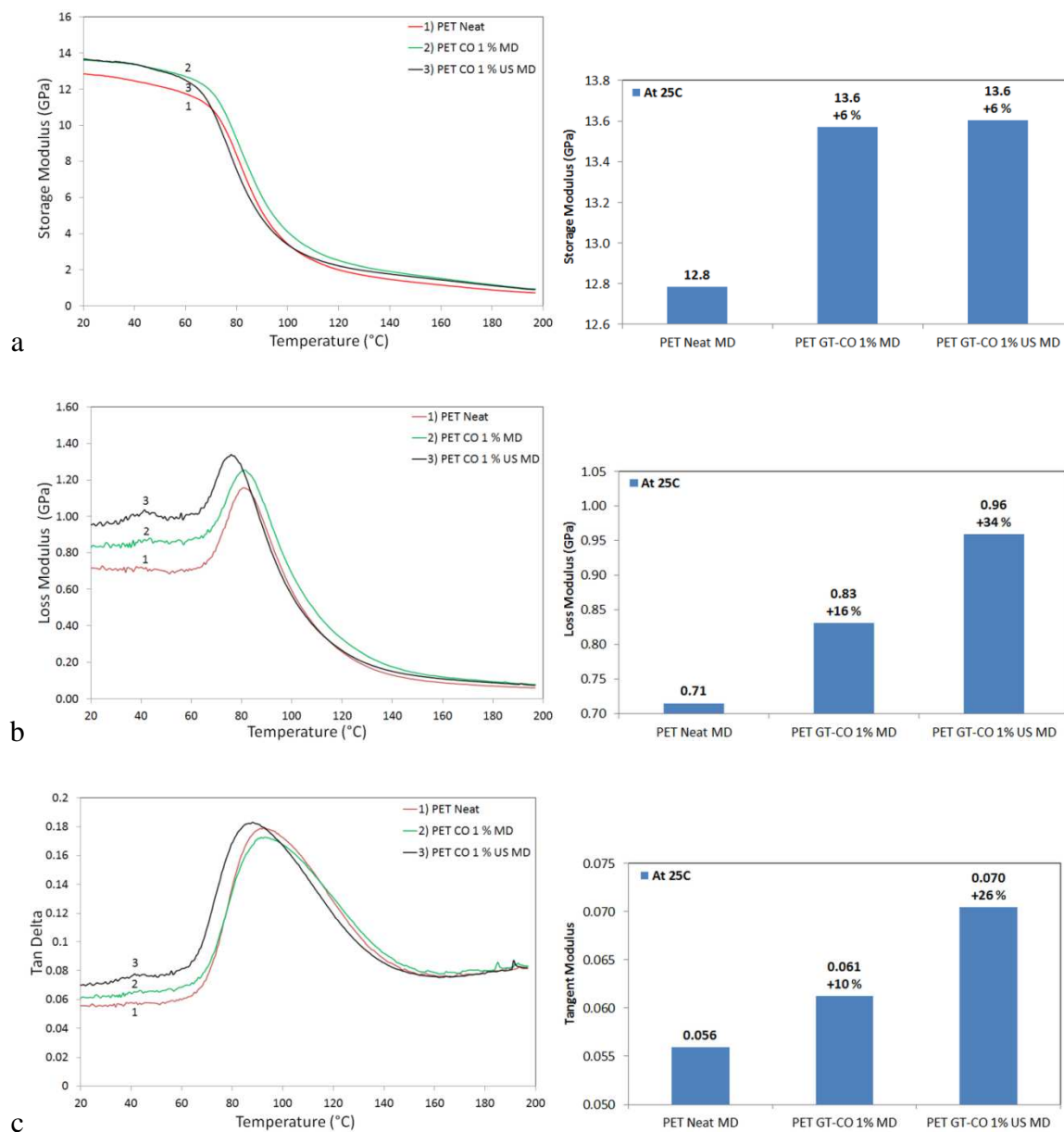


Figure 8-6 DMA of melt dispersed PET GT-CO 1 % graphene with and without ultrasonication a) Storage Modulus b) Loss Modulus c) Tan Delta (with bar graphs comparing properties at 25 °C)

PET MD properties were compared at 25 °C and showed that stored energy (storage modulus a measure of interfacial interactions) increased (+6 %) for composites with and without ultrasonication, but this was not significant.

However, the energy dissipated as heat (loss modulus a measure of viscoelasticity) increased most (+34 %) with ultrasonication of GT-CO graphene 1% and dispersion in PET using melt dispersion.

Damping (tan delta), a move to a more liquid state and an increase in free volume, increased most (+26 %) for ultrasonicated graphenes. The tan delta curves are very broad spanning almost 100 °C indicating distribution of relaxation and more constrained molecules. Broad low peaks are typical of semi-crystalline polymers. The peak measures only the amorphous component. Both peak position and width at half height were barely changed.

Even graphene dispersed without ultrasonication increased the loss of energy as heat (loss modulus) via a damping (tan delta) effect. However, without ultrasonication, the increases in loss modulus (+16 %) and tan delta (+10 %) were less than half as large. Thus ultrasonicated GT-CO graphene in PET increased energy loss as heat as damping increased.

8.4 Conclusion

PET-graphene GT-CO 1 % composites, were created using melt dispersion (MD) with ultrasonication to assist graphene dispersion, wetting and exfoliation. The composites could be visually distinguished: neat PET was a cream colour, without ultrasonication grey and with ultrasonication black (suggesting improved reduction and dispersion). Using a light optical microscope, it was possible to see that graphene without ultrasonication was poorly dispersed and that ultrasonication resulted in significantly reduced agglomeration. TEM microscopy demonstrated that single layer graphene existed even without ultrasonication, but the layering of graphene sheets suggested that more single layer graphene existed when ultrasonication was used. Stress-strain measurements showed that deformation (end strain) increased with ultrasonication of graphene consistent with improved PET ductility and fracture toughness. Interfacial interactions between graphene (storage modulus) were insignificant but with ultrasonication energy lost through increased viscoelasticity (loss modulus) and damping (tan delta) both increased. Thus PET performance was modified by the addition of ultrasonicated graphene, and the performance changes were most dramatic in the areas of deformation (strain), the energy dissipated by heat (loss modulus) and damping (tan delta).

Chapter 9 Polycarbonate-Graphene Composites

9.1 Introduction

High-performance, low filler content composites of low defect graphene are described in this chapter. Polycarbonate (PC) is a thermoplastic polymer with high impact resistance²²⁹ which has poor environmental stress crack resistance, especially on exposure to esters, aromatics and surfactants or detergents, which limits its applications. Polycarbonate is used for roofing, motorcycle helmets and electrical equipment. PC is an electrical insulator²³⁰ which resists high temperatures²³¹ and thermal degradation²²⁹. PC's repeating group (Figure 9-1) contains two aromatic rings and a carbonate ($-\text{O}-(\text{C}=\text{O})-\text{O}-$).

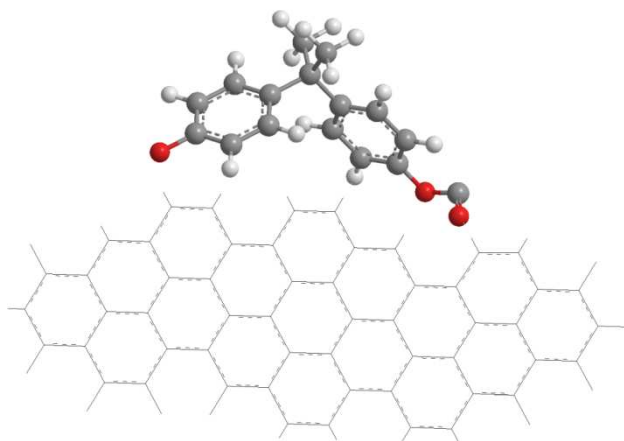


Figure 9-1 Molecular representation of the polycarbonate monomer and graphene sheet

Polycarbonate was chosen as the test polymer because it has a high glass temperature ($T_g \sim 140-150\text{ }^\circ\text{C}$)^{232, 233}, is amorphous²²⁹ and its aromatic structure complements that of graphene. A high T_g allows a polymer to be tested across a wider temperature range²²⁹.

Amorphous polymers avoid the complexity that arises with polymers that form crystal structures²²⁹ such as polyethylene, poly(ethylene terephthalate) and polytetrafluoroethylene. Crystal structure growth can vary greatly as conditions are varied making interpretation more difficult. Interpretation is especially problematic when investigating the effect of reinforcing nanomaterials such as graphene. Semi-crystalline polymers make it difficult to determine which effects are due to crystalline structures and which effects are caused by the addition of the nanomaterial (graphene). Additional complications include the need to consider whether

the nanomaterial acts as a nucleation point for polymer crystallisation²¹³ and how the crystals grow as conditions are varied. Amorphous polymers require none of these complicating considerations. Thus performance enhancements in amorphous polymers can be more definitively attributed to the reinforcing nanomaterial.

High-performance applications of PC could be enhanced by graphene as they are by glass fibre. It would be expected that stacking between the PC and the graphene via π - π type interactions would improve dispersion and prevent agglomeration of the graphene²³⁴. Polycarbonate (C₁₆ H₁₄ O₃)_n has 14 hydrogen atoms (8 aromatic and 6 methyl) per monomer (elemental analysis C 75.58 % H 5.55 %) which can interact with graphene. As graphene is non-polar, the non-polar methyl group (-CH₃) on PC ought to also assist its solubility in graphene. There is also potential for improved dispersion due to π -interactions between the π electrons (C=O) of the carbonate group (-O-CO-O-) in PC and graphene. Two different graphenes were chosen because previous experiments have demonstrated that the reducing gas used in production changes the properties of the graphene and this is reflected in graphene-polymer interactions¹⁸¹.

The aim of this experiment was to use ultrasonication on graphene to separate layers and suspend it in a liquid. To use melt dispersion with an amorphous, aromatic and high T_g polymer where interactions between graphene and aromatic rings, contribute to a strong interface. To compare H₂ and CO graphene treatments in PC which, despite these properties, is not brittle making it a suitable matrix for evaluating low defect graphene at low loading (0.1 %·w/w).

9.2 Experimental

Material information, preparation of nanocomposites and characterisation methods are detailed in Chapter 3.

9.3 Results and Discussion

Hydrogen reduced and CO reduced graphene were introduced to polycarbonate (Figure 9-1) at 0.1 %·w/w. Ultrasonication was used to optimise dispersion, exfoliation and reduction⁵² of the graphene in melt dispersed polycarbonate.

9.3.1 Visual Characterisation

The three polymer composites were clearly defined between neat PC (transparent) and PC-graphene (dark yet transparent). The distribution of graphene throughout the PC is even (no agglomeration) in both composites, but PC with GT-CO reduced graphene is slightly darker compared to the GT-H₂ graphene composite. The darker colour is typical of greater reduction^{67, 227}, improved dispersion and exfoliation.

It was noted that uneven movement of the polymer through the mould during pressing would create an uneven distribution of graphene. Allowing a greater length of time for PC to melt before pressing resulted in the even dispersion of graphene throughout the PC.



Figure 9-2 Photograph of polycarbonate melt dispersed with 0.1% ultrasonicated graphene
a) neat b) GT-H₂ c) GT-CO (from left to right)

9.3.2 Microscopy

9.3.2.1 Optical Microscopy

Optical microscopy (Figure 9-3) was used to characterise the macroscopic dispersion of graphene in PC composites. Three images of the edge of a pressed sheet of melt dispersed PC are shown at a uniform magnification (250x) a) Neat b) GT-H₂ 0.1 % and c) GT-CO 0.1 %. The neat PC is clear with no inclusions. Both GT-H₂ and GT-CO graphenes were ultrasonicated before melt dispersion which helps increase reduction⁵². Both GT-H₂ and GT-CO composites are very dark and uniform despite the low loading of 0.1 % suggesting reduction, good dispersion and high compatibility with PC. A shiny skin is visible on the top surface of all three PC composites. Similar research has shown that this is a thin skin layer of PC of about 10 μm which interferes with conductivity²²⁹. Differences between GT-H₂ and GT-CO dispersion methods were not evident at the macroscopic level.

Thus ultrasonication with high shear dispersion helps optimise dispersion of low defect graphenes and is particularly effective in PC.



Figure 9-3 PC melt dispersed with 0.1 % ultrasonicated graphene with 200 µm scale bar
a) Neat b) GT-H₂ c) GT-CO

9.3.2.2 Electron Microscopy

Electron microscopy was used to characterise graphenes and polycarbonate-graphene composites. It was used to confirm the quality of the graphene and reveal detail about the structure of PC-graphene composites.

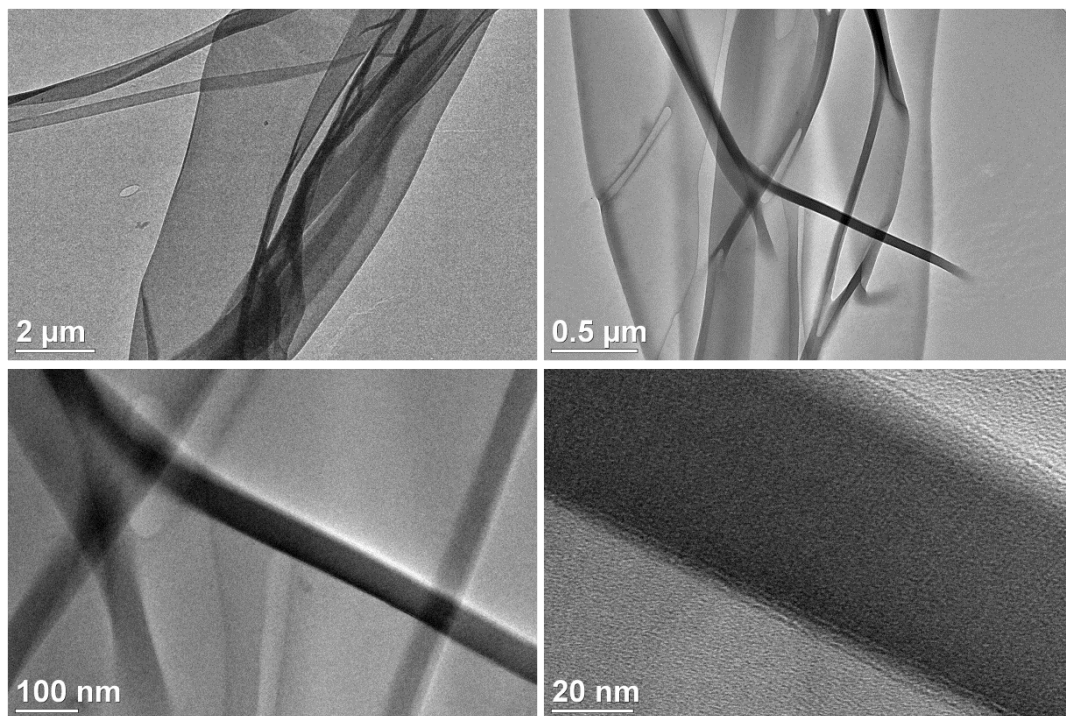


Figure 9-4 TEM images of PC GT-H₂ 0.1 % US MD a) 2 µm b) 500 nm c) 100 nm d) 20 nm

Transmission electron microscopy (TEM) was required to resolve individual graphene layers. Individual graphene layers are often difficult to distinguish in a polymer as they tend to be

oriented edgewise: moulding aligns graphenes in the plane and microtoming is done at 90° to the plane. This flow-induced orientation may improve stiffness and barrier properties while reducing electrical conductivity²²⁹.

PC GT-H₂ (0.1 %) polymer composites (Figure 9-4) shows no visible clumping of graphene, no discernible multi-layer graphene and no small graphene particles even at high resolution. The black lines are folds in the polymer. The composite shows no signs of tearing and fringes are smooth. The PC composite is lying on an amorphous carbon layer which reduced charging and ensured that small particles were captured on the TEM grid.

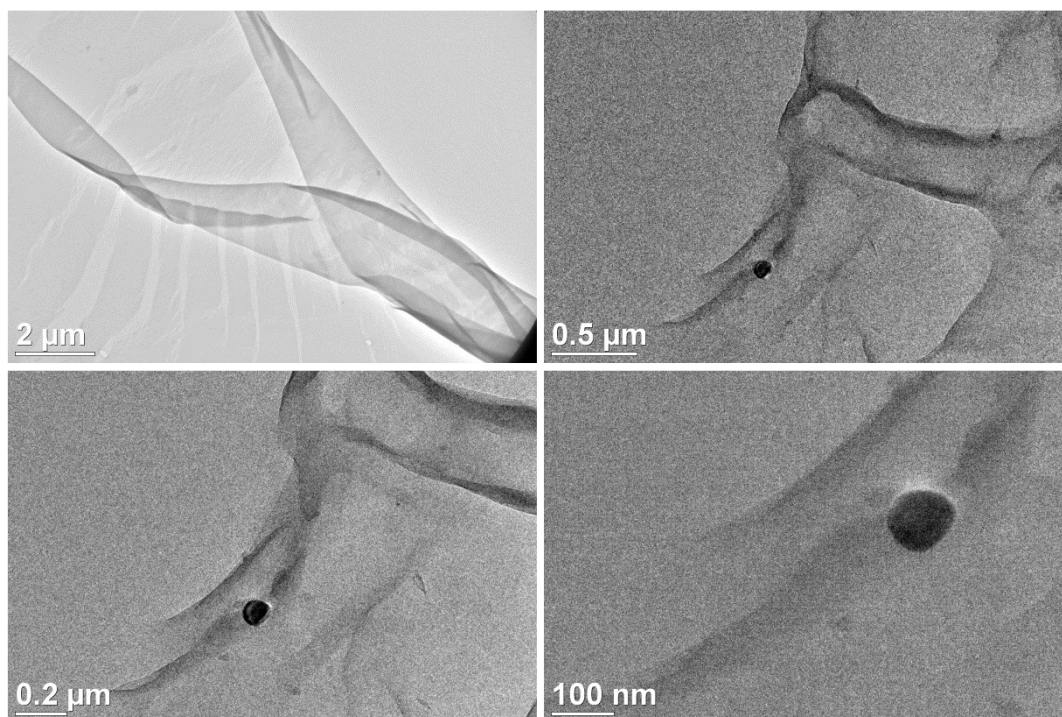


Figure 9-5 TEM images of PC GT-CO 0.1 % US MD a) 2 μm b) 500 nm c) 200 nm d) 100 nm

PC GT-CO (0.1 %) polymer composites (Figure 9-5) showed an even dispersion with no visible clumping, no discernible multi-layer graphene and one imperfection or inclusion. The dark areas appear to show broad graphene scrolling. There are no tears or fringes in the polymer. The striations in the first image are from the underlying carbon grid.

The TEM images showed that both GT-H₂ and GT-CO graphenes dispersed well in polycarbonate which is consistent with similar research²²⁹. Scrolling of the graphene was only visible when GT-CO reduced graphene was used. Scrolling was associated with low

defect graphene, which has low surface energy (the minimisation of surface energy), few layers and had been ultrasonicated (which provides activation energy)⁵².

9.3.3 Mechanical Properties

Dynamic Mechanical Analysis (DMA) is used to characterise materials and compare their response at different temperatures. As the temperature is increased storage modulus (elasticity), loss modulus (viscoelasticity) and tan delta (damping) are measured at a given frequency (1 Hz).

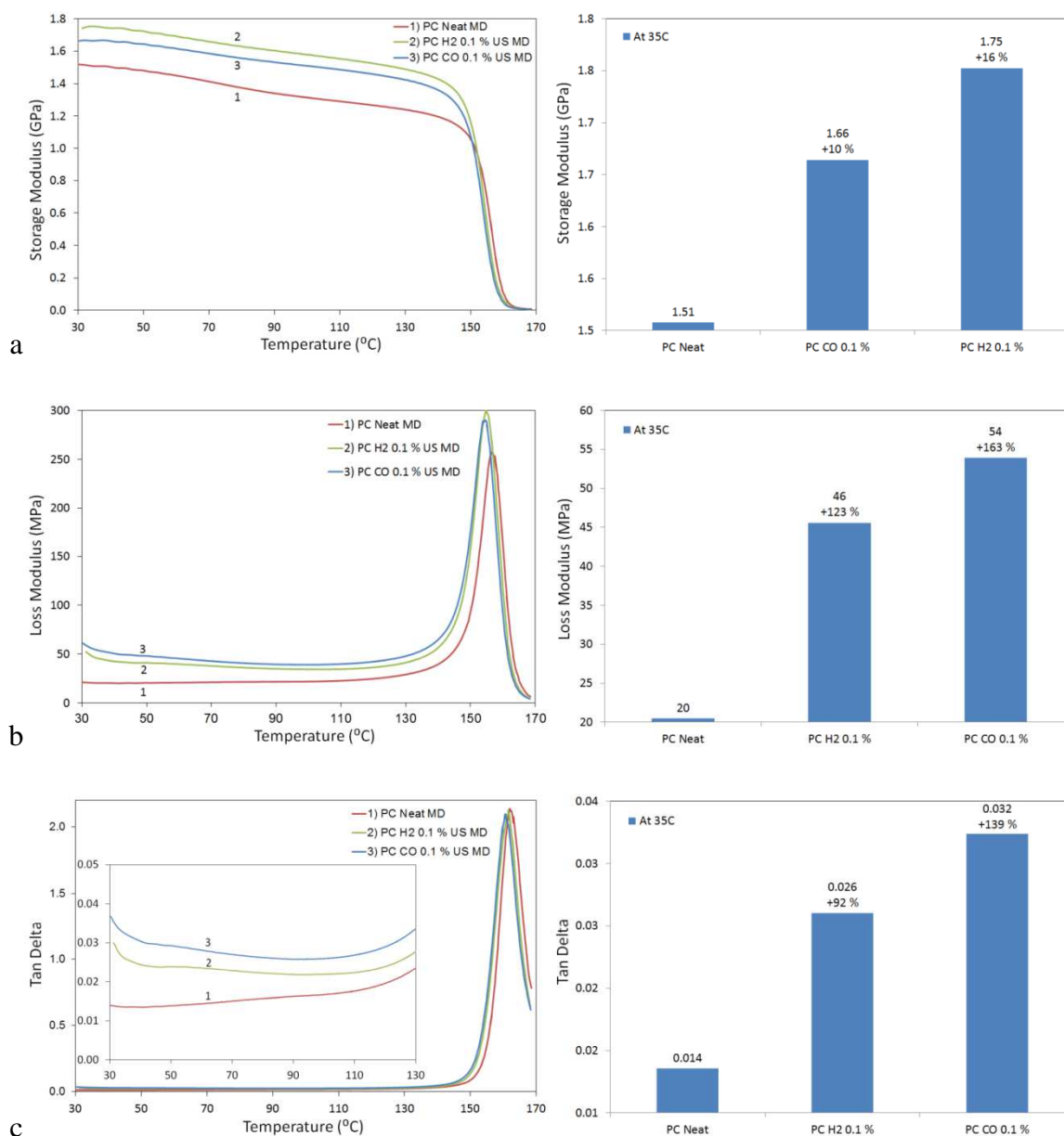


Figure 9-6 Polycarbonate with ultrasonication and melt dispersion of Neat, GT-H₂ and GT-CO 0.1 % composites a) Storage Modulus b) Loss Modulus c) TanDelta

PC composites properties were compared with PC without any graphene at 35 °C. Storage modulus increased when adding GT-CO reduced graphene (1.66 GPa +10 %) and GT-H₂ reduced graphene (1.75 GPa +16 %). Storage modulus measures stored energy (elastic portion) and an increase indicates improved interfacial interaction of PC with graphene. The slight increase in interfacial bonding may be due to increased hydrogen bonding.

Loss modulus increased for GT-H₂ reduced graphene (46 MPa +123 %) and GT-CO reduced graphene (54 MPa +163 %). Loss modulus measures time-dependent energy loss (viscous portion) thus an increase means that the viscoelastic properties increase when graphene is added to PC.

Tan delta (damping) in PC increased with GT-H₂ reduced graphene (0.026 +92 %) and with GT-CO reduced graphene (0.032 +129 %). Damping is the ratio of loss/storage modulus which describes the balance between energy loss and storage. The increased damping signals that the free volume is increasing. Values of tan delta above unity ($\tan(>45^\circ) > 1$) indicate more liquid properties (loss modulus > storage modulus) while values less than unity indicate more solid properties (regardless of viscosity). Thus as damping is increasing PC graphene composites are exhibiting fewer solid properties and the more efficient it is at safe energy absorption and dispersal (energy is converted to safer levels or frequencies). However, the low force of the loss modulus makes any increase in tan delta negligible. The tall sharp peak is typical of an amorphous polymer and less constrained molecules.

PC composites with a graphene showed some improvement of properties even at very low loadings of 0.1 %·w/w. The largest increases in magnitude were in the storage modulus with GT-CO and GT-H₂ reduced graphene. The increases suggest that CO and H₂ reduced graphene may be advantageous for improving storage modulus.

9.3.4 Dispersion

The structures obtained from the *ab initio* molecular dynamics (MD) simulations of the polycarbonate monomer adsorbed on graphene are presented in Figure 9-8.

The simulations show that the binding energy (BE) between the graphene and PC is almost identical after a 3.5 ps (-0.58 eV) and 5.3 ps (-0.62 eV) simulation time. The distances between PC and graphene (as measured between the closest carbon atoms on each structure) was the same (0.326 nm) for both structures while the distance between the nearest PC hydrogen atom and graphene C atom was 0.258 or 0.249 nm. The shortest distance between

the PC oxygen atom and a graphene C atom was 0.328 or 0.342 nm. These small differences in the adsorption distances and binding energies indicate that the PC has reached equilibrium. However, there is flexibility in the geometry of the PC on the graphene.

The simulations also give us an idea of the geometry of the interaction between PC and graphene. It has already been shown that there are two types of interactions that can occur between graphene and aromatic type compounds and involve graphene-like carbons or benzene-like carbons⁷³. The former are C atoms having three covalent bonds with adjacent carbons (as in polycyclic aromatic compounds) while the other are C atoms covalently linked to two carbons and one hydrogen atom (as in benzene). Hence, when the compounds align with face-to-face stacking, as in the AB stacking of graphite planes, both types of carbons can interact with the graphene. Further, it has been shown that the benzene-like carbons form a stronger interaction than the graphene-like carbon and therefore the magnitude of the π - π stacking interactions can increase significantly as the number of benzene-like carbons increases in the molecule.

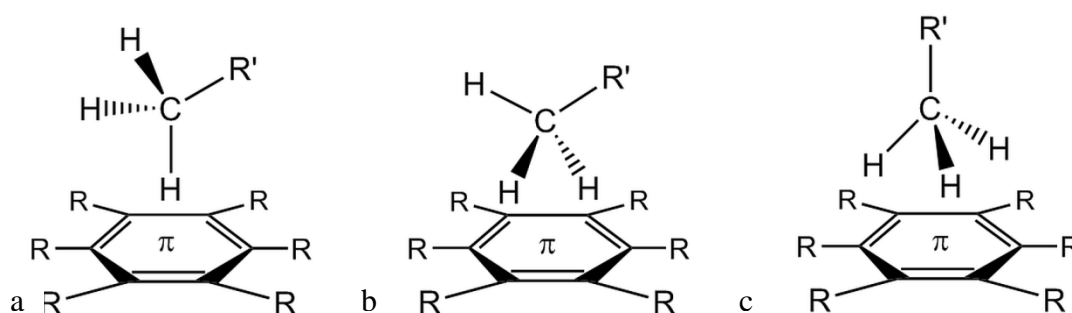


Figure 9-7 Three R'-CH/graphene complexes demonstrating weak hydrogen bonds (R' = H, phenyl, xylene or variable R = carbon part of molecular network) where a) is the most stable (modified from reference)²³⁵

Hence for PC, both types of interactions could be expected to occur with the graphene. Other types of interactions that could occur between the PC and the graphene could be with the methyl groups on the PC. It has been previously shown that CH/ π type interactions can occur between a soft acid (CH) and a soft base (π group) and have been called CH/ π hydrogen bonds^{74, 236, 237}. Examples of these types of interactions have been demonstrated to occur between methane, for instance, and an aromatic ring (Figure 9-7). The preferred orientation for this interaction is structure a, where one of the C-H bonds of the methane is directed to

the centre of the aromatic ring. It might be expected that such interactions are possible with PC and graphene due to the presence of methyl groups on the PC monomer.

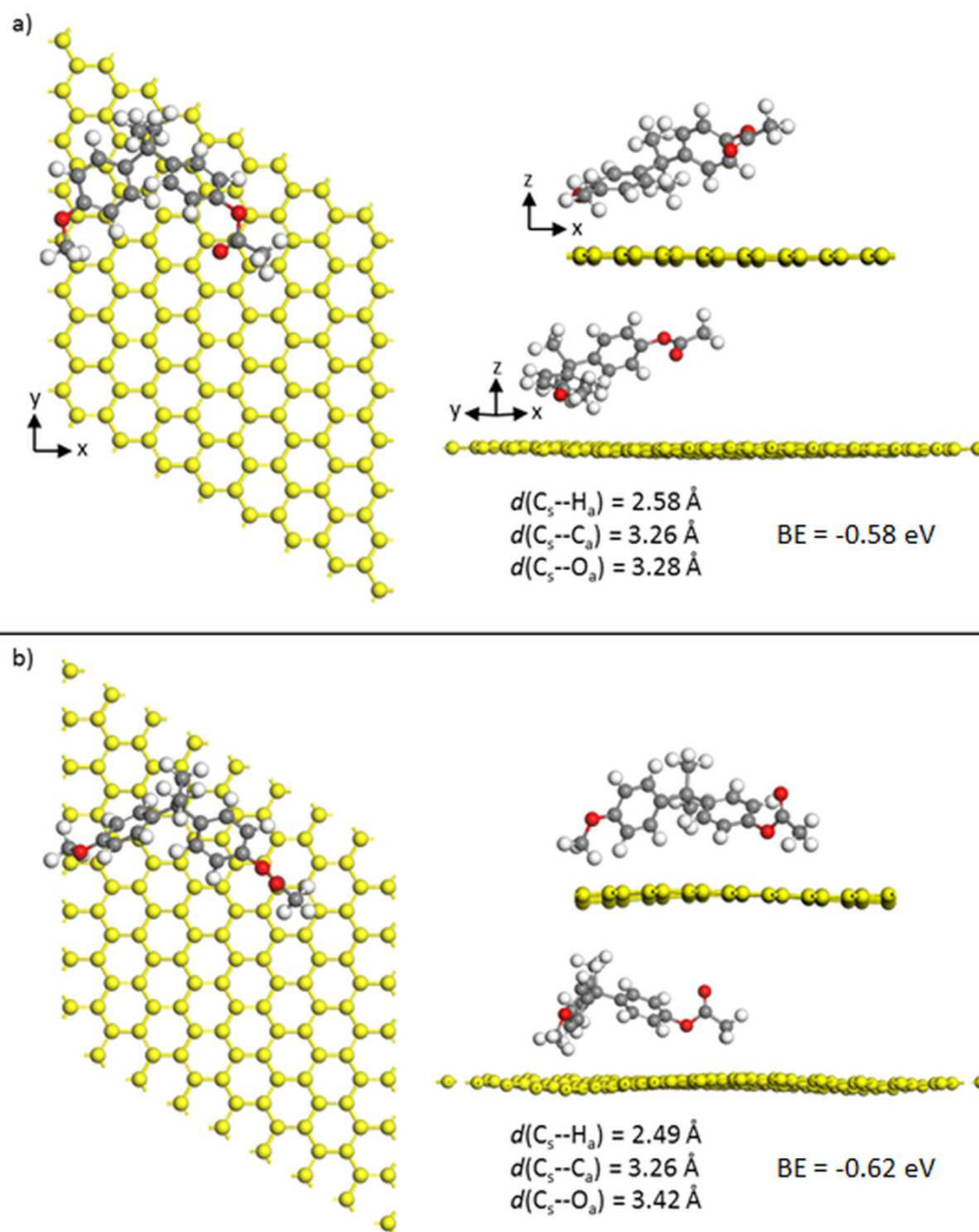


Figure 9-8 Optimised structures of PC monomer adsorbed on graphene after a simulation time of a) 3.5 ps and b) 5.3 ps

From Figure 9-8 the closest hydrogen atom in the PC monomer is 26 % closer to graphene than the nearest PC carbon atom. From the side view, it can be seen that some of the hydrogen atoms attached to the ring in the PC fragment are oriented directly above the graphene sheet suggesting there is an affinity between these atoms and the graphene (Figure

9-7). These results are consistent with the previous DFT calculations which showed that hydrogen atoms attached to aromatic rings play a significant role in aromatic interactions⁷³ and that weak hydrogen bonds (CH/ π) exist between a soft acid (CH) and a soft base (π group)^{74, 236, 237}.

From Figure 9-8 the top down view shows that at 3.5 ps, one of the aromatic rings in PC is aligned almost parallel to the graphene plane while the second aromatic ring is edge on (almost perpendicular) to the graphene. Edge on and skewed stacking are common in aromatic π -interactions⁷⁴. At 5 ps the aromatic ring in the SBS is offset to the graphene in a similar fashion to the AB stacking of graphite⁸ while the other ring is edge on to the graphene. Thus the two aromatic rings are $\sim 90^\circ$ offset to each other for the interaction with graphene to be maximised. Also, the methyl groups on the PC are oriented towards the graphene forming a possible CH/ π -type interaction. The complexity of the PC monomer and the fact that it has two aromatic rings and two methyl groups means that the interactions with graphene are not purely one or the other but seem to be a combination of π - π and CH/ π type interactions.

9.4 Conclusion

Low defect graphene at a low loading (0.1 %·w/w), prepared by hydrogen and carbon monoxide reduction, was dispersed in polycarbonate using ultrasonication and melt dispersion. GT-CO and GT-H₂ graphene treatments were compared. Visual inspection showed GT-CO reduced graphene in PC was slightly darker suggesting greater reduction, dispersion and exfoliation. Optical and TEM microscopy showed the even distribution in PC with no evidence of any multi-layer graphene. The largest effect on polycarbonate performance was by carbon monoxide reduced graphene which increased viscoelasticity (loss modulus) of polycarbonate. However, the loss modulus in PC is very low, and this makes the increase less noteworthy. Storage modulus which is an indication of stronger interfacial interactions is a significant feature of PC and increases favoured hydrogen reduced graphene suggesting increased hydrogen bonding. DFT calculations showed that there is an interaction between the PC polymer and the graphene. While this interaction is relatively weak, the aromatic rings and the methyl groups in the monomer both play a significant role in the attraction with graphene via π -interactions. GT-CO reduced graphene showed evidence of scrolling while GT-H₂ reduced graphene may involve increased hydrogen bonding which may explain the performance difference between the two alternative graphenes.

Chapter 10 Polyether Sulfone-Graphene Composites

10.1 Introduction

In this chapter, a solvent dispersion method was employed with an ultrasonic dispersion of graphene for the preparation of high-performance polymer composites. Polyethersulfone (PES) is a tough polymer (high modulus, tensile yield and impact strength), with high-temperature stability ($T_g \sim 220\text{-}230\text{ }^\circ\text{C}$)^{233, 238-240}. It is commonly used in water filtration^{105, 241, 242}, medical applications^{12, 239, 243} and as a flame retardant but its resistance to weathering and some organic solvents is poor²⁴⁰. The repeat unit (Figure 10-1) contains a series of four aromatic rings, ether (R-O-R') and a sulfone (R-SO₂-R').

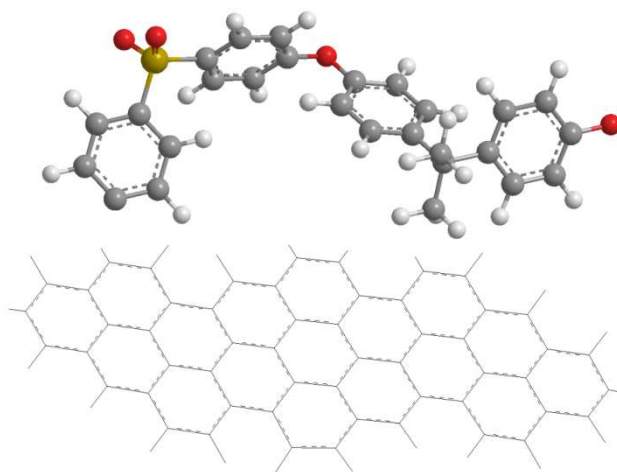


Figure 10-1 Molecular representation of the PES monomer and graphene sheet

PES is an amorphous polymer (has no crystallinity)²⁴⁴. Amorphous polymers make it easier to establish which reinforcing effects are due to the addition of nanomaterials such as graphene²²⁹. A further consideration was that PES has a high glass temperature (T_g) which allows the polymer to be tested across a wider temperature range.

Previous research has demonstrated the ability of graphene to improve the properties of aromatic polymers through its affinity for π -interactions¹⁸¹. The ring structure of PES complements that of graphene. Thus the π -interactions between the PES and graphene rings can be used to improve dispersion and prevent agglomeration of the graphene. π -interactions can occur between the π -electrons (double bonds) of the sulfone group (O=S=O) and graphene. The magnitude of those π - π interactions (adsorption energy $E_{CC} = 49.2\text{ meV}$) also

increases significantly in aromatic molecules as the number of hydrogen atoms ($E_{\text{CH}} = 80.1 \text{ meV}$) increases⁷³. The PES monomer has four hydrogen atoms attached to each of the aromatic rings (16 hydrogens in total) that can increase π - π interactions. Weak hydrogen bonding also exists between a soft acid (CH) and a soft base (π -group)^{74, 236, 237}. PES (C₂₇H₂₂O₄S)_n has 22 hydrogen atoms in total (elemental analysis C 73.3 % H 5.01 %) which can interact with graphene.

Solvent dispersion is a simple laboratory technique, compatible with PES, which permits small composite mass making it ideal for rapid iterative investigations. These considerations all make PES a good candidate for a test polymer.

The aim of this experiment was to prepare PES-graphene composites using H₂ and CO reduced graphenes, ultrasonication and solvent dispersion. The effectiveness of interactions in the composites due to combining the polar sulfone group with aromatic groups will be established by observing dispersion and measuring performance.

10.2 Experimental

Material information, preparation of nanocomposites and characterisation methods are detailed in Chapter 3.

10.3 Results and Discussion

10.3.1 Microscopy

Electron microscopy was used to characterise graphenes and PES-graphene composites. It was used to confirm the quality of the graphene and reveal detail about the structure of PES-graphene composites.

Transmission electron microscopy (TEM) was required to resolve individual graphene layers. Individual graphene layers are often stacked on top of each other making it hard to determine if they are multi-layer or single layer. The number of layers can be determined by observing if graphene sheets overlap in a disordered manner (single layer) or if they exhibit regularly spaced fringes (multi-layer). Another problem is that as the concentration of graphene in the polymer increases it can be harder to identify single layer graphene. Thus areas of high contrast are ideal to establish the dispersion of graphene and the number of layers. A series of images at increasing resolutions were taken in the same location to allow useful comparison.

PES GT-H₂ 1 % polymer composites (Figure 10-2) show no visible clumping of graphene, no discernible multi-layer graphene and no small graphene particles even at high resolution. A sheet of graphene is visible at resolutions of 200, 100, 50 and 20 nm. As no fringes are visible at the edges (Figure 10-2d), it is identified as a single layer of graphene. The polymer edges are slightly uneven (Figure 10-2a), but the polymer-graphene interface is even (no gaps) demonstrating good interfacial compatibility and adhesion.

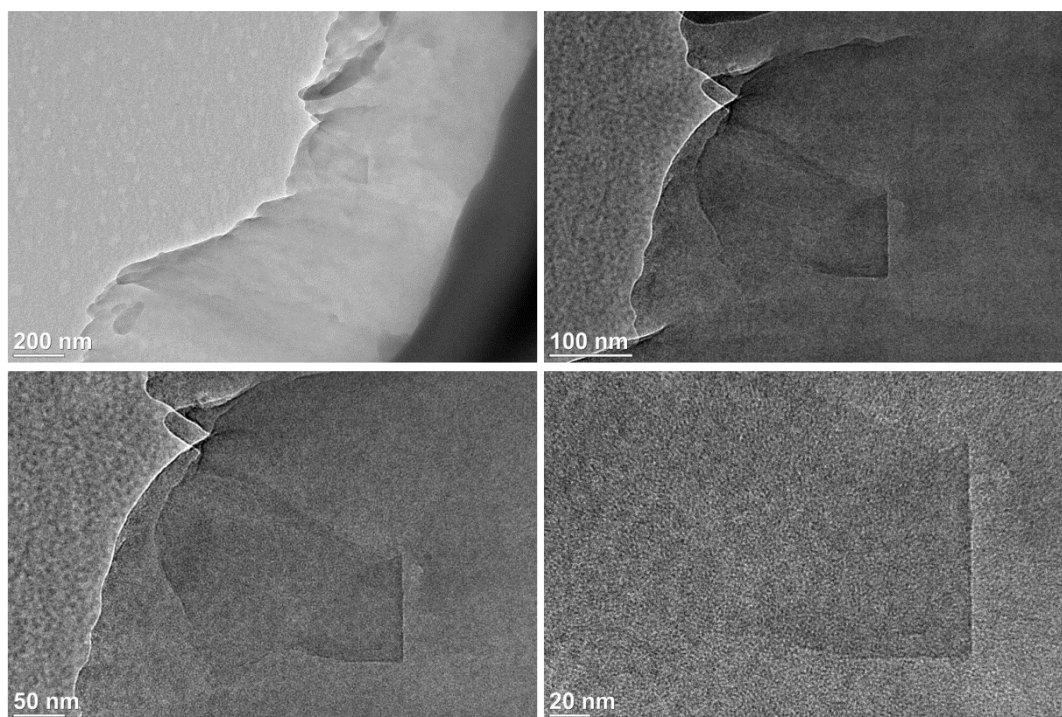


Figure 10-2 TEM images of PES GT-H₂ 1 % US and SD a) 200 nm b) 100 nm c) 50 nm d) 20 nm

PES GT-CO 1 % polymer composites (Figure 10-3) showed no visible clumping of graphene and no discernible multi-layer graphene. The dark areas show apparent graphene scrolling. The effect is unlike that visible in the GT-H₂ reduced composite (Figure 10-2). At higher resolution (Figure 10-3d) graphenes appeared to be single layer (no striated edges). The polymer shows a smooth PES-graphene interface demonstrating good compatibility and adhesion. Comparable PES-graphene oxide (0.5 %) covalently bonded composites had a much less even dispersion of graphene²⁴⁵.

TEM images of both PES composites showed an even distribution of graphene with good compatibility (evidence of adhesion). However, GT-CO reduced graphene appeared more prone to rolling or scrolling which created darker lines throughout the PES. Scrolling is

expected of pristine graphene²⁴⁶ and is triggered by ultrasonication especially in low defect graphene⁵². Scrolling increases the aspect (width to height) ratio of graphene which makes it easier for them to touch (similar to nanotubes)^{22, 247} providing improved electrical and thermal conductivity.

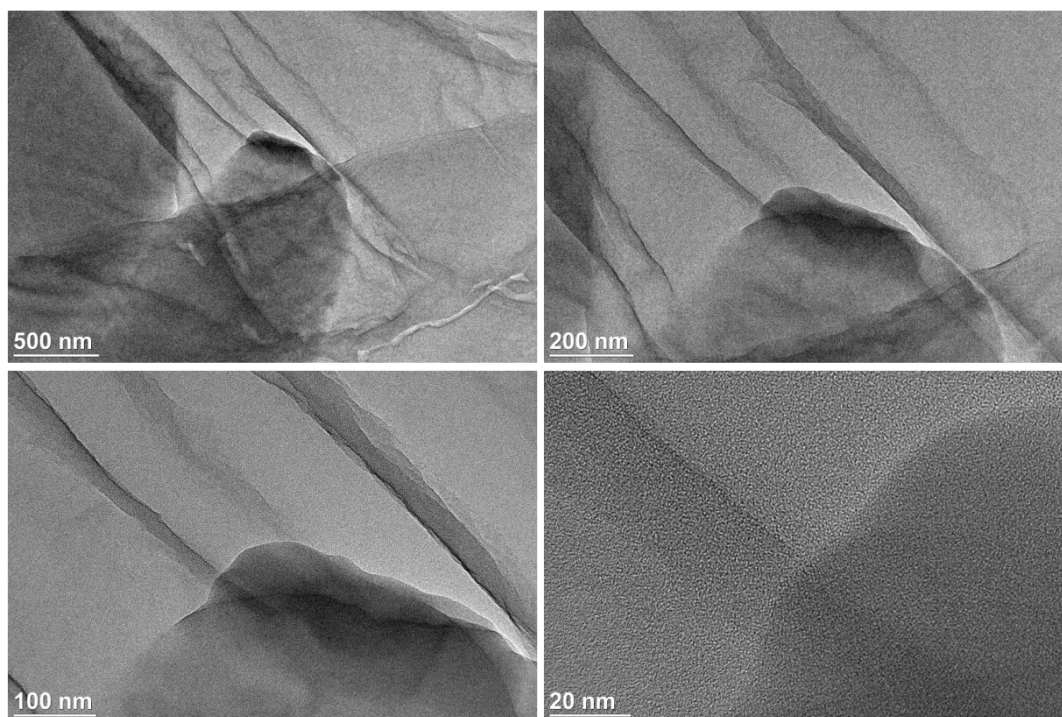


Figure 10-3 TEM images of PES GT-CO 1 % US and SD a) 500 nm b) 200 nm c) 100 nm d) 20 nm

10.3.2 Mechanical Properties

10.3.2.1 Tensile Mechanical Analysis

Stress-strain tensile mechanical analysis (SS-MA) was used to characterise and compare the mechanical performance of PES-graphene composites. A hysteresis curve was created to provide information about the reversible performance of PES by applying and then removing a ramped force of 18 N.

The tangent modulus (stress/strain Figure 10-4) was compared to neat PES at a strain of 0.05 %. PES GT-H₂ 1 % increased in stiffness (+18 %) while the PES GT-CO 1 % decreased in stiffness (-7 %). In a similar study, utilising covalent bonding, the elastic modulus (stress/strain) of sulfonated PES increased (+35 %) upon the addition of 10 % graphene oxide²⁴¹. Thus PES GT-H₂ 1 % achieved half (51 %) of the elastic modulus using much less graphene (-90 %). A second study with covalently bonded PES-graphene oxide 1 %

composites achieved a 17 % (187 MPa versus 218 MPa) increase in tensile modulus (stress/strain)²⁴⁵ which is similar to that achieved using PES GT-H₂. These results suggest that depending on which graphene was used the stiffness of PES could be increased or decreased using only π -interactions. However sampling uniformity and experimental error may make these changes insignificant.

The hysteresis curves for the two PES composites were compared to neat PES. Max strain for the PES GT-H₂ 1 % composite showed reduced stretching (-19 %) whereas the PES GT-CO 1 % composite showed an insignificant increase (+1 %). When end strain was compared, PES GT-H₂ showed a reduction in deformation (-42 %) on recovery. Reduced stretching and deformity suggest stronger cross-linking between GT-H₂ graphene and PES possibly due to increased hydrogen bonding. Permanent deformation is an undesirable outcome for most polymers, and thus a reduction is usually welcome.

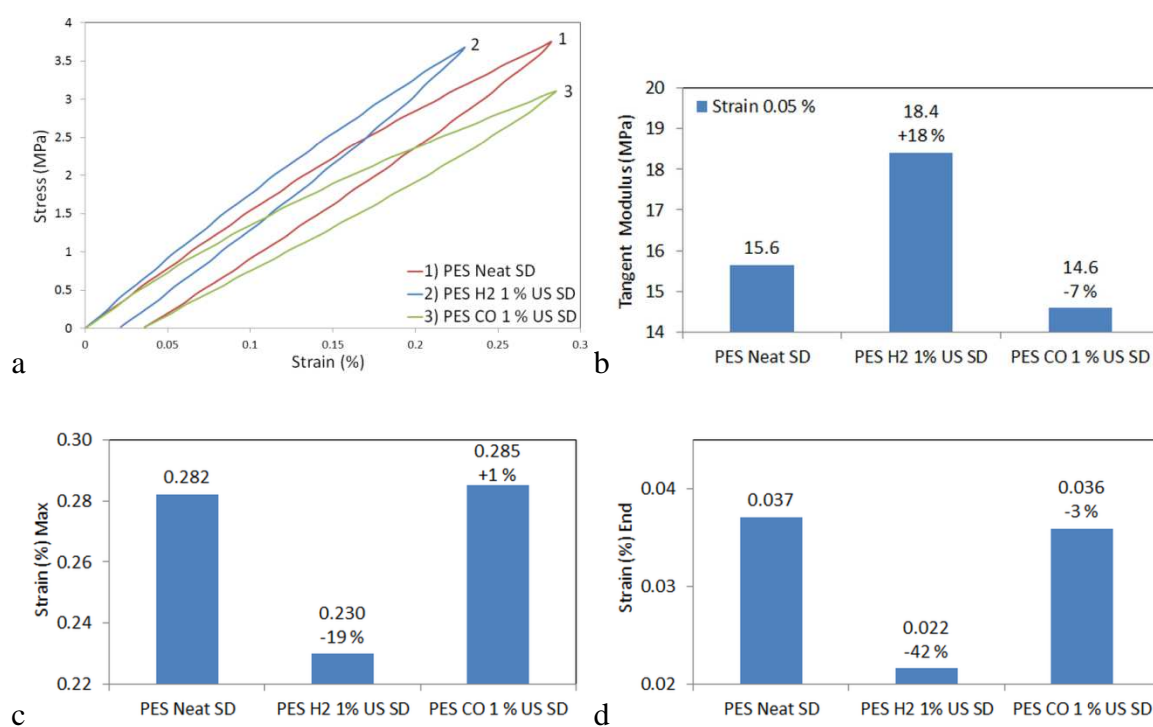


Figure 10-4 Stress-strain mechanical analysis a) Hysteresis curves b) Tangent modulus
c) Max strain d) End strain

SS-MA results demonstrated that GT-H₂ (1 %) reduced graphene with ultrasonication and solvent dispersion increased stiffness (+18 %), decreased stretching of PES under load (-19 %) and decreased deformation on recovery (-42 %) while GT-CO reduced graphene had

a negligible effect on all three metrics. However, given the relatively small changes in absolute terms, these results may not be significant.

10.3.2.2 Dynamic Mechanical Analysis

Dynamic Mechanical Analysis (DMA Figure 10-5) is used to characterise materials and compare them at different temperatures. As the temperature was increased storage modulus (elasticity), loss modulus (viscoelasticity) and tan delta (damping) were measured at a given frequency (1 Hz).

The storage modulus of PES composites at 40 °C was compared to neat PES (1.1 GPa). Compared to neat PES the storage modulus of PES GT-H₂ 1 % (1.8 GPa +63 %) and PES GT-CO 1 % (2.2 GPa +98 %). The storage modulus of PES GT-CO composites was +35 % higher than that of PES GT-H₂. Storage modulus measures the immediate response of stored energy (elastic portion), and an increase indicates improved interfacial interaction of PES with graphene. A similar study using sulphonated PEEK (poly(ether ether ketone)) and covalent bonding with graphene oxide (GO) obtained an ~86 % (+0.65 GPa) increase in storage modulus²⁴⁸. Thus stronger interfacial interactions are demonstrated between PES and GT-CO reduced graphene using only π -interactions and can be similar to those achieved with covalent bonding.

The loss modulus of PES composites at 40 °C was compared to neat PES (48 MPa). PES GT-H₂ 1 % (57 MPa +19 %) and PES GT-CO 1 % (63 MPa +33 %) both showed increases compared to neat PES. However, the loss modulus of PES GT-CO was higher (+14 %) than that of PES GT-H₂. This means the time-dependent delayed response (viscous portion) increased when graphene was added to PES.

Tan delta of PES composites at 40 °C was compared to neat PES (0.043). PES GT-H₂ 1% (0.031 -27 %) and PES GT-CO 1 % (0.029 -33 %) both showed reductions compared to neat PES. This decrease in damping (movement to a more solid state) can be attributed to a decrease in free volume (enhanced interfacial interactions) and the graphene hindering the motion of the matrix (PES) chains. The enhanced interfacial interaction of GT-CO reduced graphene over GT-H₂ reduced graphene may indicate less steric hindrance due to decreased oxide levels or greater surface area due to better exfoliation. However given that the tan delta range is 0-2 the differences are negligible.

The DMA probe demonstrates that both GT-H₂ 1 % and GT-CO 1 % reduced graphene when combined with ultrasonication and solvent dispersion improved the elasticity (storage) and viscoelasticity (loss) while lessening the damping of PES. However, GT-CO reduced graphene had the greatest effect on storage (+98 %), loss (+33 %) and tan delta (-33 %) demonstrating improved interactions between GT-CO reduced graphene and PES even at a relatively low loading.

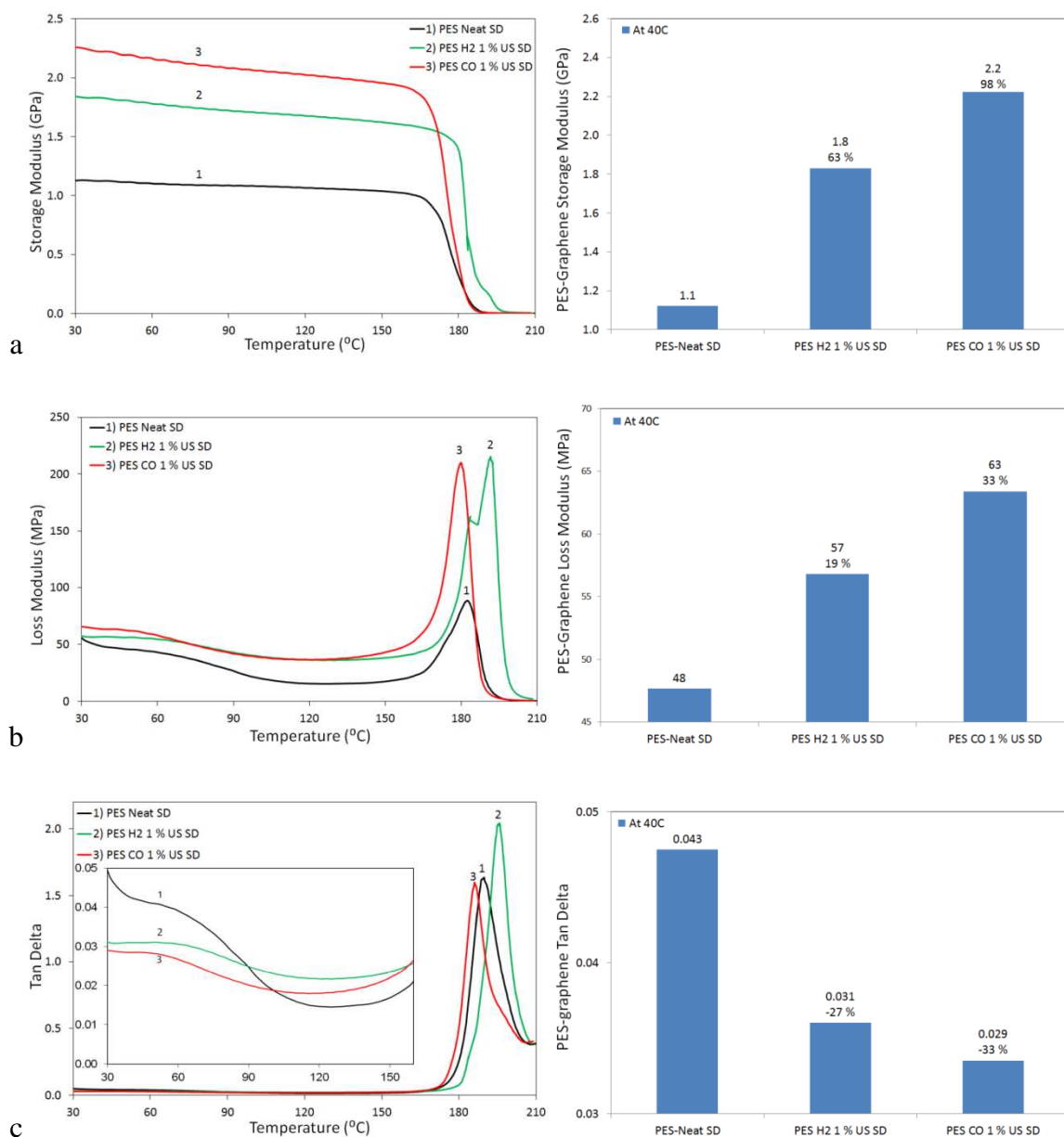


Figure 10-5 PES CO 1 % SD a) Storage modulus b) Loss Modulus c) Tan Delta

10.4 Conclusion

Polyethersulfone graphene (1 %) composites prepared using ultrasonication and cast using solvent dispersion compared the effectiveness of interactions of GT-H₂ and GT-CO reduced graphenes with the polymer. TEM microscopy showed that both GT-H₂ and GT-CO reduced graphenes were compatible with PES with good interfacial adhesion. However, GT-CO reduced graphene showed darker lines which appeared to be rolling or scrolling of graphene. Stress-strain measurements demonstrated that GT-H₂ (1 %) reduced graphene decreased deformation of PES as stiffness increased while GT-CO (1 %) reduced graphene had a negligible effect on deformation, stiffness and strain on recovery. However, absolute differences were small, so the results may not be significant. Increased interfacial interactions, increased viscoelasticity with decreased free volume demonstrated that interactions between PES GT-CO increased indicating a move to a more solid state and an increase in the elastic nature of PES. These results established that PES binds well with graphene (non-covalent bonding) and matched the performance of covalently bonded graphene.

However, scrolling of GT-CO reduced graphenes may be of greatest interest because the increased cross-sectional area of such graphenes may lead to improved thermal and electrical conductivity.

Chapter 11 Conclusion

11.1 Conclusion

This research aimed to prepare graphene, and to reactively modify its surface to enhance exfoliation and facilitate bonding to chosen matrix polymers; to characterise the prepared materials and determine their physical and mechanical properties. Five research objectives were formulated to accomplish the research aim. These objectives are composed of two key parts: 1) Preparation of graphene and 2) Combination of graphene with polymers. To achieve these objectives, a thermal expansion method was used to produce low-defect graphene using inert or reducing gases and to improve its dispersion using ultrasonication. Four types of thermoplastic polymers were used as examples to bond with the graphene: poly(styrene-*b*-butadiene-*b*-styrene), poly(ethylene terephthalate), polycarbonate and polyether sulfone. Two major dispersion methods were used: solvent and melt dispersion.

Graphene was successfully produced using a thermal (air) expansion method. Defects in the graphene sheets (and specifically oxides) were successfully removed using inert (N_2) or reducing gases (H_2 and CO). Other graphene defects (voids and inclusions) were repaired using CO. The results were compared to a commercial graphene (CT). To overcome the problem of graphene agglomeration, exfoliation of the graphene sheets was achieved by using aromatic solvents (*p*-xylene) and ultrasonication. The *p*-xylene was shown to bond to the graphene using π -interactions that assisted with exfoliation of the layers. Raman spectroscopy showed that CO reduction produced the lowest D/G ratio (a measure of defects) and the highest 2D/G ratio (indicating the fewest number of graphene layers). Contact angle measurements showed CO reduction produced the most hydrophobic graphene (the highest contact angle and lowest surface energy). Electron microscopy showed that single layer graphene (with some scrolling) was being produced using CO reduction. Density functional theory calculations were used to show that *p*-xylene adsorbed parallel to the graphene plane leading to the enhanced dispersion of graphene. These tests showed CO-reduced graphene was superior to the other graphenes. Low defect graphene is uncommon and has previously not been available in larger quantities which were shown can be produced using this method.

Graphene was dispersed in an aromatic polymer using π -interactions. SBS graphene 1 %·w/w composites were prepared using thermally expanded (Air, N_2 , H_2), functionalised (Fe_3O_4) and commercial (CT) graphenes with ultrasonication and solvent dispersion. SBS composites

using thermally expanded H₂ reduced graphene had stronger interfacial interactions (storage modulus) and lost more energy (loss modulus) than any other graphene. Graphene dispersion using ultrasonic shear depended on π -interactions between the aromatic rings of the solvent, graphene and polystyrene to disperse the graphene in the polymer and stabilise the dispersion against agglomeration. The formation of π -interactions avoided the creation of new defects in graphene and maintained the perfect sp² structure of a low defect graphene. The dispersion of low defect graphene in polymers is uncommon as they have previously not been available in sufficient quantity.

The amount of graphene that was dispersed in an aromatic polymer was varied. SBS composites were prepared with up to 20 %·w/w low defect GT-CO reduced graphene using ultrasonication and solvent dispersion. The effectiveness of the dispersion was demonstrated by the performance of the SBS that was enhanced by the GT-CO reduced graphene to 20 %·w/w: showing that its deformation decreased as the stiffness increased. The existence of single layer graphene (with some scrolling) in SBS was verified using TEM, and the interactions between the SBS and graphene were validated using DFT calculations. They confirmed that π -interactions between the components were effective for dispersing graphene even at higher loadings. Further improvements in performance were shown to be possible with longer ultrasonication times at higher graphene loadings.

Graphene was dispersed using melt dispersion and solvent dispersion. PET GT-H₂ 1 %·w/w reduced low defect graphene composites were prepared using melt dispersion (without ultrasonication) and solvent dispersion (with ultrasonication). The addition of reduced graphene did not affect crystallinity in PET composites. Reduced graphene increased permeation of O₂, and the effect was largest with ultrasonication. This effect is opposite to that of oxidised graphene (which reduces O₂ permeation). Ultrasonication produced composites with raised fracture lines (observed using SEM) and fewer multi-layer graphenes (revealed using TEM) suggesting better separation of graphene sheets. Melt dispersion produced composites which had higher stiffness, reduced deformation, better interfacial interactions, greater energy loss through increased viscoelasticity while moving toward a liquid state with increasing free volume. DFT calculations of the PET-graphene interactions validated the dispersion of graphene in PET. The results suggested that ultrasonication and melt dispersion ought to be combined.

Graphenes were dispersed with and without ultrasonication. PET GT-CO 1 % reduced graphene composites were prepared using melt dispersion with and without ultrasonication. Ultrasonication produced composites that were black, typical of reduced graphene, compared to those without ultrasonication which were grey. Ultrasonication significantly reduced graphene agglomeration. Single layer graphene existed in both ultrasonicated and non-ultrasonicated composites, but more single layer graphene existed when ultrasonication was used. Ultrasonication of graphene before dispersion in PET increased stiffness, energy lost through increased viscoelasticity and damping.

Polycarbonate composites with low loadings (0.1 %·w/w) of ultrasonicated GT-H₂ and GT-CO low defect graphenes were prepared using melt dispersion. PC GT-CO composites showed increased energy lost due to viscoelasticity and a move to a more liquid state (greater free volume). However, the absolute values were small, so any improvements were insignificant. PC interfacial interactions (storage modulus) increased slightly for both GT-CO and GT-H₂ reduced graphene but favoured hydrogen reduced graphene. TEM microscopy showed single layer graphene in both composites with no evidence of any multi-layer graphene. GT-CO reduced graphene showed signs of scrolling (greater cross-sectional area) while GT-H₂ reduced graphenes implied increased hydrogen bonding and this may explain the performance difference between the two alternative graphenes. DFT calculations were used to show that the PC and graphene interacted via π -interactions.

Polyethersulfone graphene (1 %) composites were prepared using ultrasonication and solvent dispersion compared the performance enhancing effects of GT-H₂ and GT-CO reduced graphene. TEM microscopy showed that both GT-H₂ and GT-CO reduced graphenes were present as single layers in PES. However, GT-CO reduced graphene showed darker lines which appeared to be rolling or scrolling of graphene. Stress-strain measurements revealed that GT-H₂ reduced graphene decreased the maximum deformation of PES and increased stiffness but had no effect on the strain on recovery. GT-CO reduced graphene had a negligible effect on deformation, stiffness and strain on recovery. Increases in interfacial interactions, energy lost through viscoelasticity and slight move to a more solid state (with less free volume) showed the greatest changes occurred with GT-CO reduced graphene.

Thermal expansion and repair, in a reducing carbon monoxide atmosphere, was an efficient and effective means to produce low defect graphenes. Dispersed in aromatic solvents these graphenes were solution or melt dispersible in aromatic thermoplastic polymers such as SBS,

PET, PC or PES provided reinforcement with graphenes due to π -interactions and weak hydrogen bonding. Melt dispersion combined with ultrasonication was the most efficient method of dispersing graphene in polymers. DMA measurements of energy storage (storage modulus), energy loss (loss modulus) and their ratio (tan delta) were the most sensitive to changes in aromatic polymers when graphene was added. The enhanced properties of aromatic polymers continued to increase up to a graphene loading of 20 %. The performance of aromatic polymers using low defect graphene was similar to that reported when incorporating high defect graphene via covalent bonding. Scrolling of GT-CO reduced graphenes may be of great interest because the increased cross-sectional area of such graphenes may lead to improved thermal and electrical conductivity.

11.2 Applications of This Work

The immediate uses of this research could include the greater use of low defect graphene and the improved dispersion of graphene in aromatic polymers. Industries that could immediately benefit include those of aerospace and electronics. Possible products where the low-defect graphene could be used include 3D printing, safety equipment (such as helmets) and electronically or thermally conductive polymers.

11.3 Future Ideas

11.3.1 Improved Dispersions

Improve dispersion of graphene using ultrasonication could be achieved using a Rosette cooling cell and a glass cooling cell which both improve the circulation and cooling. It is estimated that better circulation would halve the ultrasonication time. Better cooling is likely to also reduce ultrasonication time by around 50 %²⁴⁹.

11.3.2 Bonding With Other Polymers

The use of non-aromatic polymers to disperse low-defect graphene using melt dispersion (with ultrasonication) could be tried. It could be expected that mechanical dispersion forces and hydrogen bonding will prevent the agglomeration of graphenes. Thus by achieving good graphene dispersion before adding to a polymer, *many* of the desirable properties may be retained.

11.3.3 Other Improved Properties

Low defect graphenes offer an advantage over high defect graphenes as they are more likely to be conductive. The tendency of low defect graphenes to scroll, especially after ultrasonication, makes them somewhat similar in profile to nanotubes which achieve conductivity at much lower concentrations than graphene. A question may be asked at what %·w/w level do polymer composites become conductive? Aromatic polymers are assumed to be advantageous for such experiments, but non-aromatic polymers may encourage graphenes to curl as they are not likely to contain rigid aromatic rings.

Further investigation of which aromatic polymers properties (e.g. cracking, heat transfer, durability, capacitance, EMF shielding) are most enhanced by the addition of low defect graphene could be attempted. Graphene is non-polar and thus non-polar polymers should be preferred.

Investigation of the effect of graphene loading on the storage modulus, loss modulus and tan delta of the polymer composites would be useful. These properties showed the greatest improvements, but it was unclear if they would continue to improve as the loading of graphene increased past 3 % (the loading limit in other studies). Other research in this area has primarily concentrated on covalently bonded graphene, but it would be useful to know how low-defect graphene behaves and what is the maximum loading achievable before these properties stop improving.

Other research questions that might be addressed are: Can low defect graphene be used to reinforce polymers such as PDMS to increase the speed of gas filtration²⁵⁰? Do low oxide levels provide an advantage?

How much does low defect graphene improve fracture toughness in brittle polymers such as epoxy? Improved fracture toughness is of keen interest in the aerospace industry and where high performance is required (such as for motorcycle helmets). It is likely that dispersions of 0.1 % or less may have meaningful benefits¹¹. Such low loadings would be cost effective and should be easy to achieve.

11.3.4 Improved Production Methods

Investigation of other methods for improving the production of low-defect graphene could be pursued. Methods of improving production could include low-cost sources of CO, reducing energy losses and high-temperature laser expansion.

11.3.5 Scalability

To produce sufficient quantities of graphene for commercialisation, the lab techniques discovered in this work need to be scalable. By using upscaled ultrasonication: larger 1,000 W, 1,500 W, etc... ultrasonicators can treat larger quantities of graphene (using bigger tips) and decrease the ultrasonication time by 50 % (or more). To be commercially useful for larger projects the time to treat larger amounts of graphene (1 kg or more) needs to be ~1 hour or less.

Also investigation of alternative cavitation techniques which are more scalable than ultrasonication could be useful. Companies such as Hydrodynamics have cavitation techniques that replace ultrasonication but can handle huge volumes with rapid throughput.

References

- 1 *John Mackenzie Grant Cowie, and Valeria Arrighi, Polymers: Chemistry and Physics of Modern Materials (CRC press, 2007).*
- 2 *Ron Beech, 'Nanoscale Graphene Platelets Taking Its Place as an Emerging Class of Nanomaterials', Nanotechnology Law & Business, 8 (2011), 3.*
- 3 *Hyunwoo Kim, Ahmed A. Abdala, and Christopher W. Macosko, 'Graphene/Polymer Nanocomposites', Macromolecules, 43 (2010), 6515-30.*
- 4 *Hyunwoo Kim, Yutaka Miura, and Christopher W. Macosko, 'Graphene/Polyurethane Nanocomposites for Improved Gas Barrier and Electrical Conductivity', Chemistry of Materials, 22 (2010), 3441-50.*
- 5 *Kostyantyn V. Zakharchenko, Annalisa Fasolino, J. H. Los, and M. I. Katsnelson, 'Melting of Graphene: From Two to One Dimension', Journal of Physics: Condensed Matter, 23 (2011), 202202.*
- 6 *Nobel Prize, 'Nobel Prize in Physics 2010' (2010) <http://nobelprize.org/nobel_prizes/physics/laureates/2010/press.html> [Accessed 27/5/11 2011].*
- 7 *Mohammed Khenfouch, U. Buttner, and Mimouna Ba, 'Synthesis and Characterization of Mass Produced High Quality Few Layered Graphene Sheets Via a Chemical Method', Graphene, 2014 (2014).*
- 8 *Eric Pop, Vikas Varshney, and Ajit K. Roy, 'Thermal Properties of Graphene: Fundamentals and Applications', MRS Bulletin, 37 (2012), 1273-81.*
- 9 *Chintamani. N. R. Rao, A. K. Sood, Rakesh Voggu, and K. S. Subrahmanyam, 'Some Novel Attributes of Graphene', The Journal of Physical Chemistry Letters, 1 (2010), 572-80.*
- 10 *Andre K. Geim, and Konstantin S. Novoselov, 'The Rise of Graphene', Nature materials, 6 (2007), 183-91.*
- 11 *Shuying Wu, Raj B. Ladani, Jin Zhang, Ehsan Bafekrpour, Kamran Ghorbani, Adrian P. Mouritz, Anthony J. Kinloch, and Chun H. Wang, 'Aligning Multilayer Graphene Flakes with an External Electric Field to Improve Multifunctional Properties of Epoxy Nanocomposites', Carbon, 94 (2015), 607-18.*
- 12 *Tahmineh Forati, M. Atai, A. M. Rashidi, M. Imani, and A. Behnamghader, 'Physical and Mechanical Properties of Graphene Oxide/Polyethersulfone Nanocomposites', Polymers for Advanced Technologies, 25 (2014), 322-28.*

- 13 *Rahul. R. Nair, P. Blake, A. N. Grigorenko, K. S. Novoselov, T. J. Booth, T. Stauber, N. M. R. Peres, and A. K. Geim, 'Fine Structure Constant Defines Visual Transparency of Graphene', Science, 320 (2008), 1308-08.*
- 14 *Zhu Shou-En, Yuan Shengjun, and G. C. A. M. Janssen, 'Optical Transmittance of Multilayer Graphene', EPL (Europhysics Letters), 108 (2014), 17007.*
- 15 *Christopher C. Ibeh, 'Nanoscale Trends, Opportunities and Emerging Markets'.*
- 16 *Jenny Malig, J. M. Englert, A. Hirsch, and D. M. Guldi, 'Wet Chemistry of Graphene', Electrochemical Society Interface (2011), 53.*
- 17 *'Grafguard Expandable Graphite Flake', (Graphtech, 2011).*
- 18 *Sophie Duquesne, Michel Le Bras, Serge Bourbigot, René Delobel, Hervé Vezin, Giovanni Camino, Berend Eling, Chris Lindsay, and Toon Roels, 'Expandable Graphite: A Fire Retardant Additive for Polyurethane Coatings', Fire and Materials, 27 (2003), 103-17.*
- 19 *Mario Martin-Gallego, R. Verdejo, M. A. Lopez-Manchado, and M. Sangermano, 'Epoxy-Graphene UV-Cured Nanocomposites', Polymer, 52 (2011), 4664-69.*
- 20 *Pingan Song, Zhenhu Cao, Yuanzheng Cai, Liping Zhao, Zhengping Fang, and Shenyuan Fu, 'Fabrication of Exfoliated Graphene-Based Polypropylene Nanocomposites with Enhanced Mechanical and Thermal Properties', Polymer, 52 (2011), 4001-10.*
- 21 *Jeffrey R. Potts, Shanthi Murali, Yanwu Zhu, Xin Zhao, and Rodney S. Ruoff, 'Microwave-Exfoliated Graphite Oxide/Polycarbonate Composites', Macromolecules, 44 (2011), 6488-95.*
- 22 *Ming Fang, Kaigang Wang, Hongbin Lu, Yuliang Yang, and Steven Nutt, 'Covalent Polymer Functionalization of Graphene Nanosheets and Mechanical Properties of Composites', Journal of Materials Chemistry, 19 (2009), 7098-105.*
- 23 *Carola Esposito Corcione, Fabrizio Freuli, and Alfonso Maffezzoli, 'The Aspect Ratio of Epoxy Matrix Nanocomposites Reinforced with Graphene Stacks', Polymer Engineering & Science, 53 (2012), 531-39.*
- 24 *Nobel Foundation, 'Nobel Prize in Physics 2010'2010) <http://nobelprize.org/nobel_prizes/physics/laureates/2010/press.html> [Accessed 27/5/11 2011].*
- 25 *Michio Inagaki, Y. A. Kim, and M. Endo, 'Graphene: Preparation and Structural Perfection', Journal of Materials Chemistry, 21 (2011), 3280-94.*
- 26 *Changgu Lee, Xiaoding Wei, Jeffrey W. Kysar, and James Hone, 'Measurement of the Elastic Properties and Intrinsic Strength of Monolayer Graphene', Science, 321 (2008), 385-88.*

- 27 *Rahul. R. Nair, H. A. Wu, P. N. Jayaram, I. V. Grigorieva, and A. K. Geim, 'Unimpeded Permeation of Water through Helium-Leak-Tight Graphene-Based Membranes', Science, 335 (2012), 442-44.*
- 28 *Kian Ping Loh, Q. Bao, P. K. Ang, and J. Yang, 'The Chemistry of Graphene', Journal of Materials Chemistry, 20 (2010), 2277-89.*
- 29 *Daniel R. Dreyer, S. Park, C. W. Bielawski, and R. S. Ruoff, 'The Chemistry of Graphene Oxide', Chemical Society Reviews, 39 (2010), 228-40.*
- 30 *Yu Teng Liang, and Mark C. Hersam, 'Towards Rationally Designed Graphene-Based Materials and Devices', Macromolecular Chemistry and Physics, 213 (2012), 1091-100.*
- 31 *Rama K. Layek, and Arun K. Nandi, 'A Review on Synthesis and Properties of Polymer Functionalized Graphene', Polymer, 54 (2013), 5087-103.*
- 32 *Vijay Kumar Rana, Myeon-Cheon Choi, Jin-Yeon Kong, Gwang Yeon Kim, Mi Ju Kim, Sun-Hee Kim, Satyendra Mishra, Raj Pal Singh, and Chang-Sik Ha, 'Synthesis and Drug-Delivery Behavior of Chitosan-Functionalized Graphene Oxide Hybrid Nanosheets', Macromolecular Materials and Engineering, 296 (2011), 131-40.*
- 33 *Jun Ma, Qingshi Meng, Izzuddin Zaman, Shenmin Zhu, Andrew Michelmore, Nobuyuki Kawashima, Chun H Wang, and Hsu-Chiang Kuan, 'Development of Polymer Composites Using Modified, High-Structural Integrity Graphene Platelets', Composites Science and Technology, 91 (2014), 82-90.*
- 34 *Marco Sangermano, Sophie Marchi, Luca Valentini, Silvia Bittolo Bon, and Paola Fabbri, 'Transparent and Conductive Graphene Oxide/Poly(Ethylene Glycol) Diacrylate Coatings Obtained by Photopolymerization', Macromolecular Materials and Engineering (2010).*
- 35 *Laura J. Cote, R. Cruz-Silva, and J. Huang, 'Flash Reduction and Patterning of Graphite Oxide and Its Polymer Composite', Journal of the American Chemical Society, 131 (2009), 11027-32.*
- 36 *Cristina Gómez-Navarro, Jannik C. Meyer, Ravi S. Sundaram, Andrey Chuvilin, Simon Kurasch, Marko Burghard, Klaus Kern, and Ute Kaiser, 'Atomic Structure of Reduced Graphene Oxide', Nano Letters, 10 (2010), 1144-48.*
- 37 *Martin Cadek, Otto Vostrowsky, and Andreas Hirsch, 'Carbon, 7. Fullerenes and Carbon Nanomaterials', in Ullmann's Encyclopedia of Industrial Chemistry (Wiley-VCH Verlag GmbH & Co. KGaA, 2000).*
- 38 *Sharmistha Basu-Dutt, Marilyn L. Minus, Rahul Jain, Dhriti Nepal, and Satish Kumar, 'Chemistry of Carbon Nanotubes for Everyone', Journal of Chemical Education, 89 (2011), 221-29.*

- 39 Yi-Tao Liu, Xu-Ming Xie, and Xiong-Ying Ye, 'High-Concentration Organic Solutions of Poly(Styrene-co-Butadiene-co-Styrene)-Modified Graphene Sheets Exfoliated from Graphite', *Carbon*, 49 (2011), 3529-37.
- 40 Goki Eda, James Ball, Cecilia Mattevi, Muge Acik, Luca Artiglia, Gaetano Granozzi, Yves Chabal, Thomas D. Anthopoulos, and Manish Chhowalla, 'Partially Oxidized Graphene as a Precursor to Graphene', *Journal of Materials Chemistry*, 21 (2011), 11217-23.
- 41 Waleed E. Mahmoud, 'Morphology and Physical Properties of Poly(Ethylene Oxide) Loaded Graphene Nanocomposites Prepared by Two Different Techniques', *European Polymer Journal*, 47 (2011), 1534-40.
- 42 Khaled Parvez, Sheng Yang, Xinliang Feng, and Klaus Müllen, 'Exfoliation of Graphene Via Wet Chemical Routes', *Synthetic Metals*, 210 (2015), 123-32.
- 43 William S. Hummers Jr, and Richard E. Offeman, 'Preparation of Graphitic Oxide', *Journal of the American Chemical Society*, 80 (1958), 1339-39.
- 44 Dominik Eder, and Robert Schlägl, *Nanocarbon-Inorganic Hybrids (De Gruyter, 2014)*.
- 45 Jeffrey R. Potts, Daniel R. Dreyer, Christopher W. Bielawski, and Rodney S. Ruoff, 'Graphene-Based Polymer Nanocomposites', *Polymer*, 52 (2011), 5-25.
- 46 Sanjeev Gambhir, Rouhollah Jalili, David L. Officer, and Gordon G. Wallace, 'Chemically Converted Graphene: Scalable Chemistries to Enable Processing and Fabrication', *NPG Asia Materials*, 7 (2015), e186.
- 47 Markus Antonietti, Theresa Badosz, Gabriele Centi, Rubén Costa, Rudolfo Cruz-Silva, Jiangtao Di, Xinliang Feng, Benjamin Frank, Paul Gebhardt, and Dirk Michael Guldi, *Nanocarbon-Inorganic Hybrids: Next Generation Composites for Sustainable Energy Applications (Walter de Gruyter GmbH & Co KG, 2014)*.
- 48 Peter Steurer, R. Wissert, R. Thomann, and R. Mülhaupt, 'Functionalized Graphenes and Thermoplastic Nanocomposites Based Upon Expanded Graphite Oxide', *Macromolecular Rapid Communications*, 30 (2009), 316-27.
- 49 'Expandable Graphite', (Graphit Kropfmühl AG, 2011).
- 50 Robert. A. Shanks, Spoljaric S., Kong I., Czajka M., Daud N., Mustapa I. R. Zhai Y. M., 'Preparation of Functional Nano-Particles for Dispersion to Form Polymer Nano-Composites', in *Australia-India Joint Symposium on Smart Nanomaterials in Victoria (RMIT University: 2011)*, p. p. 62.
- 51 Peter Blake, Paul D. Brimicombe, Rahul R. Nair, Tim J. Booth, Da Jiang, Fred Schedin, Leonid A. Ponomarenko, Sergey V. Morozov, Helen F. Gleeson, and Ernie W. Hill, 'Graphene-Based Liquid Crystal Device', *Nano Letters*, 8 (2008), 1704-08.

- 52 Carlo A. Amadei, Itai Y. Stein, Gregory J. Silverberg, Brian L. Wardle, and Chad D. Vecitis, 'Fabrication and Morphology Tuning of Graphene Oxide Nanoscrolls', *Nanoscale*, 8 (2016), 6783-91.
- 53 Jin Ho Bang, and Kenneth S. Suslick, 'Applications of Ultrasound to the Synthesis of Nanostructured Materials', *Advanced Materials*, 22 (2010), 1039-59.
- 54 James M. Tour, 'Top-Down Versus Bottom-up Fabrication of Graphene-Based Electronics', *Chemistry of Materials*, 26 (2014), 163-71.
- 55 Christopher R. Herron, Karl S. Coleman, Rebecca S. Edwards, and Budhika G. Mendis, 'Simple and Scalable Route for the 'Bottom-up' Synthesis of Few-Layer Graphene Platelets and Thin Films', *Journal of Materials Chemistry*, 21 (2011), 3378-83.
- 56 Zhengzong Sun, Zheng Yan, Jun Yao, Elvira Beitler, Yu Zhu, and James M. Tour, 'Growth of Graphene from Solid Carbon Sources', *Nature*, 471 (2011), 124-24.
- 57 Xiaoyin Yang, Xi Dou, Ali Rouhanipour, Linjie Zhi, Hans Joachim Räder, and Klaus Müllen, 'Two-Dimensional Graphene Nanoribbons', *Journal of the American Chemical Society*, 130 (2008), 4216-17.
- 58 Ruiyi Chen, Suprem R. Das, Changwook Jeong, Mohammad Ryyan Khan, David B. Janes, and Muhammad A. Alam, 'Co-Percolating Graphene-Wrapped Silver Nanowire Network for High Performance, Highly Stable, Transparent Conducting Electrodes', *Advanced Functional Materials*, 23 (2013), 5150-58.
- 59 Sungjin Park, Jinho An, Jeffrey R. Potts, Aruna Velamakanni, Shanthi Murali, and Rodney S. Ruoff, 'Hydrazine-Reduction of Graphite- and Graphene Oxide', *Carbon*, 49 (2011), 3019-23.
- 60 Hassan M. A. Hassan, V. Abdelsayed, S. K. Abd El Rahman, K. M. AbouZeid, J. Turner, M. S. El-Shall, S. I. Al-Resayes, and A. A. El-Azhary, 'Microwave Synthesis of Graphene Sheets Supporting Metal Nanocrystals in Aqueous and Organic Media', *Journal of Materials Chemistry*, 19 (2009), 3832-37.
- 61 Jian Gao, Fang Liu, Yiliu Liu, Ning Ma, Zhiqiang Wang, and Xi Zhang, 'Environment-Friendly Method to Produce Graphene That Employs Vitamin C and Amino Acid', *Chemistry of Materials*, 22 (2009), 2213-18.
- 62 Yan Wang, ZiXing Shi, and Jie Yin, 'Facile Synthesis of Soluble Graphene Via a Green Reduction of Graphene Oxide in Tea Solution and Its Biocomposites', *ACS Applied Materials & Interfaces*, 3 (2011), 1127-33.
- 63 Brianna C. Thompson, Eoin Murray, and Gordon G. Wallace, 'Graphite Oxide to Graphene. Biomaterials to Bionics', *Advanced Materials*, 27 (2015), 7563-82.
- 64 Ludovic F. Dumée, Chunfang Feng, Li He, Francois-Marie Allieux, Zhifeng Yi, Weimin Gao, Connie Banos, Justin B. Davies, and Lingxue Kong, 'Tuning the Grade

- of Graphene: Gamma Ray Irradiation of Free-Standing Graphene Oxide Films in Gaseous Phase*, *Applied Surface Science*, 322 (2014), 126-35.
- 65 Hwee Ling Poh, Filip Šaněk, Adriano Ambrosi, Guanxia Zhao, Zdeněk Sofer, and Martin Pumera, 'Graphenes Prepared by Staudenmaier, Hofmann and Hummers Methods with Consequent Thermal Exfoliation Exhibit Very Different Electrochemical Properties', *Nanoscale*, 4 (2012), 3515-22.
- 66 Badri Narayanan, Stephen L. Weeks, Bhavin N. Jariwala, Bart Macco, Jan-Willem Weber, Somilkumar J. Rathi, Mauritius C. M. van de Sanden, Peter Sutter, Sumit Agarwal, and Cristian V. Ciobanu, 'Carbon Monoxide-Induced Reduction and Healing of Graphene Oxide', *Journal of Vacuum Science & Technology A: Vacuum, Surfaces, and Films*, 31 (2013), 040601-8.
- 67 Maher F. El-Kady, and Richard B. Kaner, 'Scalable Fabrication of High-Power Graphene Micro-Supercapacitors for Flexible and on-Chip Energy Storage', *Nature Communications*, 4 (2013), 1475.
- 68 Chih-Jen Shih, Shangchao Lin, Michael S. Strano, and Daniel Blankschtein, 'Understanding the Stabilization of Liquid-Phase-Exfoliated Graphene in Polar Solvents: Molecular Dynamics Simulations and Kinetic Theory of Colloid Aggregation', *Journal of the American Chemical Society*, 132 (2010), 14638-48.
- 69 Zhenyu Sun, Xing Huang, Fang Liu, Xiaoning Yang, Christoph Rösler, Roland A Fischer, Martin Muhler, and Wolfgang Schuhmann, 'Amine-Based Solvents for Exfoliating Graphite to Graphene Outperform the Dispersing Capacity of N-Methyl-Pyrrolidone and Surfactants', *Chemical Communications*, 50 (2014), 10382-85.
- 70 Deepthi Konatham, and Alberto Striolo, 'Molecular Design of Stable Graphene Nanosheets Dispersions', *Nano Letters*, 8 (2008), 4630-41.
- 71 Yewen Cao, Jiachun Feng, and Peiyi Wu, 'Alkyl-Functionalized Graphene Nanosheets with Improved Lipophilicity', *Carbon*, 48 (2010), 1683-85.
- 72 Shiren Wang, Yue Zhang, Nouredine Abidi, and Luis Cabrales, 'Wettability and Surface Free Energy of Graphene Films', *Langmuir*, 25 (2009), 11078-81.
- 73 Jonas Björk, Felix Hanke, Carlos-Andres Palma, Paolo Samori, Marco Cecchini, and Mats Persson, 'Adsorption of Aromatic and Anti-Aromatic Systems on Graphene through Π - Π Stacking', *The Journal of Physical Chemistry Letters*, 1 (2010), 3407-12.
- 74 Edward R. T. Tiekink, and Julio Zukerman-Schpector, *The Importance of Pi-Interactions in Crystal Engineering: Frontiers in Crystal Engineering* (Wiley. com, 2012).
- 75 Sung Min Kang, S. Park, D. Kim, S. Y. Park, R. S. Ruoff, and H. Lee, 'Simultaneous Reduction and Surface Functionalization of Graphene Oxide by Mussel-Inspired Chemistry', *Advanced Functional Materials*, 21 (2011), 108-12.

- 76 *Márcia Maria Lucchese, F. Stavale, E. H. Martins Ferreira, C. Vilani, M. V. O. Moutinho, Rodrigo B. Capaz, C. A. Achete, and A. Jorio, 'Quantifying Ion-Induced Defects and Raman Relaxation Length in Graphene', Carbon, 48 (2010), 1592-97.*
- 77 *Mildred S. Dresselhaus, A. Jorio, L. G. Cançado, G. Dresselhaus, and R. Saito, 'Raman Spectroscopy: Characterization of Edges, Defects, and the Fermi Energy of Graphene and Sp² Carbons', Graphene Nanoelectronics (2012), 15-55.*
- 78 *Jisook Lee, Sangdeok Shim, Bongsoo Kim, and Hyeon Suk Shin, 'Surface-Enhanced Raman Scattering of Single- and Few-Layer Graphene by the Deposition of Gold Nanoparticles', Chemistry—A European Journal, 17 (2011), 2381-87.*
- 79 *Xiaohong An, Trevor Simmons, Rakesh Shah, Christopher Wolfe, Kim M. Lewis, Morris Washington, Saroj K. Nayak, Saikat Talapatra, and Swastik Kar, 'Stable Aqueous Dispersions of Noncovalently Functionalized Graphene from Graphite and Their Multifunctional High-Performance Applications', Nano Letters, 10 (2010), 4295-301.*
- 80 *Andrew J. Pollard, and Debdulal Roy, 'Graphene Characterisation and Standardisation Via Raman Spectroscopy', Spectroscopy Europe, 27 (2015), 9-12.*
- 81 *Ardavan Zandiatashbar, Gwan-Hyoung Lee, Sung Joo An, Sunwoo Lee, Nithin Mathew, Mauricio Terrones, Takuya Hayashi, Catalin R. Picu, James Hone, and Nikhil Koratkar, 'Effect of Defects on the Intrinsic Strength and Stiffness of Graphene', Nature Communications, 5 (2014).*
- 82 *Otakar Frank, Georgia Tsoukleri, John Parthenios, Konstantinos Papagelis, Ibtisam Riaz, Rashid Jalil, Kostya S. Novoselov, Martin Kalbáč, Ladislav Kavan, and Costas Galiotis, 'Graphene under Uniaxial Deformation: A Raman Study', Nanocon 2011 (2011), 225-30.*
- 83 *Luiz Gustavo Cançado, A. Jorio, E. H. Martins Ferreira, F. Stavale, C. A. Achete, R. B. Capaz, M. V. O. Moutinho, A. Lombardo, T. S. Kulmala, and A. C. Ferrari, 'Quantifying Defects in Graphene Via Raman Spectroscopy at Different Excitation Energies', Nano Letters, 11 (2011), 3190-96.*
- 84 *Andrea C. Ferrari, J. C. Meyer, V. Scardaci, C. Casiraghi, Michele Lazzeri, Francesco Mauri, S. Piscanec, Da Jiang, K. S. Novoselov, and S. Roth, 'Raman Spectrum of Graphene and Graphene Layers', Physical Review Letters, 97 (2006), 187401.*
- 85 *Fanyan Zeng, Yafei Kuang, Ye Wang, Zhongyuan Huang, Chaopeng Fu, and Haihui Zhou, 'Facile Preparation of High-Quality Graphene Scrolls from Graphite Oxide by a Microexplosion Method', Advanced Materials, 23 (2011), 4929-32.*
- 86 *Izzuddin Zaman, Tam Thanh Phan, Hsu-Chiang Kuan, Qingshi Meng, Ly Truc Bao La, Lee Luong, Osama Youssf, and Jun Ma, 'Epoxy/Graphene Platelets Nanocomposites with Two Levels of Interface Strength', Polymer, 52 (2011), 1603-11.*

- 87 *Mustafa Lotya, Yenny Hernandez, Paul J. King, Ronan J. Smith, Valeria Nicolosi, Lisa S. Karlsson, Fiona M. Blighe, Sukanta De, Zhiming Wang, and I. T. McGovern, 'Liquid Phase Production of Graphene by Exfoliation of Graphite in Surfactant/Water Solutions', Journal of the American Chemical Society, 131 (2009), 3611-20.*
- 88 *Han Hu, Zongbin Zhao, Yury Gogotsi, and Jieshan Qiu, 'Compressible Carbon Nanotube–Graphene Hybrid Aerogels with Superhydrophobicity and Superoleophilicity for Oil Sorption', Environmental Science & Technology Letters, 1 (2014), 214-20.*
- 89 *Daewha Hong, KiEun Bae, Sangjin Yoo, Kyungtae Kang, Byoungwook Jang, Jinkyu Kim, Sehun Kim, Seokwoo Jeon, Yoonkey Nam, Yang-Gyun Kim, and Insung S. Choi, 'Generation of Cellular Micropatterns on a Single-Layered Graphene Film', Macromolecular Bioscience (2013).*
- 90 *Peichao Lian, Xuefeng Zhu, Shuzhao Liang, Zhong Li, Weishen Yang, and Haihui Wang, 'Large Reversible Capacity of High Quality Graphene Sheets as an Anode Material for Lithium-Ion Batteries', Electrochimica Acta, 55 (2010), 3909-14.*
- 91 *Diana Olteanu, Adriana Filip, Crina Socaci, Alexandru Radu Biris, Xenia Filip, Maria Coros, Marcela Corina Rosu, Florina Pogacean, Camelia Alb, and Ioana Baldea, 'Cytotoxicity Assessment of Graphene-Based Nanomaterials on Human Dental Follicle Stem Cells', Colloids and Surfaces B: Biointerfaces, 136 (2015), 791-98.*
- 92 *Youbin Kim, Jinsup Lee, Min Sun Yeom, Jae Won Shin, Hyungjun Kim, Yi Cui, Jeffrey W. Kysar, James Hone, Yousung Jung, Seokwoo Jeon, and Seung Min Han, 'Strengthening Effect of Single-Atomic-Layer Graphene in Metal–Graphene Nanolayered Composites', Nature Communications, 4 (2013).*
- 93 *Alireza Fadavi Boostani, S. Tahamtan, Z. Y. Jiang, Dongbin Wei, Siamak Yazdani, R. Azari Khosroshahi, R. Taherzadeh Mousavian, Jianzhong Xu, X. Zhang, and Dianyao Gong, 'Enhanced Tensile Properties of Aluminium Matrix Composites Reinforced with Graphene Encapsulated Sic Nanoparticles', Composites Part A: Applied Science and Manufacturing, 68 (2015), 155-63.*
- 94 *Dhiraj Prasai, Juan Carlos Tuberquia, Robert R Harl, G Kane Jennings, and Kirill I Bolotin, 'Graphene: Corrosion-Inhibiting Coating', ACS Nano, 6 (2012), 1102-08.*
- 95 *Ajay Krishnamurthy, Venkataramana Gadhamshetty, Rahul Mukherjee, Bharath Natarajan, Osman Eksik, S. Ali Shojaee, Don A. Lucca, Wencai Ren, Hui-Ming Cheng, and Nikhil Koratkar, 'Superiority of Graphene over Polymer Coatings for Prevention of Microbially Induced Corrosion', Scientific reports, 5 (2015).*
- 96 *Sasha Stankovich, Dmitriy A. Dikin, Geoffrey H. B. Dommett, Kevin M. Kohlhaas, Eric J. Zimney, Eric A. Stach, Richard D. Piner, SonBinh T. Nguyen, and Rodney S. Ruoff, 'Graphene-Based Composite Materials', Nature, 442 (2006), 282-86.*
- 97 *Tanmoy Rath, and Yongjin Li, 'Nanocomposites Based on Polystyrene-*b*-Poly(Ethylene-*r*-Butylene)-*b*-Polystyrene and Exfoliated Graphite Nanoplates: Effect*

- of Nanoplatelet Loading on Morphology and Mechanical Properties', Composites Part A: Applied Science and Manufacturing, 42 (2011), 1995-2002.*
- 98 *Jingchao Wang, Xianbao Wang, Chunhui Xu, Min Zhang, and Xiaopeng Shang, 'Preparation of Graphene/Poly(Vinyl Alcohol) Nanocomposites with Enhanced Mechanical Properties and Water Resistance', Polymer International, 60 (2011), 816-22.*
 - 99 *Ruijuan Liao, Yanda Lei, Jingjing Wan, Zhenghai Tang, Baochun Guo, and Liqun Zhang, 'Dispersing Graphene in Hydroxypropyl Cellulose by Utilizing Its Lcst Behavior', Macromolecular Chemistry and Physics, 213 (2012), 1370-77.*
 - 100 *Sepidar Sayyar, Eoin Murray, B. C. Thompson, Johnson Chung, David L. Officer, Sanjeev Gambhir, Geoffrey M. Spinks, and Gordon G. Wallace, 'Processable Conducting Graphene/Chitosan Hydrogels for Tissue Engineering', Journal of Materials Chemistry B, 3 (2015), 481-90.*
 - 101 *Chengpeng Li, Chunfang Feng, Zheng Peng, Wei Gong, and Lingxue Kong, 'Ammonium-Assisted Green Fabrication of Graphene/Natural Rubber Latex Composite', Polymer Composites, 34 (2013), 88-95.*
 - 102 *Nair Ajalesh Balachandran, Kurian Philip, and Joseph Rani, 'Effect of Expanded Graphite on Thermal, Mechanical and Dielectric Properties of Ethylene–Propylene–Diene Terpolymer/Hexafluoropropylene–Vinylidene fluoride Dipolymer Rubber Blends', European Polymer Journal, 49 (2013), 247-60.*
 - 103 *Bin Shen, Wentao Zhai, Dingding Lu, Wenge Zheng, and Qing Yan, 'Fabrication of Microcellular Polymer/Graphene Nanocomposite Foams', Polymer International, 61 (2012), 1693-702.*
 - 104 *Gabriel Gedler, M. Antunes, T. Borca-Tasciuc, J. I. Velasco, and R. Ozisik, 'Effects of Graphene Concentration, Relative Density and Cellular Morphology on the Thermal Conductivity of Polycarbonate–Graphene Nanocomposite Foams', European Polymer Journal, 75 (2016), 190-99.*
 - 105 *Sirus Zinadini, Ali Akbar Zinatizadeh, Masoud Rahimi, Vahid Vatanpour, and Hadis Zangeneh, 'Preparation of a Novel Antifouling Mixed Matrix Pes Membrane by Embedding Graphene Oxide Nanoplates', Journal of Membrane Science, 453 (2014), 292-301.*
 - 106 *Lan Yu, Yun-Soo Lim, Jong Hun Han, Kunnyun Kim, Jong Yun Kim, Sung-Yool Choi, and Kwonwoo Shin, 'A Graphene Oxide Oxygen Barrier Film Deposited Via a Self-Assembly Coating Method', Synthetic Metals, 162 (2012), 710-14.*
 - 107 *Jie Jin, R. Rafiq, Y. Q. Gill, and M. Song, 'Preparation and Characterization of High Performance of Graphene/Nylon Nanocomposites', European Polymer Journal, 49 (2013), 2617-26.*

- 108 Luis Ibarra, and David Panos, 'Dynamic Properties of Thermoplastic Butadiene–Styrene (SBS) and Oxidized Short Carbon Fiber Composite Materials', *Journal of Applied Polymer Science*, 67 (1998), 1819-26.
- 109 María Elena Leyva, Guilherme M. O. Barra, Ana C. F. Moreira, Bluma G. Soares, and Dipak Khastgir, 'Electric, Dielectric, and Dynamic Mechanical Behavior of Carbon Black/Styrene-Butadiene-Styrene Composites', *Journal of Polymer Science Part B: Polymer Physics*, 41 (2003), 2983-97.
- 110 'Tufprene', (Tokyo, Japan: Asahi Kasei, 2010).
- 111 Vladimir V. Frolkis, V. G. Nikolaev, L. N. Bogatskaya, A. S. Stupina, E. V. Shcherbitskaya, A. I. Kovtun, G. I. Paramonova, V. E. Sabko, V. M. Shaposhnikov, Yu E. Rushkevich, Kh K. Muradian, and N. P. Adamenko, 'Enterisorption in Prolonging Old Animal Lifespan', *Experimental Gerontology*, 19 (1984), 217-25.
- 112 Vladimir V. Frolkis, V. G. Nikolaev, G. I. Paramonova, E. V. Shchorbitskaya, L. N. Bogatskaya, A. S. Stupina, A. I. Kovtun, V. E. Sabko, V. M. Shaposhnikov, and Kh K. Muradian, 'Effect of Enterisorption on Animal Lifespan', *Biomaterials, artificial cells and artificial organs*, 17 (1989), 341-51.
- 113 Paul Taylor, *The Biochar Revolution: Transforming Agriculture & Environment* (Global Publishing Group, 2010).
- 114 Junjie Du, Xiangang Hu, and Qixing Zhou, 'Graphene Oxide Regulates the Bacterial Community and Exhibits Property Changes in Soil', *RSC Advances*, 5 (2015), 27009-17.
- 115 Pasi Kuusisto, Vesa Manninen, Heikki Vapaatalo, Jussi K. Huttunen, and Pertti J. Neuvonen, 'Effect of Activated Charcoal on Hypercholesterolaemia', *The Lancet*, 328 (1986), 366-67.
- 116 Pertti J. Neuvonen, P. Kuusisto, V. Manninen, H. Vapaatalo, and T. A. Miettinen, 'The Mechanism of the Hypocholesterolaemic Effect of Activated Charcoal', *European Journal of Clinical Investigation*, 19 (1989), 251-54.
- 117 Hamid Tayebi Khosroshahi, and Kamyar Kalantar-zadeh, 'Dialysis Free Protocol for Some End Stage Renal Disease Patients (Khosroshahi Protocol)', *Functional Foods in Health and Disease*, 2 (2012), 300-06.
- 118 Carlos G. Musso, H. Michelangelo, J. Reynaldi, B. Martinez, F. Vidal, M. Quevedo, M. Parot, G. Waisman, and L. Algranati, 'Combination of Oral Activated Charcoal Plus Low Protein Diet as a New Alternative for Handling in the Old End-Stage Renal Disease Patients', *Saudi Journal of Kidney Diseases and Transplantation*, 21 (2010), 102.
- 119 David O. Cooney, *Activated Charcoal: Antidotal and Other Medical Uses. Vol. 9* (Marcel Dekker Incorporated, 1980).

- 120 Masao Shibuya, Motoshi Kato, Masaki Ozawa, P. H. Fang, and Eiji sawa, 'Detection of Buckminsterfullerene in Usual Soots and Commercial Charcoals', *Fullerene Science and Technology*, 7 (1999), 181-93.
- 121 Toshimitsu Hata, Yuji Imamura, Emiko Kobayashi, Kenji Yamane, and Kohtaro Kikuchi, 'Onion-Like Graphitic Particles Observed in Wood Charcoal', *Journal of Wood Science*, 46 (2000), 89-92.
- 122 Eiji Sawa, 'Natural Fullerenes-Will They Offer a Hint to the Selective Synthesis of Fullerenes?', *Fullerene Science and Technology*, 7 (1999), 637-52.
- 123 Marie Pontier Johnson, J. B. Donnet, T. K. Wang, C. C. Wang, R. W. Locke, B. E. Brinson, and T. Marriott, 'A Dynamic Continuum of Nanostructured Carbons in the Combustion Furnace', *Carbon*, 40 (2002), 189-94.
- 124 Jim Baggott, *Perfect Symmetry: The Accidental Discovery of Buckminsterfullerene* (Oxford University Press, 1994).
- 125 Tarek Baati, Fanchon Bourasset, Najla Gharbi, Leila Njim, Manef Abderrabba, Abdelhamid Kerkeni, Henri Szwarc, and Fathi Moussa, 'The Prolongation of the Lifespan of Rats by Repeated Oral Administration of [60] Fullerene', *Biomaterials*, 33 (2012), 4936-46.
- 126 Roger Taylor, and David R. M. Walton, 'The Chemistry of Fullerenes', *Nature*, 363 (1993), 685-93.
- 127 Georgii G. Gnesin, 'Carbon in Inorganic Materials: From Charcoal to Graphene', *Powder Metallurgy and Metal Ceramics*, 54 (2015), 241-51.
- 128 Manav Saxena, and Sabyasachi Sarkar, 'Involuntary Graphene Intake with Food and Medicine', *RSC Advances*, 4 (2014), 30162-67.
- 129 Jae Hoon Shin, Sung Gu Han, Jin Kwon Kim, Boo Wook Kim, Joo Hwan Hwang, Jong Seong Lee, Ji Hyun Lee, Jin Ee Baek, Tae Gyu Kim, and Keun Soo Kim, '5-Day Repeated Inhalation and 28-Day Post-Exposure Study of Graphene', *Nanotoxicology*, 9 (2015), 1023-31.
- 130 Tobias Lammel, Paul Boisseaux, Maria-Luisa Fernández-Cruz, and José M Navas, 'Internalization and Cytotoxicity of Graphene Oxide and Carboxyl Graphene Nanoplatelets in the Human Hepatocellular Carcinoma Cell Line Hep G2', *Particle and Fibre Toxicology*, 10 (2013), 1.
- 131 Jong Ho Lee, Yong Cheol Shin, Oh Seong Jin, Seok Hee Kang, Yu-Shik Hwang, Jong-Chul Park, Suck Won Hong, and Dong-Wook Han, 'Reduced Graphene Oxide-Coated Hydroxyapatite Composites Stimulate Spontaneous Osteogenic Differentiation of Human Mesenchymal Stem Cells', *Nanoscale*, 7 (2015), 11642-51.
- 132 Bingan Lu, Ting Li, Haitao Zhao, Xiaodong Li, Caitian Gao, Shengxiang Zhang, and Erqing Xie, 'Graphene-Based Composite Materials Beneficial to Wound Healing', *Nanoscale*, 4 (2012), 2978-82.

- 133 Yang Qiu, Zhongying Wang, Alisa C. E. Owens, Indrek Kulaots, Yantao Chen, Agnes B. Kane, and Robert H. Hurt, 'Antioxidant Chemistry of Graphene-Based Materials and Its Role in Oxidation Protection Technology', *Nanoscale*, 6 (2014), 11744-55.
- 134 Daniele Frasca, D. Schulze, V. Wachtendorf, C. Huth, and B. Schartel, 'Multifunctional Multilayer Graphene/Elastomer Nanocomposites', *European Polymer Journal*, 71 (2015), 99-113.
- 135 Shakil A. Awan, A. Lombardo, A. Colli, G. Privitera, T. S. Kulmala, J. M. Kivioja, M. Koshino, and A. C. Ferrari, 'Transport Conductivity of Graphene at Rf and Microwave Frequencies', *2D Materials*, 3 (2016), 015010.
- 136 Kevin T. Chan, J. B. Neaton, and Marvin L. Cohen, 'First-Principles Study of Metal Adatom Adsorption on Graphene', *Physical Review B*, 77 (2008), 235430.
- 137 'Periodic Table', Wikipedia, (2016) <https://en.wikipedia.org/wiki/Periodic_table> [Accessed 20/4/16 2016].
- 138 Eric C. Mattson, Haihui Pu, Shumao Cui, Marvin A. Schofield, Sonny Rhim, Ganhua Lu, Michael J. Nasse, Rodney S. Ruoff, Michael Weinert, and Marija Gajdardziska-Josifovska, 'Evidence of Nanocrystalline Semiconducting Graphene Monoxide During Thermal Reduction of Graphene Oxide in Vacuum', *ACS Nano*, 5 (2011), 9710-17.
- 139 Nanditha D. M. M. Dissanayake, A. Ashraf, D. Dwyer, K. Kisslinger, L. Zhang, Y. Pang, H. Efstathiadis, and M. D. Eisaman, 'Spontaneous and Strong Multi-Layer Graphene N-Doping on Soda-Lime Glass and Its Application in Graphene-Semiconductor Junctions', *Scientific Reports*, 6 (2016).
- 140 Xiaowei Yang, Junwu Zhu, Ling Qiu, and Dan Li, 'Bioinspired Effective Prevention of Restacking in Multilayered Graphene Films: Towards the Next Generation of High-Performance Supercapacitors', *Advanced Materials*, 23 (2011), 2833-38.
- 141 Jing Su, Minhua Cao, Ling Ren, and Changwen Hu, 'Fe₃O₄-Graphene Nanocomposites with Improved Lithium Storage and Magnetism Properties', *The Journal of Physical Chemistry C*, 115 (2011), 14469-77.
- 142 Dongyun Chen, Ge Ji, Yue Ma, Jim Yang Lee, and Jianmei Lu, 'Graphene-Encapsulated Hollow Fe₃O₄ Nanoparticle Aggregates as a High-Performance Anode Material for Lithium Ion Batteries', *ACS Applied Materials & Interfaces*, 3 (2011), 3078-83.
- 143 Qihua Wu, Guangying Zhao, Cheng Feng, Chun Wang, and Zhi Wang, 'Preparation of a Graphene-Based Magnetic Nanocomposite for the Extraction of Carbamate Pesticides from Environmental Water Samples', *Journal of Chromatography A*, 1218 (2011), 7936-42.
- 144 Xiaoying Yang, Xiaoyan Zhang, Yanfeng Ma, Yi Huang, Yinsong Wang, and Yongsheng Chen, 'Superparamagnetic Graphene Oxide-Fe₃O₄ Nanoparticles Hybrid for Controlled Targeted Drug Carriers', *Journal of Materials Chemistry*, 19 (2009), 2710-14.

- 145 Folke Johannes Tölle, Martin Fabritius, and Rolf Mülhaupt, 'Emulsifier-Free Graphene Dispersions with High Graphene Content for Printed Electronics and Freestanding Graphene Films', *Advanced Functional Materials*, 22 (2012), 1136-44.
- 146 Marco Sangermano, Sophie Marchi, Luca Valentini, Silvia Bittolo Bon, and Paola Fabbri, 'Transparent and Conductive Graphene Oxide/Poly(Ethylene Glycol) Diacrylate Coatings Obtained by Photopolymerization', *Macromolecular Materials and Engineering*, 296 (2011), 401-07.
- 147 Jae-Hwang Lee, Phillip E. Loya, Jun Lou, and Edwin L. Thomas, 'Dynamic Mechanical Behavior of Multilayer Graphene Via Supersonic Projectile Penetration', *Science*, 346 (2014), 1092-96.
- 148 Chang-Duk Kim, Bong-Ki Min, and Woo-Sik Jung, 'Preparation of Graphene Sheets by the Reduction of Carbon Monoxide', *Carbon*, 47 (2009), 1610-12.
- 149 Daniel T. Oldfield, Dougal G. McCulloch, Chi P. Huynh, Kallista Sears, and Stephen C. Hawkins, 'Multilayered Graphene Films Prepared at Moderate Temperatures Using Energetic Physical Vapour Deposition', *Carbon*, 94 (2015), 378-85.
- 150 Shigeki Kawai, Andrea Benassi, Enrico Gnecco, Hajo Söde, Rémy Pawlak, Xinliang Feng, Klaus Müllen, Daniele Passerone, Carlo A Pignedoli, and Pascal Ruffieux, 'Superlubricity of Graphene Nanoribbons on Gold Surfaces', *Science*, 351 (2016), 957-61.
- 151 Michael Czajka, 'Identification and Characterisation of a Proprietary Bonding Surface Treatment for Metals (Project Report Onps 2186)', (RMIT, 2010).
- 152 S. Hu, M. Lozada-Hidalgo, F. C. Wang, A. Mishchenko, F. Schedin, R. R. Nair, E. W. Hill, D. W. Boukhvalov, M. I. Katsnelson, and R. A. W. Dryfe, 'Proton Transport through One-Atom-Thick Crystals', *Nature*, 516 (2014), 227-30.
- 153 David Cohen-Tanugi, and Jeffrey C. Grossman, 'Mechanical Strength of Nanoporous Graphene as a Desalination Membrane', *Nano Letters*, 14 (2014), 6171-78.
- 154 Minmin Xue, Hu Qiu, and Wanlin Guo, 'Exceptionally Fast Water Desalination at Complete Salt Rejection by Pristine Graphyne Monolayers', *Nanotechnology*, 24 (2013), 505720.
- 155 Leon Tsetseris, and S. T. Pantelides, 'Graphene: An Impermeable or Selectively Permeable Membrane for Atomic Species?', *Carbon*, 67 (2014), 58-63.
- 156 Nobuo Narita, Sumiaki Nagai, Shugo Suzuki, and Kenji Nakao, 'Optimized Geometries and Electronic Structures of Graphyne and Its Family', *Physical Review B*, 58 (1998), 11009.
- 157 Rafal Sitko, Beata Zawisza, and Ewa Malicka, 'Graphene as a New Sorbent in Analytical Chemistry', *TrAC Trends in Analytical Chemistry*, 51 (2013), 33-43.

- 158 *Hunain Alkhateb, Ahmed Al-Ostaz, Alexander H-D Cheng, and Xiaobing Li, 'Materials Genome for Graphene-Cement Nanocomposites', Journal of Nanomechanics and Micromechanics, 3 (2013), 67-77.*
- 159 *Samuel Chuah, Zhu Pan, Jay G. Sanjayan, Chien Ming Wang, and Wen Hui Duan, 'Nano Reinforced Cement and Concrete Composites and New Perspective from Graphene Oxide', Construction and Building Materials, 73 (2014), 113-24.*
- 160 *Francis Cerezo, 'Thermal Stability and Mechanical Property of Polymer Layered Graphite Oxide Composites (Phd Thesis)' (RMIT University, 2006).*
- 161 *Francis T. Cerezo, C. M. L. Preston, and R. A. Shanks, 'Structural, Mechanical and Dielectric Properties of Poly(Ethylene-Co-Methyl Acrylate-Co-Acrylic Acid) Graphite Oxide Nanocomposites', Composites Science and Technology, 67 (2007), 79-91.*
- 162 *Frances T. Cerezo, Christopher M. L. Preston, and Robert A. Shanks, 'Morphology, Thermal Stability, and Mechanical Behavior of [Poly(Propylene)-Grafted Maleic Anhydride]-Layered Expanded Graphite Oxide Composites', Macromolecular Materials and Engineering, 292 (2007), 155-68.*
- 163 *Robert A. Shanks, and Frances T. Cerezo, 'Preparation and Properties of Poly (Propylene-G-Maleic Anhydride) Filled with Expanded Graphite Oxide', Composites Part A: Applied Science and Manufacturing (2012).*
- 164 *Gerald H. Pollack, The Fourth Phase of Water: Beyond Solid, Liquid, and Vapor (Ebner & Sons, 2013).*
- 165 *D Li, and AW Neumann, 'Equation of State for Interfacial Tensions of Solid-Liquid Systems', Advances in Colloid and Interface Science, 39 (1992), 299-345.*
- 166 *Georg Kresse, and Jürgen Furthmüller, 'Efficiency of Ab-Initio Total Energy Calculations for Metals and Semiconductors Using a Plane-Wave Basis Set', Computational Materials Science, 6 (1996), 15-50.*
- 167 *———, 'Efficient Iterative Schemes for ab Initio Total-Energy Calculations Using a Plane-Wave Basis Set', Physical Review B, 54 (1996), 11169.*
- 168 *Georg Kresse, and J. Hafner, 'ab Initio Molecular Dynamics for Open-Shell Transition Metals', Physical Review B, 48 (1993), 13115-18.*
- 169 *Peter E. Blöchl, 'Projector Augmented-Wave Method', Physical Review B, 50 (1994), 17953-79.*
- 170 *John P. Perdew, Kieron Burke, and Matthias Ernzerhof, 'Generalized Gradient Approximation Made Simple', Physical Review Letters, 77 (1996), 3865.*

- 171 Stefan Grimme, 'Semiempirical Gga-Type Density Functional Constructed with a Long-Range Dispersion Correction', *Journal of Computational Chemistry*, 27 (2006), 1787-99.
- 172 L. Staudenmaier, 'Verfahren Zur Darstellung Der Graphitsäure', *Berichte der Deutschen Chemischen Gesellschaft*, 31 (1898), 1481-87.
- 173 Ulrich Hofmann, and Rudolf Holst, 'Über Die Säurenatur Und Die Methylierung Von Graphitoxyd', *Berichte der Deutschen Chemischen Gesellschaft (A and B Series)*, 72 (1939), 754-71.
- 174 Ulrich Hofmann, and Ernst König, 'Untersuchungen Über Graphitoxyd', *Zeitschrift für Anorganische und Allgemeine Chemie*, 234 (1937), 311-36.
- 175 Mildred S. Dresselhaus, and G. Dresselhaus, 'Intercalation Compounds of Graphite', *Advances in Physics*, 51 (2002), 1-186.
- 176 John Daintith, *A Dictionary of Chemistry* ('Oxford University Press', 2008).
- 177 Da Zhan, Li Sun, Zhen Hua Ni, Lei Liu, Xiao Feng Fan, Yingying Wang, Ting Yu, Yeng Ming Lam, Wei Huang, and Ze Xiang Shen, 'FeCl₃-Based Few-Layer Graphene Intercalation Compounds: Single Linear Dispersion Electronic Band Structure and Strong Charge Transfer Doping', *Advanced Functional Materials*, 20 (2010), 3504-09.
- 178 R.A. Greinke, 'Expandable Graphite and Method', (Google Patents, 2000).
- 179 Michael J. McAllister, Je-Luen Li, Douglas H. Adamson, Hannes C. Schniepp, Ahmed A. Abdala, Jun Liu, Margarita Herrera-Alonso, David L. Milius, Roberto Car, Robert K. Prud'homme, and Ilhan A. Aksay, 'Single Sheet Functionalized Graphene by Oxidation and Thermal Expansion of Graphite', *Chemistry of Materials*, 19 (2007), 4396-404.
- 180 Hannes C. Schniepp, Je-Luen Li, Michael J. McAllister, Hiroaki Sai, Margarita Herrera-Alonso, Douglas H. Adamson, Robert K. Prud'homme, Roberto Car, Dudley A. Saville, and Ilhan A. Aksay, 'Functionalized Single Graphene Sheets Derived from Splitting Graphite Oxide', *The Journal of Physical Chemistry B*, 110 (2006), 8535-39.
- 181 Michael Czajka, Robert A. Shanks, and Ing Kong, 'Preparation of Graphene and Inclusion in Composites with Poly (Styrene-*b*-Butadiene-*b*-Styrene)', *Science and Engineering of Composite Materials*, 22 (2015), 7-16.
- 182 Axel Eckmann, Alexandre Felten, Artem Mishchenko, Liam Britnell, Ralph Krupke, Kostya S. Novoselov, and Cinzia Casiraghi, 'Probing the Nature of Defects in Graphene by Raman Spectroscopy', *Nano Letters*, 12 (2012), 3925-30.
- 183 Yingjuan Huang, Y. Qin, N. Wang, Y. Zhou, H. Niu, J.Y. Dong, J. Hu, and Y. Wang, 'Reduction of Graphite Oxide with a Grignard Reagent for Facile in Situ Preparation of Electrically Conductive Polyolefin/Graphene Nanocomposites', *Macromolecular Chemistry and Physics* (2012).

- 184 Sergey Mikhailov, *'Physics and Applications of Graphene-Experiments'*, Tech Janeza Trdine, Rijeka, Croatia (2011).
- 185 Ado Jorio, Erlon H. Martins Ferreira, Luiz G. Cançado, Carlos A. Achete, and Rodrigo B. Capaz, *Measuring Disorder in Graphene with Raman Spectroscopy (INTECH Open Access Publisher Rijeka, Croatia, 2011)*.
- 186 Mark Wall, *'Raman Spectroscopy'*, *Advanced Materials & Processes*, 170 (2012), 35-38.
- 187 Mohammad Choucair, P. Thordarson, and J. A. Stride, *'Gram-Scale Production of Graphene Based on Solvothermal Synthesis and Sonication'*, *Nature Nanotechnology*, 4 (2008), 30-33.
- 188 Seong Min Oh, Kyung Min Oh, Trung Dung Dao, Hyung-il Lee, Han Mo Jeong, and Byung Kyu Kim, *'The Modification of Graphene with Alcohols and Its Use in Shape Memory Polyurethane Composites'*, *Polymer International*, 62 (2013), 54-63.
- 189 Filippo Mangolini, J. Brandon McClimon, Franck Rose, and Robert W. Carpick, *'Accounting for Nanometer-Thick Adventitious Carbon Contamination in X-Ray Absorption Spectra of Carbon-Based Materials'*, *Analytical chemistry*, 86 (2014), 12258-65.
- 190 Fereshte Taherian, Valentina Marcon, Nico F. A. van der Vegt, and Frédéric Leroy, *'What Is the Contact Angle of Water on Graphene?'*, *Langmuir*, 29 (2013), 1457-65.
- 191 C. I. Pereni, Q. Zhao, Y. Liu, and E. Abel, *'Surface Free Energy Effect on Bacterial Retention'*, *Colloids and Surfaces B: Biointerfaces*, 48 (2006), 143-47.
- 192 JinTaek Choi, DongHoon Kim, KwangSun Ryu, Hyung-il Lee, HanMo Jeong, CheolMin Shin, JungHo Kim, and ByungKyu Kim, *'Functionalized Graphene Sheet/Polyurethane Nanocomposites: Effect of Particle Size on Physical Properties'*, *Macromolecular Research*, 19 (2011), 809-14.
- 193 F. Tuinstra, and J. L. Koenig, *'Raman Spectrum of Graphite'*, *The Journal of Chemical Physics*, 53 (2003), 1126-30.
- 194 Zhijun Yang, Jun Liu, Ruijuan Liao, Ganwei Yang, Xiaohui Wu, Zhenghai Tang, Baochun Guo, Liqun Zhang, Yong Ma, and Qiuhai Nie, *'Rational Design of Covalent Interfaces for Graphene/Elastomer Nanocomposites'*, *Composites Science and Technology*, 132 (2016), 68-75.
- 195 Zhonghua Chen, and Runcai Feng, *'Preparation and Characterization of Poly(Styrene-*b*-Butadiene-*b*-Styrene)/Montmorillonite Nanocomposites'*, *Polymer Composites*, 30 (2009), 281-87.
- 196 Yeon-Ran Shin, Sun-Min Jung, In-Yup Jeon, and Jong-Beom Baek, *'The Oxidation Mechanism of Highly Ordered Pyrolytic Graphite in a Nitric Acid/Sulfuric Acid Mixture'*, *Carbon*, 52 (2013), 493-98.

- 197 Adriano Ambrosi, Alessandra Bonanni, Zdeněk Sofer, Jeffrey S. Cross, and Martin Pumera, 'Electrochemistry at Chemically Modified Graphenes', *Chemistry – A European Journal*, 17 (2011), 10763-70.
- 198 Jinhong Du, and Hui-Ming Cheng, 'The Fabrication, Properties, and Uses of Graphene/Polymer Composites', *Macromolecular Chemistry and Physics*, 213 (2012), 1060-77.
- 199 Esmaeil Narimissa, Rahul K. Gupta, Hyoungh J. Choi, Nhol Kao, and Margaret Jollands, 'Morphological, Mechanical, and Thermal Characterization of Biopolymer Composites Based on Polylactide and Nanographite Platelets', *Polymer Composites*, 33 (2012), 1505-15.
- 200 Yunho Lee, Dowan Kim, Jongchul Seo, Haksoo Han, and Sher Bahadar Khan, 'Preparation and Characterization of Poly(Propylene Carbonate)/Exfoliated Graphite Nanocomposite Films with Improved Thermal Stability, Mechanical Properties and Barrier Properties', *Polymer International*, 62 (2013), 1386-94.
- 201 Iosif Tantis, G. C. Psarras, and D. L. Tasis, 'Functionalized Graphene–Poly(Vinyl Alcohol) Nanocomposites: Physical and Dielectric Properties', *Express Polymer Letters*, 6 (2012), 283-92.
- 202 ASTM, in *E 111-97 Standard Test Method for Young's Modulus, Tangent Modulus and Chord modulus* (1997).
- 203 Sara M. Butterfield, Paresma R. Patel, and Marcey L. Waters, 'Contribution of Aromatic Interactions to A-Helix Stability', *Journal of the American Chemical Society*, 124 (2002), 9751-55.
- 204 Marcey L. Waters, 'Aromatic Interactions in Model Systems', *Current Opinion in Chemical Biology*, 6 (2002), 736-41.
- 205 Suting Liu, Ming Tian, Bingyue Yan, Yang Yao, Liqun Zhang, Toshio Nishi, and Nanying Ning, 'High Performance Dielectric Elastomers by Partially Reduced Graphene Oxide and Disruption of Hydrogen Bonding of Polyurethanes', *Polymer*, 56 (2015), 375-84.
- 206 Shamik Chowdhury, and Rajasekhar Balasubramanian, 'Recent Advances in the Use of Graphene-Family Nanoadsorbents for Removal of Toxic Pollutants from Wastewater', *Advances in Colloid and Interface Science*, 204 (2014), 35-56.
- 207 Mathew J. Allen, V. C. Tung, and R. B. Kaner, 'Honeycomb Carbon: A Review of Graphene', *Chemical Reviews*, 110 (2009), 132-45.
- 208 Kellar Autumn, Metin Sitti, Yiching A. Liang, Anne M. Peattie, Wendy R. Hansen, Simon Sponberg, Thomas W. Kenny, Ronald Fearing, Jacob N. Israelachvili, and Robert J. Full, 'Evidence for Van Der Waals Adhesion in Gecko Setae', *Proceedings of the National Academy of Sciences*, 99 (2002), 12252-56.

- 209 Changgu Lee, Qunyang Li, William Kalb, Xin-Zhou Liu, Helmuth Berger, Robert W Carpick, and James Hone, 'Frictional Characteristics of Atomically Thin Sheets', *Science*, 328 (2010), 76-80.
- 210 Jianbing Zang, Yanhui Wang, Linyan Bian, Jinhui Zhang, Fanwei Meng, Yuling Zhao, Rui Lu, Xuanhui Qu, and Shubin Ren, 'Graphene Growth on Nanodiamond as a Support for a Pt Electrocatalyst in Methanol Electro-Oxidation', *Carbon*, 50 (2012), 3032-38.
- 211 Hui Wang, Zengxi Li, Yanqing Liu, Xiangping Zhang, and Suojiang Zhang, 'Degradation of Poly(Ethylene Terephthalate) Using Ionic Liquids', *Green Chemistry*, 11 (2009), 1568-75.
- 212 Guodong Liang, Junting Xu, Suping Bao, and Weibing Xu, 'Polyethylene/Maleic Anhydride Grafted Polyethylene/Organic-Montmorillonite Nanocomposites. I. Preparation, Microstructure, and Mechanical Properties', *Journal of Applied Polymer Science*, 91 (2004), 3974-80.
- 213 Beatriz Mayoral, Peter R. Hornsby, Tony McNally, Tara L. Schiller, Kevin Jack, and Darren J. Martin, 'Quasi-Solid State Uniaxial and Biaxial Deformation of Pet/Mwcnt Composites: Structural Evolution, Electrical and Mechanical Properties', *RSC Advances*, 3 (2013), 5162-83.
- 214 Shigeru Aoyama, Yong Tae Park, Toshiaki Ougizawa, and Christopher W. Macosko, 'Melt Crystallization of Poly(Ethylene Terephthalate): Comparing Addition of Graphene Vs. Carbon Nanotubes', *Polymer*, 55 (2014), 2077-85.
- 215 Jamal Seyyed Monfared Zanjani, Burcu Saner Okan, and Yusuf Menciloglu, 'Manufacturing of Multilayer Graphene Oxide/Poly(Ethylene Terephthalate) Nanocomposites with Tunable Crystallinity, Chain Orientations and Thermal Transitions', *Materials Chemistry and Physics*, 176 (2016), 58-67.
- 216 Sudheer Bandla, and Jay C. Hanan, 'Microstructure and Elastic Tensile Behavior of Polyethylene Terephthalate-Exfoliated Graphene Nanocomposites', *Journal of Materials Science*, 47 (2012), 876-82.
- 217 Ibrahim M. Inuwa, A. Hassan, and S. A. Shamsudin, 'Thermal Properties, Structure and Morphology of Graphene Reinforced Polyethylene Terephthalate/Polypropylene Nanocomposites', *Malaysian Journal of Analytical Sciences*, 18 (2014), 466-77.
- 218 Svetla D. Chakarova-Käck, Elsebeth Schröder, Bengt I. Lundqvist, and David C. Langreth, 'Application of Van Der Waals Density Functional to an Extended System: Adsorption of Benzene and Naphthalene on Graphite', *Physical Review Letters*, 96 (2006), 146107.
- 219 Ahmad Al-Jabareen, Hammam Al-Bustami, Hannah Harel, and Gad Marom, 'Improving the Oxygen Barrier Properties of Polyethylene Terephthalate by Graphite Nanoplatelets', *Journal of Applied Polymer Science*, 128 (2013), 1534-39.

- 220 Kai Liu, Li Chen, Yao Chen, Jieli Wu, Weiyi Zhang, Feng Chen, and Qiang Fu, 'Preparation of Polyester/Reduced Graphene Oxide Composites Via in Situ Melt Polycondensation and Simultaneous Thermo-Reduction of Graphene Oxide', *Journal of Materials Chemistry* (2011).
- 221 Arthur Jaeton Glover, Minzhen Cai, Kyle R. Overdeep, David E. Kranbuehl, and Hannes C. Schniepp, 'In Situ Reduction of Graphene Oxide in Polymers', *Macromolecules*, 44 (2011), 9821-29.
- 222 Haixiong Tang, Gregory J. Ehlert, Yirong Lin, and Henry A. Sodano, 'Highly Efficient Synthesis of Graphene Nanocomposites', *Nano Letters*, 12 (2011), 84-90.
- 223 Feng You, Dongrui Wang, Jianping Cao, Xinxin Li, Zhi-Min Dang, and Guo-Hua Hu, 'In Situ Thermal Reduction of Graphene Oxide in a Styrene–Ethylene/Butylene–Styrene Triblock Copolymer Via Melt Blending', *Polymer International*, 63 (2014), 93-99.
- 224 Lowell H. Hall, and C. T. Story, 'Boiling Point and Critical Temperature of a Heterogeneous Data Set: Qsar with Atom Type Electrotopological State Indices Using Artificial Neural Networks', *Journal of Chemical Information and Computer Sciences*, 36 (1996), 1004-14.
- 225 Ashivni Shekhawat, and Robert O. Ritchie, 'Toughness and Strength of Nanocrystalline Graphene', *Nature Communications*, 7 (2016).
- 226 Mitchell Bacon, Siobhan J. Bradley, and Thomas Nann, 'Graphene Quantum Dots', *Particle & Particle Systems Characterization*, 31 (2014), 415-28.
- 227 James G. Radich, Anthony L. Krenselewski, Jiadong Zhu, and Prashant V. Kamat, 'Is Graphene a Stable Platform for Photocatalysis? Mineralization of Reduced Graphene Oxide with UV-Irradiated TiO₂ Nanoparticles', *Chemistry of Materials*, 26 (2014), 4662-68.
- 228 Yaxin Qiu, Jun Wang, Defeng Wu, Zhifeng Wang, Ming Zhang, Ye Yao, and Nengxin Wei, 'Thermoplastic Polyester Elastomer Nanocomposites Filled with Graphene: Mechanical and Viscoelastic Properties', *Composites Science and Technology*, 132 (2016), 108-15.
- 229 Hyunwoo Kim, and Christopher W. Macosko, 'Processing-Property Relationships of Polycarbonate/Graphene Composites', *Polymer*, 50 (2009), 3797-809.
- 230 Tapas Kuilla, Sambhu Bhadra, Dahu Yao, Nam Hoon Kim, Saswata Bose, and Joong Hee Lee, 'Recent Advances in Graphene Based Polymer Composites', *Progress in Polymer Science*, 35 (2010), 1350-75.
- 231 Mitra Yoonessi, and James R. Gaier, 'Highly Conductive Multifunctional Graphene Polycarbonate Nanocomposites', *ACS Nano*, 4 (2010), 7211-20.

- 232 Huimin Guo, and Vipin Kumar, 'Some Thermodynamic and Kinetic Low-Temperature Properties of the PC-CO₂ System and Morphological Characteristics of Solid-State PC Nanofoams Produced with Liquid CO₂', *Polymer*, 56 (2015), 46-56.
- 233 Perkin Elmer, 'MP, T_g and Structure of Common Polymers', (2011).
- 234 Bin Shen, Wentao Zhai, Mimi Tao, Dingding Lu, and Wenge Zheng, 'Enhanced Interfacial Interaction between Polycarbonate and Thermally Reduced Graphene Induced by Melt Blending', *Composites Science and Technology*, 86 (2013), 109-16.
- 235 Motohiro Nishio, 'The CH/II Hydrogen Bond in Chemistry. Conformation, Supramolecules, Optical Resolution and Interactions Involving Carbohydrates', *Physical Chemistry Chemical Physics*, 13 (2011), 13873-900.
- 236 Osamu Takahashi, Yuji Kohno, and Motohiro Nishio, 'Relevance of Weak Hydrogen Bonds in the Conformation of Organic Compounds and Bioconjugates: Evidence from Recent Experimental Data and High-Level *ab Initio* MO Calculations', *Chemical Reviews*, 110 (2010), 6049-76.
- 237 Motohiro Nishio, Minoru Hirota, and Yoji Umezawa, *The CH/II Interaction: Evidence, Nature, and Consequences. Vol. 21* (John Wiley & Sons, 1998).
- 238 Linlin Duan, Yuanming Wang, Yatao Zhang, and Jindun Liu, 'Graphene Immobilized Enzyme/Polyethersulfone Mixed Matrix Membrane: Enhanced Antibacterial, Permeable and Mechanical Properties', *Applied Surface Science*, 355 (2015), 436-45.
- 239 Wen Zou, Hui Qin, Wenbin Shi, Shudong Sun, and Changsheng Zhao, 'Surface Modification of Poly(Ether Sulfone) Membrane with a Synthesized Negatively Charged Copolymer', *Langmuir*, 30 (2014), 13622-30.
- 240 Benoît Lecouvet, Michel Sclavons, S. Bourbigot, and Christian Bailly, 'Thermal and Flammability Properties of Polyethersulfone/Halloysite Nanocomposites Prepared by Melt Compounding', *Polymer Degradation and Stability*, 98 (2013), 1993-2004.
- 241 Swati Gahlot, Prem P. Sharma, Hariom Gupta, Vaibhav Kulshrestha, and Prafulla K. Jha, 'Preparation of Graphene Oxide Nano-Composite Ion-Exchange Membranes for Desalination Application', *RSC Advances*, 4 (2014), 24662-70.
- 242 B. M. Ganesh, Arun M. Isloor, and Ahmad Fauzi Ismail, 'Enhanced Hydrophilicity and Salt Rejection Study of Graphene Oxide-Polysulfone Mixed Matrix Membrane', *Desalination*, 313 (2013), 199-207.
- 243 Mariana Ionita, Eugenia Vasile, Livia Elena Crica, Stefan Ioan Voicu, Andreea Madalina Pandele, Sorina Dinescu, Loredana Predoiu, Bianca Galateanu, Anca Hermenean, and Marieta Costache, 'Synthesis, Characterization and in Vitro Studies of Polysulfone/Graphene Oxide Composite Membranes', *Composites Part B: Engineering*, 72 (2015), 108-15.
- 244 Fei Li, Yu Liu, Cheng-Bing Qu, Hong-Mei Xiao, Yang Hua, Guo-Xin Sui, and Shao-Yun Fu, 'Enhanced Mechanical Properties of Short Carbon Fiber Reinforced

- Polyethersulfone Composites by Graphene Oxide Coating*, *Polymer*, 59 (2015), 155-65.
- 245 Mariana Ionita, Andreea Madalina Pandele, Livia Crica, and Luisa Pilan, 'Improving the Thermal and Mechanical Properties of Polysulfone by Incorporation of Graphene Oxide', *Composites Part B: Engineering*, 59 (2014), 133-39.
- 246 Zhao Qin, and Markus Buehler, 'Bioinspired Design of Functionalised Graphene', *Molecular Simulation*, 38 (2012), 695-703.
- 247 Rui Zhang, Hua Deng, Renata Valenca, Junhong Jin, Qiang Fu, Emiliano Bilotti, and Ton Peijs, 'Strain Sensing Behaviour of Elastomeric Composite Films Containing Carbon Nanotubes under Cyclic Loading', *Composites Science and Technology*, 74 (2013), 1-5.
- 248 Yuseon Heo, Hyungu Im, and Jooheon Kim, 'The Effect of Sulfonated Graphene Oxide on Sulfonated Poly(Ether Ether Ketone) Membrane for Direct Methanol Fuel Cells', *Journal of Membrane Science*, 425 (2013), 11-22.
- 249 Tatsuki Yasumitsu, Gang Liu, Jean-Marc Leveque, Shuji Aonuma, Laurent Duclaux, Takahide Kimura, and Naoki Komatsu, 'A Rosette Cooling Cell: More Effective Container for Solubilization of Single-Walled Carbon Nanotubes under Probe-Type Ultrasonic Irradiation', *Ultrasonics Sonochemistry*, 20 (2013), 37-39.
- 250 Kyle Berean, Jian Zhen Ou, Majid Nour, Kay Latham, Chris McSweeney, David Paull, Andri Halim, Sandra Kentish, Cara M. Doherty, Anita J. Hill, and Kourosh Kalantar-zadeh, 'The Effect of Crosslinking Temperature on the Permeability of PDMS Membranes: Evidence of Extraordinary CO₂ and CH₄ Gas Permeation', *Separation and Purification Technology*, 122 (2014), 96-104.

Appendix A: Publications

Michael Czajka, Robert A. Shanks and Ing Kong*

Preparation of graphene and inclusion in composites with poly(styrene-*b*-butadiene-*b*-styrene)

Abstract: The aim of this work was to prepare and characterize nanocomposites containing graphene from intercalated graphite. The graphene was produced by rapid thermal expansion using expandable graphite oxide or obtained commercially. The polymer used was poly(styrene-*b*-butadiene-*b*-styrene) (SBS). The SBS was dissolved in *p*-xylene and the graphene was ultrasonically suspended in the xylene solution. The morphology, dynamic mechanical, electrical, and thermal properties of composites were characterized. Graphene at 1% (w/w) (hydrogen atmosphere) was found to increase the storage modulus (68%) and loss modulus (147%) of the glassy state of polybutadiene in SBS. The damping factor of SBS was enhanced by 74% corresponding to the polystyrene phase of SBS using Cheap Tubes graphene. The composites were insulators at 1% (w/w). The styrene groups in SBS strongly adsorb onto the graphenes, preventing a percolation network that would enhance electrical permittivity. Graphene enhanced physical crosslinks of the polystyrene phase to increase the modulus at low concentration. Graphene dispersion using ultrasonic shear depended on π - π interactions between the aromatic rings of the solvent, graphene, and polystyrene. This is a simple, fast, cheap, and scalable way of making high-quality graphene and a new way of graphene dispersal in polymers.

Keywords: block copolymer; elastomer; graphene; graphite; intercalation.

*Corresponding author: Ing Kong, School of Applied Sciences, RMIT University, Box 2476 GPO, Melbourne, Victoria 3001, Australia; and Department of Mechanical, Materials and Manufacturing Engineering, University of Nottingham Malaysia Campus, Jalan Broga, 43500 Semenyih, Selangor, Malaysia.
e-mail: ing.kong@rmit.edu.au

Michael Czajka and Robert A. Shanks: School of Applied Sciences, RMIT University, Box 2476 GPO, Melbourne, Victoria 3001, Australia

1 Introduction

Graphene was first isolated in 2004 by Andre Geim and Konstantin Novoselov. They were awarded the 2010 Nobel Prize in Physics for this [1]. Since then, graphene

has been the most cited substance in science. Graphene is a hexagonal matrix of carbon that looks like chicken wire but is only one atom thick. Graphene is the stiffest and strongest material yet discovered (tensile modulus of 1 TPa and ultimate strength of 130 GPa). It has a greater surface area (2630 m²/g) [2] and it is more electrically conductive (6000 S/cm) [3] than any other material. Graphene is impermeable to gases, resists high temperatures (estimated $T_m=4900$ K) [4], and is highly thermally conductive (5000 W/mK) [3]. However, the high price of graphenes, and thus availability for ready experimentation, hampers experimenters [4–6]. Keeping graphene sheets apart to utilize their unique properties is a secondary challenge.

Graphene can be produced either top down or bottom up. The bottom-up method involves either plasma deposition or chemical vapor deposition. The bottom-up methods require 300 million layers of graphene to make a stack 10 cm high. The top-down method (separating graphite into individual layers) is probably the one best suited to making large amounts of graphene. The main top-down method of creating graphene is chemical oxidation (Hummers method). However, oxidation methods result in a large number of defects in the graphene. One method to produce low defect graphene is the intercalation method (oxides are placed between graphite layers) [7]. This results in expandable graphite, which can be used to create low defect graphene. Graphene flakes created by this method still have sheets very close together. Ultrasonication has been used to separate graphite and create graphene flakes without further oxidation [8]. Thermally expanded graphene, while low defect, still has some oxides on its surface. Oxides on the surface of graphene can be removed. However, removing oxides often requires hazardous chemicals (hydrazine). An alternative is to use an inert gas or a reducing gas. The most common method of dispersing graphene in a polymer is by functionalization. Functionalization requires the creation of defects. The creation of defects can be avoided by using π - π interactions [9] to disperse graphene [10]. Thus, a low defect graphene can be retained in the final product and more of the potential of graphene can be utilized.

The aim was to prepare and characterize nanocomposites containing graphene from intercalated graphite, characterize their structure, and evaluate their

Carbon Monoxide Reduced Low-Defect Graphene Nanocomposites with Poly(styrene-*b*-butadiene-*b*-styrene)

Michael Czajka, Robert Shanks and Daniel Oldfield,
School of Applied Sciences, RMIT University, Box 2476 GPO, Melbourne 3001, Australia
E-mail: Michael.Czajka@rmit.edu.au

Abstract

The aim was to prepare poly(styrene-*b*-butadiene-*b*-styrene) (SBS) graphene nano-composites with effective dispersion to enhance physical and mechanical properties and investigate the effect of increasing low defect graphene from 1–20 % w/w. Graphene was produced by rapid thermal expansion using expandable graphite oxide and compared to a commercial graphene. The graphene was further reduced and repaired with carbon monoxide (CO). The matrix phase was SBS. SBS was dissolved in benzene and the graphene was ultrasonically suspended in the benzene solution. A range of analyses: Raman spectroscopy and characterisation techniques: stress-strain tensile mechanical analysis (TMA), thermogravimetry (TGA), and transmission electron microscopy (TEM) were used. CO reduction of graphene removed 84 % of oxide groups and produced the least defects (0.41 D/G ratio). Ultrasonication improved the exfoliation and dispersion of graphene. Dispersion of graphenes in SBS utilised π -interactions. SBS physical properties improved by the addition of GT-CO: the tangent modulus increased 100 % and strain decreased 94 % as graphene loading increased to 20 % w/w.

Introduction

SBS is a block co-polymer, thermoplastic elastomer used in adhesives, sealants, and molded or extruded products where flexibility and toughness is important. Graphene is a single layer of hexagonally bonded carbon atoms with extreme modulus, strength and conductivity [1-3]. These are desirable properties to incorporate into a polymer.

Most research into graphene polymer composites has concentrated on covalent bonding of graphenes with the chosen polymer matrix [4]. To achieve this oxides (hydroxides, peroxides or carboxyls) are created on graphene to provide sites for bonding. However these functional groups interrupt the perfect sp^2 matrix of graphene creating defects. Most methods of graphene production result in many voids that are defects. It is common for graphenes to have up to 40 % of such defects [5, 6]. It is generally accepted that it is not possible to reinforce a polymer with graphene without such damage. However it is possible to avoid such defects by using low defect graphene production method such as thermal

expansion. The problem of bonding can be by-passed by using π -interactions to disperse graphenes. In previous research it was demonstrated that such a reinforcing approach was possible with SBS [7]. However research suggests that the mechanical percolation threshold for exfoliated graphites and graphenes in a polymer is 2-3 % [8-10]

The aim of this research is to establish whether the dispersion and reinforcement of SBS can be achieved at up to 20 % w/w graphene using π -interactions to maintain the perfect sp^2 structure of a low defect graphene.

Materials

Graphtech (GT) 220-50N expandable graphite. HDPlas (Cheap Tubes) (CT) $>700 \text{ m}^2/\text{g}$ nano platelets (grade 4) 1-2 μm diameter $< 3 \text{ nm}$ 1-3 layers; poly(styrene-*b*-butadiene-*b*-styrene) (SBS) from Aldrich CAS 9003-55-8; benzene and N-methylpyrrolidone (NMP) from Merck;

Preparation

GT (in 1 g amounts) was expanded in air for 30 s in a furnace preheated to 1000 °C. The GT was heated in a ceramic tube furnace at 1000 °C for 8 h in a reducing atmosphere of CO 10 % (GT-CO) (Figure 1).

Disks of 2 cm diameter (~0.5 mm thick) were formed from expanded GT by applying a 9 t load for 5 min in a hydraulic press.

GT-CO 1–20 % w/w was ultrasonicated in benzene (2 mL) for 10–20 min. Ultrasonication (20 kHz and amplitude 25 %) was continued until no more large (un-exfoliated) particles of graphene were visible. A Sonics Autotune series high intensity Ultrasonic Processor Model: GEX 500 (power 500 W) was used.

SBS (1 g) was dissolved in benzene (10 mL) by standing overnight at 23 °C. SBS and graphene solutions were combined and ultrasonicated (to disperse graphene).

Composites were precipitated with methanol, dried and consolidated in a heated press at 155 °C and 6 t pressure. A small round mould of ~4.2 mm diameter and 0.5 mm thickness was used. Polytetrafluoroethylene (PTFE) sheets were placed on both sides and sandwiched between metal plates. The mould was ~30 % overfilled to force out any bubbles and holes.

Hydrogen-reduced Low-defect Graphene with Poly(ethylene terephthalate) Composites

Michael Czajka, Robert A. Shanks, Michelle Spencer and Daniel Oldfield
School of Applied Sciences, RMIT University
Box 2476 GPO, Melbourne, VIC 3001, Australia
E-mail: Michael.Czajka@rmit.edu.au

Abstract

The aim was to prepare and characterise poly(ethylene terephthalate) (PET) composites with hydrogen-reduced graphene (HG) created using thermally expanded intercalated graphite oxide. Melt dispersion (MD) and ultrasonicated solvent-dispersion (SD) methods were contrasted. The structure, response to modulated force, temperature and permeability to gases were measured. A commercially sourced research grade graphene, sourced from Cheap Tubes, was used for comparison. PET-HG was melt dispersed using a Haake mixer with 1 % w/w HG added. PET solution dispersion was performed using o-chlorophenol with ultrasonication. Characterisation techniques used were Raman spectroscopy and wide-angle X-ray scattering (WAXS) with molecular dynamics simulations for validation of dispersion. Properties were measured using dynamic mechanical analysis (DMA), thermogravimetry (TGA), oxygen permeation (MOCON) scanning electron microscopy (SEM) and transmission electron microscopy (TEM). Low defect graphene (1 % w/w), with a Raman D/G peak ratio of 0.53 (lowest D/G ratio) and TGA mass loss of 0.38 % (84 % less oxygen groups) under nitrogen purge, in PET MD was found to increase tensile storage modulus (+43 %) and loss modulus (+96 %) compared with neat PET MD (at 20 °C). Oxygen permeation increased when reduced graphene was added to PET. Melt dispersion of graphene in PET was not as effective as ultrasonic solvent dispersion of graphenes in solvent cast films. Stress-strain showed decreased deformation (-86 %) and smaller hysteresis loop when graphene (1 %) was melt dispersed into PET.

Keywords: polymer composite, nanotechnology, nanocomposite, graphene preparation,

Introduction

Poly(ethylene terephthalate) PET is a high performance commodity; it is a semi crystalline thermoplastic used in bottles, films, fibres and moulded products. It is produced by the polymerisation of ethylene glycol and terephthalic acid. Its repeating group contains one aromatic ring and two ester (R-CO-O-R') groups. Graphene is a single layer of hexagonally bonded carbon atoms with extreme modulus and strength (tensile modulus 1 TPa, tensile strength 130 GPa)[1] and conductivity (electrical: 6,000 S/cm and thermal: 5,000 W/m.k)[2]. The Nobel prize in physics was awarded to Andre Geim and Konstantin Novoselov in 2010 for isolating graphene[3]. Ever since graphene has been the most cited substance in science. Polymer-graphene composites have the ability to significantly enhance the properties of the polymer. Determining if PET permeability, storage modulus, loss modulus and damping factor would be improved by the addition of graphene was the aim of this work.

The production of graphene is considered a major challenge. Producing graphene top down (from graphite) is ideal for mass production. However typical chemical exfoliation methods (Hummers)[4] used to produce graphene require functionalisation (a defect) and thus result in a large number of defects (~40 %)[5]. Intercalation, which involves less covalent bonding[6, 7] and thus creates few defects, is an alternative method to produce low defect graphene. In intercalation oxygen containing

(12) INTERNATIONAL APPLICATION PUBLISHED UNDER THE PATENT COOPERATION TREATY (PCT)

(19) World Intellectual Property
Organization
International Bureau



(10) International Publication Number

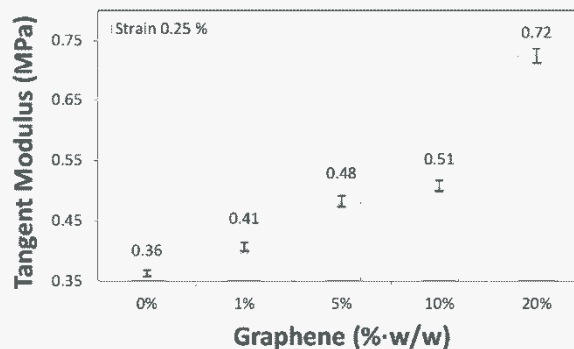
WO 2015/164916 A1

(43) International Publication Date
5 November 2015 (05.11.2015)

- (51) International Patent Classification:
C01B 31/04 (2006.01)
- (21) International Application Number:
PCT/AU2015/000257
- (22) International Filing Date:
1 May 2015 (01.05.2015)
- (25) Filing Language: English
- (26) Publication Language: English
- (30) Priority Data:
2014901584 1 May 2014 (01.05.2014) AU
- (71) Applicant: RMIT UNIVERSITY [AU/AU]; 124 La Trobe Street, Melbourne, Victoria 3000 (AU).
- (72) Inventors: CZAJKA, Michael;
SHANKS, Robert;
HUGEL, Helmut;
- (74) Agent: PHILLIPS ORMONDE FITZPATRICK; Level 21, 22 & 23, 367 Collins Street, Melbourne, Victoria 3000 (AU).
- (81) Designated States (unless otherwise indicated, for every kind of national protection available): AE, AG, AL, AM, AO, AT, AU, AZ, BA, BB, BG, BH, BN, BR, BW, BY, BZ, CA, CH, CL, CN, CO, CR, CU, CZ, DE, DK, DM, DO, DZ, EC, EE, EG, ES, FI, GB, GD, GE, GH, GM, GT, HN, HR, HU, ID, IL, IN, IR, IS, JP, KE, KG, KN, KP, KR, KZ, LA, LC, LK, LR, LS, LU, LY, MA, MD, ME, MG, MK, MN, MW, MX, MY, MZ, NA, NG, NI, NO, NZ, OM, PA, PE, PG, PH, PL, PT, QA, RO, RS, RU, RW, SA, SC, SD, SE, SG, SK, SL, SM, ST, SV, SY, TH, TJ, TM, TN, TR, TT, TZ, UA, UG, US, UZ, VC, VN, ZA, ZM, ZW.
- (84) Designated States (unless otherwise indicated, for every kind of regional protection available): ARIPO (BW, GH, GM, KE, LR, LS, MW, MZ, NA, RW, SD, SL, ST, SZ, TZ, UG, ZM, ZW), Eurasian (AM, AZ, BY, KG, KZ, RU, TJ, TM), European (AL, AT, BE, BG, CH, CY, CZ, DE, DK, EE, ES, FI, FR, GB, GR, HR, HU, IE, IS, IT, LT, LU, LV, MC, MK, MT, NL, NO, PL, PT, RO, RS, SE, SI, SK, SM, TR), OAPI (BF, BJ, CF, CG, CI, CM, GA, GN, GQ, GW, KM, ML, MR, NE, SN, TD, TG).
- Published:
— with international search report (Art. 21(3))

(54) Title: GRAPHENE PRODUCTION PROCESS

Figure 6



(57) Abstract: A process for the preparation of reduced graphene comprising the steps of: providing an expandable graphite intercalated with oxygen containing groups; heating the expandable graphite under conditions sufficient to cause expansion of the expandable graphite and formation of an expanded graphite comprising oxygen containing groups; and contacting the expanded graphite with carbon monoxide to reduce at least a portion of the oxygen containing groups and form a reduced expanded graphite comprising an array of reduced graphene. The process of the invention enables large volumes of high quality graphene to be produced.

WO 2015/164916 A1